Consiglio Nazionale delle Ricerche
ISTITUTO DI SCIENZE DEL PATRIMONIO CULTURALE

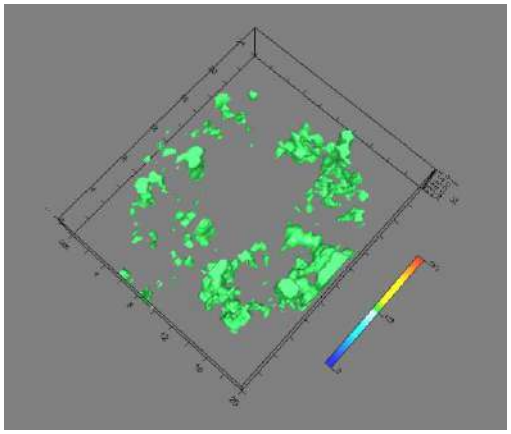

GEOPHYSICAL SURVEY IN THE HOLY CHURCH OF RESURRECTION IN JERUSALEM

The Director
Dott.ssa Costanza Miliani

The Scientific Manager
Dott. Giovanni Leucci

Firmato digitalmente da
LEUCCI GIOVANNI
C: IT

DECEMBER 2021

INDEX

INTRODUCTION

To characterize the shallow subsurface of the Holy Church of Resurrection in Jerusalem, geophysical surveys with ground-penetrating radar (GPR) were undertaken at the end of October 2021.
The surveyed areas are shown in Fig. 1.

Fig. 1: The GPR surveyed areas

The GPR data were acquired using the Sir 3000 georadar system (GSSI) with the 270MHz, and 900MHz antennae along grids with parallel profiles set 0.4 m apart for the 270MHz and 0.2m apart for 900MHz.
Data were acquired by the Laboratory of Geophysics of the Institute of Heritage Science (National Research Council) team. The team was composed by Dr Vincenzo Di Fiore (ISPC Napoli), Dr Ivan Ferrari (ISPC Lecce) and Dr Michele Punzo (ISPC Napoli). The measurements were carried out on the 22, 23 and 24 October 2021 (Fig. 2).

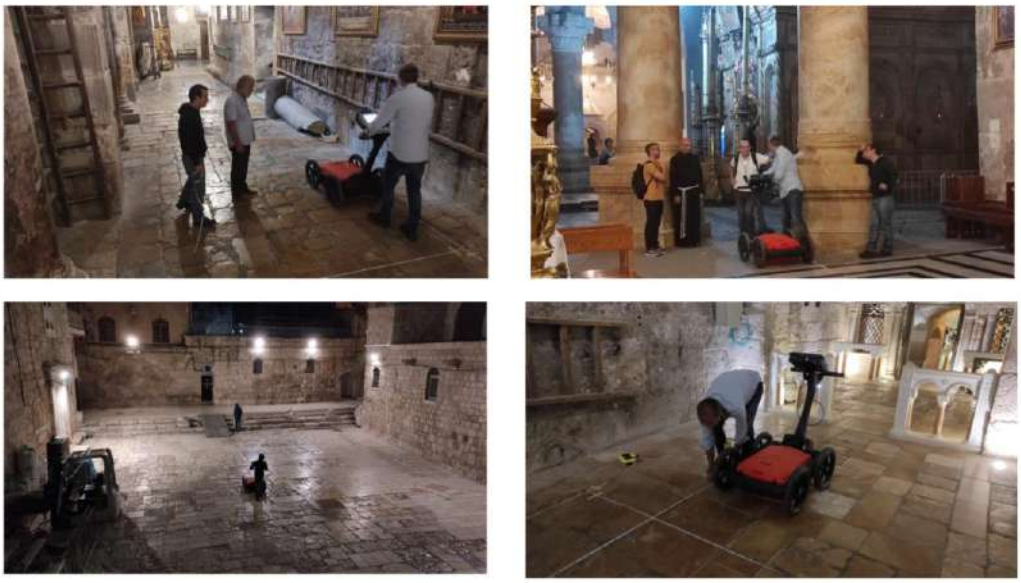

Fig. 2: Phases of GPR data acquisition

GROUND PENETRATING RADAR: BACKGROUND THEORY

GPR surveys' success is mainly dependent on soil and sediment mineralogy, clay content, ground moisture, depth of burial, surface topography, and vegetation (Conyers 2004; Leucci, 2007; Leucci, 2015; Leucci, 2019). It is not a geophysical method that can be immediately applied to any geographic or archaeological setting. However, with thoughtful modifications in acquisition and data processing methodology, GPR can adapt to many different site conditions. Most GPR practitioners have assumed that the method would only be successful in areas where soils and underlying sediment are dry (Annan and Davis 1978). Although radar wave penetration, and the
ability to reflect energy to the surface, is often enhanced in a dry environment, recent work has demonstrated that dryness is not necessarily a prerequisite for GPR surveys and even very wet environments are suitable, as long as the medium is not electrically conductive (Conyers 2004). The GPR method involves the transmission of high-frequency electromagnetic radio (radar) pulses into the earth and measuring the time elapsed between transmission, the reflection of a buried discontinuity and reception back at a surface radar antenna. A pulse of radar energy is generated on a dipole transmitting antenna placed on, or near, the ground surface. The resulting wave of electromagnetic energy propagates downward into the ground, where some energy can be reflected back to the surface at discontinuities (Fig. 3).

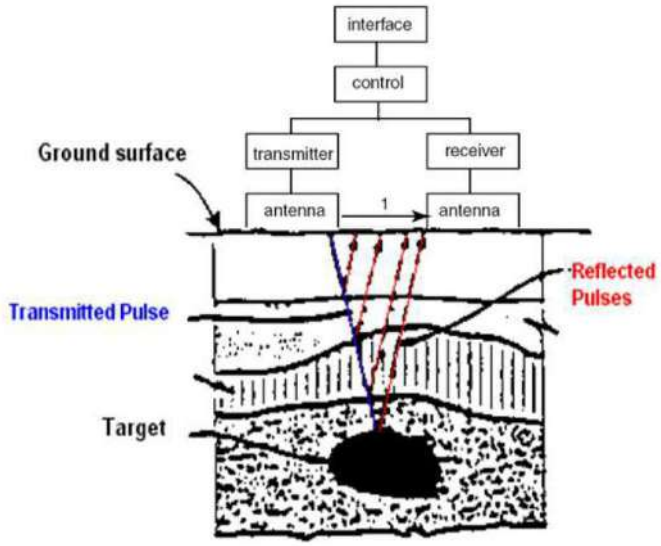

Fig. 3. A block diagram of a GPR system. The interface module enables the user to enter the system parameters and displays and records the data. The control unit generates the timing signals so that all components operate in unison. This unit also does some preliminary data processing. The pulse travel paths in order of arrival are direct air wave, direct ground wave, and reflections.

The discontinuities where reflections occur are usually created by changes in electrical properties of the sediment or soil, lithologic changes, differences in bulk density at stratigraphic interfaces and, most crucial, water content variations. Reflection can also occur at interfaces between anomalous archaeological features and the surrounding soil or sediment. Void spaces in the ground, encountered in burials, tombs, or tunnels, will also generate significant radar reflections due to a considerable change in radar wave velocity. The depth to which radar energy can penetrate and the amount of definition expected in the subsurface are partially controlled by the frequency of the radar energy transmitted. Radar energy frequency controls both the wavelength of the propagating wave and the amount of weakening, or attenuation, of the waves in the ground. Standard GPR antennas used in archaeology propagate radar energy that varies in band width from about 10 megahertz (MHz) to 2500 MHz. Antennas usually come in standard frequencies. Each antenna has one centre frequency but produces radar energy that ranges around that centre by about two octaves (one half and two times the centre frequency). The most efficient method in subsurface GPR mapping is to establish a grid across a survey area before acquiring data. Usually, rectangular grids are set with one meter or less transect spacing. Rectangular grids produce data that are easier to process and interpret. Other grid acquisition patterns may be necessary because of surface topography or other obstructions. Data from non-rectilinear surveys is just as valuable as those acquired in rectangular shaped grids. However, more field time may be necessary for surveying, and reflection data must be manipulated differently during computer processing and interpretation for reflection amplitude analysis. The two-way travel time and the amplitude and wavelength of the reflected radar waves derived from the pulses are amplified, processed and recorded for immediate viewing and later post-acquisition processing and display. During field data acquisition, radar transmission is repeated many times a second as the antennas are pulled along the ground surface in transects. The distance along each line is recorded to place all reflections within a surveyed grid accurately. In this fashion, two-dimensional profiles, which approximate vertical “slices” through the earth, are created along each grid line.
Radar energy becomes both dispersed and attenuated as it radiates into the ground. When portions of the originally transmitted signal are reflected back toward the surface, they will suffer additional

attenuation by the material they pass before finally being recorded at the surface. Therefore, to be detected as reflections, important subsurface interfaces must have sufficient electrical contrast at their boundary and must be located at a shallow enough depth where sufficient radar energy is still available for reflection. As radar energy is propagated to increasing depths, the signal becomes weaker as it spreads out over more surface area and absorbed by the ground, making it less available for reflection. The maximum depth of resolution for every site will vary with the geologic conditions and the equipment being used. Post-acquisition data filtering and other data amplification techniques (termed range-gaining) can sometimes be applied to reflection data after acquisition, enhancing some very low amplitude reflections to make them more visible. Many ground-penetrating radar novices envision the propagating radar pattern as a narrow “pencil” shaped beam focused directly down from the antenna. GPR waves radiated from standard commercial antennas radiate energy into the ground in an elliptical cone with the apex
of the cone at the centre of the transmitting antenna (Conyers 2004; Leucci, 2015, Giannino and Leucci, 2021). This elliptical cone of transmission occurs because the electrical field produced by the antenna is generated parallel to its long axis and is therefore usually radiating into the ground perpendicular to the direction of antenna movement along the ground surface. The radiation pattern is generated from a horizontal electric dipole antenna to which elements are sometimes added that effectively reduce upward radiation, called shields. Sometimes the only shielding mechanism is a radar-absorbing surface placed above the antenna to neutralize upward radiating energy. Because of cost and portability considerations (size and weight), the use of more complex radar antennas that might be able to focus energy more efficiently into the ground in a more narrow beam has to date, been limited in archaeology. Some antennas, especially those in the low-frequency range from 10 to 100 MHz, are often not shielded and radiate radar energy in all directions. Using unshielded antennas can generate reflections from a nearby person pulling the radar antenna or other objects nearby, such as trees or buildings. Discrimination of individual targets, especially those of interest in the subsurface, can be difficult if these types of antennas are used. However, if the unwanted reflections generated from unshielded antennas can be identified, they can be easily filtered out later. Suppose reflections are recorded from randomly located trees, surface obstructions, or people moving about randomly near the antenna. In that case, they are more difficult to discriminate from important subsurface reflections and interpretation of the data is much more difficult. One of the most important variables in GPR surveys is the selection of antennas with the correct operating frequency for the depth necessary and the resolution of the features of interest (Conyers 2004a). In most cases, proper antenna frequency selection can make the difference between success and failure in a GPR survey and must be planned for in advance. The greater the necessary depth of investigation, the lower the antenna frequency should be used (Leucci, 2008). But lower frequency antennas are much larger, heavier and more difficult to transport to and within the field than high-frequency antennas. For instance, a 100 MHz antenna is about 2 meters long. It is difficult to transport to and from the field but must usually be moved along transect lines using some form of wheeled vehicle or sledge. In contrast, antennas greater than 400 MHz are usually 50 centimetres or smaller in maximum dimension, weigh very little, and easily fit into a suitcase. Low-frequency antennas (10–120 MHz) generate long wave-length radar energy that can penetrate up to 50 meters in certain conditions but only resolve extensive subsurface features. In pure ice, antennas of this frequency have been known to transmit radar energy many kilometres. In contrast, the maximum depth of penetration of a 900 MHz antenna is about one meter or less in typical soils, but its generated reflections can resolve features down to a few centimetres in dimension (Conyers 2004; Leucci, 2008). A trade-off, therefore, exists between depth of penetration and subsurface resolution. The depth of penetration and the subsurface resolution is highly variable, depending on site-specific factors such as overburden composition, porosity, and retained moisture. If large amounts of electrically-conductive clay are present, then attenuation of the radar energy with depth will occur very rapidly, irrespective of radar energy

frequency. Attenuation can also occur if sediment or soils are saturated with salty water, especially sea water. The ability to resolve buried features are mostly determined by the frequency and, therefore, the wavelengths of the radar energy being transmitted into the ground. The wavelength necessary for resolution varies depending on whether a three-dimensional object or an undulating surface is investigated. For GPR to resolve three-dimensional objects, reflections from at least two surfaces, usually a top and bottom interface, must be distinct. However, the resolution of a single buried planar surface needs only one distinct reflection, and therefore wavelength is not as important in its resolution. Radar energy reflected off a buried subsurface interface that slopes away from a surface transmitting antenna will be reflected away from the receiving antenna and lost. This sloping interface would therefore go unnoticed in reflection profiles. A buried surface with this orientation would only be visible if a different traverse were located where the same buried interface is sloping toward the surface antennas. This is why it is important always to acquire lines of reflection data within a closely spaced surface grid and sometimes in transects perpendicular to each other. Some features in the subsurface may be described as “point targets”, while others are more similar to planar surfaces. Planar surfaces can be stratigraphic and soil horizons or large flat archaeological features such as floors. Point targets are features such as walls, tunnels, voids, artefacts or any other non-planar object. Depending on a planar surface’s thickness, reflectivity, orientation and depth of burial, it is potentially visible with any frequency data, constrained only by the conditions discussed above. Point sources, however, often have a little surface area with which to reflect radar energy and therefore are usually difficult to identify and map. They are sometimes indistinguishable from the surrounding material, often visible only as small reflection hyperbolas visible on one profile within a grid. In most geological and archaeological settings, the materials through which radar waves pass may contain many small discontinuities that reflect energy, which can only be described as clutter (if they are not the survey's target). The clutter resolution is dependent on the wavelength of the radar energy being propagated. Suppose both the features to be resolved and the discontinuities producing the clutter are on the order of one wavelength in size. In that case, the reflection profiles will appear to contain only clutter, and there can be no discrimination between the two. Clutter can also be produced by large discontinuities, such as cobbles and boulders, but only when a lower frequency antenna that produces a long wavelength is used. In all cases, if not a large planar surface, the features to be resolved should be much larger than the clutter and greater than one wavelength of the propagating energy in dimension (Conyers 2004). The raw reflection data collected by GPR is nothing more than a collection of many individual traces along two-dimensional transects within a grid. Each reflection trace contains a series of waves that vary in amplitude depending on the amount and intensity of energy reflection at buried interfaces. When these traces are plotted sequentially in standard two-dimensional profiles, specific amplitudes within individual traces containing important reflection information are sometimes difficult to visualize and interpret. Rarely is the standard interpretation of GPR data, which consists of viewing each profile and then mapping important reflections and other anomalies sufficient, especially when the buried features and stratigraphy are complex. In areas where buried materials are difficult to discern, different processing and interpretation methods must be used, one of which is amplitude analysis. In the past, when GPR reflection data were collected that had no discernable reflections or recognizable anomalies of any sort, the survey has usually declared a failure and little if any interpretation was conducted. With the advent of more powerful computers and sophisticated software programs that can manipulate large sets of digital data, important subsurface information in the form of amplitude changes within the reflected waves has been extracted from these types of GPR data (Conyers 2004). An analysis of the spatial distribution of the amplitudes of reflected waves is important because it is an indicator of subsurface changes in lithology and other physical properties. The higher the contrasting velocity at a buried interface, the greater the reflected wave amplitude. Suppose amplitude changes can be related to important buried features and stratigraphy. In that case, the location of higher or lower amplitudes

at specific depths can be used to reconstruct the subsurface in three dimensions. Areas of low amplitude waves indicate uniform matrix material or soils, while those of high amplitude denote areas of high subsurface contrast such as buried archaeological features, voids or important stratigraphic changes. To be correctly interpreted, amplitude differences must be analyzed in discrete slices that examine only the strength of reflections within specific depths in the ground. Each slice consists of the spatial distribution of all reflected wave amplitudes at various depths, which are indicative of these changes in sediments, soils and buried materials. Amplitude slices need not be constructed horizontally or even in equal time intervals. They can vary in thickness and orientation, depending on questions (Conyers and Goodman, 1997). Surface topography and the subsurface orientation of features and stratigraphy of a site may sometimes necessitate the construction of slices that are neither uniform in thickness nor horizontal. To compute horizontal amplitude slices, the computer compares amplitude variations within traces recorded within a defined time window (that can become depth windows if velocities are known). When this is done, both positive and negative amplitudes of reflections are compared to the norm of all amplitudes within that window. No differentiation is usually made between positive or negative amplitudes in these analyses; only the magnitude of amplitude deviation from the norm. Low amplitude variations within any one slice denote little subsurface reflection and therefore indicate the presence of fairly homogeneous material. High amplitudes indicate significant subsurface discontinuities, in many cases detecting the presence of buried features. An abrupt change between an area of low and high amplitude can be very significant and may indicate the presence of a major buried interface between two media. Degrees of amplitude variation in each time slice can be assigned arbitrary colours or shades of grey along a nominal scale. Usually, there are no specific amplitude units assigned to these colour or tonal changes.

Using three-dimensional GPR reflection data, buried features can be rendered into isosurface images, meaning that the interfaces producing the reflections are placed in a three-dimensional picture, and a pattern or colour is assigned to specific amplitudes for them to be visible (Conyers 2004; Goodman et al. 2004; Leckebusch 2003). Typical amplitudes (usually the highest ones) in programs that produce these images can be patterned or coloured while others are made transparent. To simulate sun rays, computer-generated light sources can then be used to shade and shadow the rendered features to enhance them. The elements can be rotated and shaded until the desired image results.

GPR data processing

One of the significant advantages of the GPR method is that the raw data is acquired in a manner that allows it to be easily viewed in real-time using a computer screen. Often very little processing is required for an initial interpretation of the data, with most of the effort directed towards data visualization. On the other hand, it may be necessary to perform sophisticated data processing depending on the application and target of interest. Many practitioners find that techniques common to seismic reflection, such as migration, can be applied. The outcome of processing is a cross-section of the subsurface EM properties, displayed in terms of the two-way travel time, i.e. the time taken for a wave to move from the transmitter to a reflector and return to the receiver. The amount of processing undertaken can range from basic, which allows rapid data output, to the more time-consuming application of algorithms designed for use on the seismic dataset (Ylmaz, 1987), which produce high-quality work (Conyers and Goodman, 1997). The processing sequence usually developed for GPR raw data is following done.

Zero-time adjusts (static shift) – The airwave is the first waveform to arrive at the receiver during a GPR survey. There is a delay in the arrival time of the first break of the air wave on the radar section due to the length of the cable connecting the antennae and the control unit. Therefore need to associate zero-time with zero-depth, so any time offset due to instrument recording must be removed before interpretation of the radar image.

Background removal filter (subtract average trace to remove banding) - Background noise is a repetitive signal created by slight ringing in the antennae, which produces a coherent banding effect,

parallel to the surface wave, across the section (Conyers and Goodman,1997). The filter is a simple arithmetic process that sums all the amplitudes of reflections recorded simultaneously along with a profile divided by the number of traces summed; the resulting composite digital wave, which is an average of all background noise, is then subtracted from the data set. In this process, care must be taken not to remove actual linear events in the profile. The time window where the filter operates must be specified so that the filter is not applied until after the surface wave.

Horizontal (distance) stretch to get constant trace separation (horizontal normalization) – This correction needs to remove non-constant motion effects along with the profile. Data are collected continuously and will not be represented correctly in the image if steps are not taken to correct the horizontal data coverage variable.

Gain – Gain is used to compensate for amplitude variations in the GPR image; early signal arrival times have greater amplitude than later because these early signals have not travelled as far. The loss of signal amplitude is related to geometric spreading and intrinsic attenuation. Various time-variable gain functions may be applied to equalize the amplitudes of the recorded signals. The most commonly used is an automatic gain control (AGC), a time-varying gain that runs a window of chosen length along each trace, point by point, finding the average amplitude over the length of the window about each topic. A gain function is then applied such that the average at each point is made constant along the trace.

Topographic corrections – Surveyed elevation data apply topography to the GPR survey profiles. Firstly trace windowing is used to remove all artefacts in the survey that arrived before the time zero arrivals. The elevation recorded along the GPR line is then entered into the data processing package. The time zero arrivals are hung from the topographic profile by applying a time shift to each trace.

Frequency filtering - Although GPR data are collected with source and receiver antennae of specified dominant frequency, the recorded signals include a band of frequencies around the dominant frequency component. Frequency filtering removes unwanted high and/or low frequencies to produce a more interpretable GPR image. Highpass filtering maintains the high frequencies in the signal but removes the low-frequency components. Low-pass filtering does just the opposite, eliminating high frequencies and retaining the low-frequency components. A combination of these two effects can be achieved with a band-pass filter, where the filter retains all frequencies in the pass band but removes the high and low frequencies outside of the pass band.

Deconvolution - When the time-domain GPR pulse propagates in the subsurface, convolution is the physical process that describes how the propagating wavelet interacts with the earth filter (the reflection and transmission response of the subsurface). Deconvolution is an inverse filtering operation that attempts to remove the effects of the source wavelet better to interpret GPR profiles as images of the earth structure. Deconvolution operators can degrade GPR images when the source signature is not known. Deconvolution operators are designed to assume that the propagating source wavelet is a minimum phase (i.e., most of its energy is associated with early times in the wavelet). This assumption is not necessarily valid for GPR signals. With GPR, the ground becomes part of the antennae, and the source pulse can vary from trace to trace and is not necessarily the minimum phase. All filtering operations borrowed from seismic data processing must be applied with care as some of the underlying assumptions for elastic waves generated at the earth's surface are not valid or are different for electromagnetic waves. For more, see Ylmaz (1987)

Migration - Migration is a processing technique that attempts to correct that energy in the GPR profile image is not necessarily correctly associated with depths below the 2-D survey line. As with deconvolution, migration can be seen as an inverse processing step that attempts to correct the geometry of the subsurface in the GPR image concerning the survey geometry. For example, a subsurface scattering point in a GPR image is a hyperbolic-shaped feature. Migration would associate all the energy in the wavelets making up the hyperbolic feature with the point of diffraction, and imaging the actual earth structure (the heterogeneity represented by the point diffractor) would be

imaged more clearly. Migration operators require an excellent subsurface EM wave velocity estimate to apply the correct adjustments to the GPR image. For more, see Ylmaz (1987).

F-K filter - Fourier transforms techniques, or f-k filtering, i.e. using filters designed and applied in the frequency-wavenumber (or f-k) domain (Yilmaz, 1987). It is well known that a dipping line in the x-t domain maps to a line passing through the origin and with an orientation normal to the original line in the f-k amplitude spectrum. In other words, a line of constant apparent velocity corresponds to a line of constant slope in the f-k domain. In particular, horizontal lines map to the vertical direction along the f-axis. Dipping events that overlap in the x-t domain can be separated in the f-k domain by their dips. This allows the elimination of certain types of unwanted energy from the data, representing linear coherent noise. Regardless of their location, lines with the same dip (parallel lines) map to the same radial line in the f-k amplitude spectrum, so that f-k filters could be effective for removing at the same time all undesired lines with the same slope, but impractical if one wants to remove only some of them instead of the whole family. Fan filters are generally used for dip filtering. In these cases, the amplitude spectrum of the input is multiplied by a suitable function, the amplitude response of the filter consisting of ones in a fan-shaped zone and zeros elsewhere, to obtain the amplitude spectrum of the output, whereas the phase spectrum is left unchanged. Finally, the filtered signal is received by a twodimensional inverse Fourier transform.

The Wavelet Transform is possible to decompose the radar signal into different scales where signal and certain noises may be effectively separated/isolated (multiresolution analysis). Subsequent noise muting is easily achieved in the Wavelet Transform (WT) domain operating only on the scales where the offending noise appears.

Time-slice analysis – An analysis of the spatial distribution of reflected wave amplitudes is essential because it indicates potentially meaningful subsurface changes in lithology or other physical properties of materials in the ground. If amplitude changes can be related to the presence of important buried features, the location of those changes can be used to reconstruct the subsurface in three dimensions. Areas of low-amplitude waves usually indicate uniform matrix material or soils. At the same time, those of high amplitude denote areas of high subsurface contrast such as buried archaeological features, voids, or significant stratigraphic changes. To be interpreted, amplitude differences must be analyzed in slices that examine only changes within specified depths in the ground. Each amplitude slice consists of the spatial distribution of all reflected wave amplitudes, which are indicative of these changes in sediments, soils, and buried materials. Amplitude slices need not be constructed horizontally or even in equal depth intervals. They can vary in thickness and orientation, depending on the questions. To produce horizontal amplitude slice maps, the computer compares amplitude variations within traces recorded within a defined time window. For instance, if data were recorded to a maximum of 30 nanoseconds in the ground, six slices of 5 nanoseconds in thickness would be analyzed, and the spatial distribution of amplitudes in each slice would be produced. When this is done, both positive and negative amplitudes of reflections are compared to the norm of all amplitudes within that window. No differentiation is usually made between positive or negative amplitudes in these analyses; only the magnitude of amplitude deviation from the norm is expressed. An abrupt change between an area of low and high amplitude can be very significant and may indicate the presence of an important buried interface between two media. Degrees of amplitude variation in each slice can be assigned arbitrary colours or shades of grey along a nominal scale. Usually, there are no specific amplitude units assigned to these colour or tonal changes. Slices produced in thicknesses based on radar travel time can readily be converted to depth slices if the velocity of energy movement through the material (or its RDP) is calculated. This is the preferred format for most archaeological applications. Several computer programs can estimate the velocity of radar travel times from individual reflection profiles; alternatively, direct measurements can be made in the field if open excavations are present (Conyers and Lucius 1996).

Time-depth conversion – The EM-wave velocity can be estimated from GPR data in several ways (Conyers and Goodman 1997; Huisman et al. 2003; Leucci 2019, Leucci 2020); the conventional methods involve common depth-point (CDP) and wide-angle reflection and refraction (WARR) data sets. Both methods require two antennae in separate units and relatively long acquisition times. In the first case, both antennae are simultaneously moved apart on either side of the midpoint of the profile. In the second case, the position of one antenna is fixed while the other is moved along the profile direction. The EM-wave velocity can be more quickly and easily determined from the reflection profiles acquired in continuous mode, using the characteristic hyperbolic shape of reflection from a point source (Fruhwirth et al. 1996). This is a very common method of velocity estimation, and it is based on the phenomenon that a small object reflects EM waves in almost every direction.

GPR DATA ANALYSIS: The 270 MHz antenna

The surveyed zone was divided into five main areas (Fig. 4).

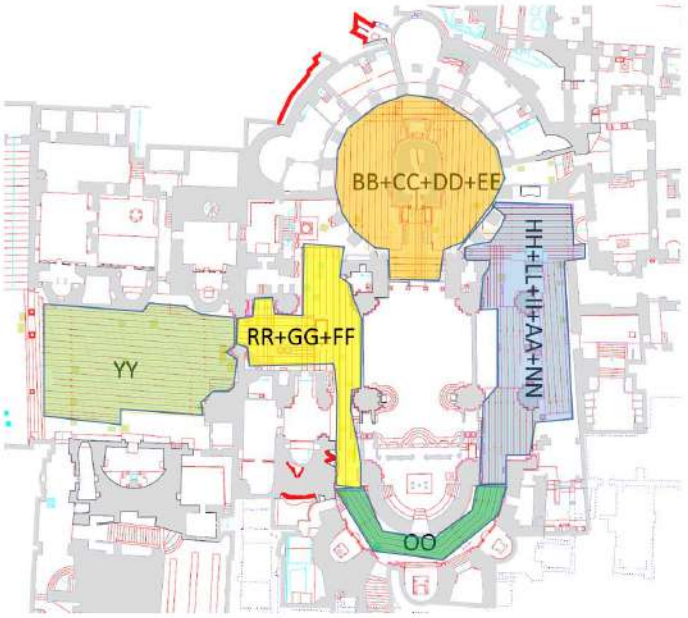

Fig. 4: surveyed areas with 270MHz antenna

Area BB+CC+DD+EE

In the area, BB+CC+DD+EE have acquired 70 GPR profiles for an extension of 649.8 meters.

The GPR data profiles were processed in 2D using GPR-slice software (GPR-SLICE Software (gpr-survey.com)). To eliminate a small noise component and make it easy to interpret GPR data, the following processing sequence was applied:

1) Zero-time adjust (static shift), to associate zero-time with zero-depth;
2) Background removal;
3) Frequency filtering, to remove high-frequency noise;
4) Migration, to correct the shape and dimension of reflection events related to the structure present in the subsoil.

Area CC: The processed GPR profiles acquired in area CC are shown in Figs. 5,…, 10.

The reflection event evidenced by a dashed yellow line (labelled B) is probably related to the bedrock. The depth of bedrock ranges from about 1.2m to 2.8m.

The T's reflection events are related to the manholes visible on the surface.

The reflection events labelled C at a depth of about 0.25-0.3m are related to a known cavity.

Some reflection events labelled V at a depth between 0.9 m and 1.1m in the radar sections 5, 6 and 7 (Fig. 6) are probably related to a void space. Also, the reflection events labelled V at a depth between 1.7m, and 2.0m (Fig. 8) are likely associated with void spaces. Here is possible to note a change in the polarity of the electromagnetic wave. The multiple reflections labelled M are probably related to the metal objects.

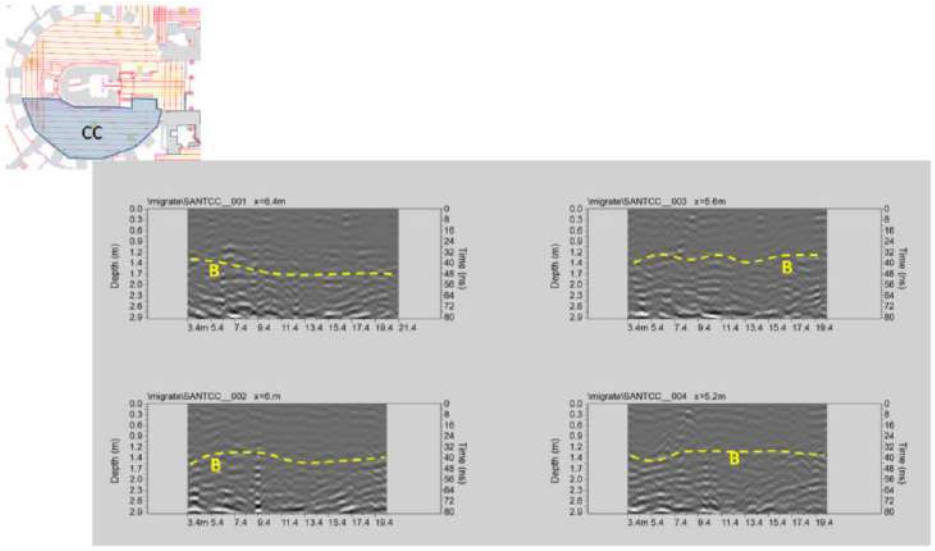

Fig. 5: Area CC: Processed GPR profiles 1,…,4 (B: bedrock)

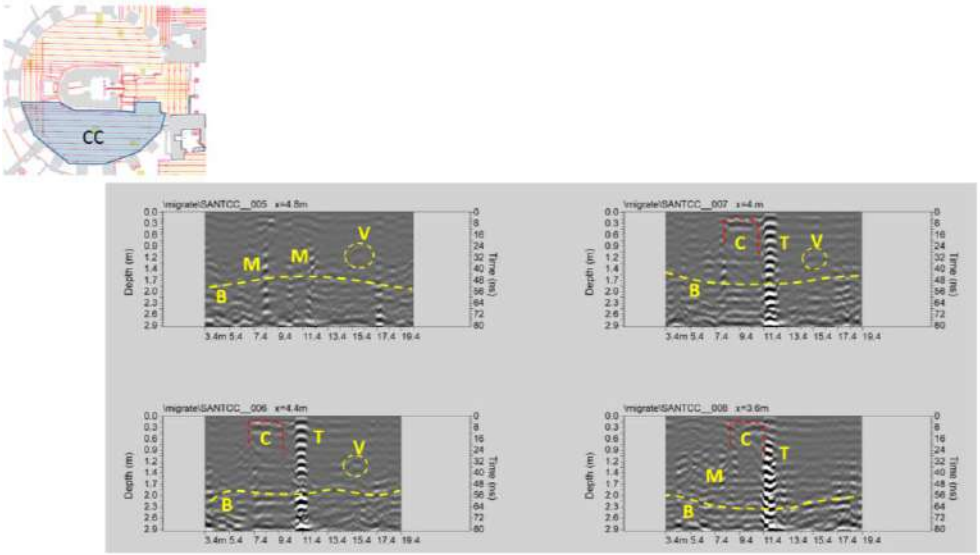

Fig. 6: Area CC: Processed GPR profiles 5,…,8 (T: manhole; C: Cavity; M: metal object; B: bedrock; V: void space).

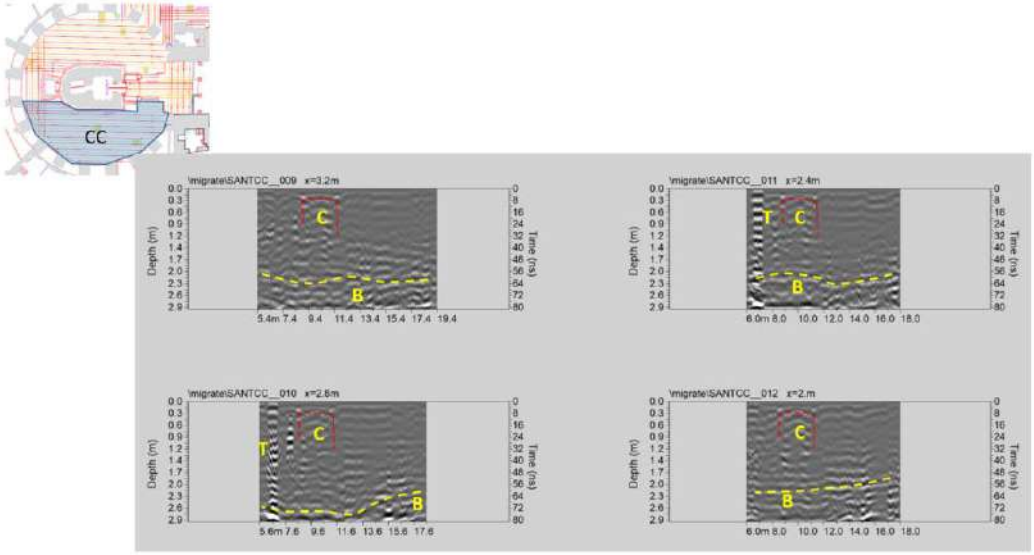

Fig. 7: Area CC: Processed GPR profiles 9,…,12 (T: manhole; C: Cavity; B: bedrock).

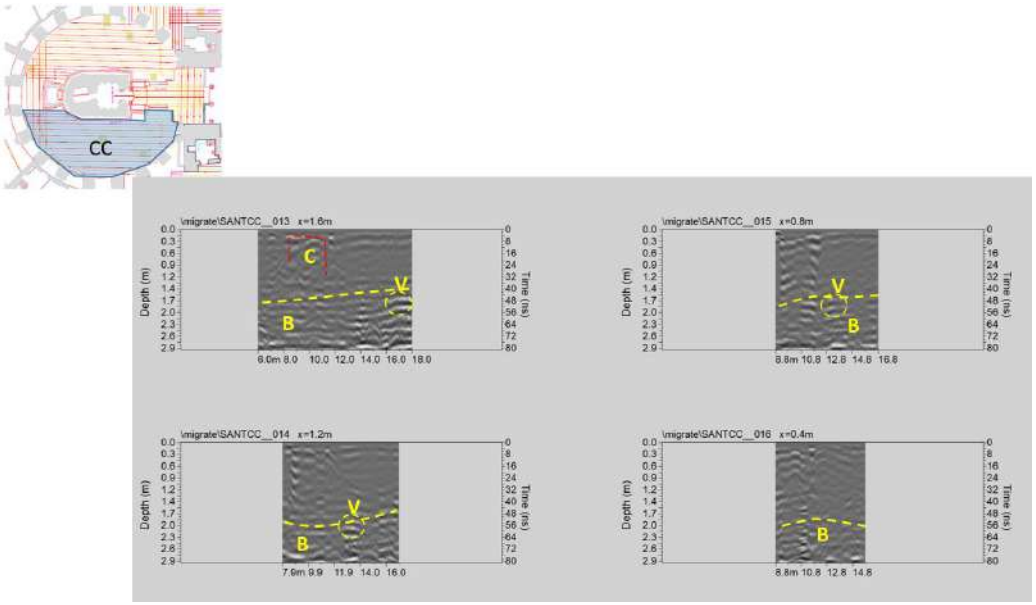

Fig. 8: Area CC: Processed GPR profiles 13,…, 16 (V: void space; C: Cavity; B: bedrock).

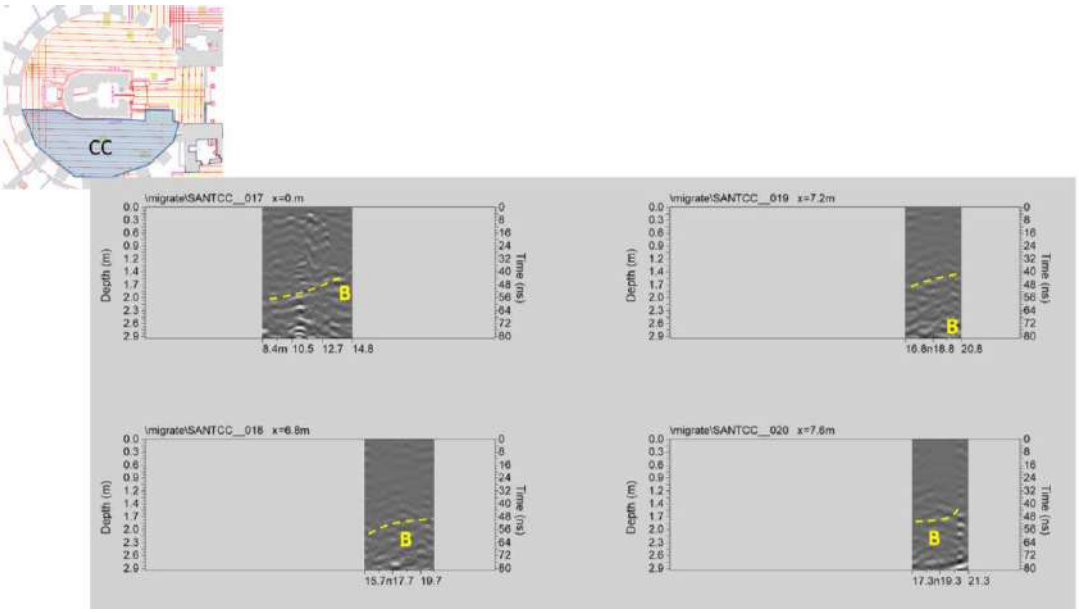

Fig. 9: Area CC: Processed GPR profiles 17,…, 20 (B: bedrock).

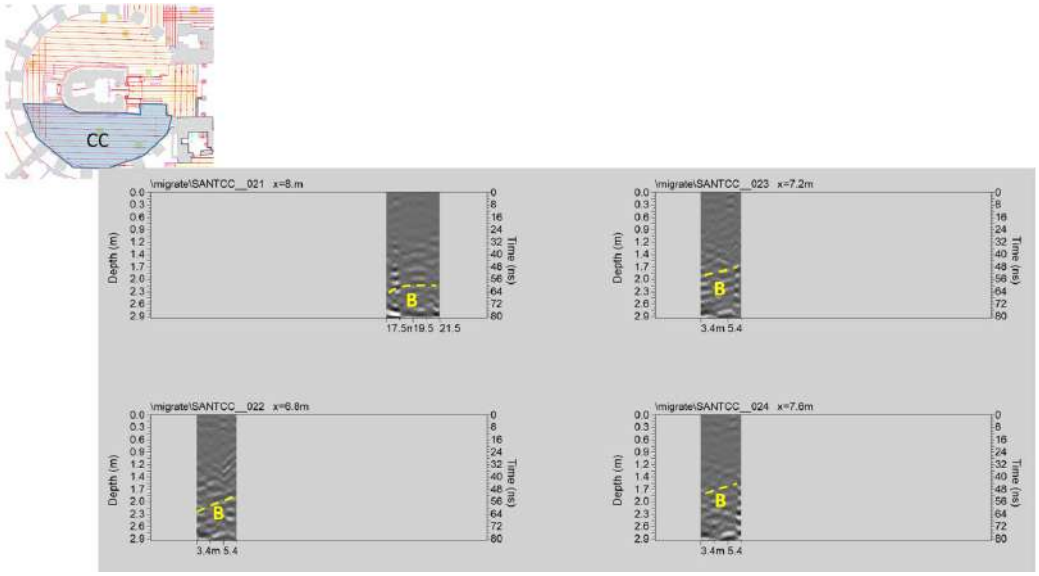

Fig. 10: Area CC: Processed GPR profiles 21,…, 24 (B: bedrock).

Area BB: The processed GPR profiles acquired in the area BB are shown in Figs. 11,…, 15.
The reflection event evidenced by a dashed yellow line (labelled B1) is probably related to the first level of the bedrock. Its depth ranges from about 0.2m to 0.6m. It is possible to evidence also a second level (B2) of the bedrock. Its depth ranges from 1.4m to 1.7m. The first bedrock level (B1) shows greater homogeneity than the second level B2. The second level, B2, offers a high sub-horizontal stratification.
The T's reflection events are related to the manholes visible on the surface.
The reflection events labelled C at a depth of about 1.2-1.7m are related to a known cavity.
Some reflection events labelled V at a depth between 1.2 m and 1.4m in the radar sections 16, 17, 18, 19, 20 and 21 (Figs. 14 and 15) are probably related to a void space. Here is possible to note a change in the polarity of the electromagnetic wave.

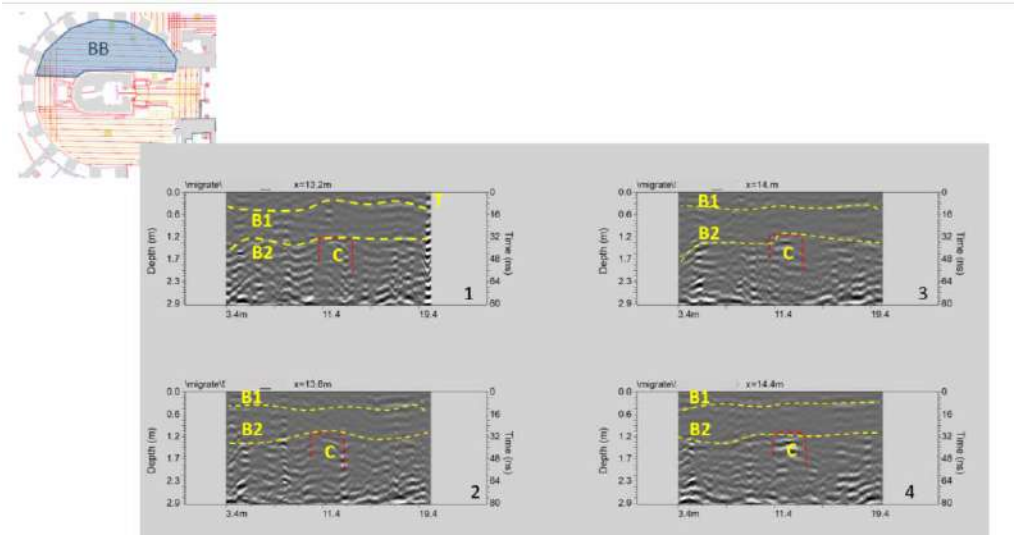

Fig. 11: Area BB: Processed GPR profiles 1,…, 4 (C: cavity; B1: first level of bedrock; B2: second level of bedrock stratified; T: manhole)

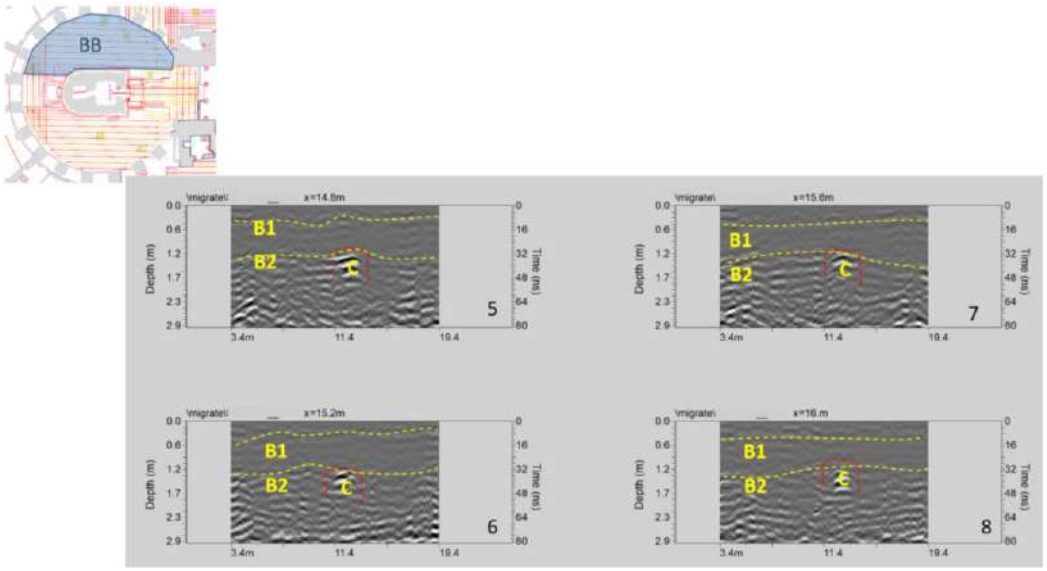

Fig. 12: Area BB: Processed GPR profiles 5,…, 8 (C: cavity; B1: first level of bedrock; B2: second level of bedrock)

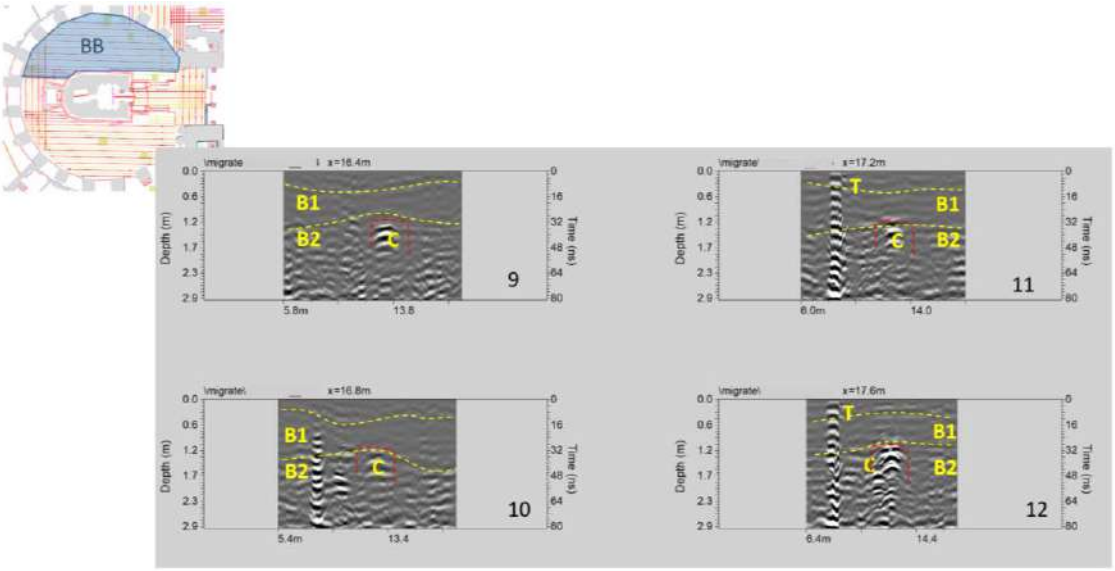

Fig. 13: Area BB: Processed GPR profiles 9,…, 12 (C: cavity; B1: first level of bedrock; B2: second level of bedrock; T: manhole)

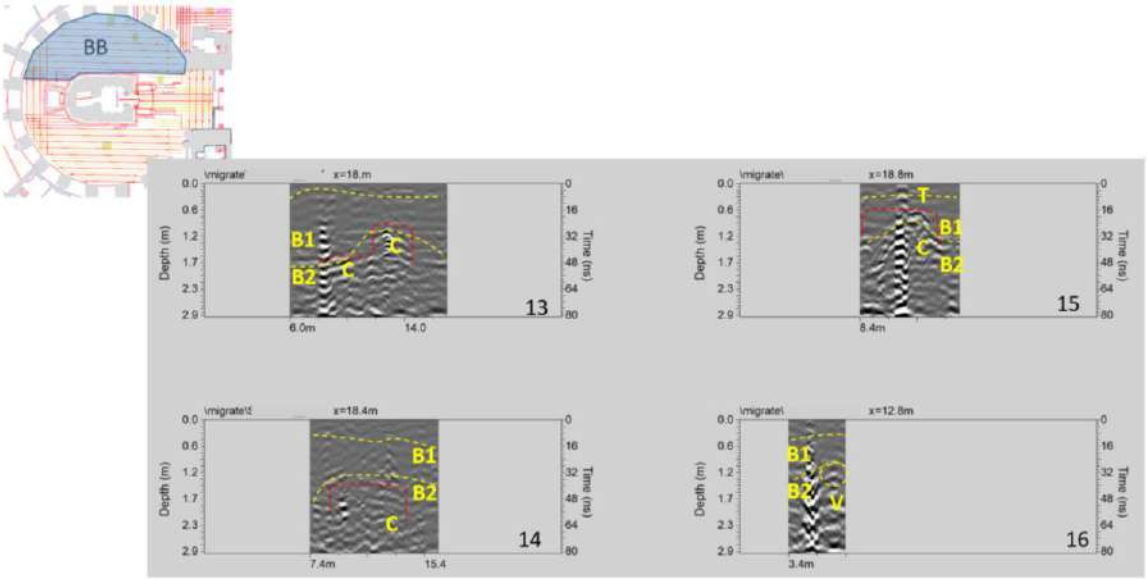

Fig. 14: Area BB: Processed GPR profiles 13,…, 16 (C: cavity; B1: first level of bedrock; B2: second level of bedrock; T: manhole; V: void space)

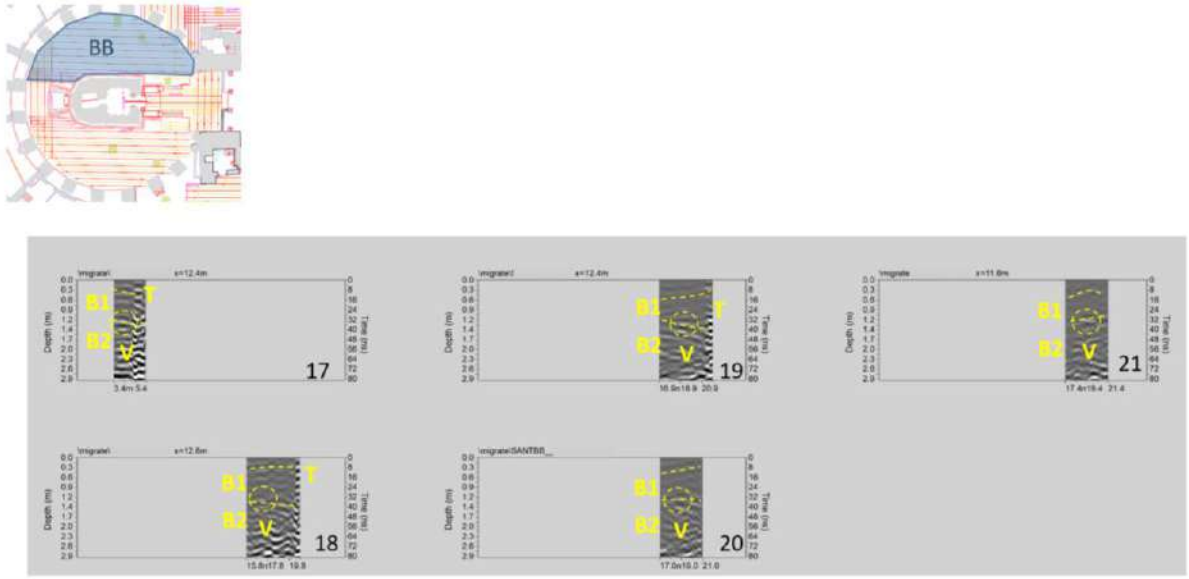

Fig. 15: Area BB: Processed GPR profiles 17,…, 20 (B1: first level of bedrock; B2: second level of bedrock; T: manhole; V: void space)

Area DD: The processed GPR profiles acquired in the area DD are shown in Figs. 16,…, 20.
The reflection event evidenced by a dashed yellow line (labelled B) is probably related to the bedrock level. Its depth ranges from about 0.2m to 0.6m. The reflection events labelled V1 and V2 are probably associated with the void spaces at a depth between 0.6m and 0.7 m (V1) and between 1.2m and 1.5m V2.
The reflection events labelled CH (Fig. 20) at a depth of about 2.8-3.0m is related to a void space (natural void?). While the reflection event labelled V (Fig. 20) at a depth of about 0.4-0.8m is related to a void space.

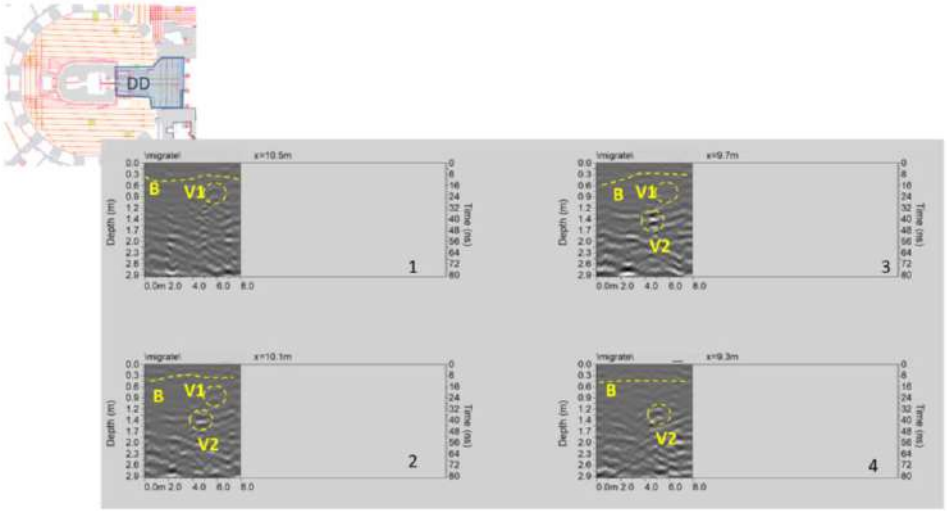

Fig. 16: Area DD: Processed GPR profiles 1,…, 4 (B: bedrock; V1 and V2: void spaces)

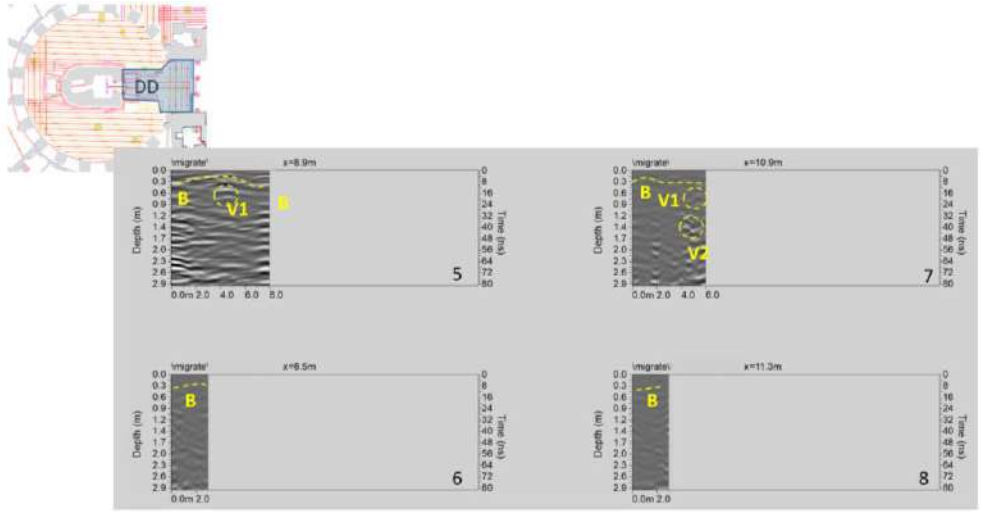

Fig. 17: Area DD: Processed GPR profiles 5,…, 8 (B: bedrock; V1 and V2: void spaces)

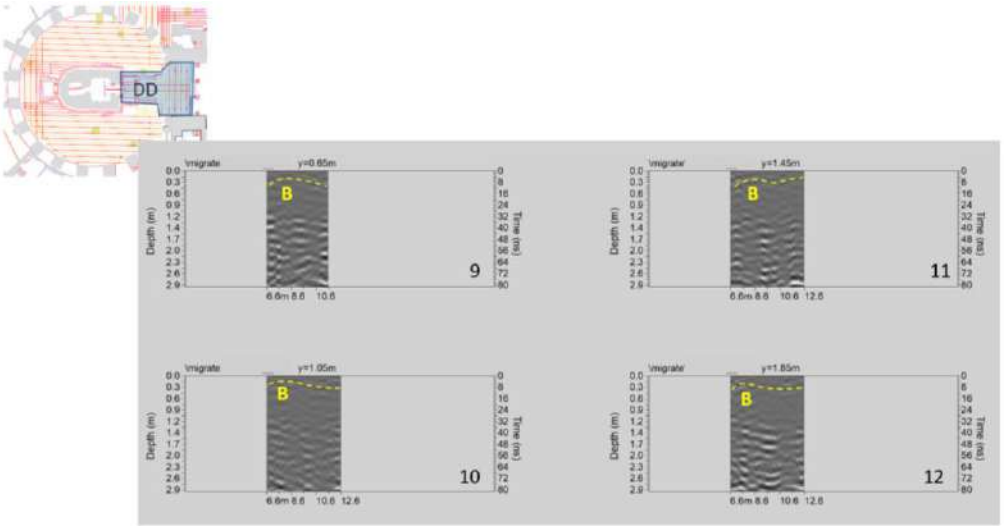

Fig. 18: Area DD: Processed GPR profiles 9,…, 12 (B: bedrock)

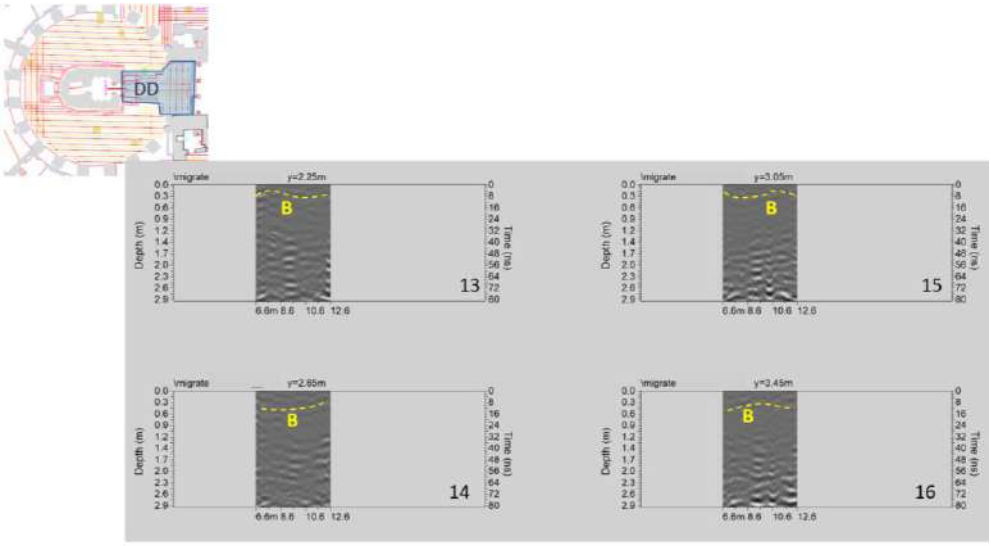

Fig. 19: Area DD: Processed GPR profiles 13,…, 16 (B: bedrock)

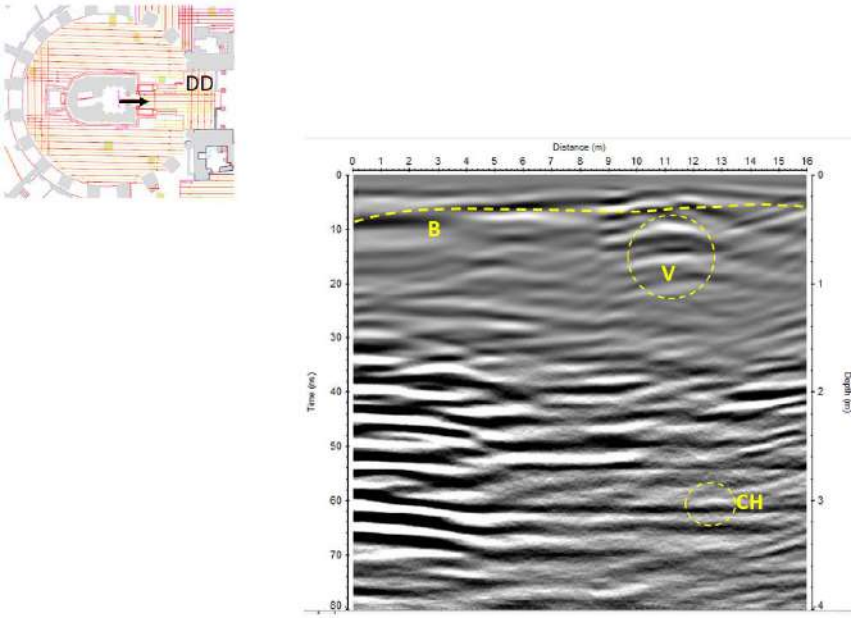

Fig. 20: Area DD: Processed GPR acquired into the "edicola" (B: bedrock; V: void space; CH: void space)

Area EE: The processed GPR profiles acquired in the area EE are shown in Figs. 21 and 22.
The reflection event evidenced by a dashed yellow line (labelled B) is probably related to the bedrock level. Its depth ranges from about 0.2m to 0.8m. The reflection events labelled C are probably associated with a cavity at a depth between 1.7m and 2.2 m. T's reflection events are due to a manhole visible on the living surface.

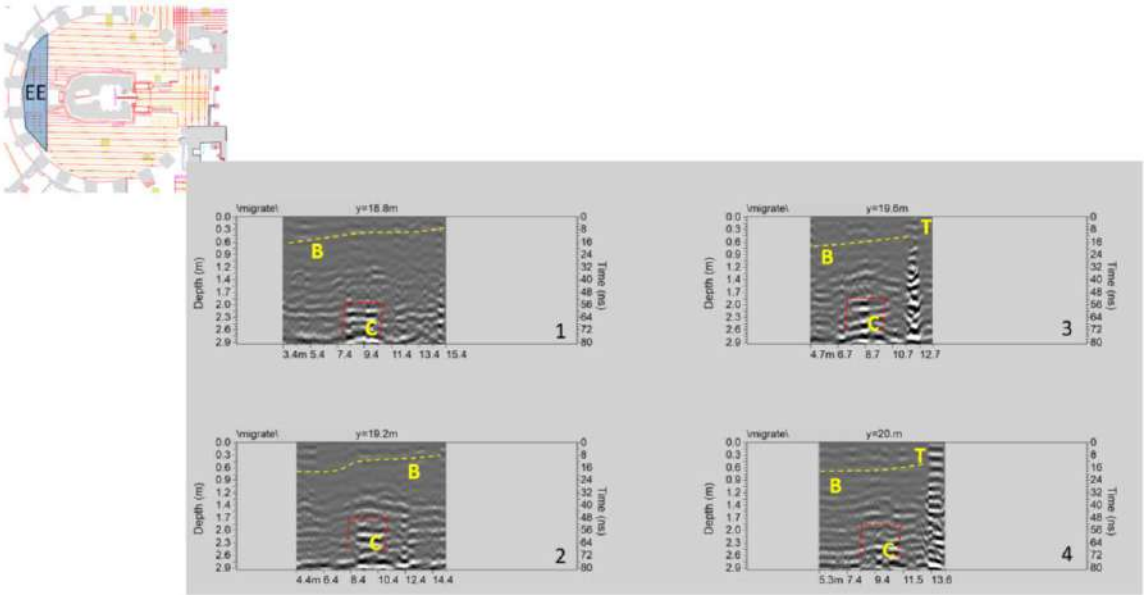

Fig. 21: Area EE: Processed GPR profiles 1,…, 4 (B: bedrock; C: cavity)

Fig. 22: Area EE: Processed GPR profiles 5,…, 9 (B: bedrock; C: cavity)

Area BB+CC+DD+EE: 3D Visualization: A way of obtaining visually useful maps for understanding the plan distribution of reflection amplitudes within specific time intervals is the creation of horizontal time slices. These are maps on which the reflection amplitudes have been projected at a specified time (or depth) with a selected time interval (Conyers, 2006). In a graphic method developed by Goodman et al. (2006), termed 'overlay analysis', the strongest and weakest reflectors at a depth of each slice are assigned specific colours. This technique allows the linkage of structures buried at different depths. This represents an improvement in imaging because subtle features indistinguishable on radargrams can be seen and interpreted more easily. The present report uses the time-slice technique to display the amplitude variations within consecutive time windows of width Δt=5 ns. Time (or depth) slices can be seen as a virtual excavation that places the interest structures at their depth.

The time slices show the amplitude using a range defined by blue as zero and red as the maximum value. Figs. 23, …, 26 shows the depth slices from 0.0 m to 2.9 m in depth.

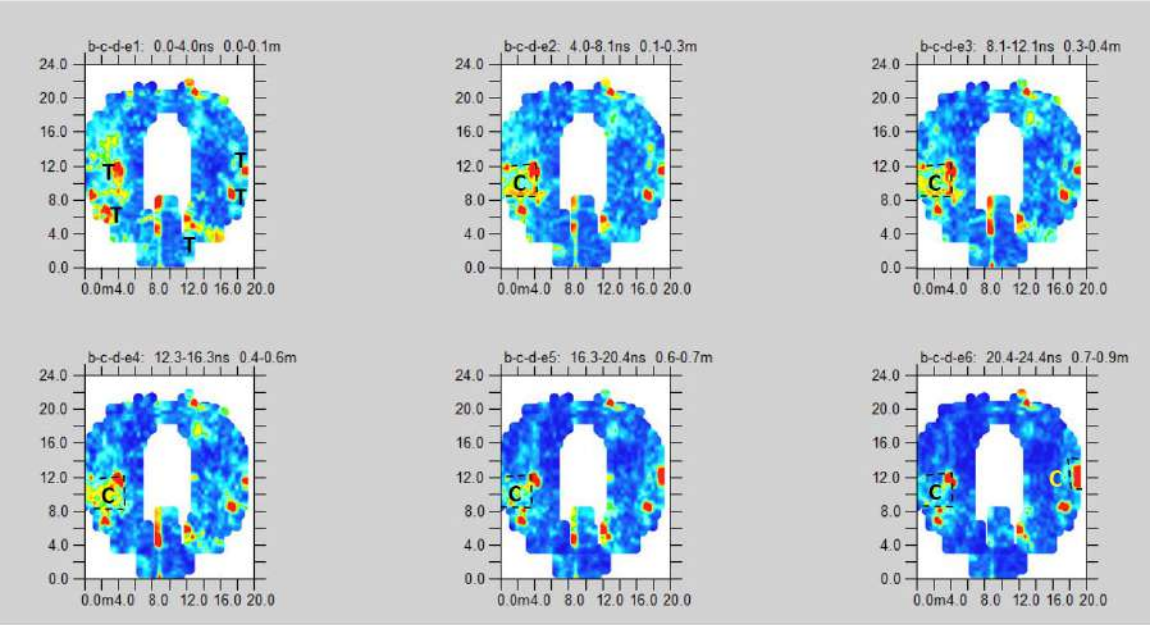

Fig. 23: the whole Area: depth slices 0.0-0.9m deep (T: manhole; C: known cavities)

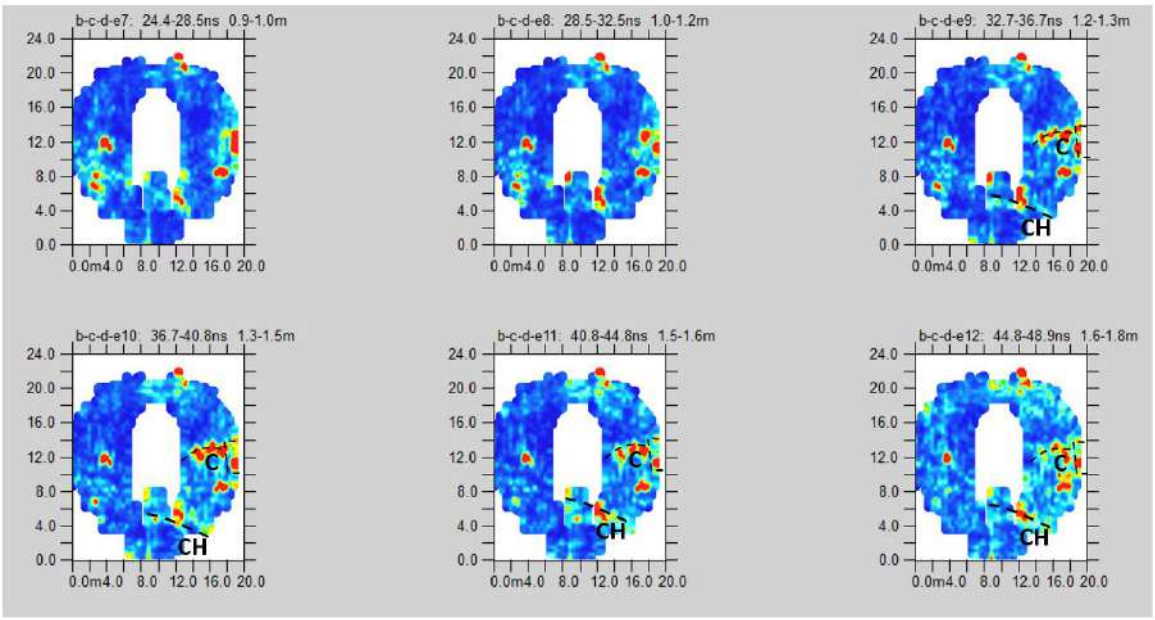

Fig. 24: the whole Area: depth slices 0.9-1.8m depth (CH: Channel; C: known cavities)

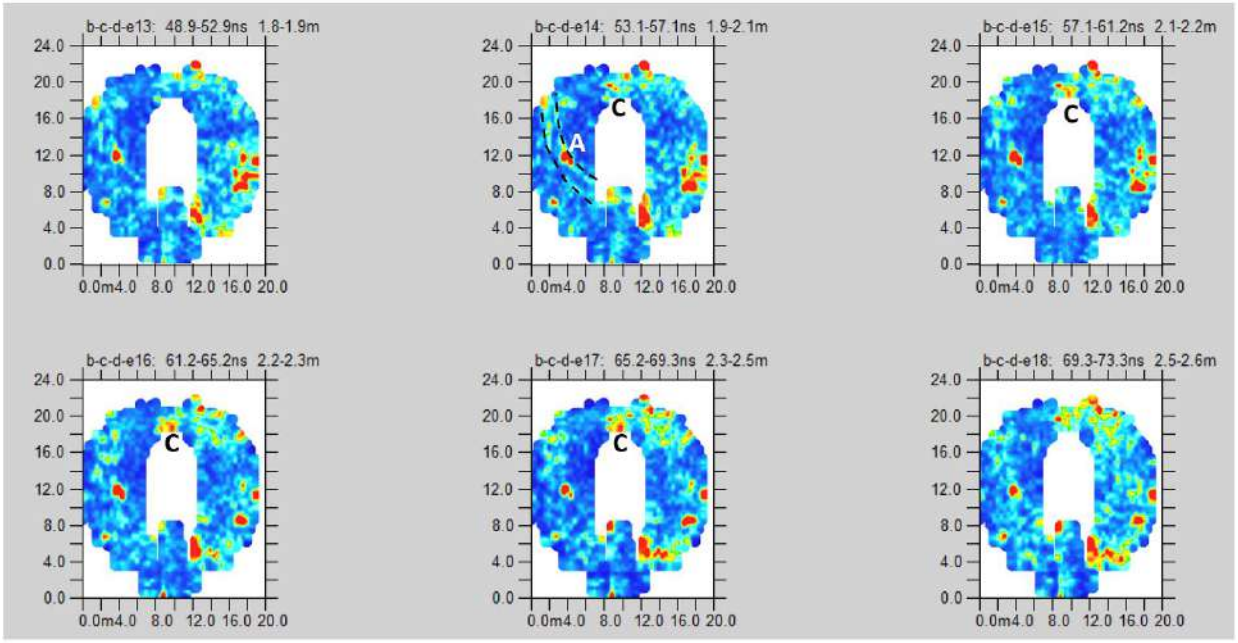

Fig. 25: the whole Area: depth slices 1.8-2.6m depth (A: road traces?; C: cavity)

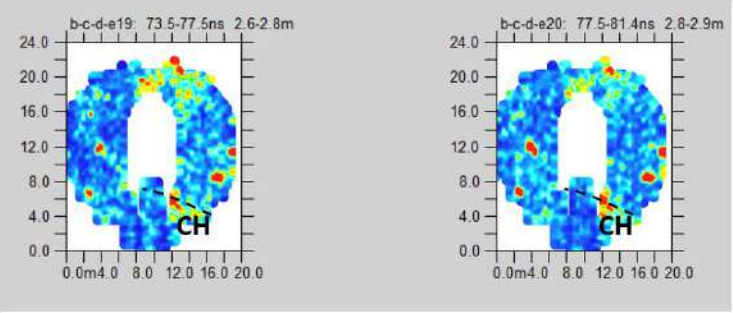

Fig. 26: the whole Area: depth slices 2.6-2.9m depth (CH: channel)

In the slices ranging from 0m to 0.1m depth (Fig. 23), relatively high-amplitude alignments (labelled T) are visible. These correspond to the anomalies labelled T in the 2D radargram. The dashed dark lines highlight a high-amplitude anomaly (labelled C) in the time slices (Fig. 23) ranging from 0.1m to 0.9m depth; the dashed dark lines highlight a high-amplitude anomaly (labelled C). This corresponds to the known cavity. The time slices ranging from 1.2 m to 1.8 m (Fig. 24) depth show other high amplitude alignments (labelled C) related to a known cavity and tunnel.
Moreover, the same depth highlights relatively high-amplitude alignments with the same direction (labelled CH). It could be correlated to the presence of a channel. Slices from 1.9m to 2.5 m depth show two high amplitude anomalies labelled A and C. The first one (A) comprises two parallel lines and could probably be related to road traces. The second (C) could be related to a cavity (natural cavity?). At deeper slices (Fig. 26) is possible to see the high amplitude anomaly labelled CH.

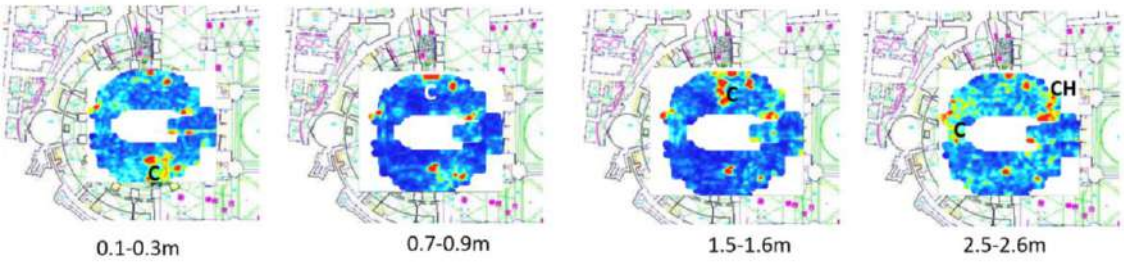

Fig. 27: the whole Area: depth slices overlapped to the planimetry

Fig 27 shows the more significant depth slices overlapped to the planimetry of the church. It is possible to see the position of the high amplitude anomalies C and CH.

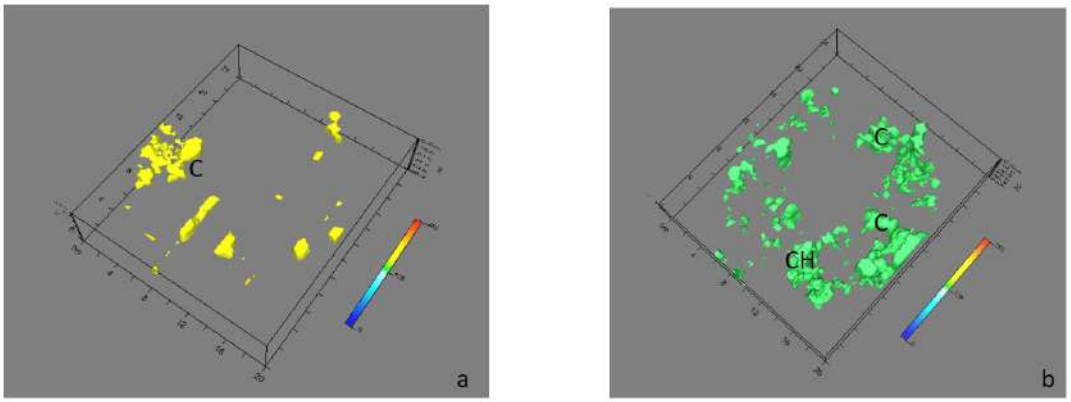

Fig. 28: the whole Area: electromagnetic amplitude isosurfaces: a) 0.0-0.6m depth threshold 60%; b) 0.7-2.9m depth threshold 50%

Moreover, the highest amplitudes were rendered into an isosurface (Conyers and Goodman, 1997; Conyers, 2004, 2012; Leucci, 2019; Leucci, 2020; Giannino and Leucci, 2021). Three-dimensional amplitude isosurface rendering displays amplitudes of equal value in the GPR study volume. Shading is usually used to illuminate these surfaces, giving the appearance of real archaeological structures. In this case, the threshold calibration is a delicate task to obtain valuable results. Fig. 28 shows the isosurfaces amplitude visualization.
Fig. 29 show a virtual excavation at two different levels. Here is possible to see the position of the anomalous zones well.

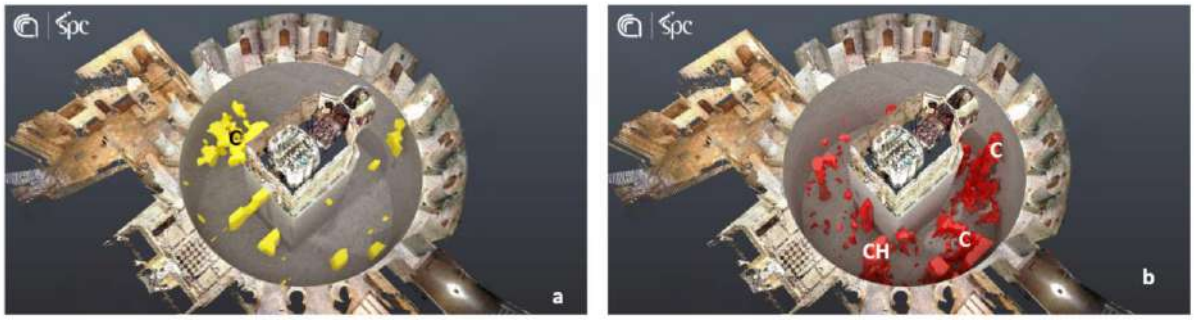

Fig. 29: the whole Area: virtual-excavation: a) 0.6m depth; b) 0.7 m depth

Area RR+GG+FF

In the area, RR+GG+FF has acquired 48 GPR profiles for an extension of 473.46 meters.
The GPR data profiles were processed in 2D using GPR-slice software (GPR-SLICE Software (gpr-survey.com)). As the above describes areas to interpret GPR data, the following processing sequence was applied:

1) Zero-time adjust (static shift), to associate zero-time with zero-depth;
2) Background removal;
3) Frequency filtering, to remove high-frequency noise;
4) Migration, to correct the shape and dimension of reflection events related to the structure present in the subsoil.

AREA FF: The profiles acquired in the area FF are shown in Fig. 30.

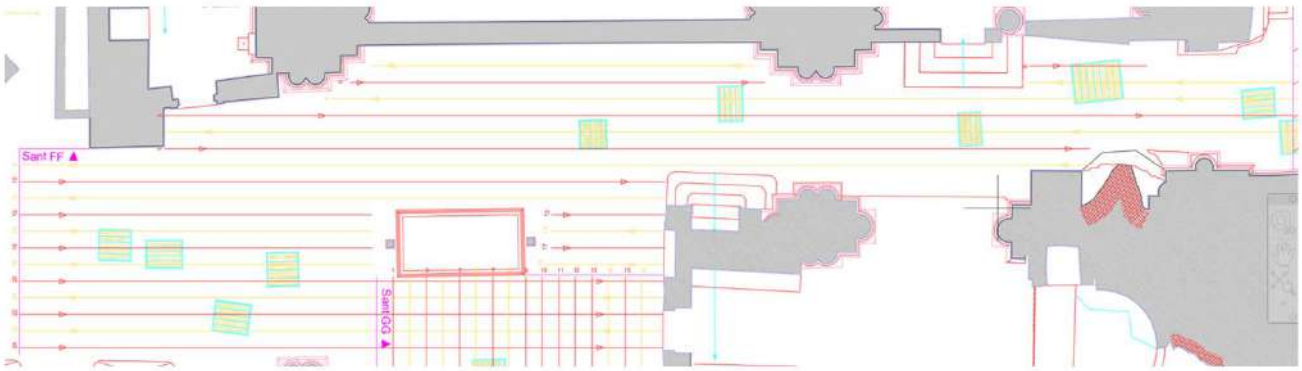

Fig. 30: Area FF: location of GPR profiles

The processed GPR profiles acquired in the area FF are shown in Figs. 31,…, 36.

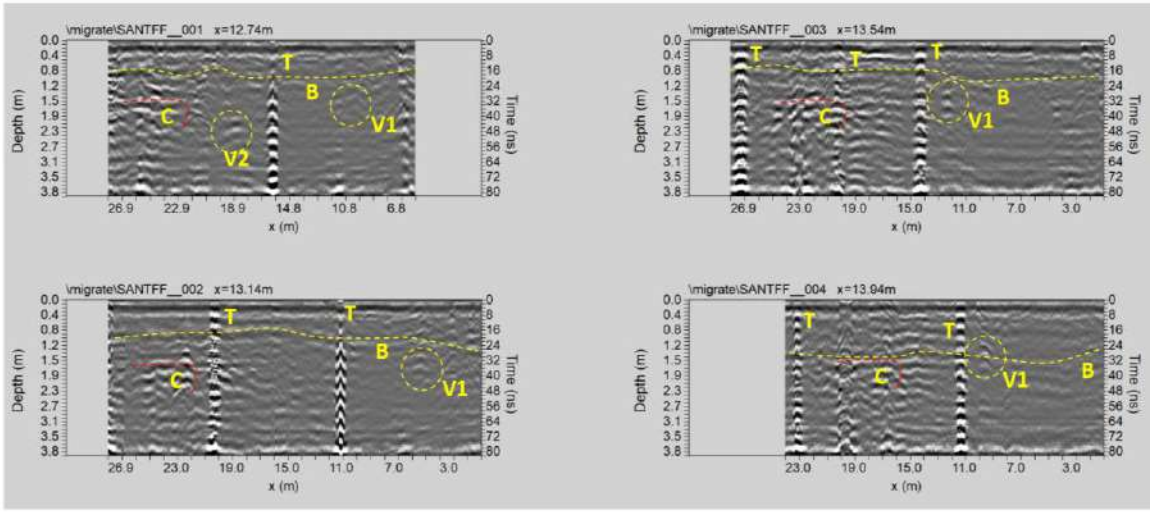

Fig. 31: Area FF: processed GPR profiles 1,.., 4 (B: bedrock; C: cavity; T: manhole; V1 and V2: void spaces)

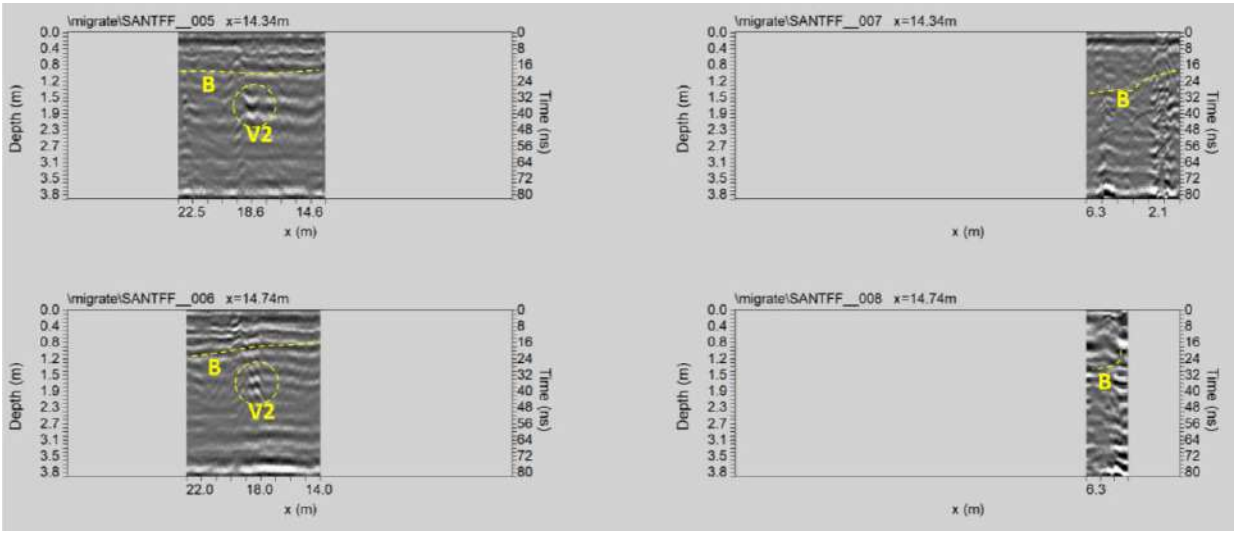

Fig. 32: Area FF: processed GPR profiles 5,.., 8 (B: bedrock; V1 and V2: void spaces)

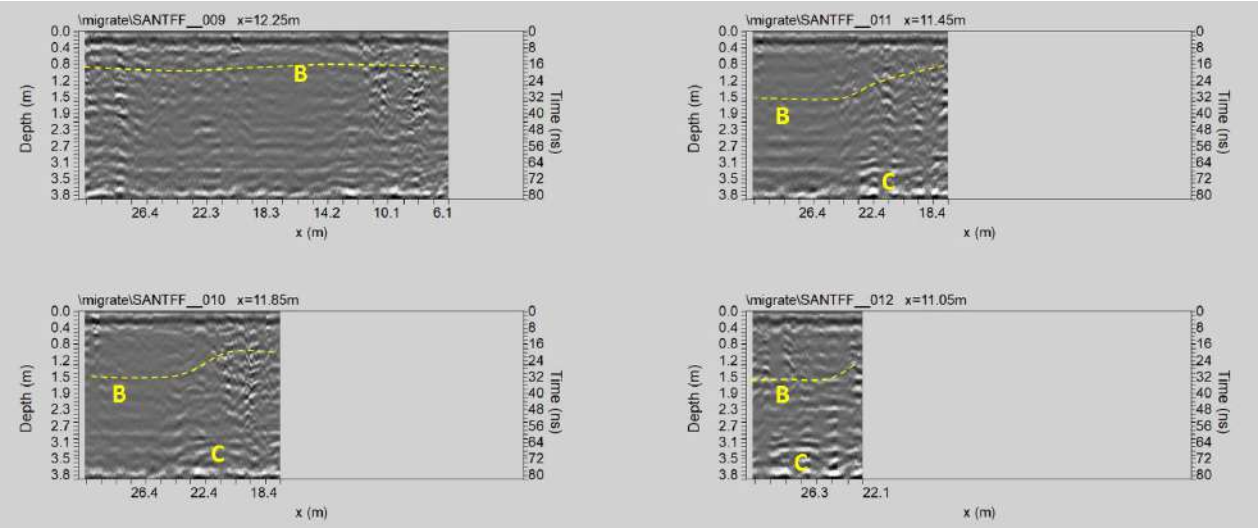

Fig. 33: Area FF: processed GPR profiles 9,.., 12 (B: bedrock; C: cavity)

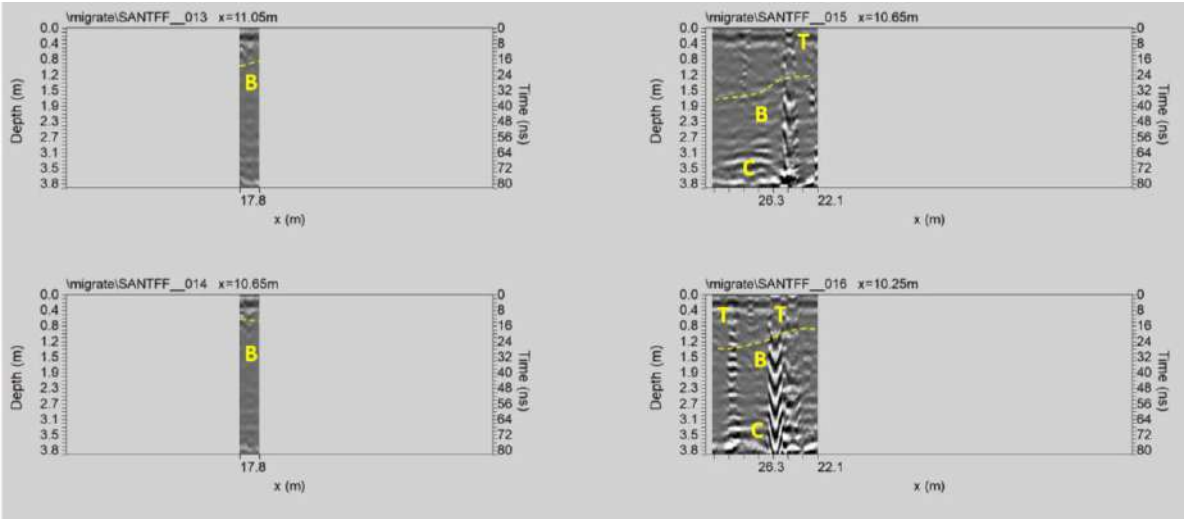

Fig. 34: Area FF: processed GPR profiles 13,.., 16 (B: bedrock; C: cavity; T: manhole)

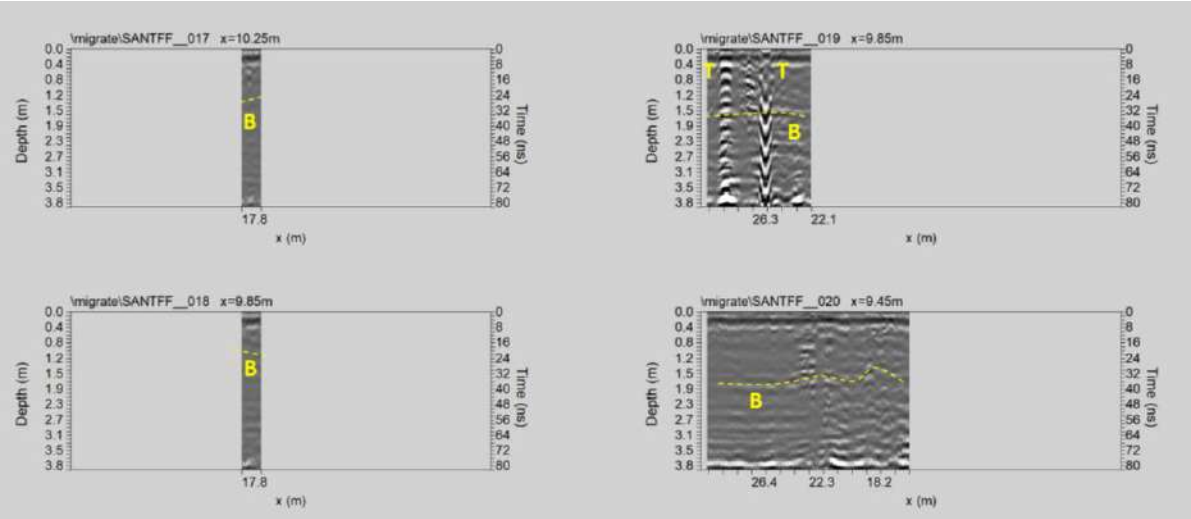

Fig. 35: Area FF: processed GPR profiles 17,.., 20 (B: bedrock; T: manhole)

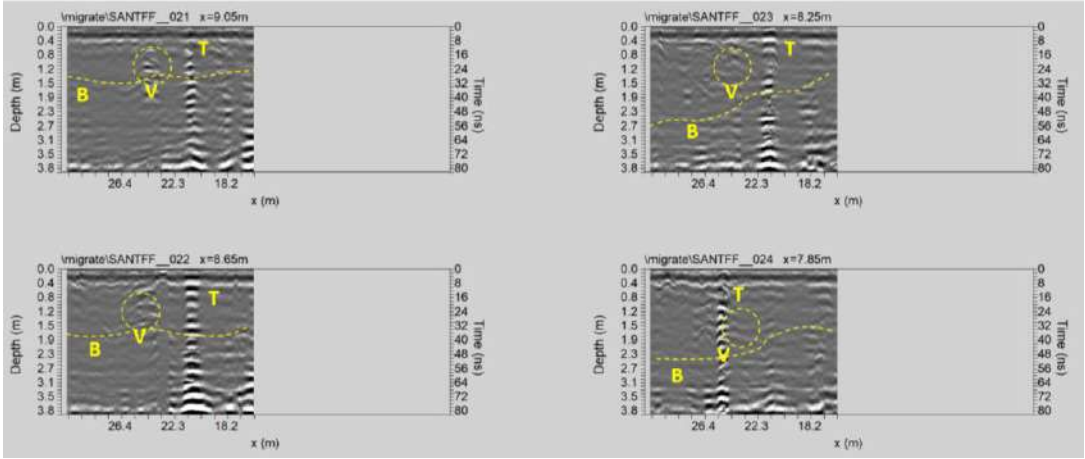

Fig. 36: Area FF: processed GPR profiles 21,.., 24 (B: bedrock; T: manhole; V: void space)

The reflection event evidenced by a dashed yellow line (labelled B) is probably related to the bedrock. The depth of bedrock ranges from about 0.8m to 2.3m.
The T's reflection events are related to the manholes visible on the surface.
The reflection events labelled C at a depth of about 3.0-3.5m are related to a cavity.
Some reflection events labelled V, V1 and V2 at depth 1.2m, 1.5m and 1.0 m, respectively, are probably related to void spaces.

AREA GG+RR: The profiles acquired in the area GG+RR are shown in Fig. 37.

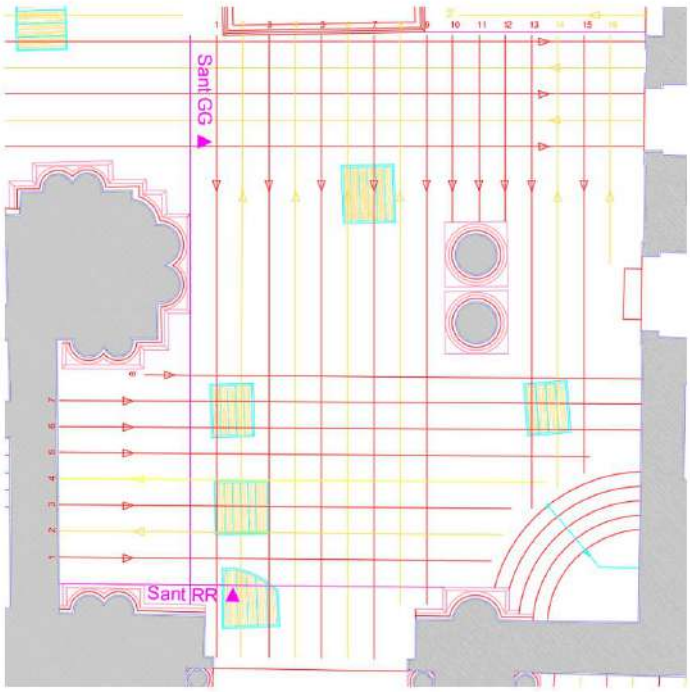

Fig. 37: Area GG+RR: location of GPR profiles

The processed GPR profiles acquired in the area GG+RR are shown in Figs. 38,…, 43.
Here it is possible to highlight the reflection event indicated by a dashed yellow line (labelled B) is probably related to the bedrock. The depth of bedrock ranges from about 0.8m to 2.3m.
The reflection events labelled T is related to the manholes visible on the surface.
The reflection events labelled C at a depth of about 0.8-1.1m are related to a cavity.
The reflection event labelled V at depth 0.8-1.0 m is probably related to void spaces.

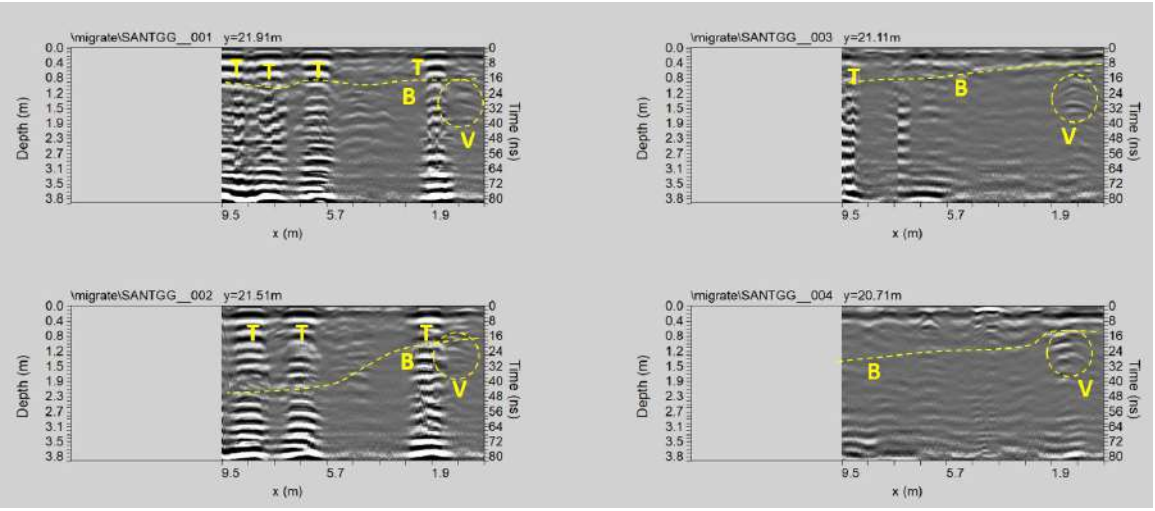

Fig. 38: Area GG: processed GPR profiles 1,.., 4 (B: bedrock; T: manhole; V: void space)

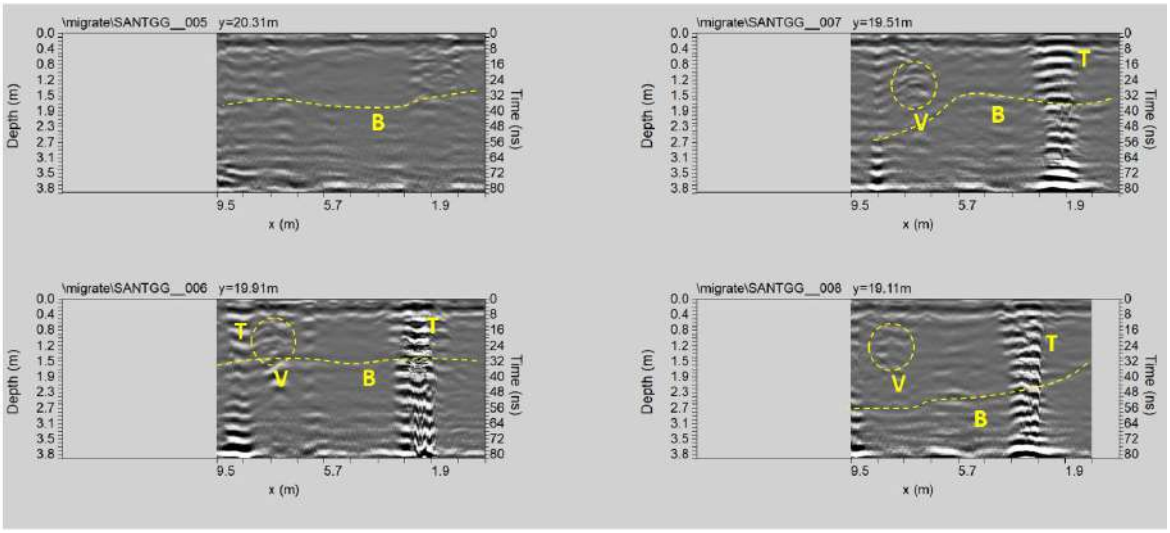

Fig. 39: Area GG: processed GPR profiles 5,.., 8 (B: bedrock; T: manhole; V: void space)

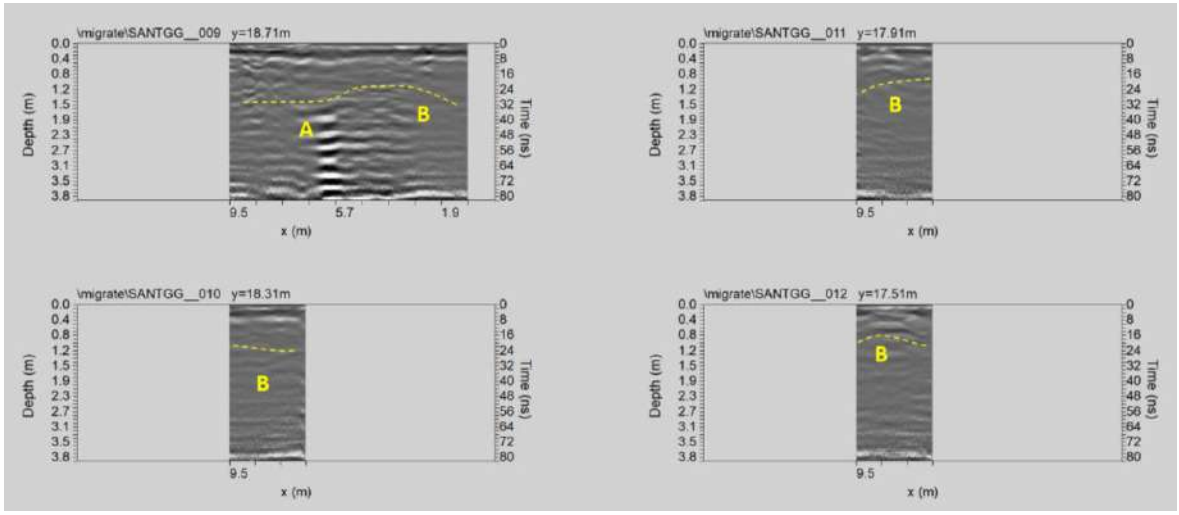

Fig. 40: Area GG: processed GPR profiles 9,.., 12 (B: bedrock; A: archaeological structure)

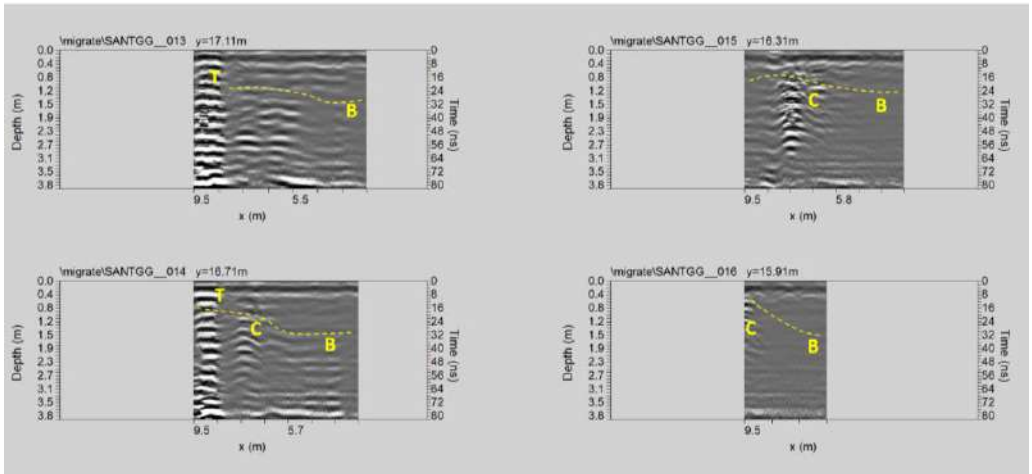

Fig. 41: Area GG: processed GPR profiles 13,.., 16 (B: bedrock; C: cavity; T: manhole)

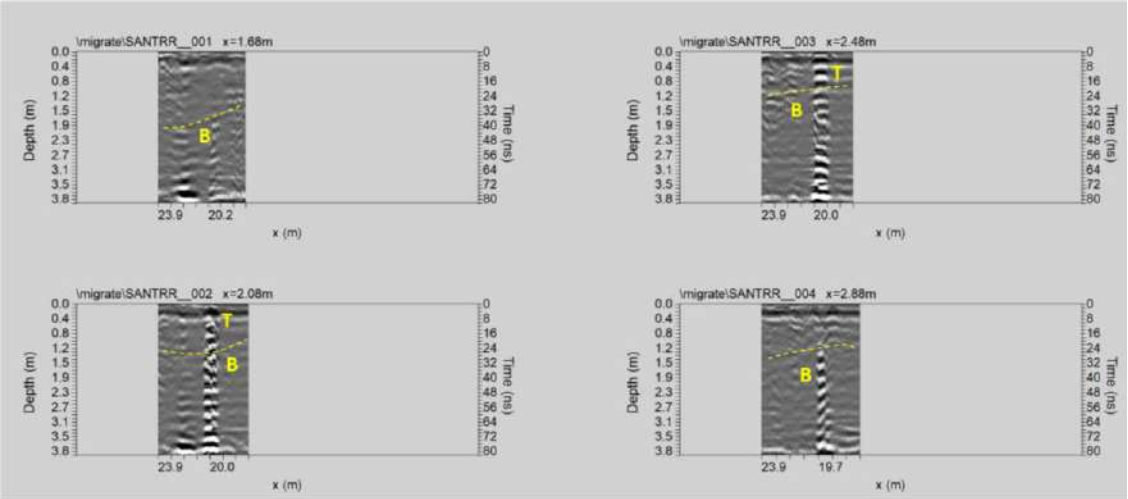

Fig. 42: Area RR: processed GPR profiles 1,.., 4 (B: bedrock; T: manhole)

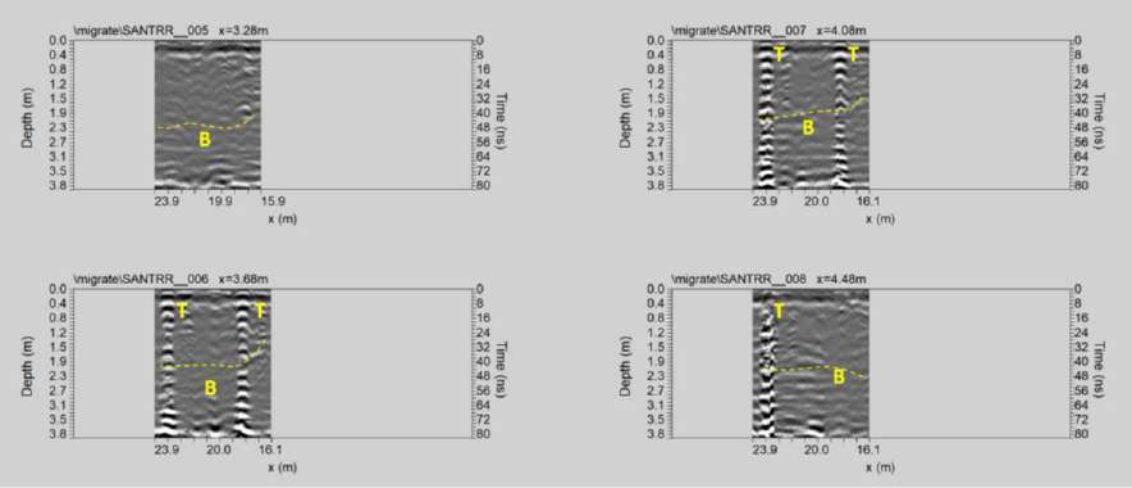

Fig. 43: Area RR: processed GPR profiles 5,.., 8 (B: bedrock; T: manhole)

Area RR+GG+FF: 3D visualization: In this case, the time-slice technique has been used to display the amplitude variations within consecutive time windows of width Δt=5 ns.
Figs. 44, …, 47 shows the depth slices from 0.0 m to 3.9 m in depth.

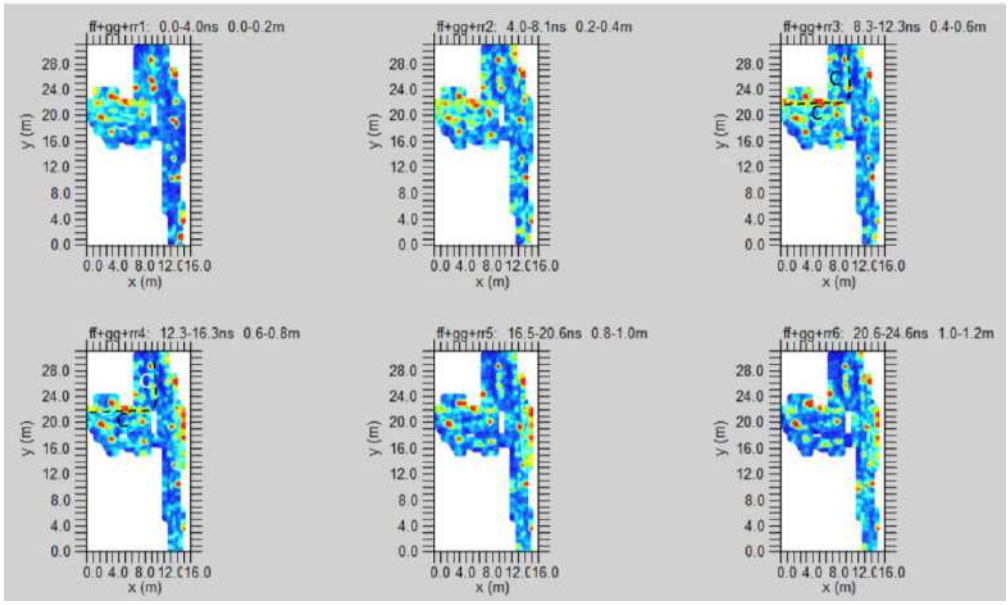

Fig. 44: the whole Area: depth slices 0.0-1.2m depth (C: cavities)

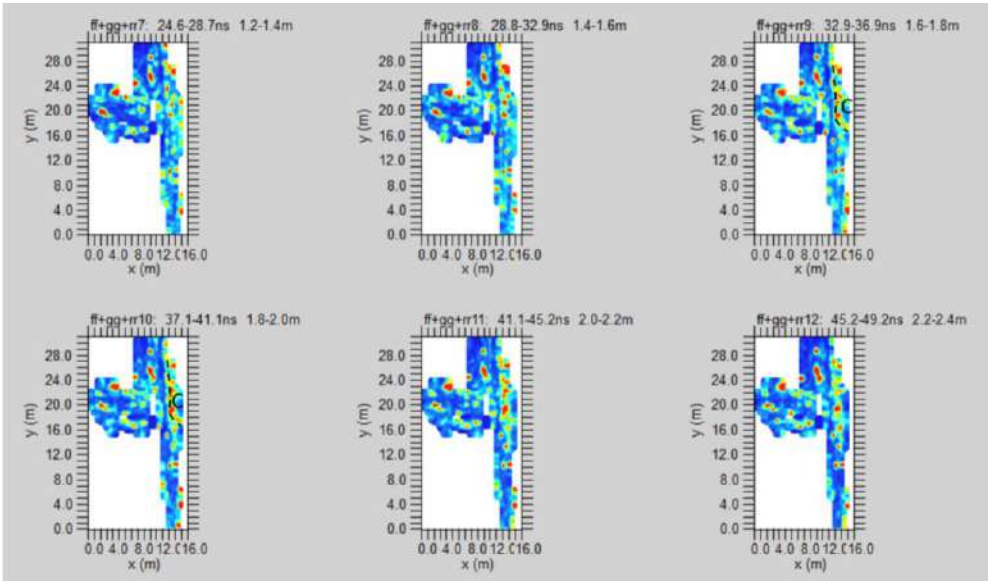

Fig. 45: the whole Area: depth slices 1.4-2.4m depth (C: cavities)

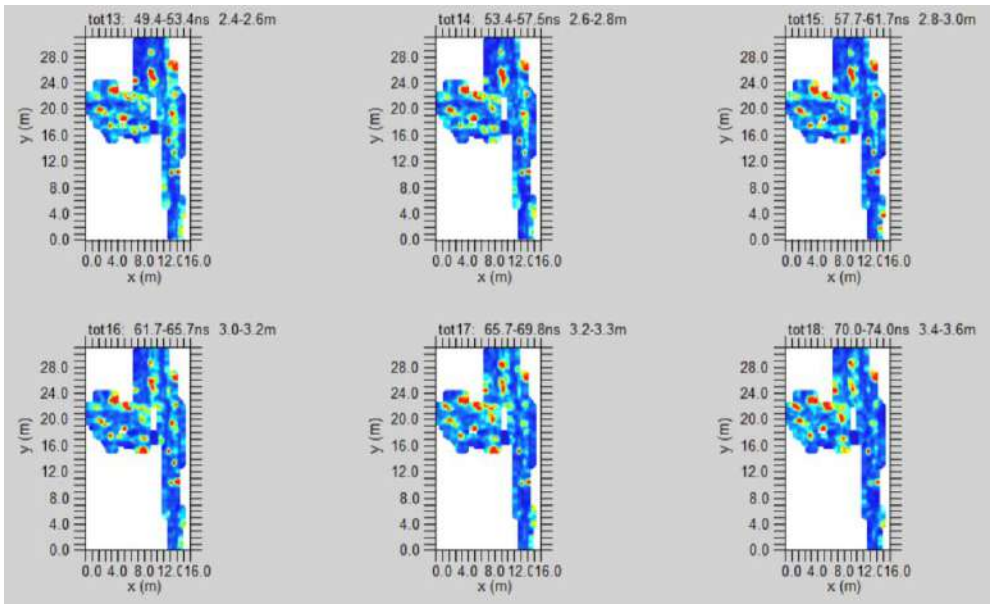

Fig. 46: the whole Area: depth slices 2.4-3.6m depth (A: road traces?; C: cavity)

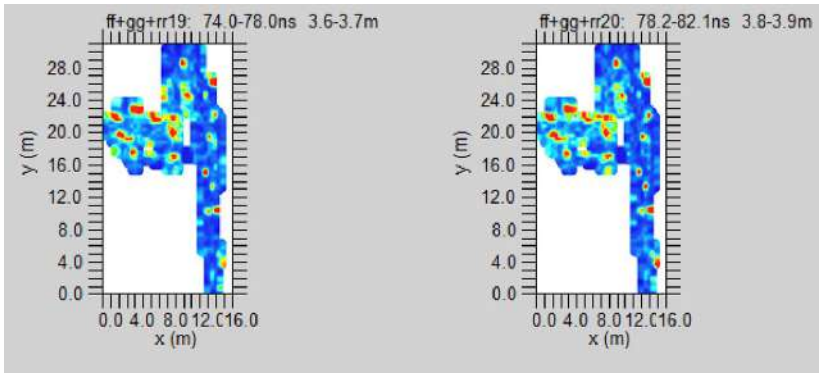

Fig. 47: the whole Area: depth slices 3.6-3.9m depth

In the slices ranging from 0.4m to 0.8m depth (Fig. 44), relatively high-amplitude alignments (labelled C) are visible. These could be related to a cavity (probable channel). The dashed dark lines highlight a high-amplitude anomaly (labelled C) in the time slices (Fig. 45) ranging from 1.6m to 2.0m depth; the dashed dark lines highlight a high-amplitude anomaly (labelled C). This corresponds to a cavity (probably channel). The deeper time slices show other high amplitude alignments. They could be correlated to old structures (archaeological interest).

Fig. 48: the whole Area: depth slices overlapped to the planimetry

Fig 48 shows the more significant depth slices overlapped to the planimetry of the church. It is possible to see the position of the high amplitude anomalies C.

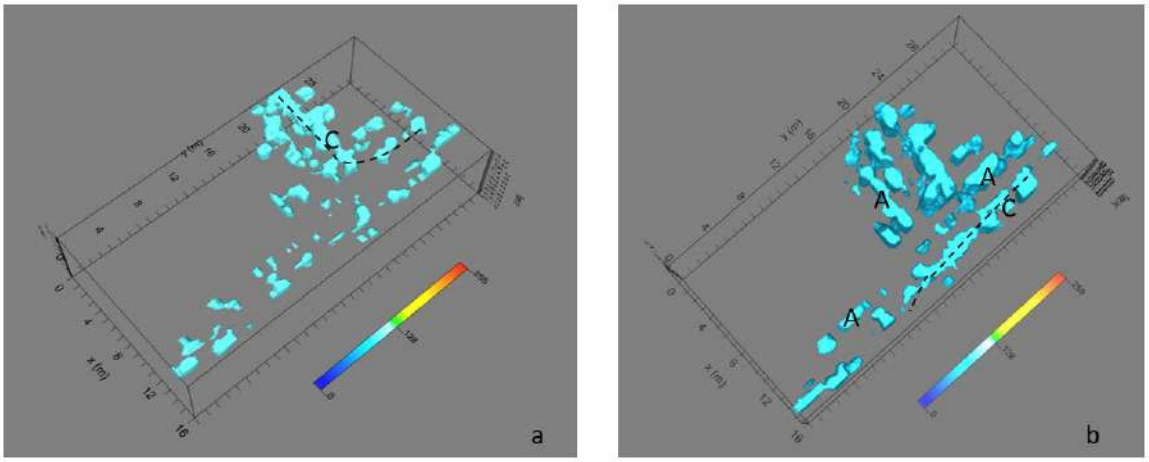

Fig. 49: the whole Area: electromagnetic amplitude isosurfaces: a) 0.0-0.8m depth threshold 40%; b) 1.6-1.8m depth threshold 30%

Fig. 49 show the isosurface visualization, and Fig. 50 offer a virtual excavation at two different levels. Here is possible to see the position of the anomalous zones well. In this case, the anomalies labelled A are well evidenced. They are probably related to structures of archaeological interest.

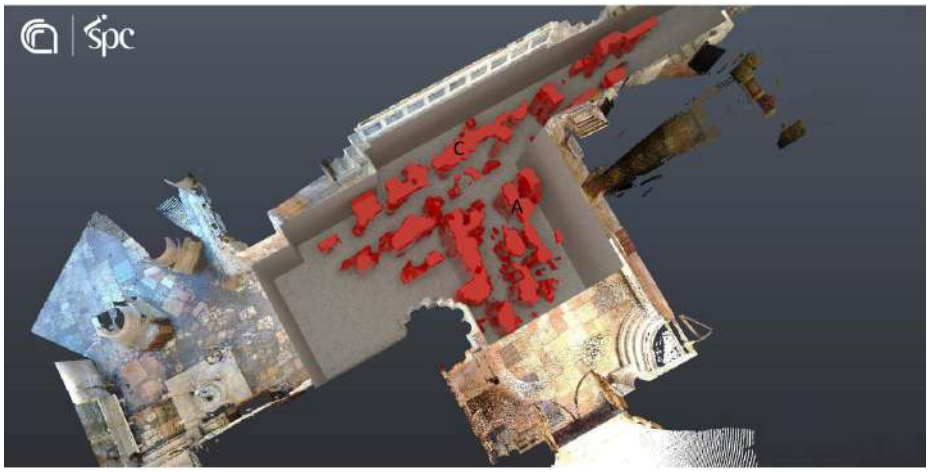

Fig. 50: the whole Area: virtual-excavation: 1.6-1.8m depth

Area AA+HH+II+LL+NN

In the area, AA+HH+II+LL+NN have acquired 61 GPR profiles for an extension of 543.47 meters.
The GPR data profiles were processed in 2D using GPR-slice software (GPR-SLICE Software (gpr-survey.com)). As the above describes areas to interpret GPR data, the following processing sequence was applied:

1) Zero-time adjust (static shift), to associate zero-time with zero-depth;
2) Background removal;
3) Frequency filtering, to remove high-frequency noise;
4) Migration, to correct the shape and dimension of reflection events related to the structure present in the subsoil.

AREA HH: The profiles acquired in the area HH are shown in Fig. 51.

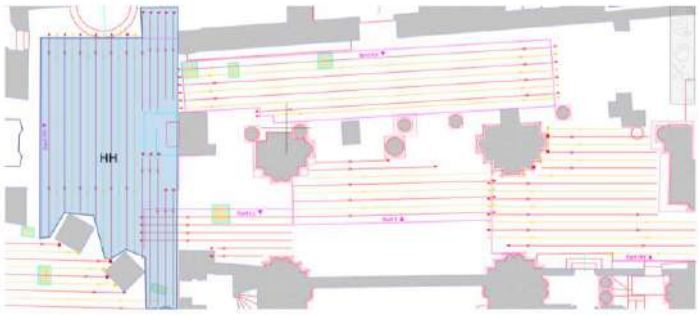

Fig. 51: Area HH: location of GPR profiles

The processed GPR profiles acquired in the area HH are shown in Figs. 52,…, 57.

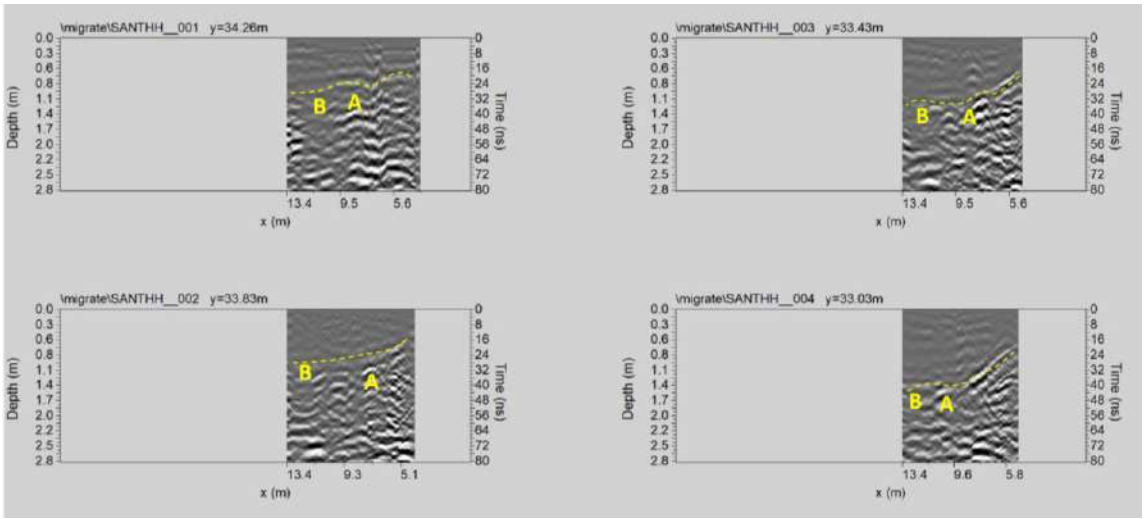

Fig. 52: Area HH: processed GPR profiles 1,.., 4 (B: bedrock; A: archaeological structure)

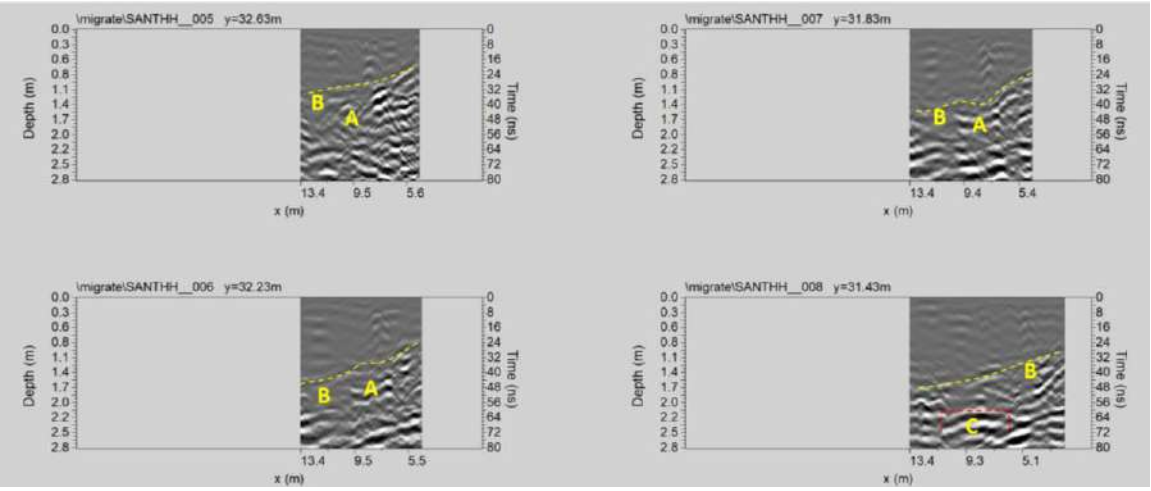

Fig. 53: Area HH: processed GPR profiles 5,.., 8 (B: bedrock; C: cavity; A: archaeological structure)

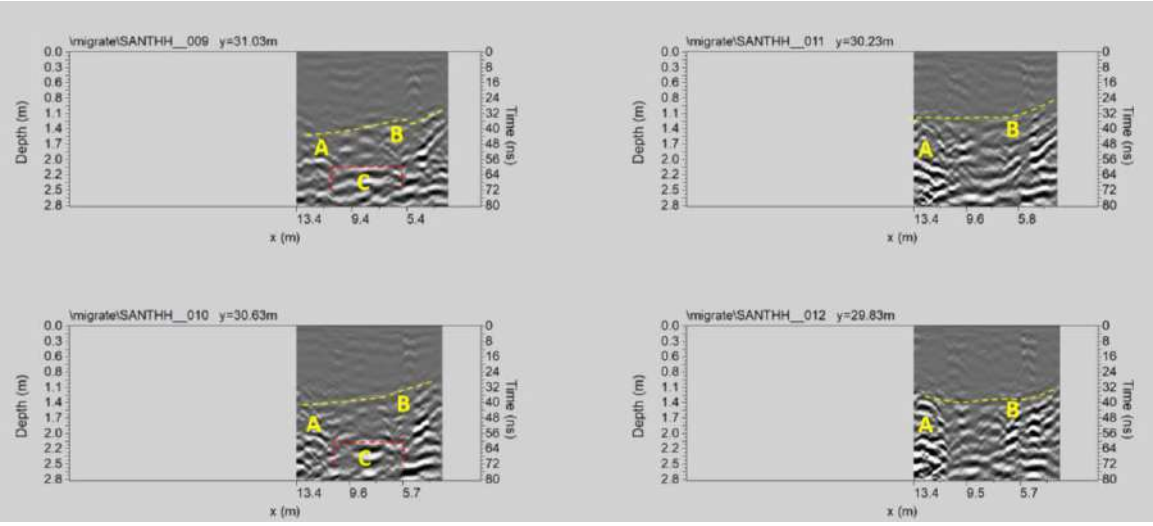

Fig. 54: Area HH: processed GPR profiles 9,.., 12 (B: bedrock; C: cavity; A: archaeological structure)

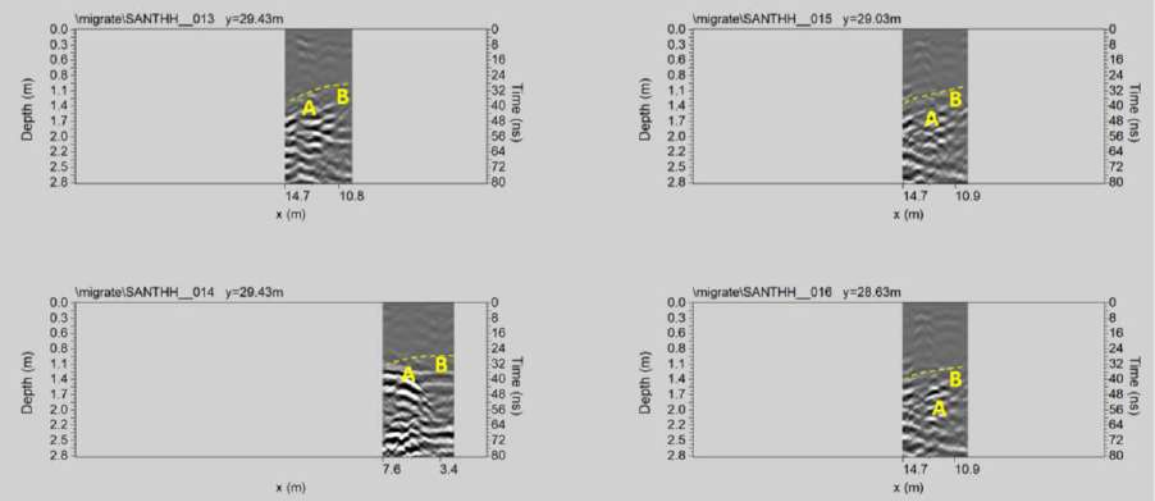

Fig. 55: Area HH: processed GPR profiles 13,.., 16 (B: bedrock; A: archaeological structure)

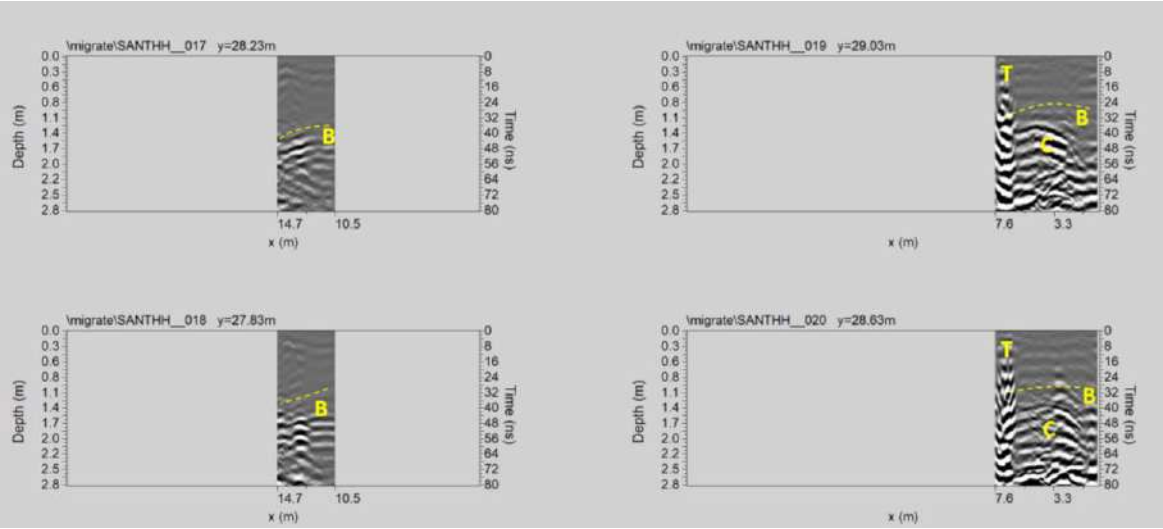

Fig. 56: Area HH: processed GPR profiles 17,.., 20 (B: bedrock; T: manhole; C: cavity)

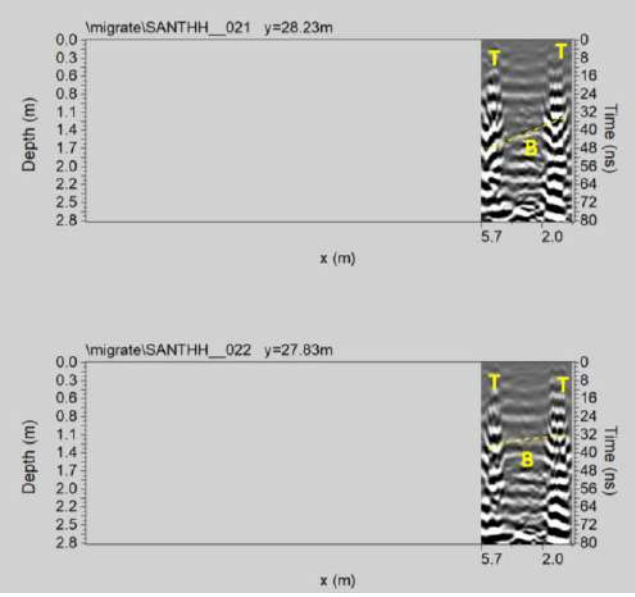

Fig. 57: Area HH: processed GPR profiles 21 and 22 (B: bedrock; T: manhole)

The reflection event evidenced by a dashed yellow line (labelled B) is probably related to the bedrock. The depth of bedrock ranges from about 0.7m to 1.7m.
The reflection events labelled T is related to the manholes visible on the surface.
The reflection events labelled C (Figs. 53 and 54) at a depth of about 2.0-2.4m are related to a cavity.
The reflection events labelled C (Fig. 56) at a depth of about 1.2-1.4m are connected to a cavity.
Some reflection events labelled A at a depth between 1.1m and 1.4m are probably related to structures of archaeological interest (probable walls).

AREA AA: The profiles acquired in the area AA are shown in Fig. 58.

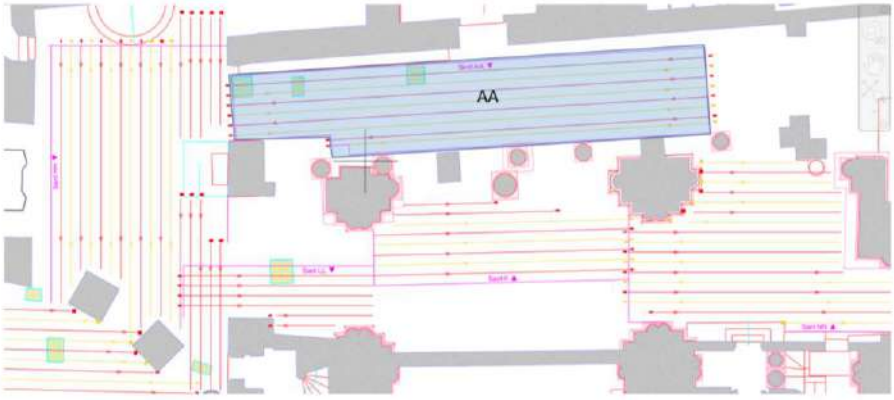

Fig. 58: Area AA: location of GPR profiles

The processed GPR profiles acquired in the area AA are shown in Figs. 59 and 60.
Here it is possible to highlight the reflection event indicated by a dashed yellow line (labelled B) is probably related to the bedrock. The depth of bedrock ranges from about 0.5m to 1.4m.
The reflection events labelled T is related to the manholes visible on the surface.
The reflection events labelled C at a depth of about 1.1-1.4m are related to a cavity.
The reflection event labelled V at depth 0.8-1.0 m is probably related to void spaces. Some reflection events marked A at a depth between 0.7m and 1.0m are likely associated with structures of archaeological interest (probable walls).

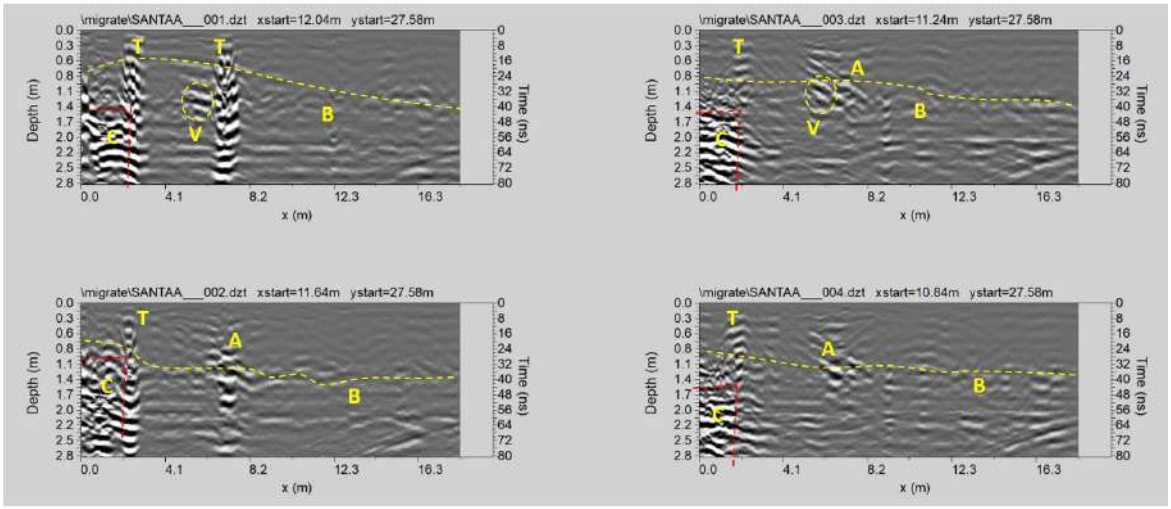

Fig. 59: Area AA: processed GPR profiles 1,.., 4 (B: bedrock; T: manhole; V: void space; C: cavity; A: archaeological structure)

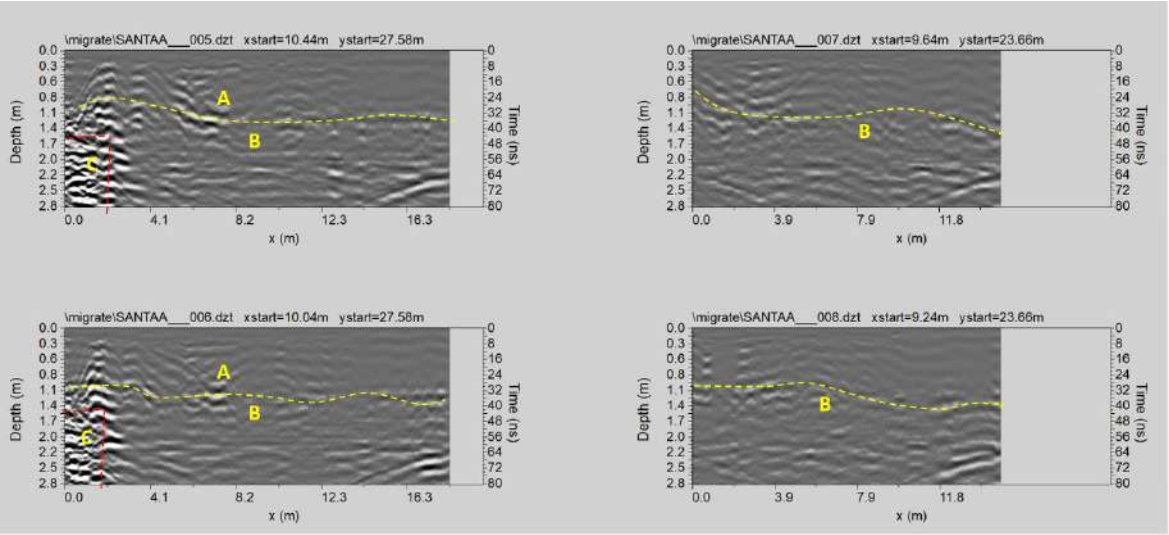

Fig. 60: Area AA: processed GPR profiles 5,.., 8 (B: bedrock; C: cavity; A: archaeological structure)

AREA II: The profiles acquired in area II are shown in Fig. 61.

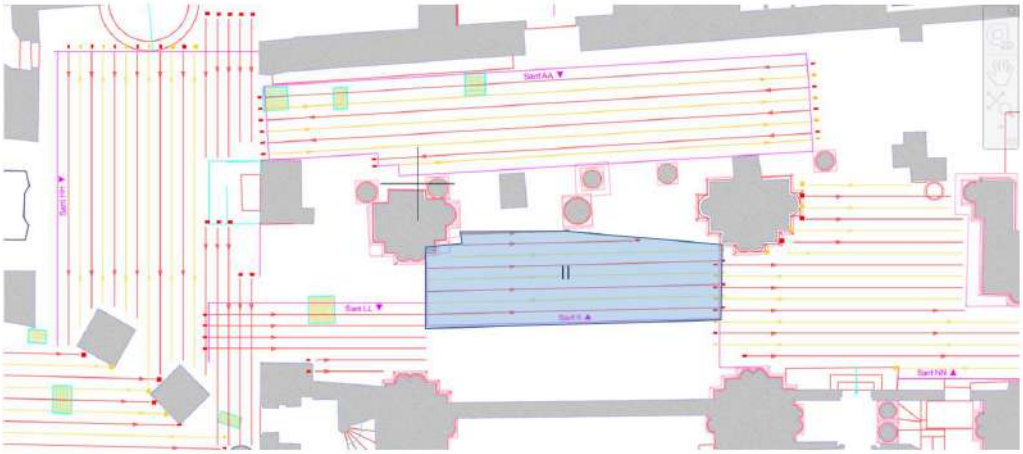

Fig. 61: Area II: location of GPR profiles

The processed GPR profiles acquired in area II are shown in Figs. 62 and 63.
Here it is possible to highlight the reflection event indicated by a dashed yellow line (labelled B) is probably related to the bedrock. The depth of bedrock ranges from about 0.8m to 2.0m.
The reflection event labelled V at depth 1.6-1.7 m is probably related to void spaces. Some reflection events marked A at a depth between 0.9m and 1.1m are probably associated with structures of archaeological interest (probable walls).

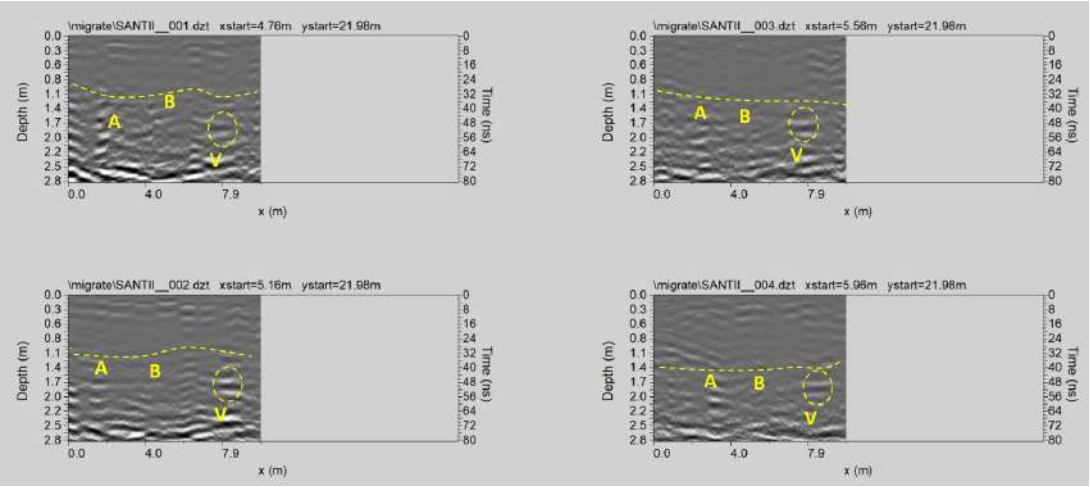

Fig. 62: Area II: processed GPR profiles 1,.., 4 (B: bedrock; V: void space; A: archaeological structure)

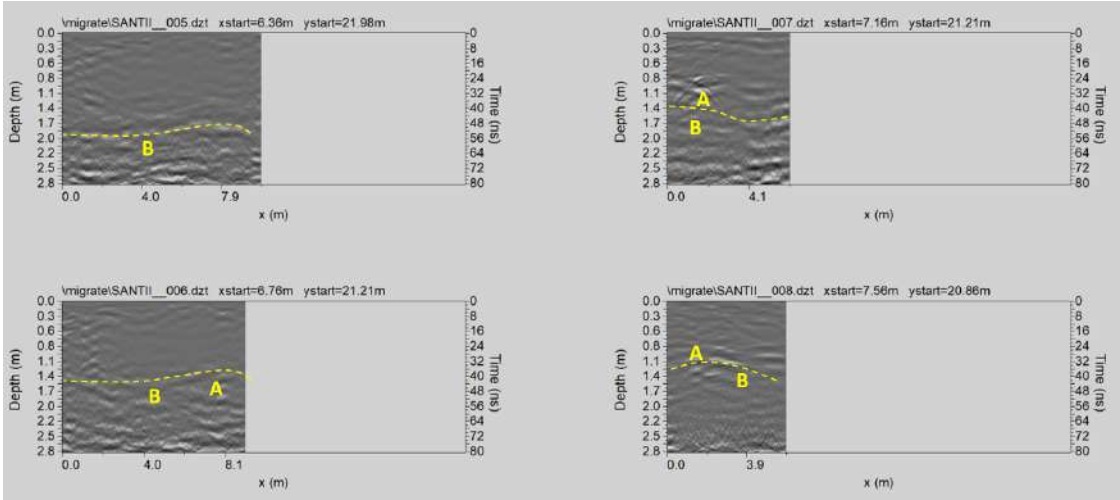

Fig. 63: Area II: processed GPR profiles 5,.., 8 (B: bedrock; A: archaeological structure)

AREA LL: The profiles acquired in the area LL are shown in Fig. 64.

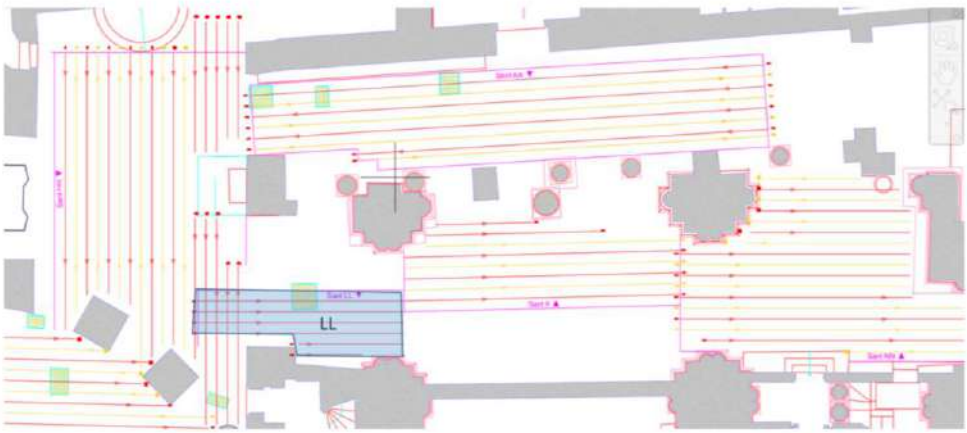

Fig. 64: Area LL: location of GPR profiles

The processed GPR profiles acquired in area LL are shown in Figs. 65 and 66.
The reflection event indicated by a dashed yellow line (labelled B) is probably related to the bedrock.
The depth of bedrock ranges from about 0.9m to 1.4m.
The reflection events labelled T is related to the manholes visible on the surface.

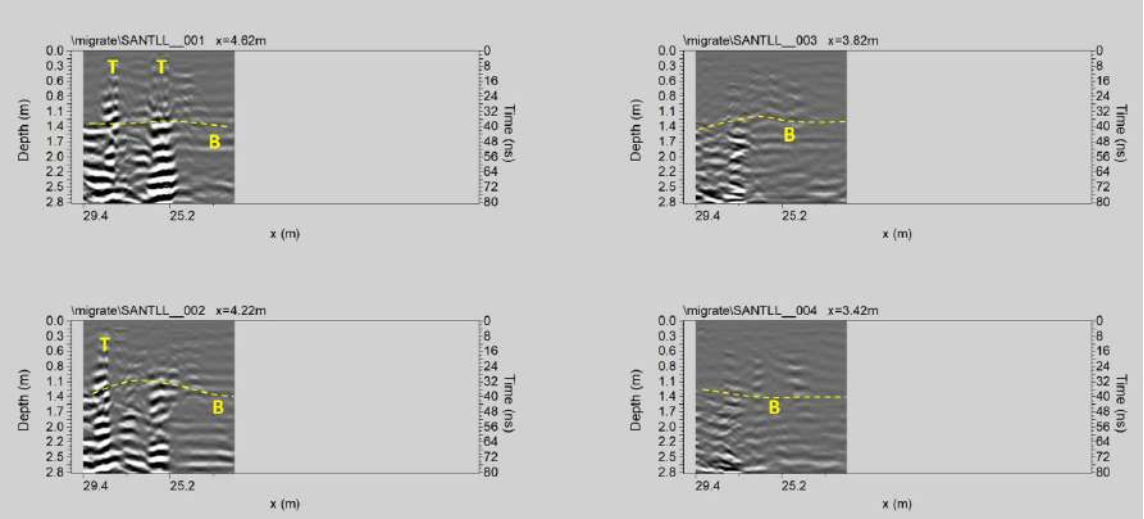

Fig. 65: Area LL: processed GPR profiles 1,.., 4 (B: bedrock; T: manhole)

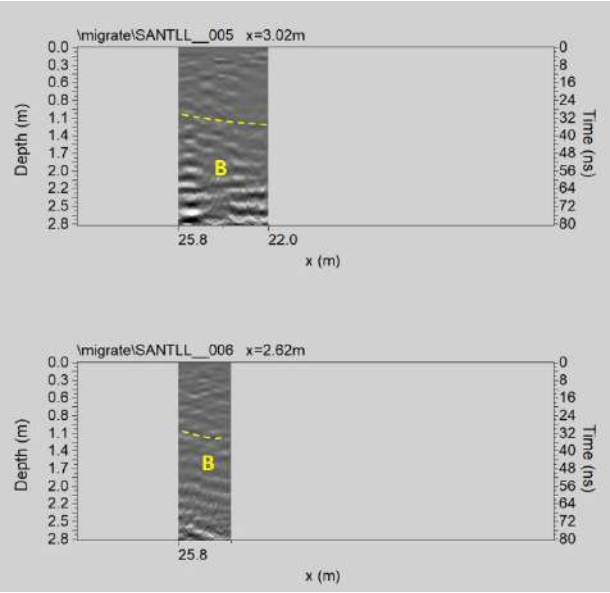

Fig. 66: Area LL: processed GPR profiles 5 and 6 (B: bedrock)

AREA NN: The profiles acquired in the area NN are shown in Fig. 67.

Fig. 67: Area NN: location of GPR profiles

The processed GPR profiles acquired in the area NN are shown in Figs. 68,…, 71.
The reflection event indicated by a dashed yellow line (labelled B) is probably related to the bedrock.
The depth of bedrock ranges from about 0.8m to 1.7m.
The reflection event labelled D at a depth between 0.6m, and 0.8m could be related to a structure.

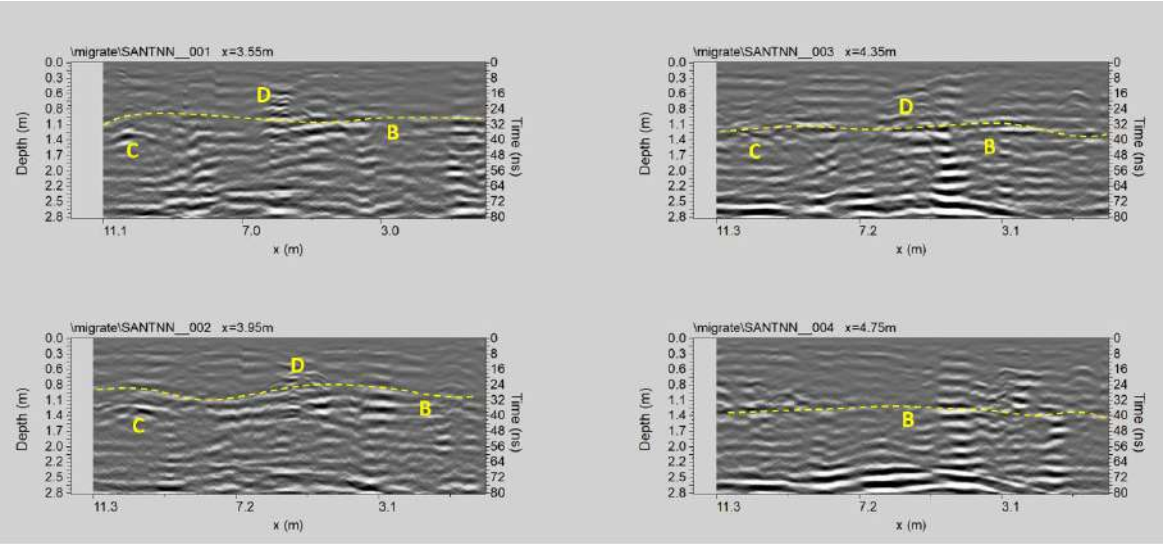

Fig. 68: Area NN: processed GPR profiles 1,…, 4 (B: bedrock; C: cavity; D: structure)

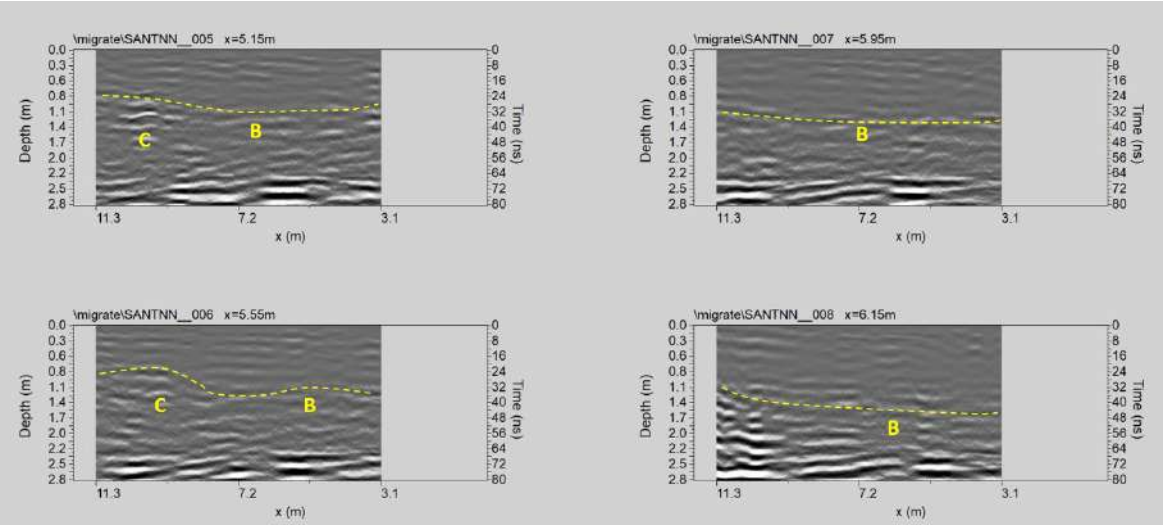

Fig. 69: Area NN: processed GPR profiles 5,…, 8 (B: bedrock; C: cavity)

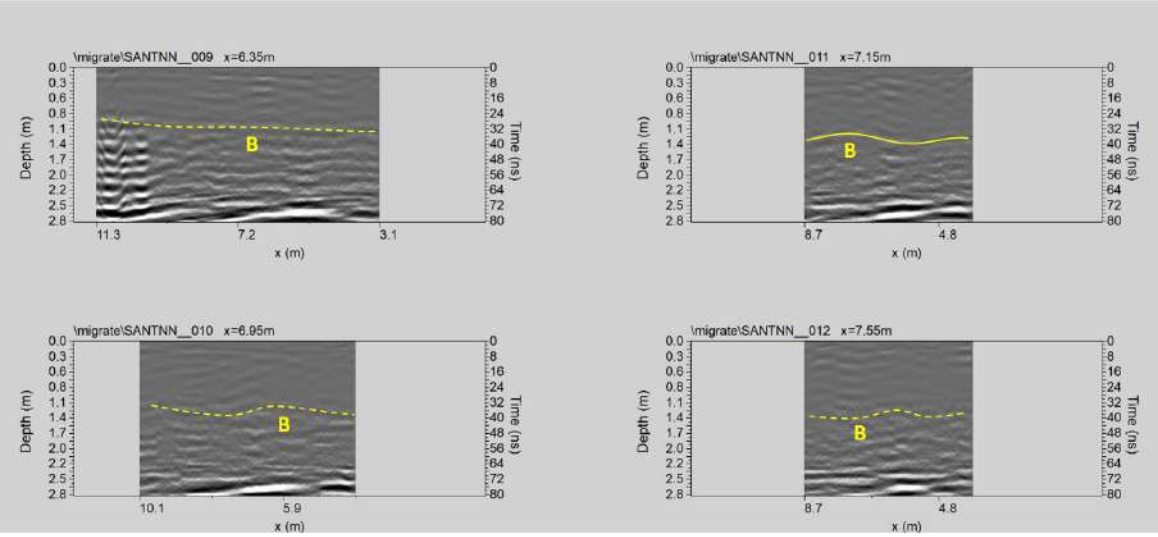

Fig. 70: Area NN: processed GPR profiles 9,…, 12 (B: bedrock)

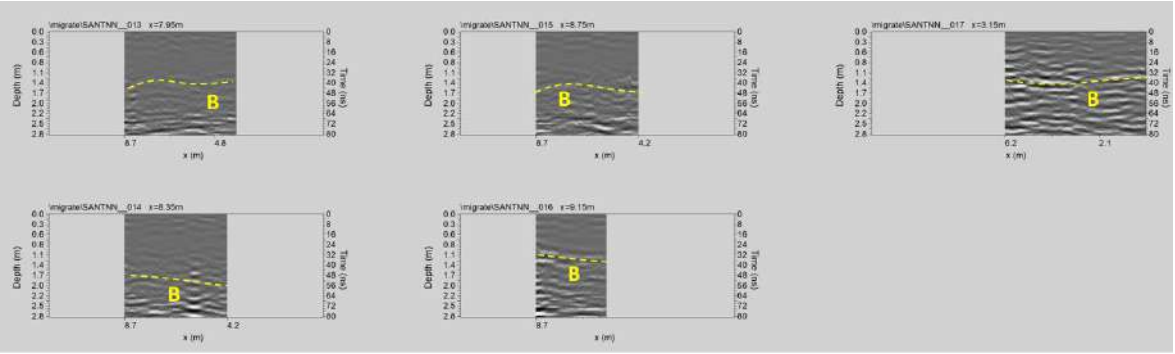

Fig. 71: Area NN: processed GPR profiles 13,…, 17 (B: bedrock)

Area AA+HH+II+LL+NN: 3D visualization: In this case, the time-slice technique has been used to display the amplitude variations within consecutive time windows of width Δt=5 ns.
Figs. 72, …, 75 shows the depth slices from 0.0 m to 2.8 m in depth.

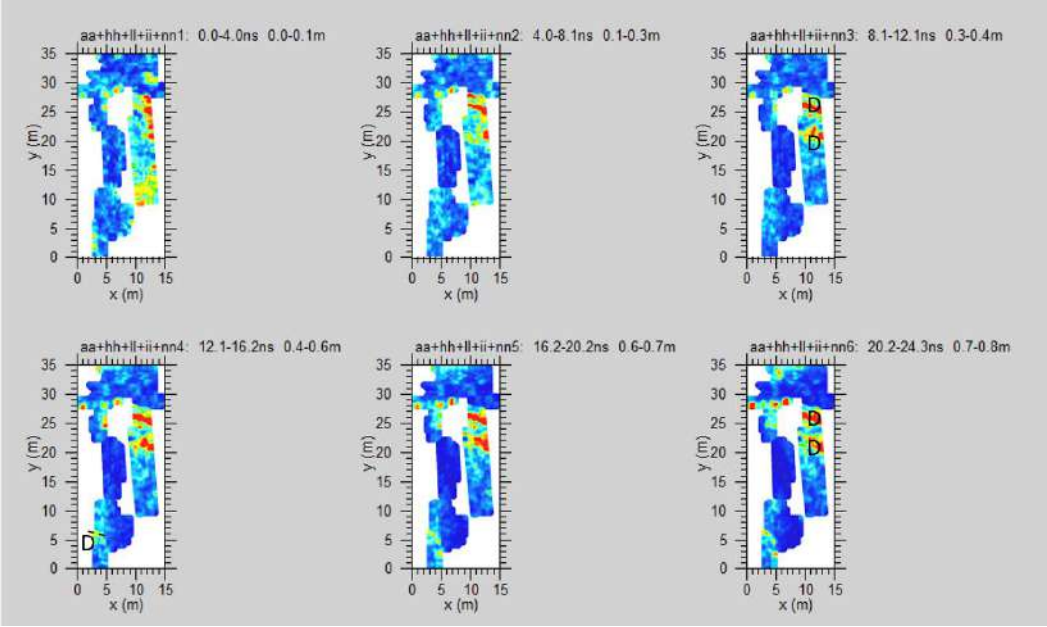

Fig. 72: the whole Area: depth slices 0.0-0.8m deep (D: structures)

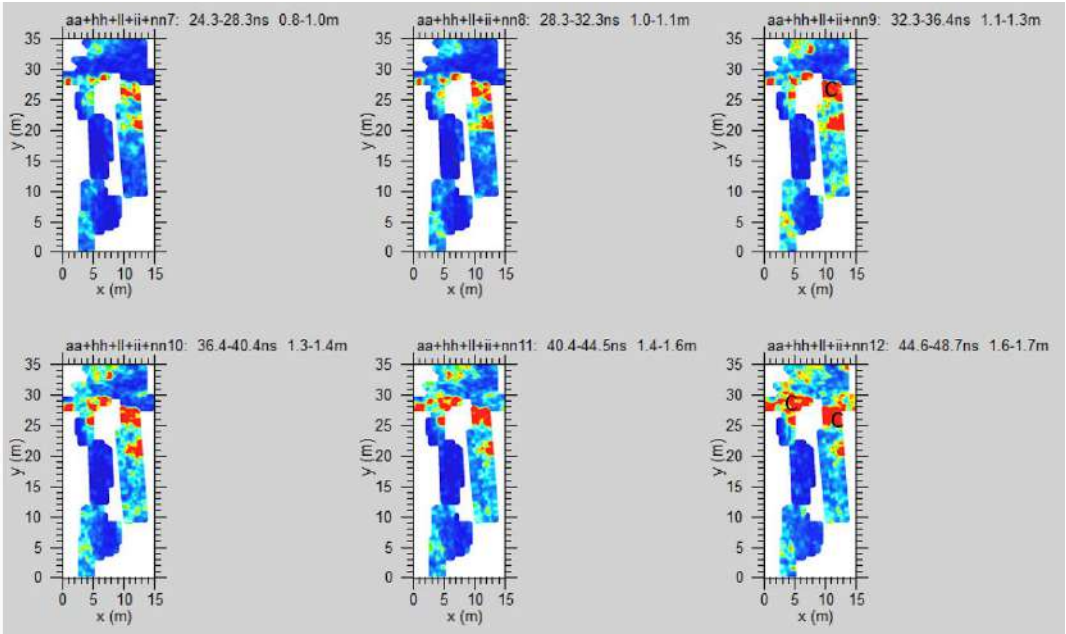

Fig. 73: the whole Area: depth slices 0.8-1.7m depth (C: cavities)

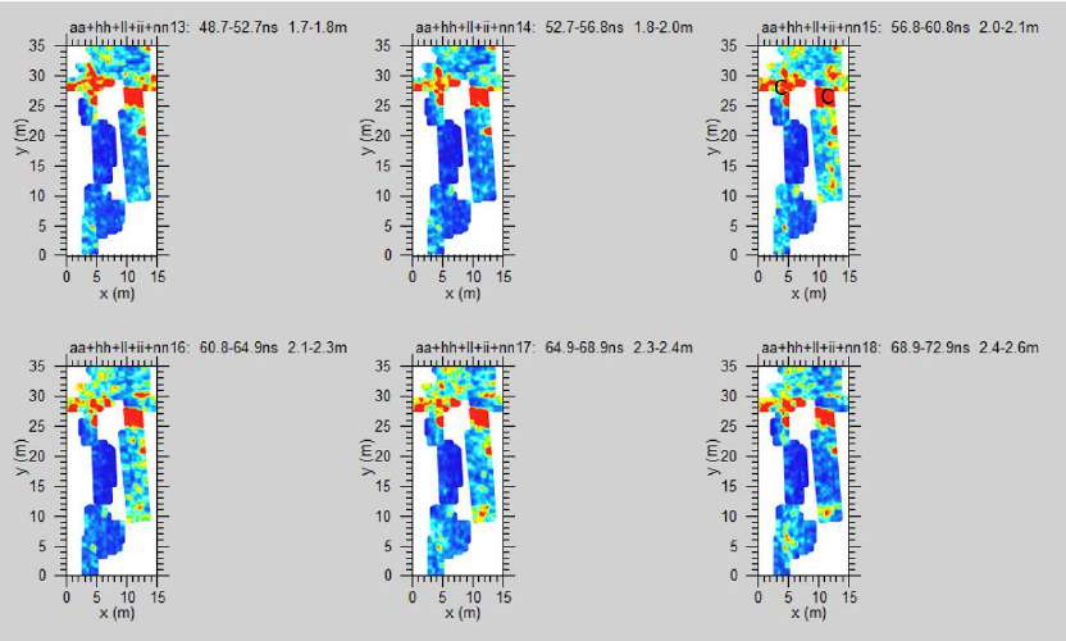

Fig. 74: the whole Area: depth slices 1.7-2.6m depth (C: cavity)

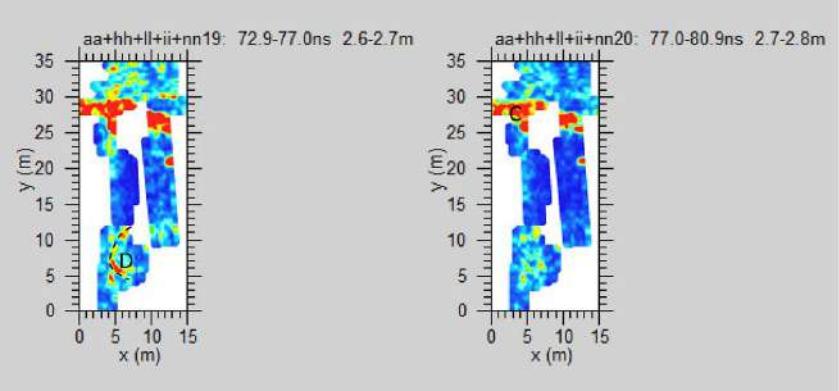

Fig. 75: the whole Area: depth slices 2.6-2.8m depth

In the slices ranging from 0.3m to 0.8m depth (Fig. 72), relatively high-amplitude alignments (labelled D) are visible. These could be related to a structure (probable channel?). In the time slices (Fig. 73, 74 and 75) ranging from 1.1m to 2.8m depth, a high-amplitude anomaly (labelled C) is visible. This corresponds to a probable cavity. The deeper time slice (Fig. 75) show other high amplitude alignments (D). They could be correlated to old structures (archaeological interest).

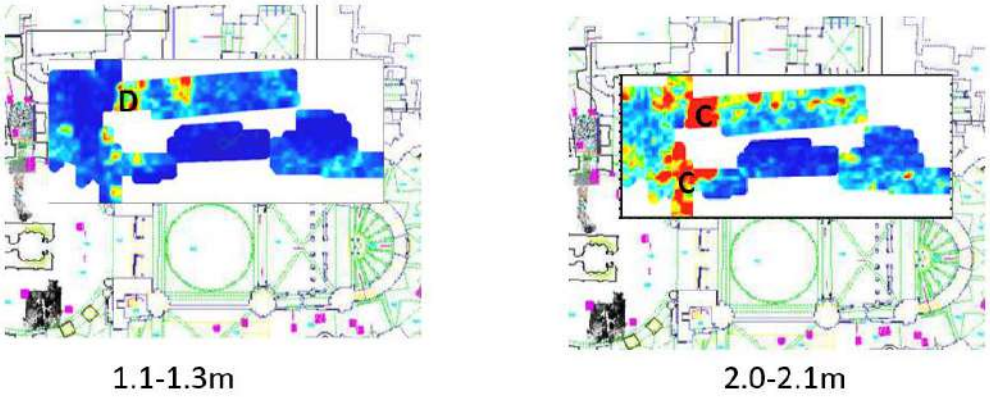

Fig. 76: the whole Area: depth slices overlapped to the planimetry

Fig 76 shows the more significant depth slices overlapped to the planimetry of the church. It is possible to see the position of the high amplitude anomalies C.

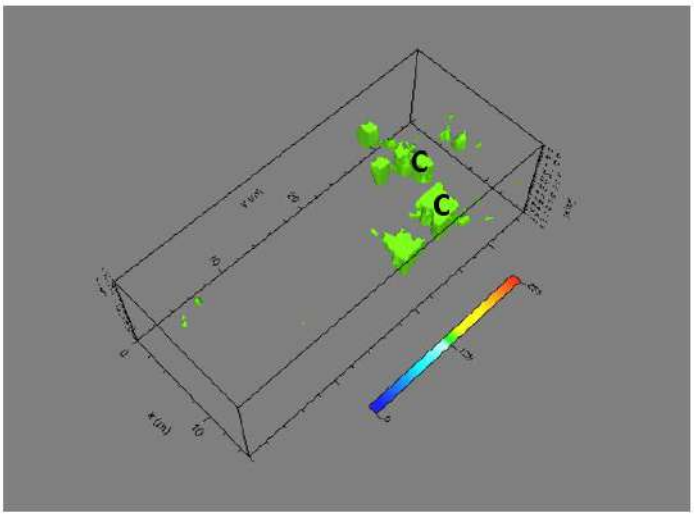

Fig. 77: the whole Area: electromagnetic amplitude isosurfaces 1.0-1.7m depth threshold 55%

Fig. 77 shows the isosurface visualization and Fig. 78 shows a virtual excavation at two levels. Here is possible to see the position of the anomalous zones well. In this case, the anomalies labelled C and D are well evidenced.

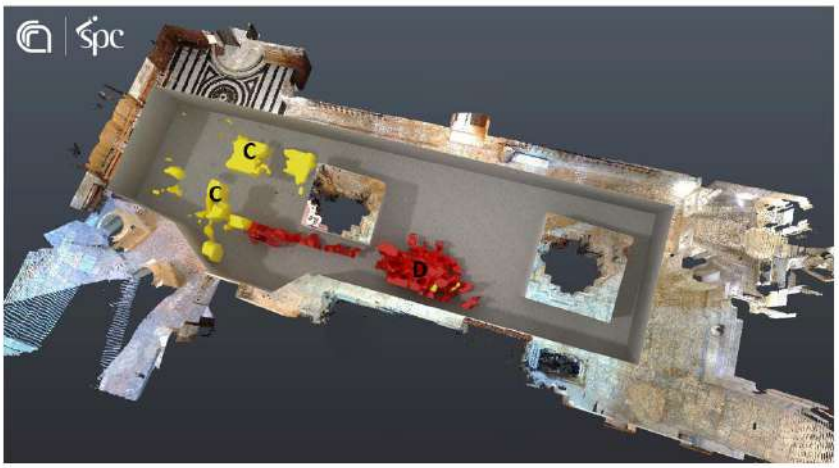

Fig. 78: the whole Area: virtual electromagnetic excavation: 1.0-2.8m depth

Area OO

In the area, OO acquired 28 GPR profiles for an extension of 183.33 meters.

The GPR data profiles were processed in 2D using GPR-slice software (GPR-SLICE Software (gpr-survey.com)). As the above describes areas to interpret GPR data, the following processing sequence was applied:

1) Zero-time adjust (static shift), to associate zero-time with zero-depth;
2) Background removal;
3) Frequency filtering, to remove high-frequency noise;
4) Migration, to correct the shape and dimension of reflection events related to the structure present in the subsoil.

The profiles acquired in the area OO are shown in Fig. 79.

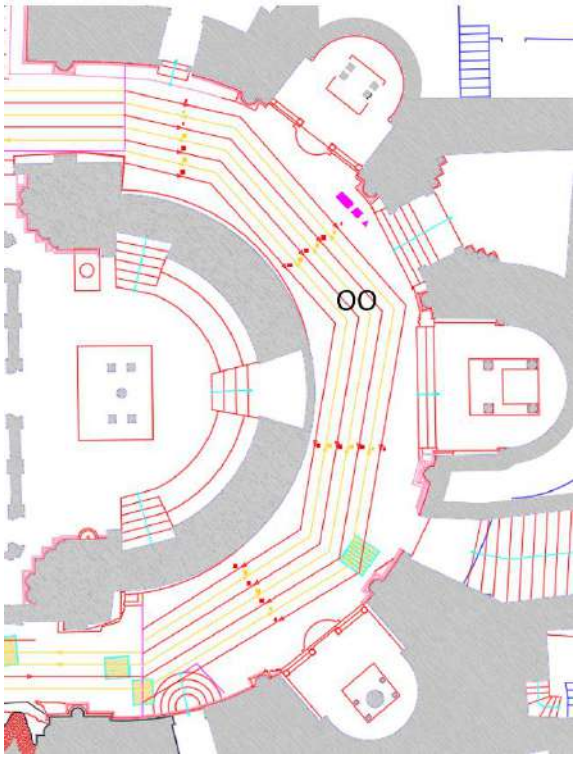

Fig. 79: Area OO: location of GPR profiles

The processed GPR profiles acquired in the area OO are shown in Figs. 80,…, 86.

The reflection event indicated by a dashed yellow line (labelled B) is probably related to the bedrock. The depth of bedrock ranges from about 1.5m to 3.1m.

The A reflection event at a depth between 0.8m and 1.3m could be related to a probable archaeological structure.

The reflection events labelled T is related to the manholes visible on the surface.

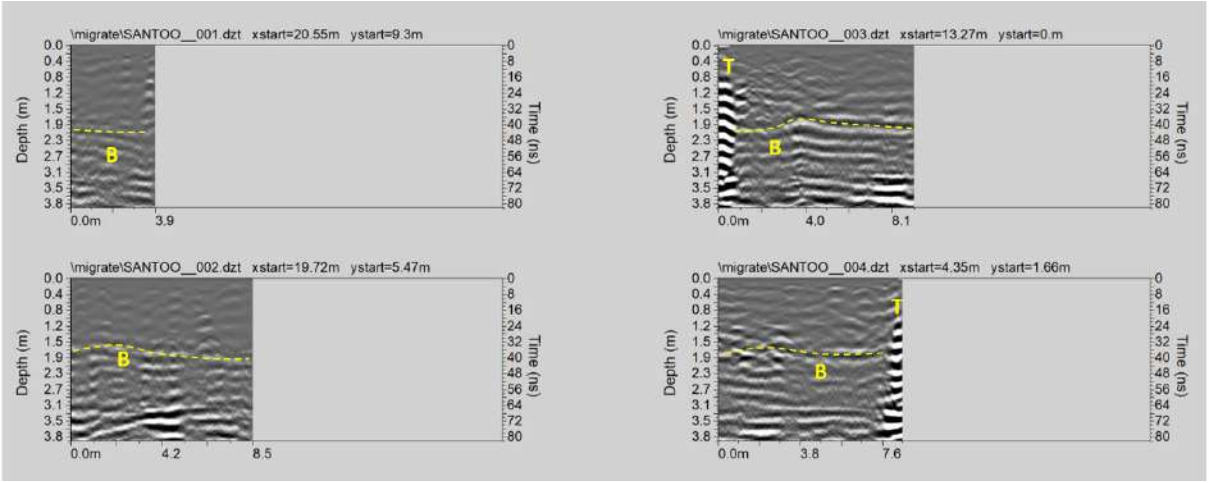

Fig. 80: Area OO: processed GPR profiles 1,.., 4 (B: bedrock; T: manhole)

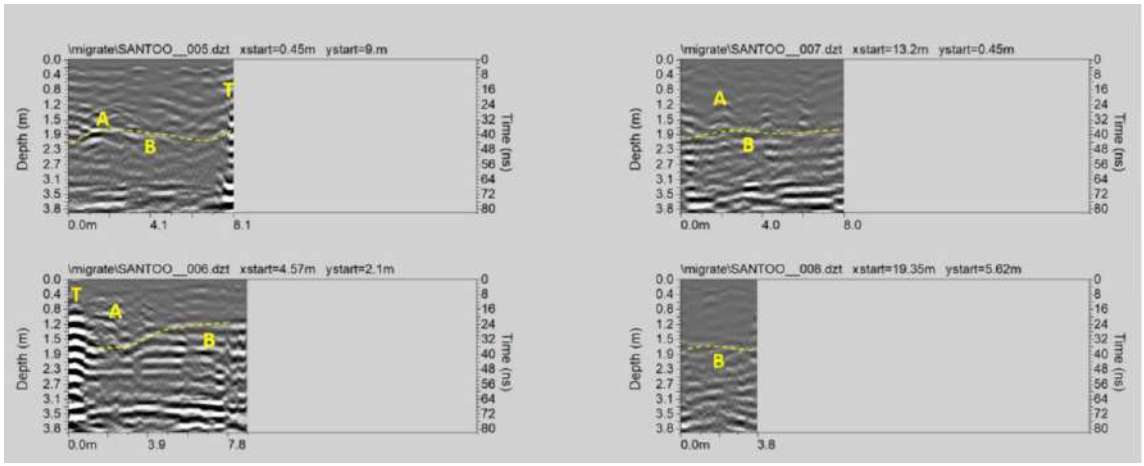

Fig. 81: Area OO: processed GPR profiles 5,.., 8 (B: bedrock; T: manhole; A: archaeological structure)

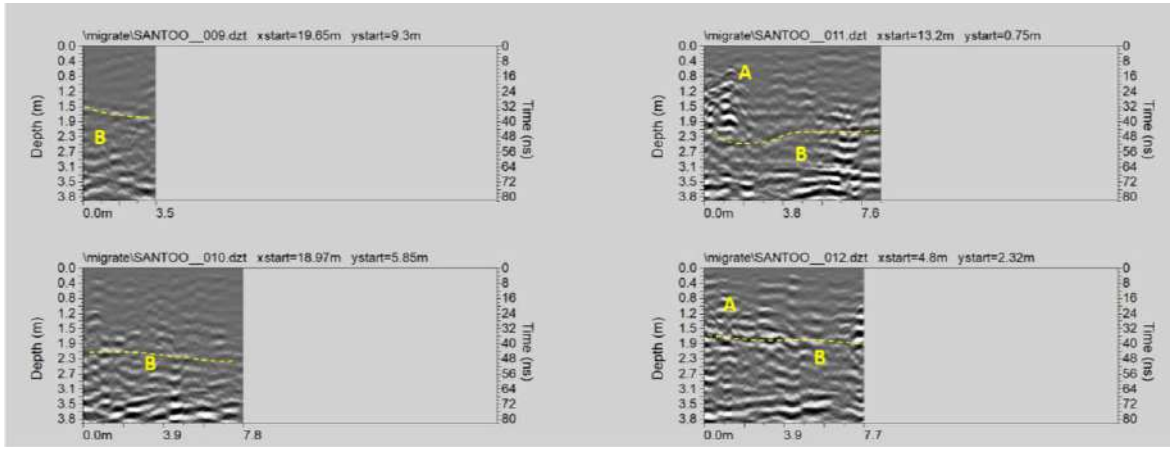

Fig. 82: Area OO: processed GPR profiles 9,.., 12 (B: bedrock; A: archaeological structure)

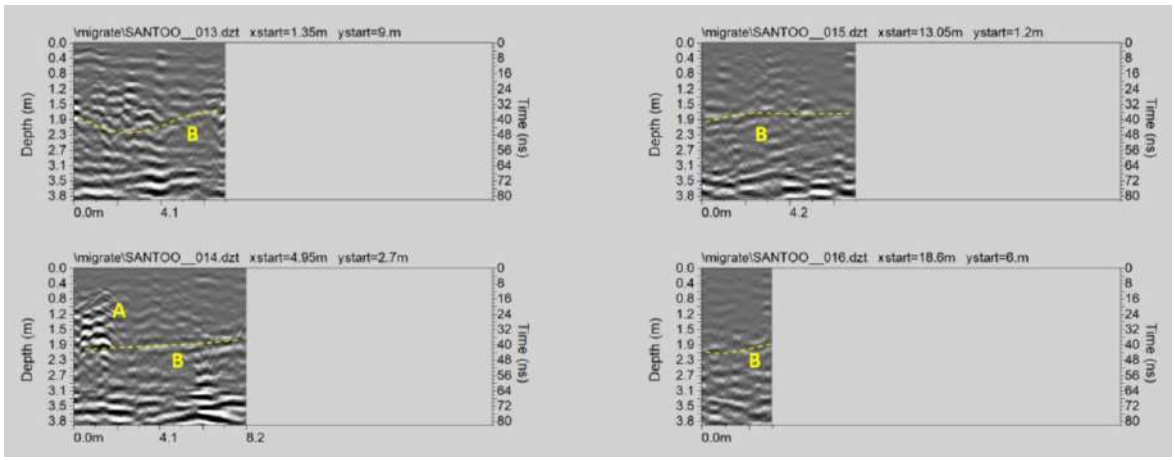

Fig. 83: Area OO: processed GPR profiles 13,.., 16 (B: bedrock; A: archaeological structure)

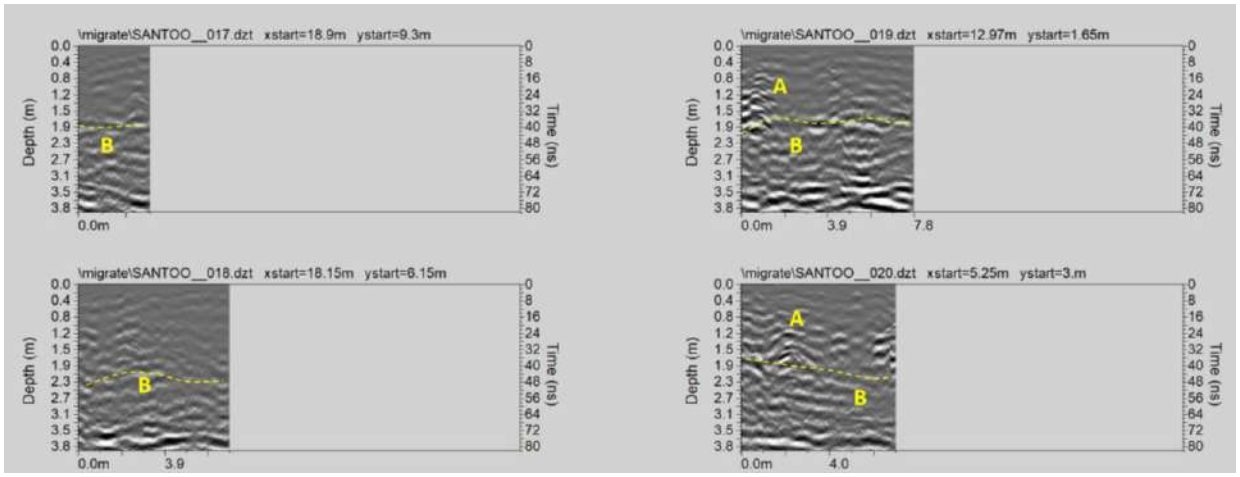

Fig. 84: Area OO: processed GPR profiles 17,.., 20 (B: bedrock; A: archaeological structure)

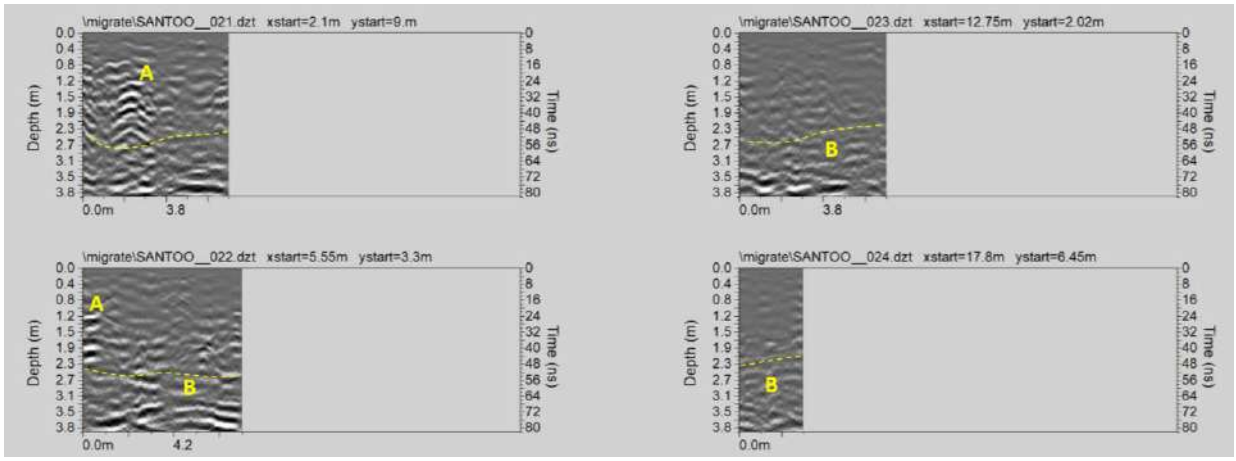

Fig. 85: Area OO: processed GPR profiles 21,.., 24 (B: bedrock; A: archaeological structure)

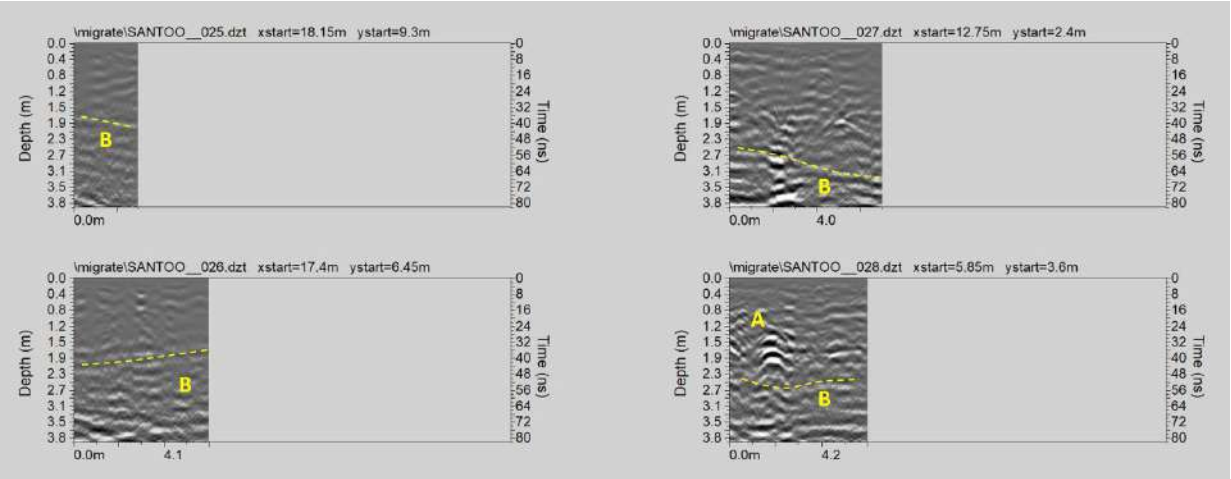

Fig. 86: Area OO: processed GPR profiles 25,.., 28 (B: bedrock; A: archaeological structure)

Area OO: 3D visualization: In this case, the time-slice technique has been used to display the amplitude variations within consecutive time windows of width Δt=5 ns.
Figs. 87 and 88 show the depth slices from 0.0 m to 3.9 m in depth.

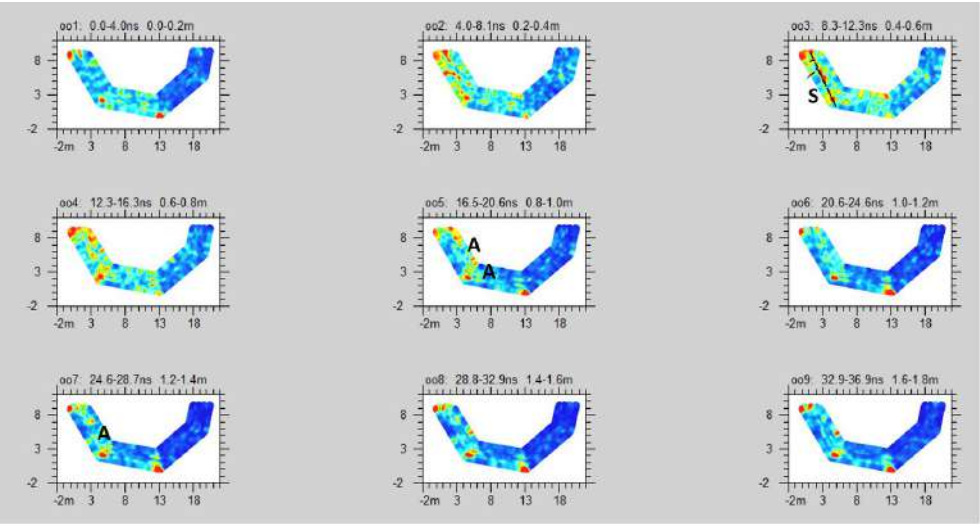

Fig. 87: Area OO: depth slices 0.0-1.8m deep (S: underground services; A: archaeological structure)

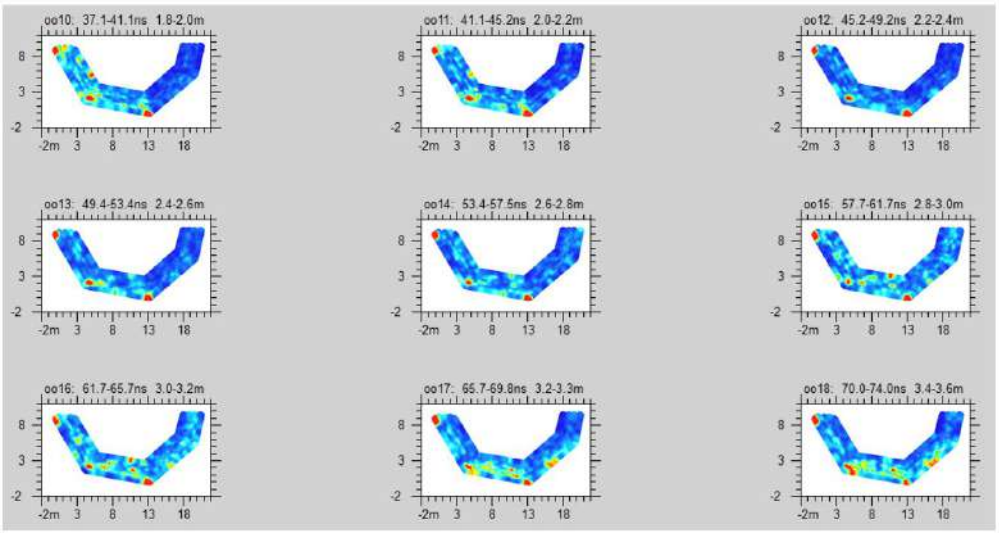

Fig. 88: Area OO: depth slices 1.8-3.6m depth

In the slices ranging from 0.4m to 0.6m depth (Fig. 87), relatively high-amplitude alignments (labelled S) are visible. These could be related to underground services. The deeper time slice -0.8-1.4m depth- (Fig. 87) show other high amplitude alignments (A). They could be correlated to old structures (archaeological interest).

Fig. 89: Area OO: depth slices overlapped to the planimetry

Fig 89 shows the more significant depth slices overlapped to the planimetry of the church. It is possible to see the position of the high amplitude anomalies A.

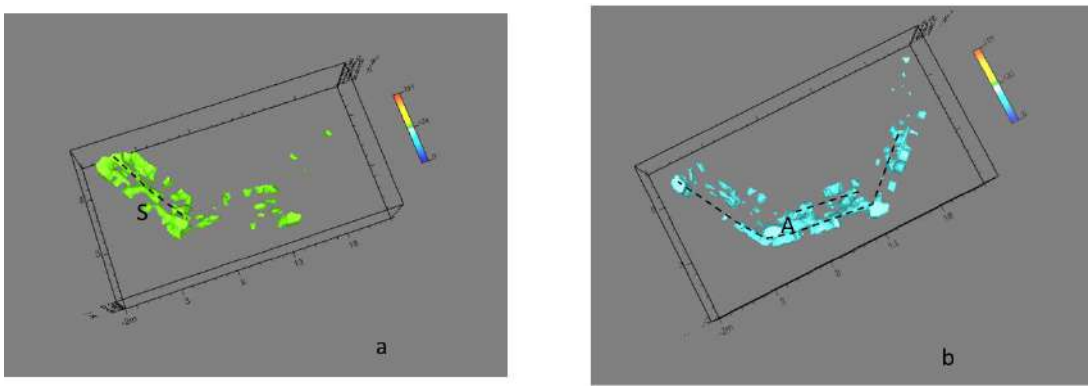

Fig. 90: Area OO: electromagnetic amplitude isosurfaces: a) 0.0-0.6m depth threshold 60%; b) 1.0-1.5m depth threshold 40%

Fig. 90 show the isosurface visualization. Here is possible to see the spatial position of the anomaly labelled A. Fig. 91 show a virtual excavation. In this case, it is likely to see the position of the anomalous zones well.

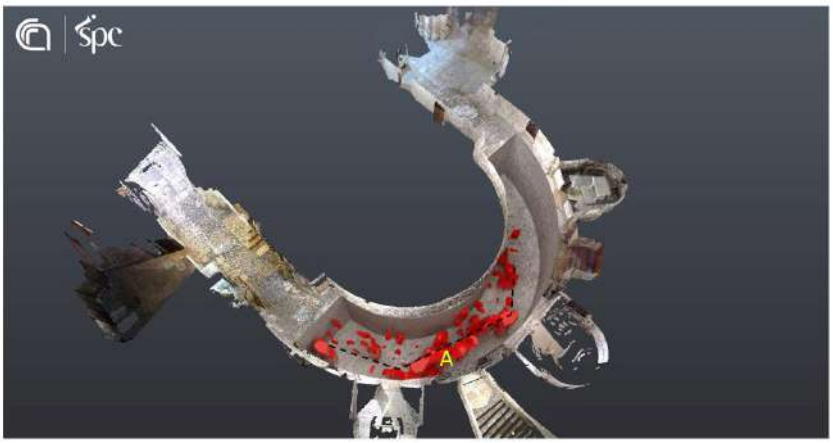

Fig. 91: Area OO: virtual excavation: 1.0-1.8m depth

Area YY

In the area, YY acquired 39 GPR profiles for an extension of 753.00 meters.

The GPR data profiles were processed in 2D using GPR-slice software (GPR-SLICE Software (gpr-survey.com)). As the above describes areas to interpret GPR data, the following processing sequence was applied:

1) Zero-time adjust (static shift), to associate zero-time with zero-depth;
2) Background removal;
3) Frequency filtering, to remove high-frequency noise;
4) Migration, to correct the shape and dimension of reflection events related to the structure present in the subsoil.

The profiles acquired in the area YY are shown in Fig. 92.

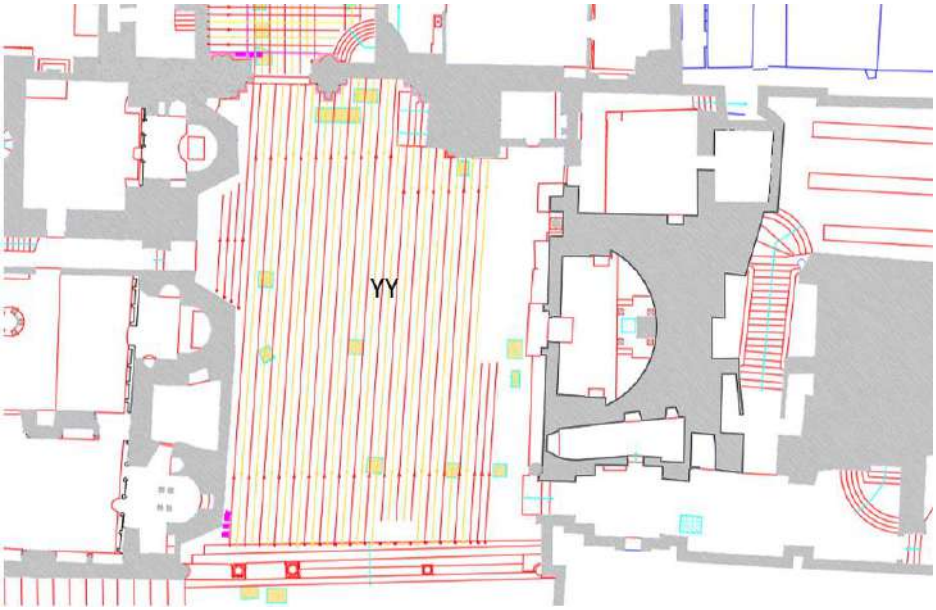

Fig. 92: Area YY: location of GPR profiles

The processed GPR profiles acquired in the area YY are shown in Figs. 93,…, 102.

The reflection event indicated by a dashed yellow line (labelled B) is probably related to the bedrock. The depth of bedrock ranges from about 0.4m to 2.2m.

The A reflection event at a depth between 1.0m and 1.3m could be related to a probable archaeological structure.

The reflection events labelled T is related to the manholes visible on the surface.

The reflection event labelled D (Figs 94 and 95) at a depth between 1.9m and 2.8m seem to be due to the presence of a probable channel.

High amplitude reflection event (CH) (figs. 94 and 95) could be related to the probable presence of a shallow channel (0.5m-1.0m depth). Another deeper (1.0m-3.3m) high amplitude anomaly labelled C is visible. It is a probable cavity.

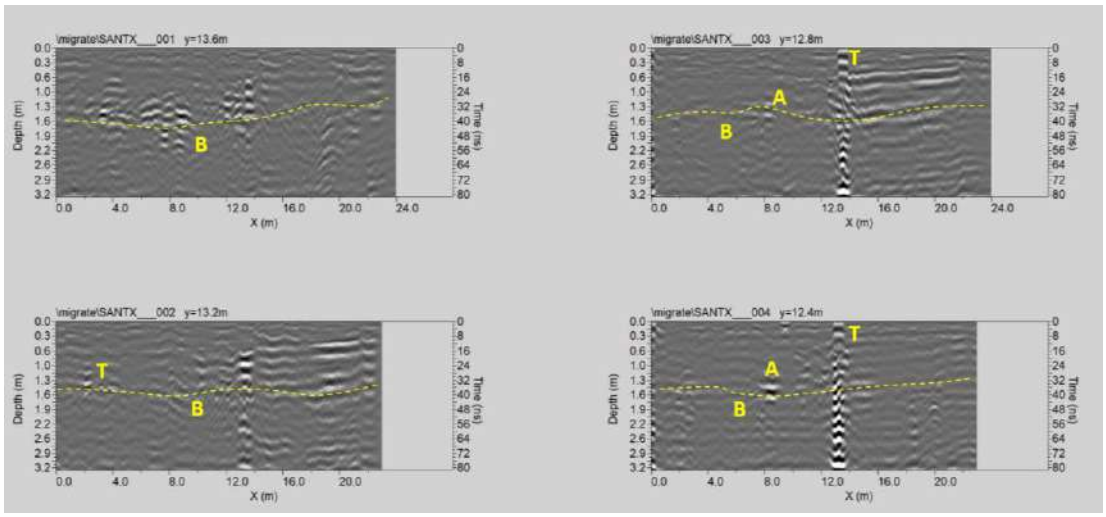

Fig. 93: Area YY: processed GPR profiles 1,.., 4 (B: bedrock; T: manhole; A: archaeological structure)

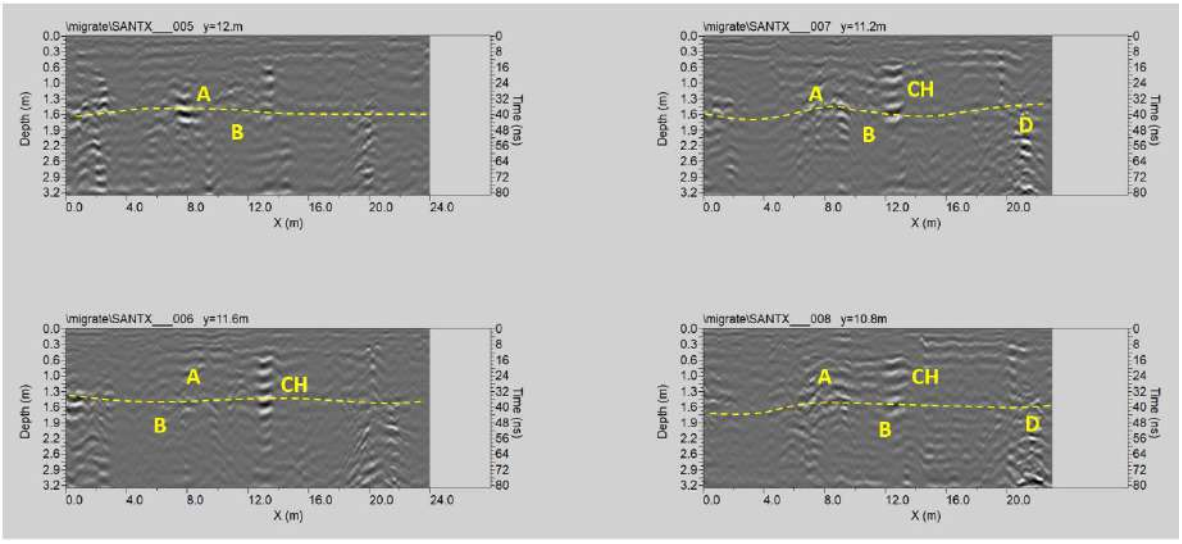

Fig. 94: Area YY: processed GPR profiles 5,.., 8 (B: bedrock; D: structure – channel?; A: archaeological structure; CH: channel)

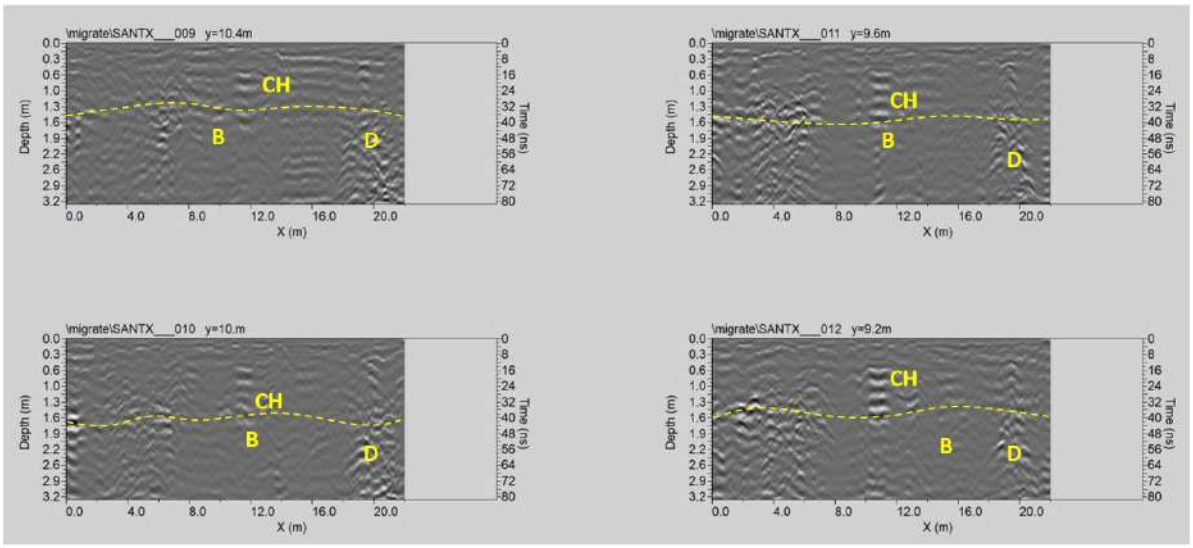

Fig. 95: Area YY: processed GPR profiles 9,.., 12 (B: bedrock; D: structure; CH: channel)

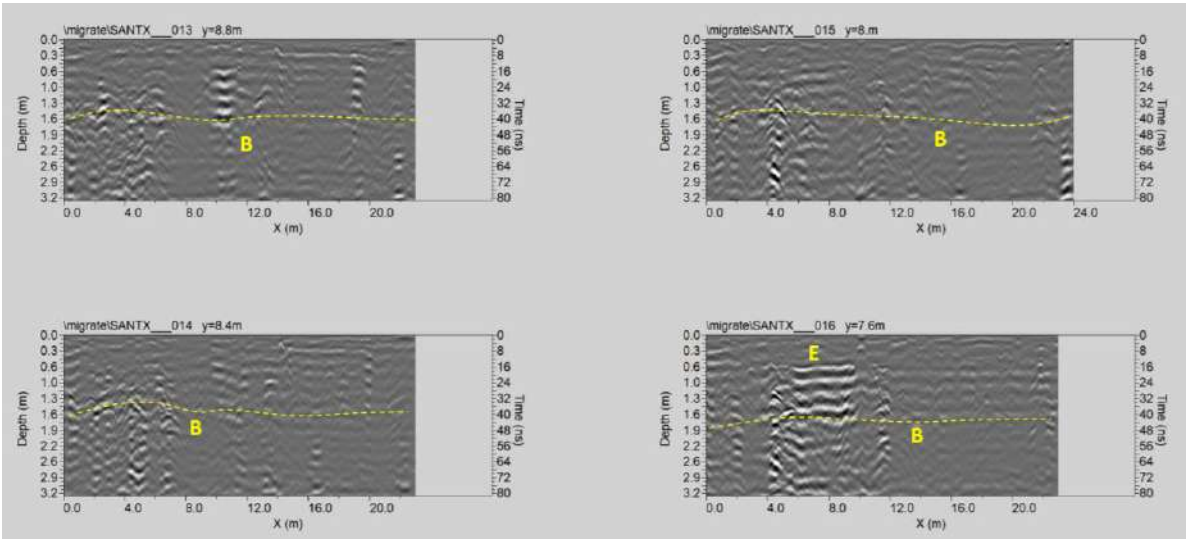

Fig. 96: Area YY: processed GPR profiles 13,.., 16 (B: bedrock; E: shallow surface hole)

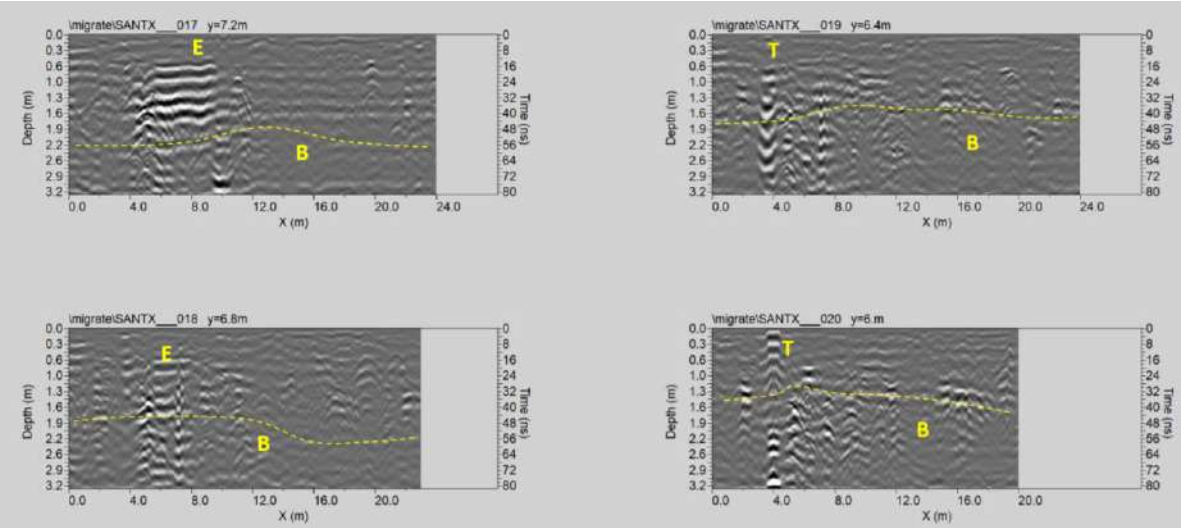

Fig. 97: Area YY: processed GPR profiles 17,.., 20 (B: bedrock; T: manhole; E: shallow surface hole)

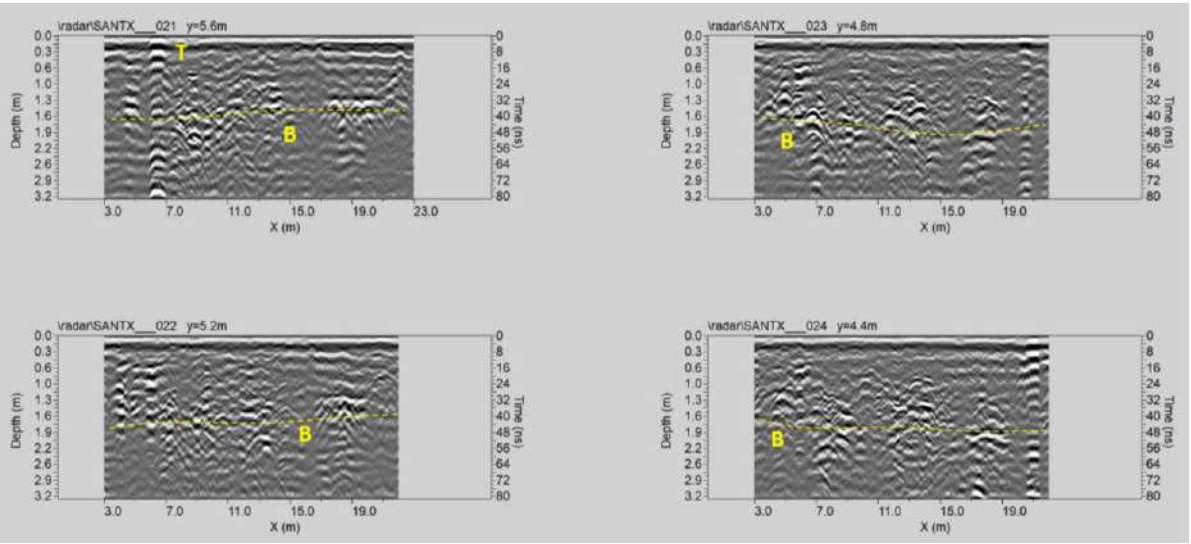

Fig. 98: Area YY: processed GPR profiles 21,.., 24 (B: bedrock; T: manhole)

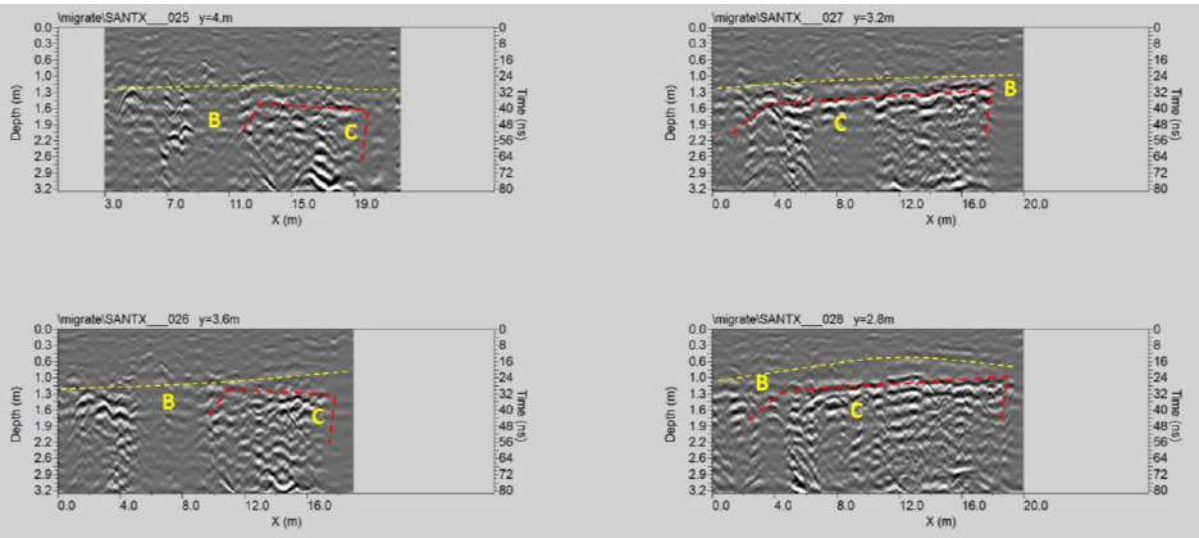

Fig. 99: Area YY: processed GPR profiles 25,.., 28 (B: bedrock; C: cavity)

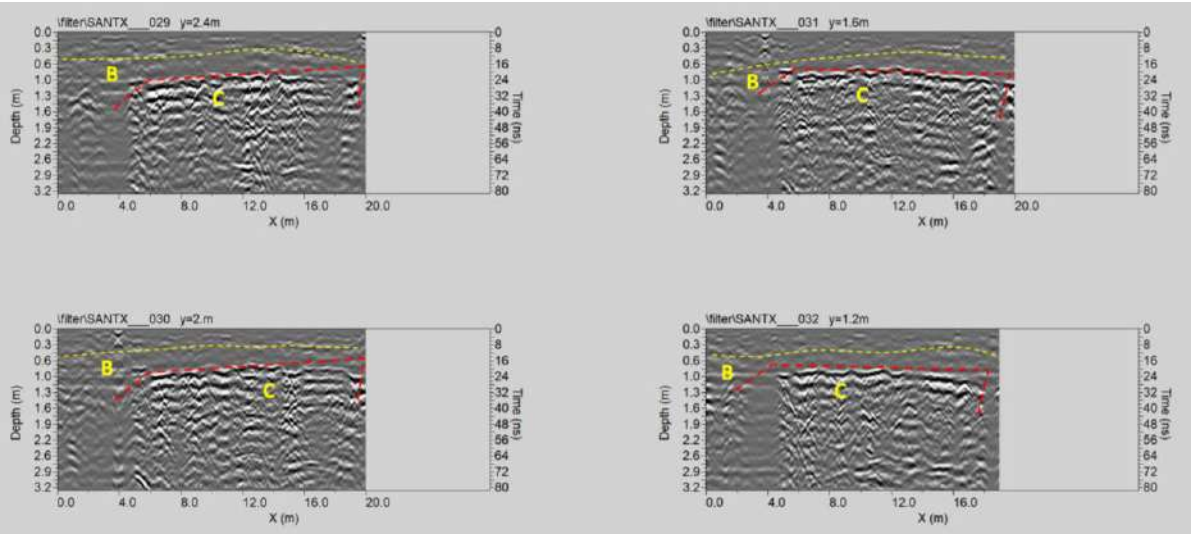

Fig. 100: Area YY: processed GPR profiles 29,.., 32 (B: bedrock; C: cavity)

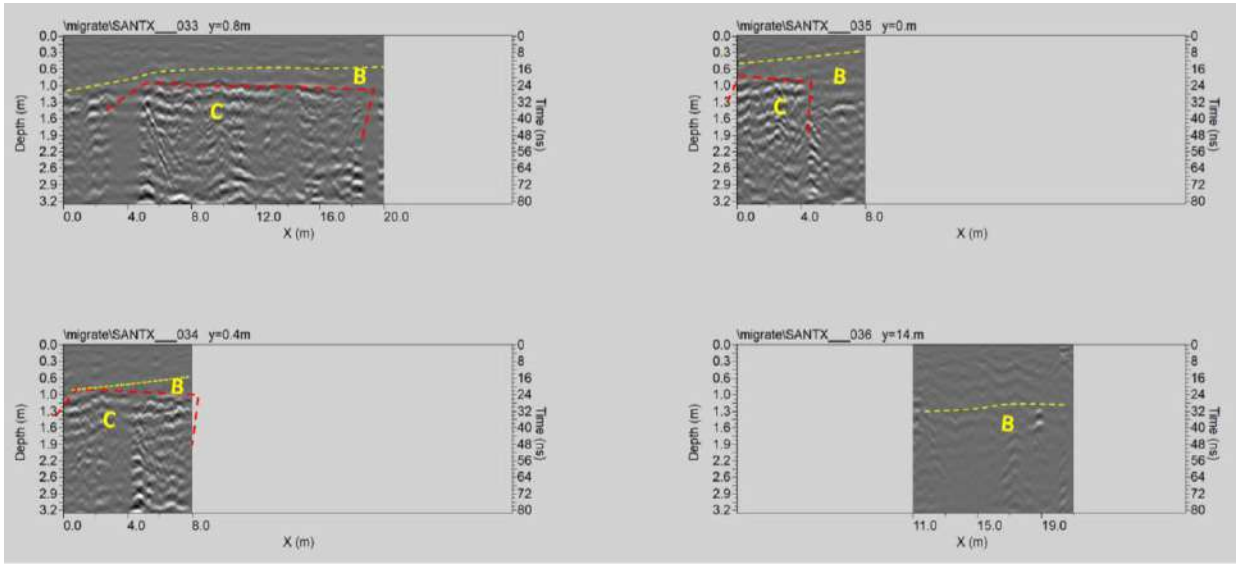

Fig. 101: Area YY: processed GPR profiles 33,.., 36 (B: bedrock; C: cavity)

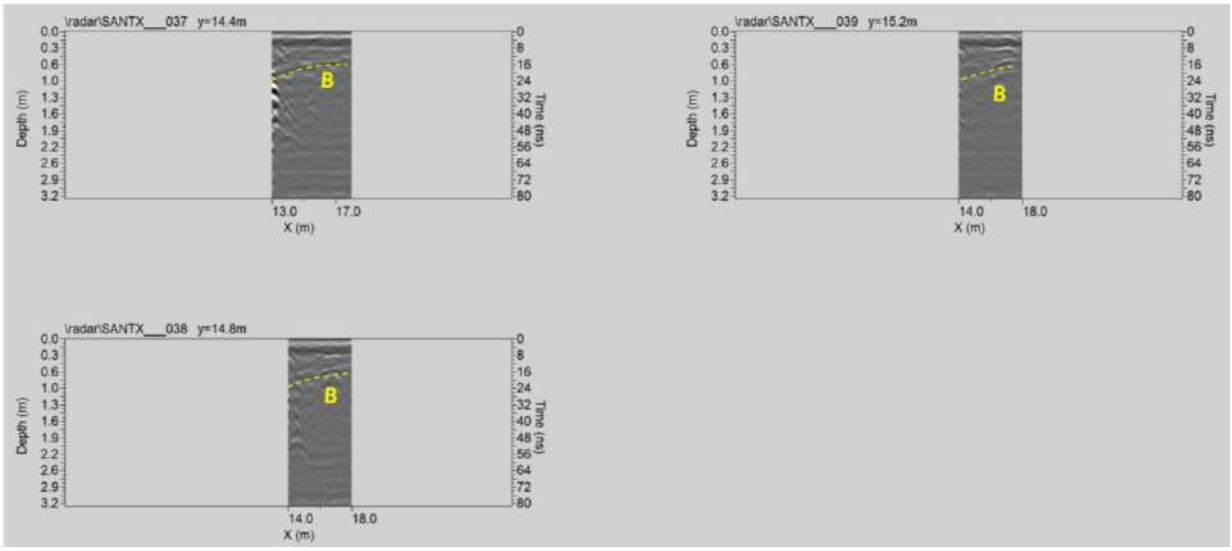

Fig. 102: Area YY: processed GPR profiles 37,.., 39 (B: bedrock)

Area YY: 3D visualization: The time-slice technique has been used to display the amplitude variations within consecutive time windows of width Δt=5 ns.
Figs. 103,…, 105 shows the depth slices from 0.0 m to 3.3 m in depth.

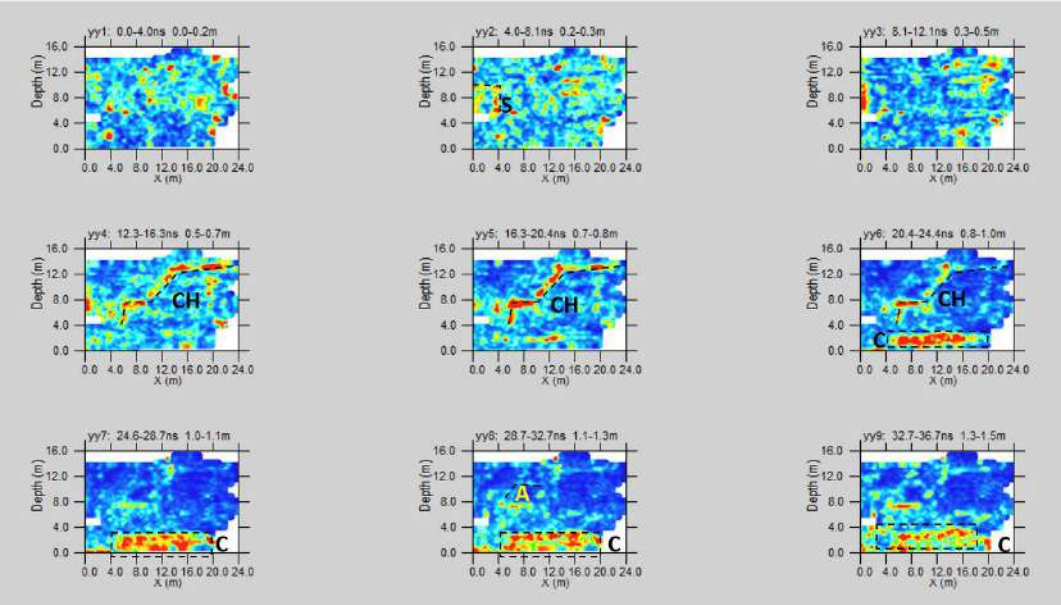

Fig. 103: Area YY: depth slices 0.0-1.5m deep (CH: channel; C: cavity; A: archaeological structure; S: underground services)

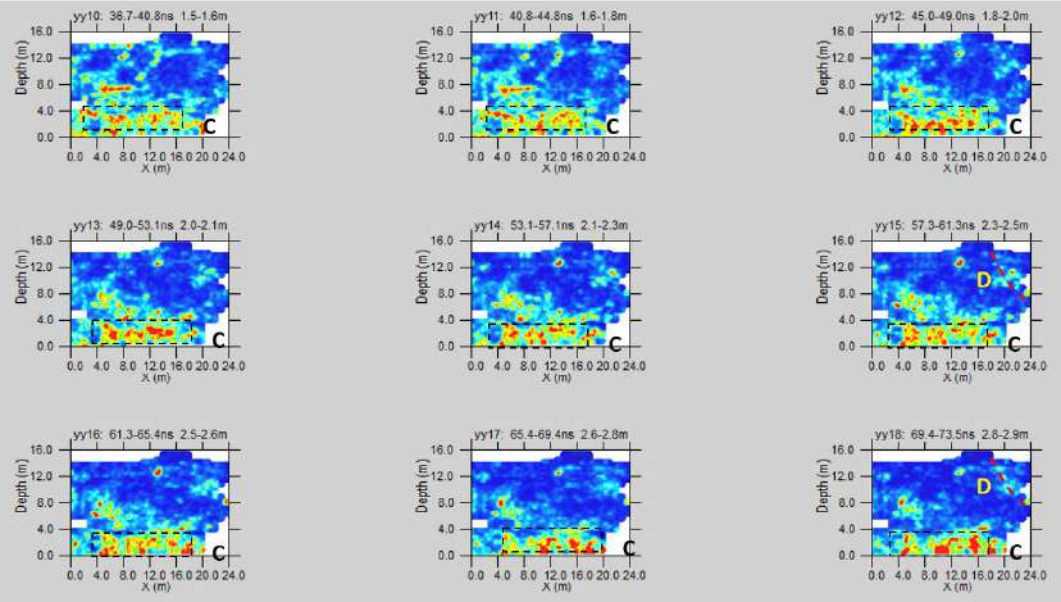

Fig. 104: Area YY: depth slices 1.5-2.9m depth (C: cavity; D: channel)

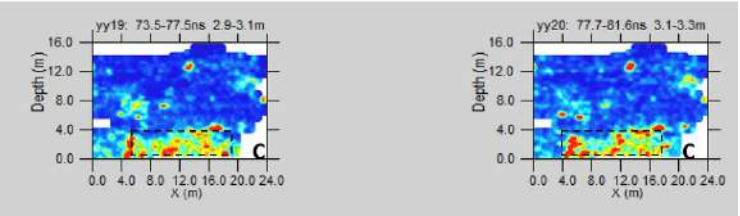

Fig. 105: Area YY: depth slices 2.9-3.3m depth (C: cavity)

In the slices ranging from 0.2m to 0.3m depth (Fig. 103), relatively high-amplitude alignments (labelled S) are visible. These could be related to underground services. At depth between 0.5m and

1.0m, the anomaly CH (Fig. 103) represent a probable channel. The deeper time slice -0.8-3.3m depth- (Figs. 103,..,105) show other high amplitude alignments (C). They could be correlated to the presence of a cavity. The anomaly A (Fig. 103) at a depth of about 1.1m could be related to an old structure (archaeological interest). At 2.3m depth (Fig. 104), the relatively high amplitude anomaly could be a channel.

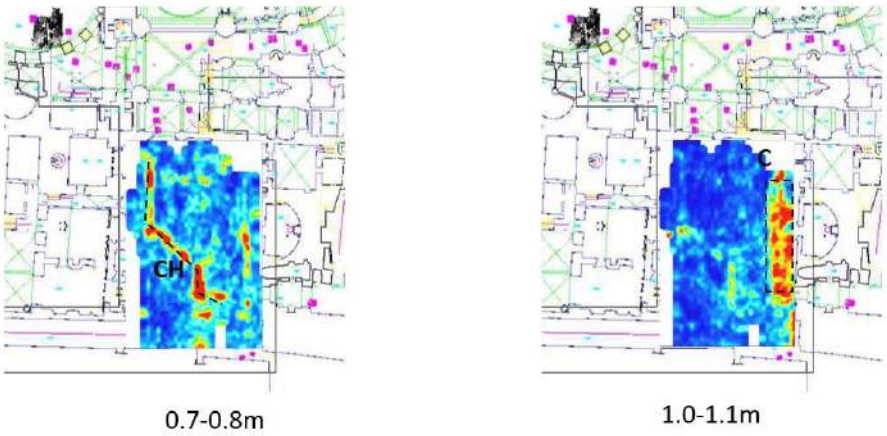

Fig. 106: Area YY: depth slices overlapped to the planimetry

Fig 89 shows the more significant depth slices overlapped to the planimetry of the church. It is possible to see the position of the high amplitude anomalies A.

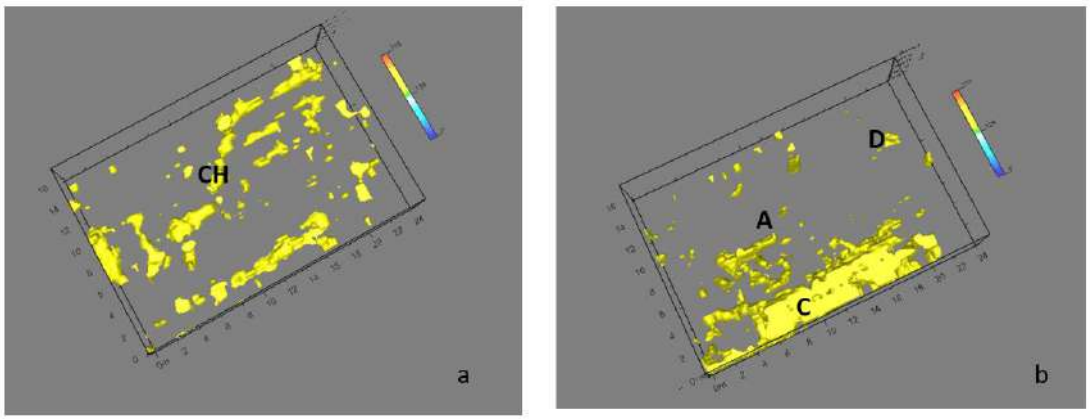

Fig. 107: Area OO: electromagnetic amplitude isosurfaces: a) 0.0-0.8m depth threshold 65%; b) 1.0-3.3m depth threshold 60%

Fig. 107 show the isosurface visualization. Here is possible to see the spatial position of the anomalies CH, A, D, and C. Fig. 108 offer a virtual excavation. In this case, it is possible to see the anomalous zones' position.

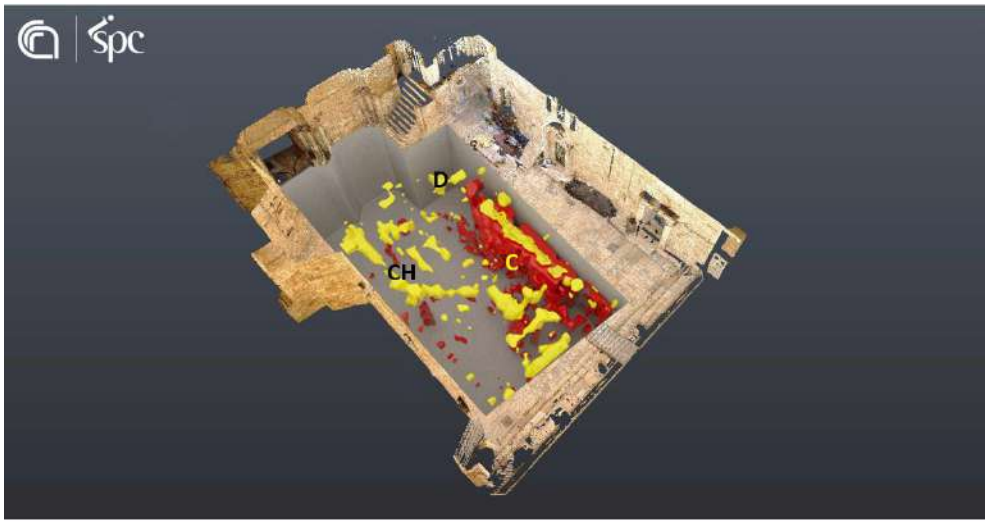

Fig. 108: Area YY: virtual excavation

Bedrock depth analysis: To obtain the bedrock's depth inside the Basilica, a geostatistical analysis was performed using the results obtained from the GPR survey. Fig. 109 show the results.

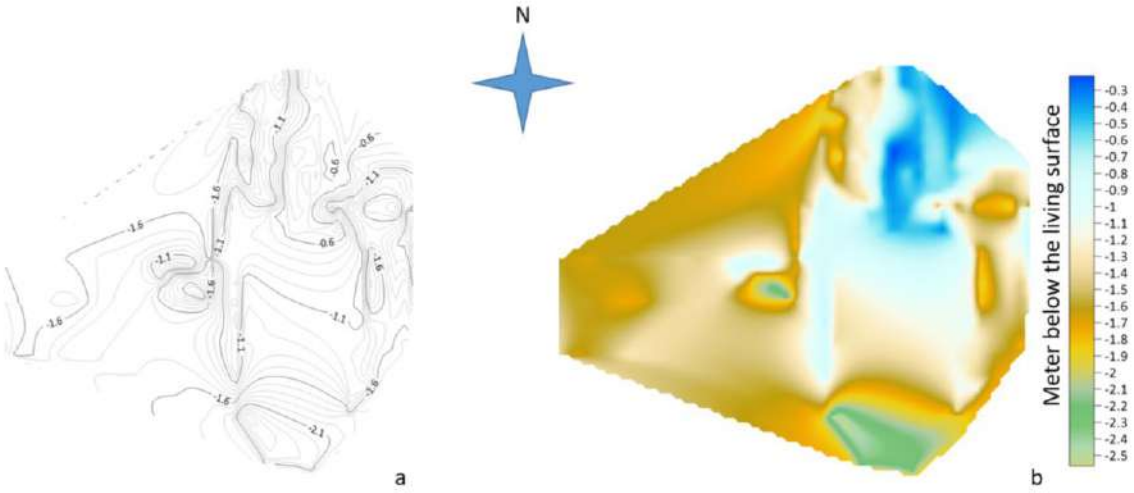

Fig. 109: the bedrock depth inside the Basilica: a) isoipse; b) colour scale

Fig. 110: the depth of the bedrock

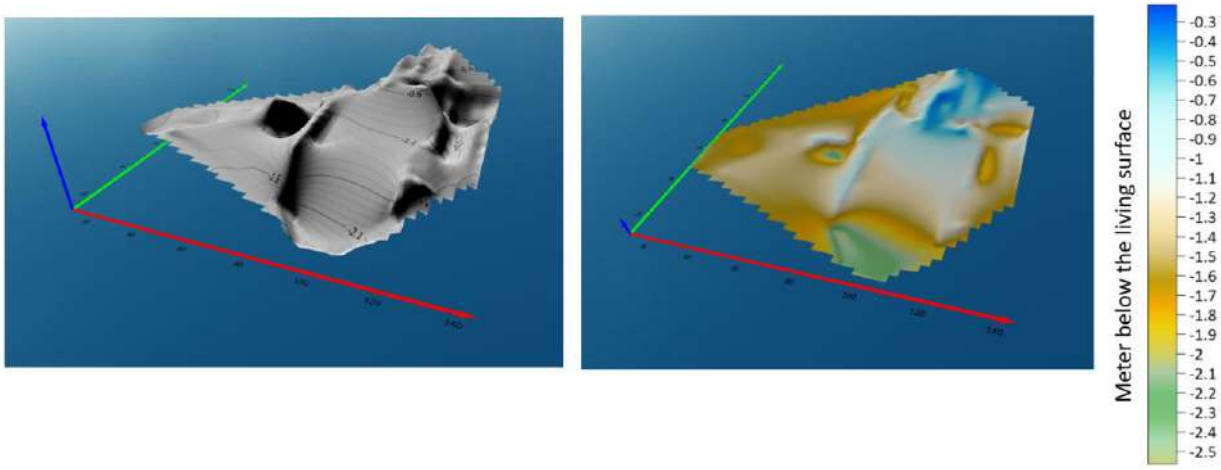

Fig. 111: the iso surfaces representing the depth of the bedrock

Figs 110 and 111 show the bedrock's depth below today living surface ranging from 0.2m in the northwest part to 2.5 in the northeast part of the Basilica.

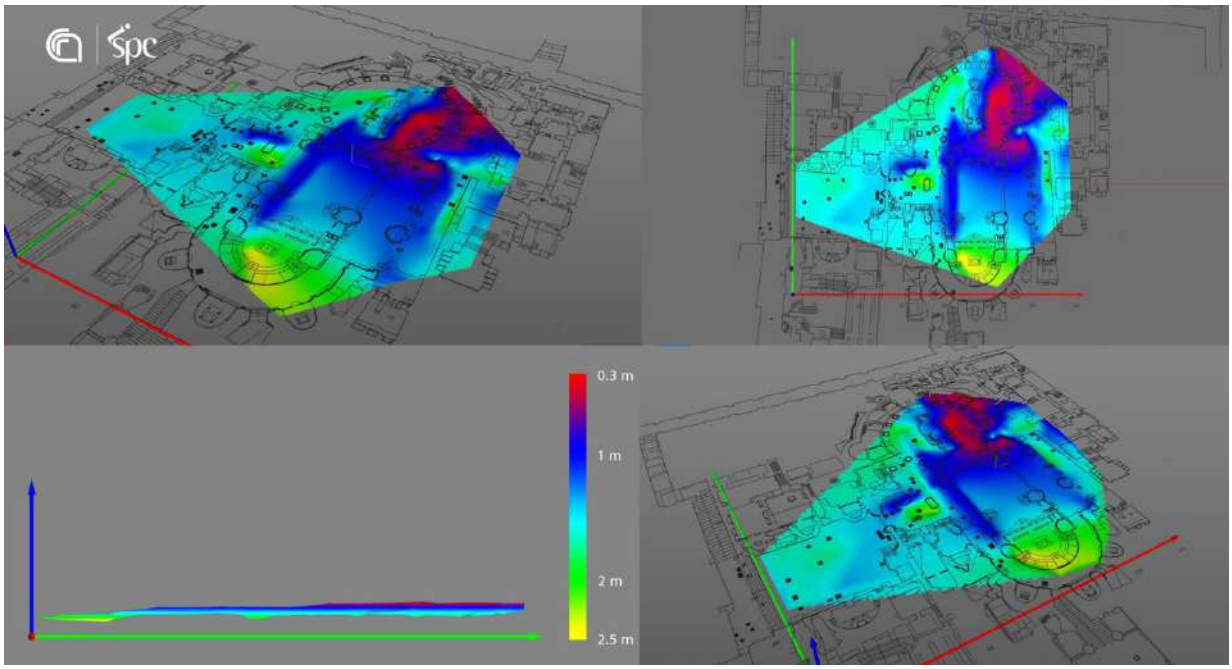

Fig. 112: pseudo-3D visualization of today living surface overlapped the iso surface bedrock representation

The 900 MHz GPR data analysis

The surveyed zone was divided into ten main areas (Fig. 113).

Fig. 113: surveyed areas with 900MHz antenna

The high-frequency survey was undertaken to obtain detailed information relating to the first meter of subsoil. In this way, information was obtained regarding the thickness of the stone paving, the volumetric water content, and probable underground utilities. For the 900MHz antenna survey, parallel profiles 0.2m spaced were acquired.

Area B+C+D+E

In the area, B+C+D+E have acquired 95 GPR profiles for an extension of 1181.0 meters (Fig. 114).
The GPR data profiles were processed in 2D using GPR-slice software (GPR-SLICE Software (gpr-survey.com)). To eliminate a small noise component and make it easy to interpret GPR data, the following processing sequence was applied:

1) Zero-time adjust (static shift), to associate zero-time with zero-depth;
2) Background removal;
3) Frequency filtering, to remove high-frequency noise;
4) Migration, to correct the shape and dimension of reflection events related to the structure present in the subsoil.

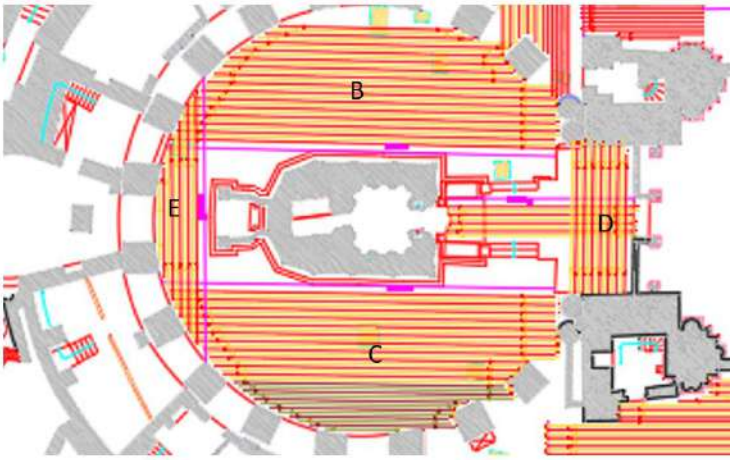

Fig. 114: Area B, C, D and E: location of GPR profiles

AREA B: The processed GPR profiles acquired in area B are shown in Figs. 115,…, 121.
The reflection event evidenced by a dashed yellow line (labelled P) is probably related to the paving. Here the thickness of the paving seems to vary between 0.1m and 0.2m.
The reflection events labelled T is related to the manholes visible on the surface.
The reflection events labelled C at a depth of about 0.4m are related to a probable channel.
The reflection events labelled R is visible nearly the surface and develops in-depth it seems to be due to a sort of reworking (excavation and filling).
Some reflection events labelled S at a depth of about 0.3 m are probably related to underground services (pipes).

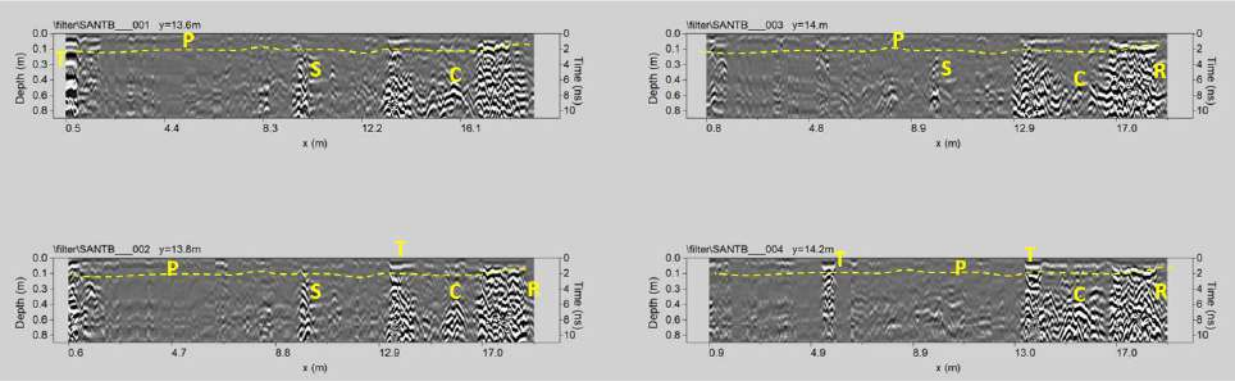

Fig. 115: Area B: processed GPR profiles 1, …, 4 (T: manhole; P: paving thickness; C: channel; R: remodelled area; S: underground services)

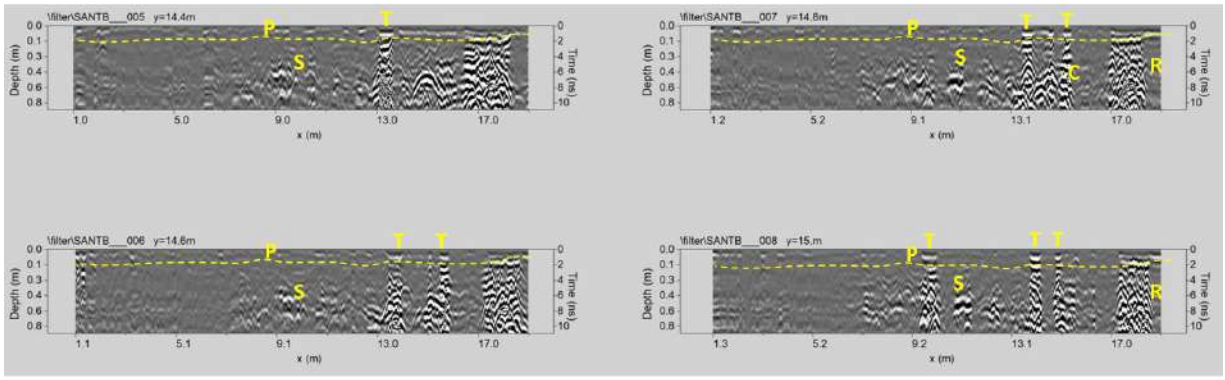

Fig. 116: Area B: processed GPR profiles 5, …, 8 (T: manhole; P: paving thickness; C: channel; R: remodelled area; S: underground services)

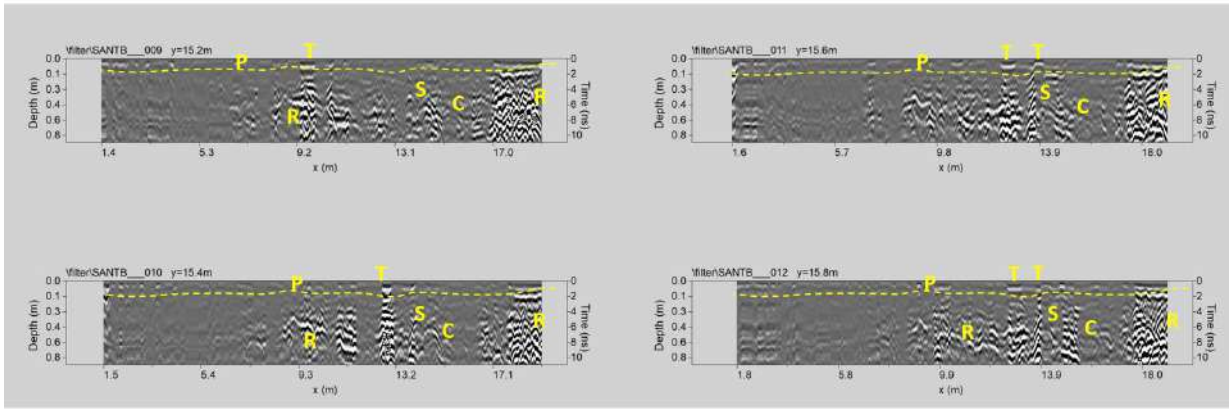

Fig. 117: Area B: processed GPR profiles 9, …, 12 (T: manhole; P: paving thickness; C: channel; R: remodelled area; S: underground services)

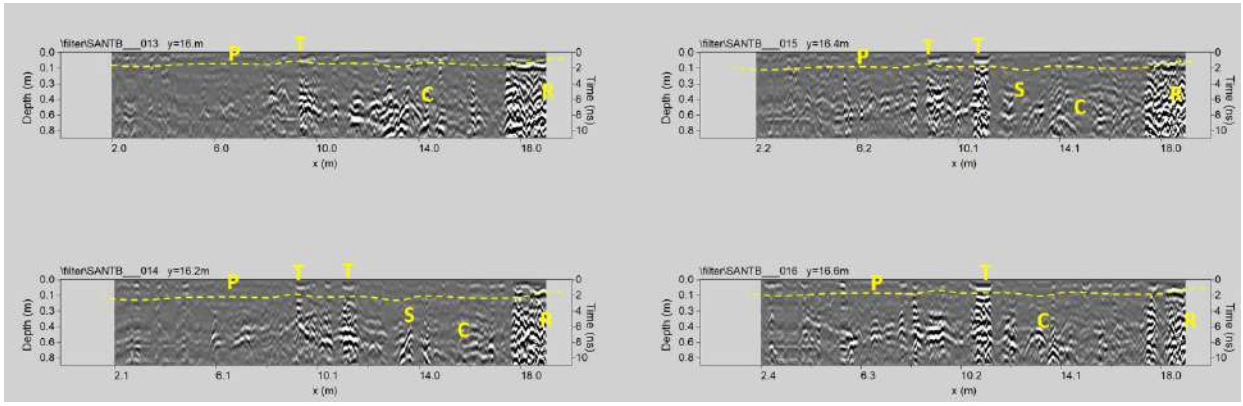

Fig. 118: Area B: processed GPR profiles 13, …, 17 (T: manhole; P: paving thickness; C: channel; R: remodelled area; S: underground services)

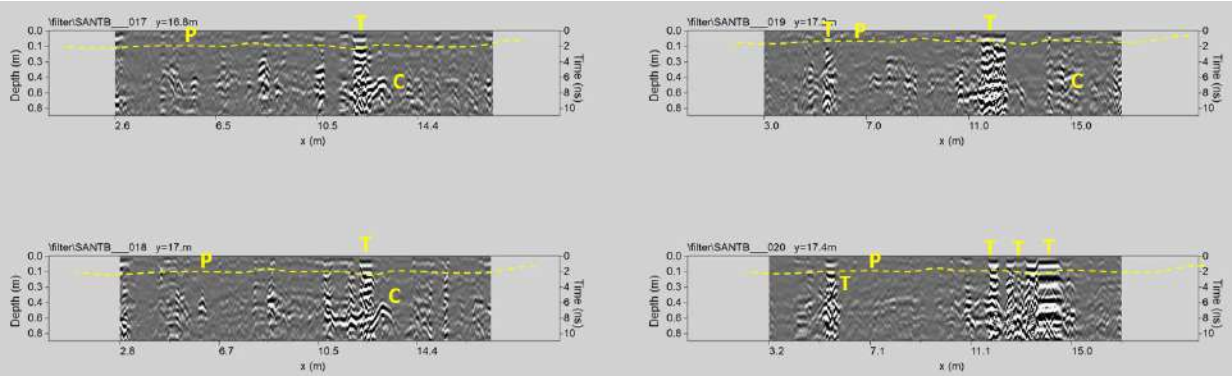

Fig. 119: Area B: processed GPR profiles 17, …, 20 (T: manhole; P: paving thickness; C: channel)

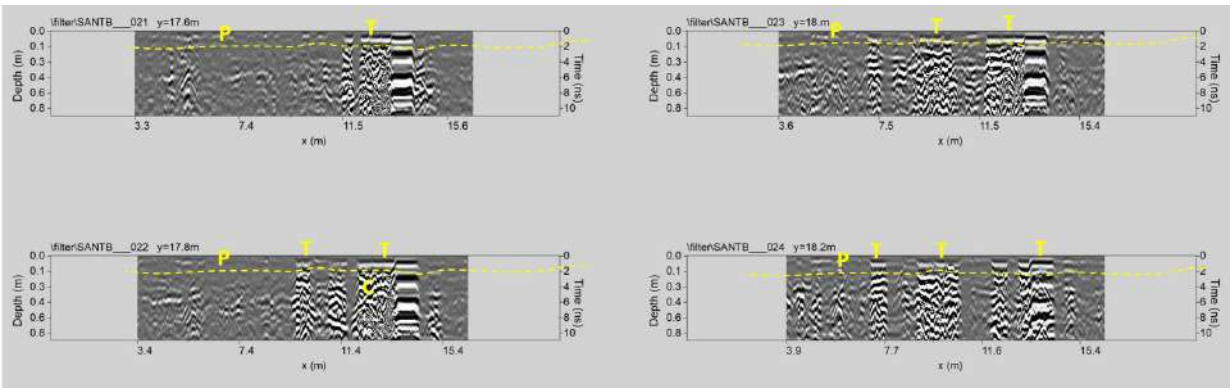

Fig. 120: Area B: processed GPR profiles 21, …, 24 (T: manhole; P: paving thickness; C: channel)

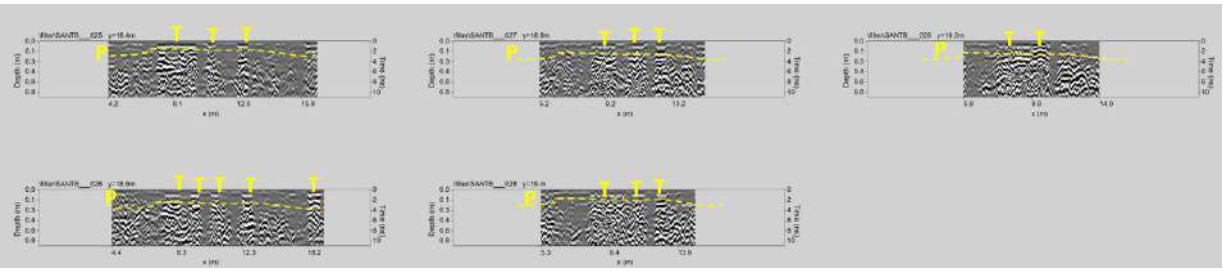

Fig. 121: Area B: processed GPR profiles 25, …, 29 (T: manhole; P: paving thickness)

AREA C: The processed GPR profiles acquired in area C are shown in Figs. 122,…, 130.
The reflection event evidenced by a dashed yellow line (labelled P) is probably related to the paving. Here the thickness of the paving seems to vary between 0.1m and 0.25m.
The reflection events labelled T is related to the manholes visible on the surface.
The reflection events labelled KC at a depth of about 0.22m are related to a known cavity.
The reflection events labelled C1 visible at about 0.5m-0.6m depth could be related to the presence of a channel.
Some reflection events labelled S at a depth of about 0.3 m are probably related to underground services (pipes).

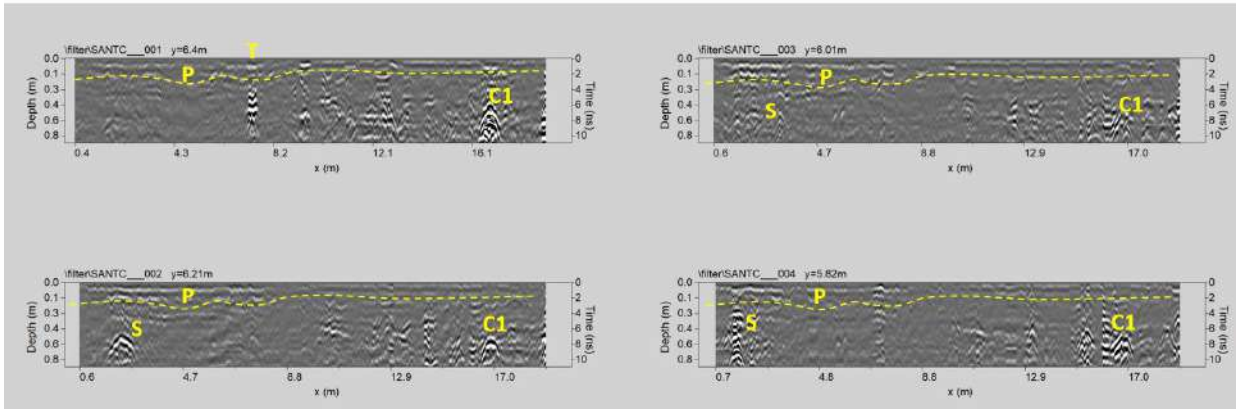

Fig. 122: Area C: processed GPR profiles 1, …, 4 (T: manhole; P: paving thickness; C1: channel; S: underground services)

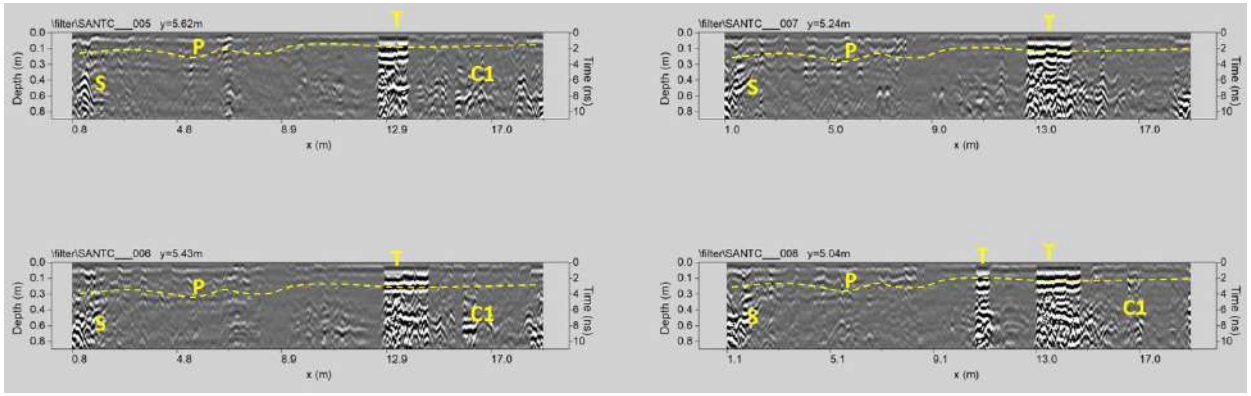

Fig. 123: Area C: processed GPR profiles 5, …, 8 (T: manhole; P: paving thickness; C1: channel; S: underground services)

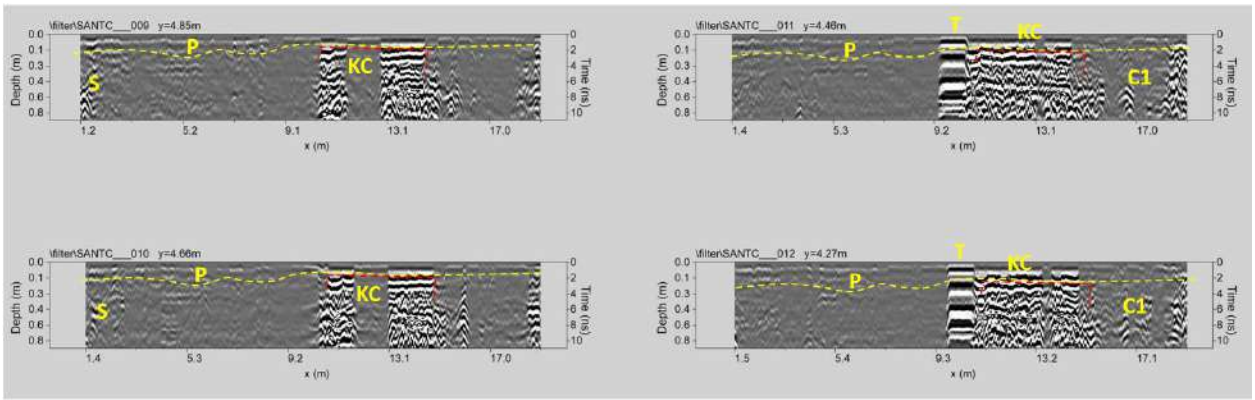

Fig. 124: Area C: processed GPR profiles 9, …, 12 (T: manhole; P: paving thickness; C1: channel; S: underground services; KC: know cavity)

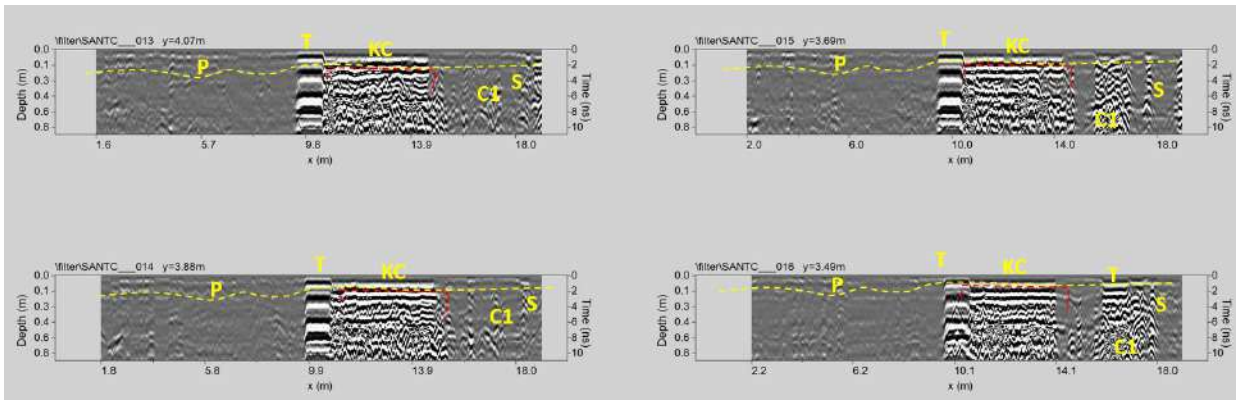

Fig. 125: Area C: processed GPR profiles 13, …, 16 (T: manhole; P: paving thickness; C1: channel; S: underground services; KC: know cavity)

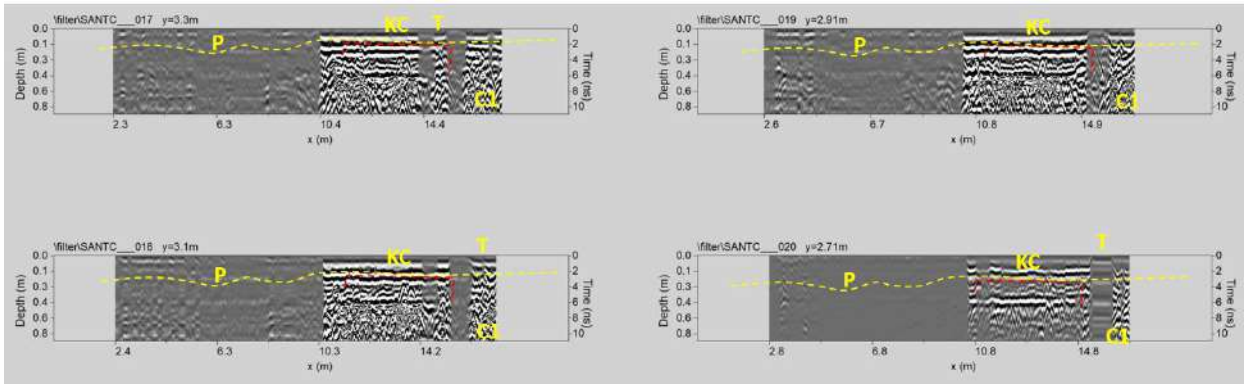

Fig. 126: Area C: processed GPR profiles 17, …, 20 (T: manhole; P: paving thickness; C1: channel; KC: know cavity)

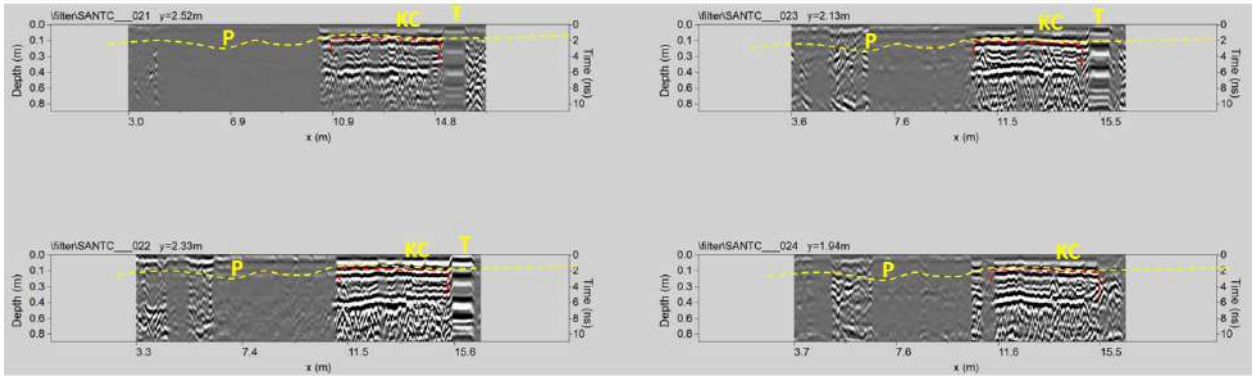

Fig. 127: Area C: processed GPR profiles 21, …, 24 (T: manhole; P: paving thickness; KC: know cavity)

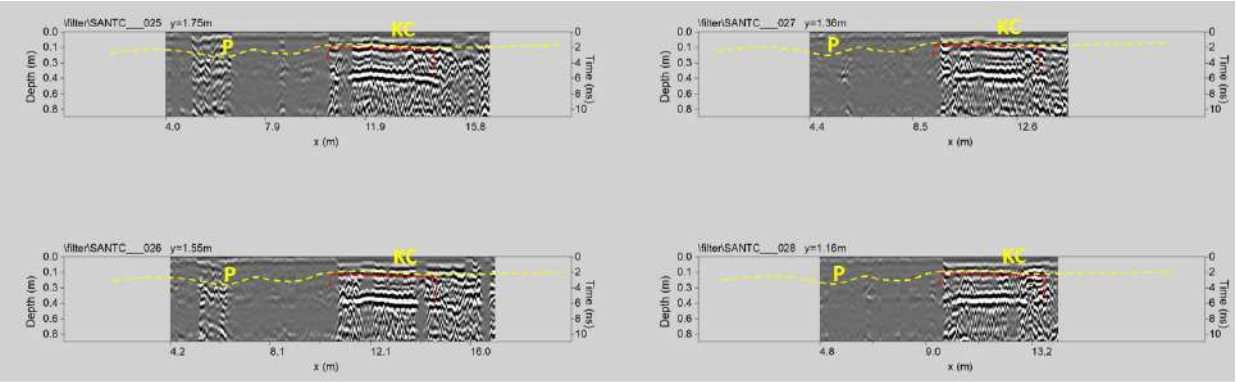

Fig. 128: Area C: processed GPR profiles 25, …, 28 (P: paving thickness; KC: know cavity)

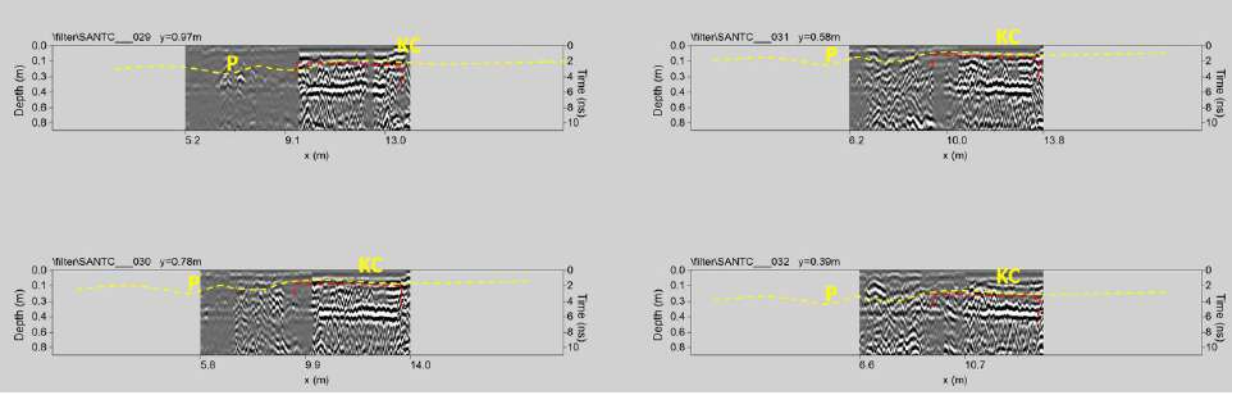

Fig. 129: Area C: processed GPR profiles 29, …, 32 (P: paving thickness; KC: know cavity)

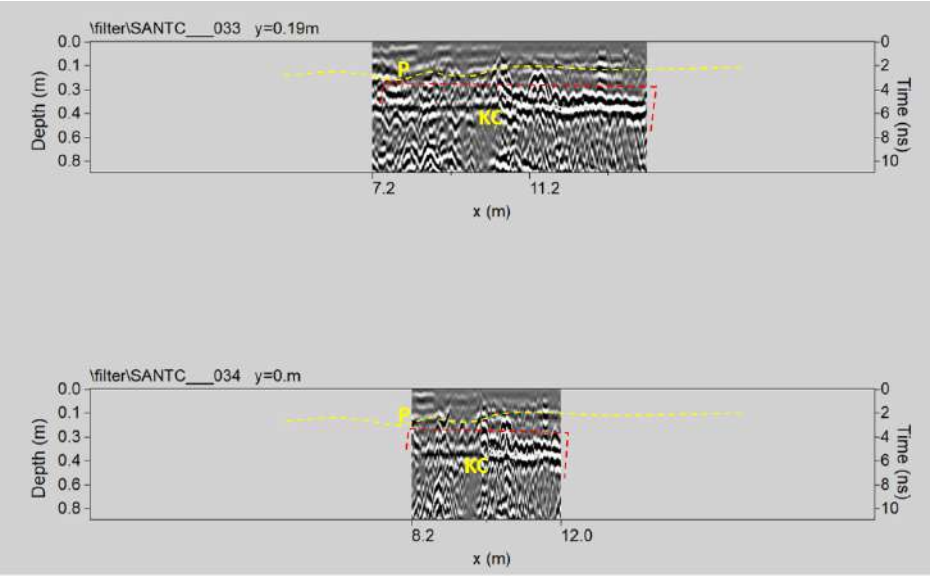

Fig. 130: Area C: processed GPR profiles 33 and 34 (P: paving thickness; KC: know cavity)

AREA D: The processed GPR profiles acquired in area D are shown in Figs. 131,…, 135.
The reflection event evidenced by a dashed yellow line (labelled P) is probably related to the paving. Here the thickness of the paving seems to vary between 0.1m and 0.2m.
The reflection events labelled C visible at about 0.5m-0.6m depth could be related to the presence of a channel.

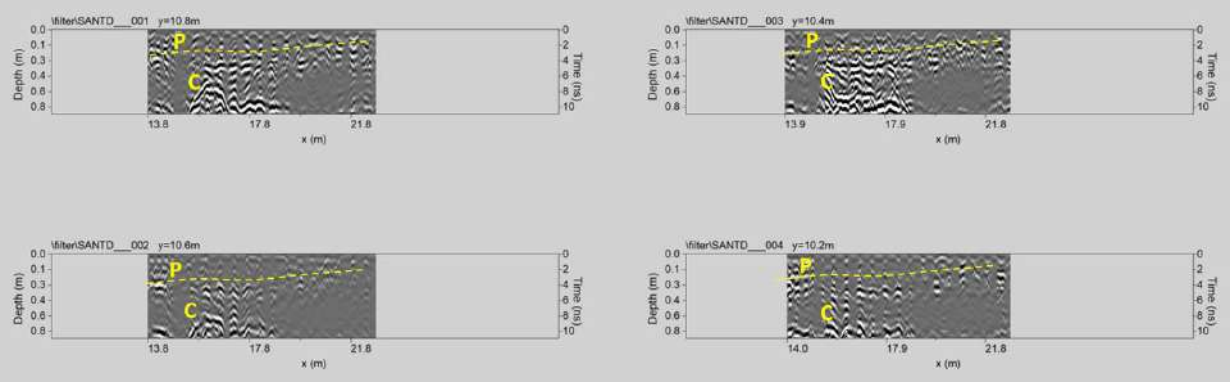

Fig. 131: Area D: processed GPR profiles 1,…, 4 (P: paving thickness; C: channel)

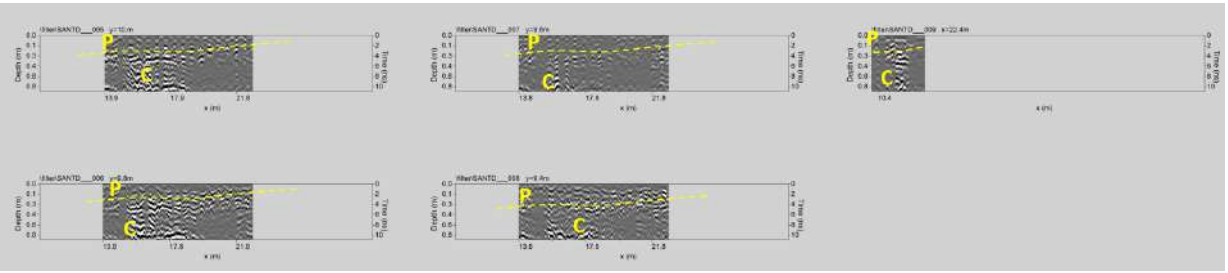

Fig. 132: Area D: processed GPR profiles 5, …, 9 (P: paving thickness; C: channel)

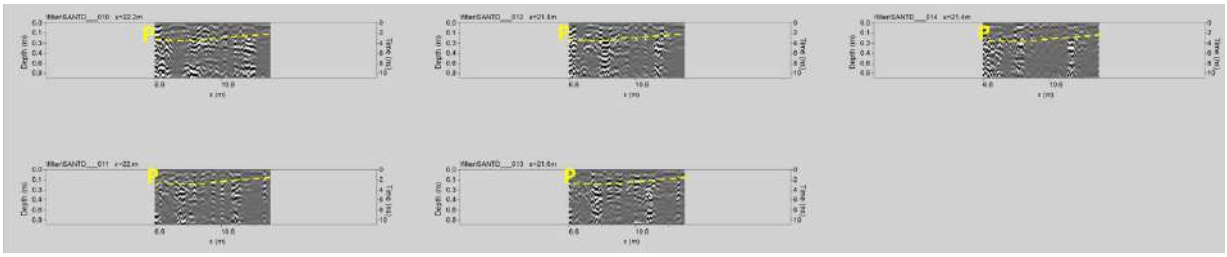

Fig. 133: Area D: processed GPR profiles 10, …14 (P: paving thickness)

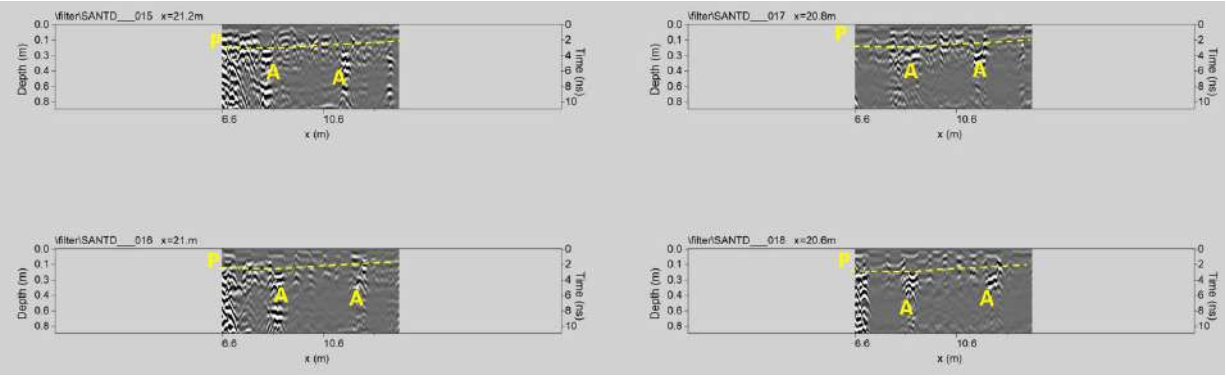

Fig. 134: Area D: processed GPR profiles 15, …, 18 (P: paving thickness; A: archaeological structures)

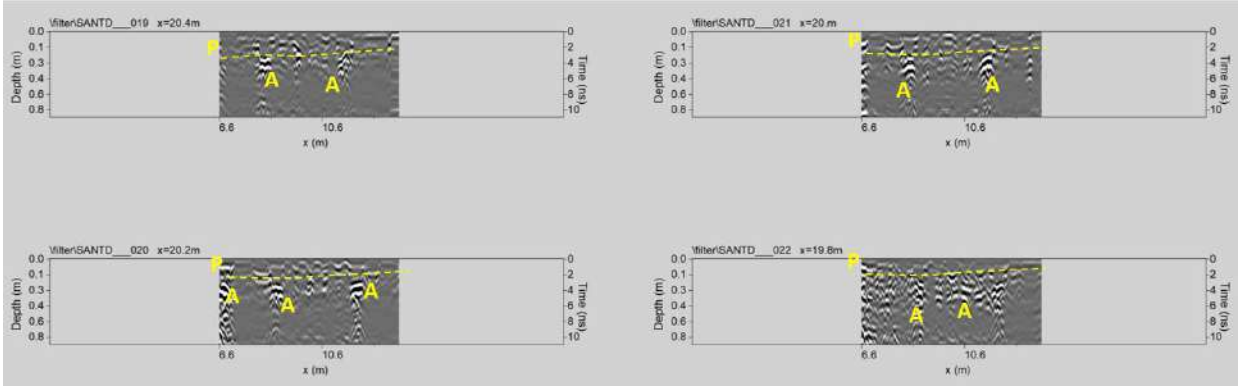

Fig. 135: Area D: processed GPR profiles 19, …, 22 (P: paving thickness; A: archaeological structures)

AREA E: The processed GPR profiles acquired in area E are shown in Figs. 136 and 137.
The reflection event evidenced by a dashed yellow line (labelled P) is probably related to the paving. Here the thickness of the paving seems to vary between 0.1m and 0.2m.
The reflection events labelled T is related to the manholes visible on the surface.
Some reflection events labelled S at a depth of about 0.3 m are probably related to underground services (pipes).

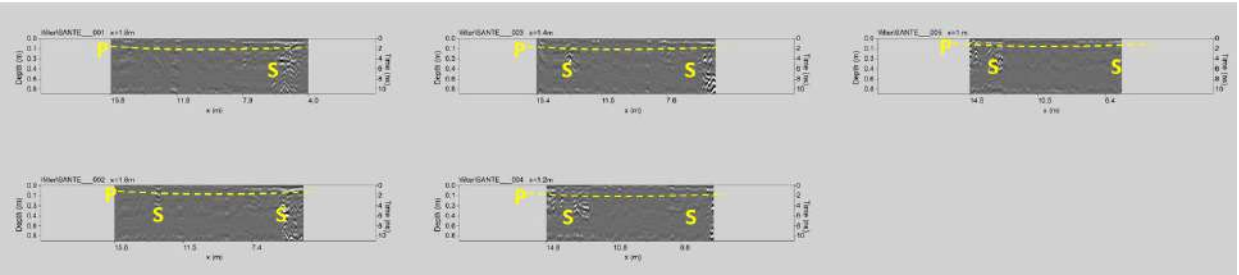

Fig. 136: Area E: processed GPR profiles 1, …, 5 (P: paving thickness; S: underground services)

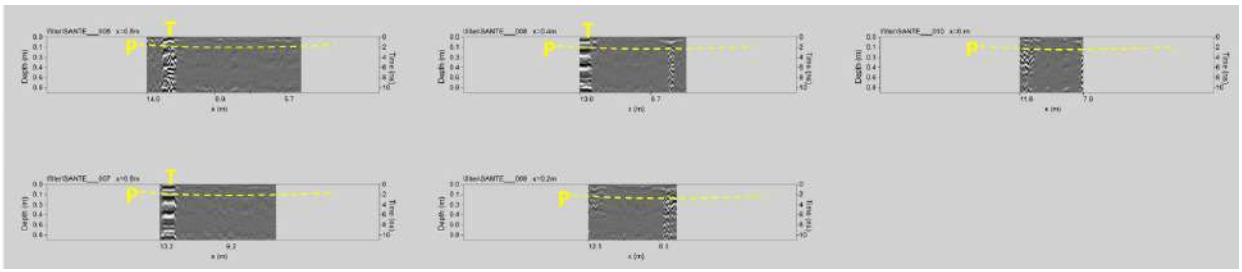

Fig. 137: Area E: processed GPR profiles 6, …, 10 (P: paving thickness; T: manhole)

Fig. 138 shows a pseudo-3D representation of the 2D GPR profiles.

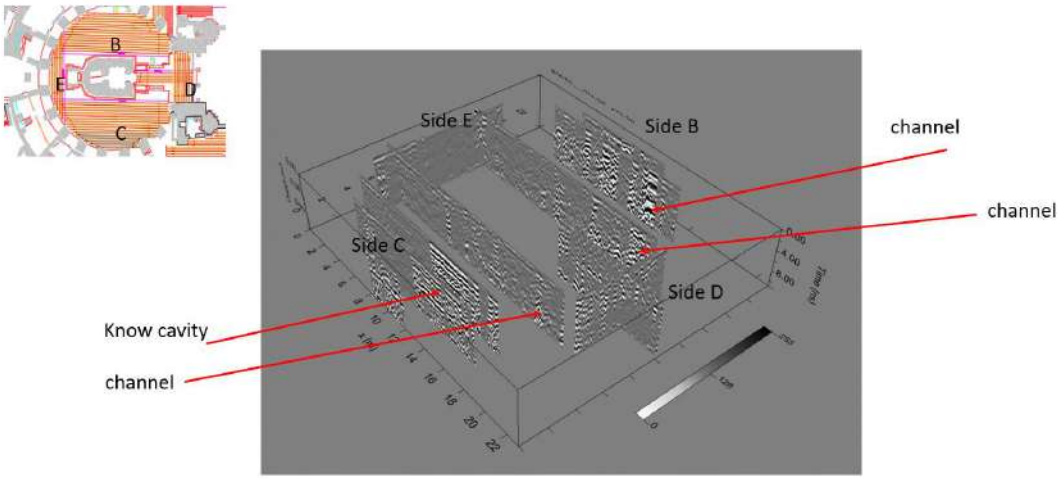

Fig. 138: the whole Area: pseudo-3D visualization of the 2D GPR profiles

Area B+C+D+E: 3D visualization: The time-slice technique has been used to display the amplitude variations within consecutive time windows of width Δt=1 ns.
Figs. 139,…, 142 shows the depth slices from 0.0 m to 0.82 m in depth.

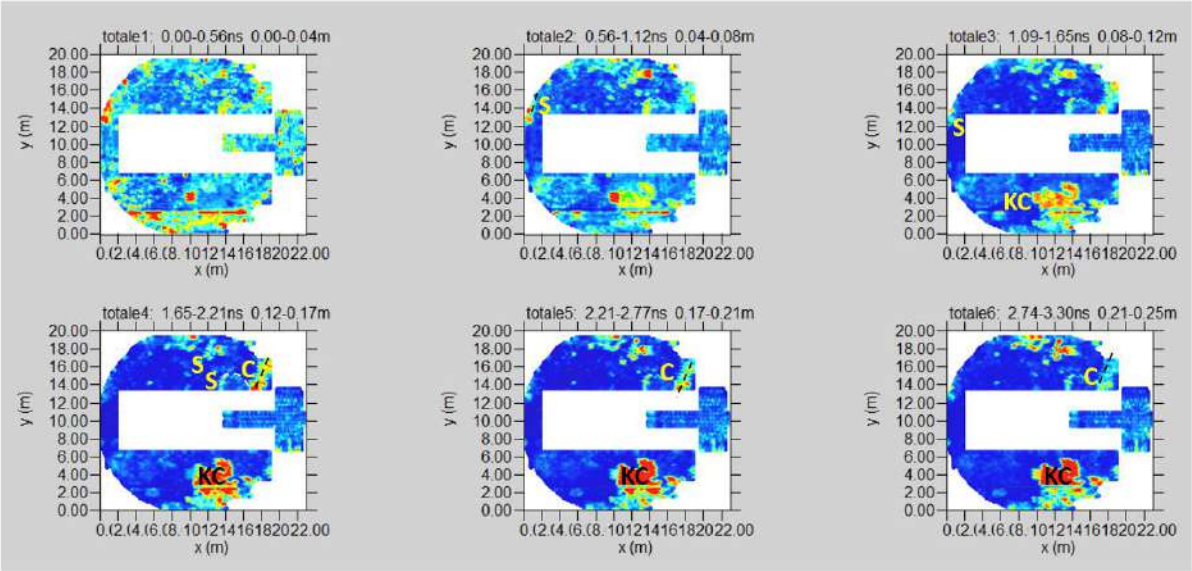

Fig. 139: the whole Area: Depth slices 0.0-0.25m (KC: Know cavity; C: channel; S: underground services –pipes)

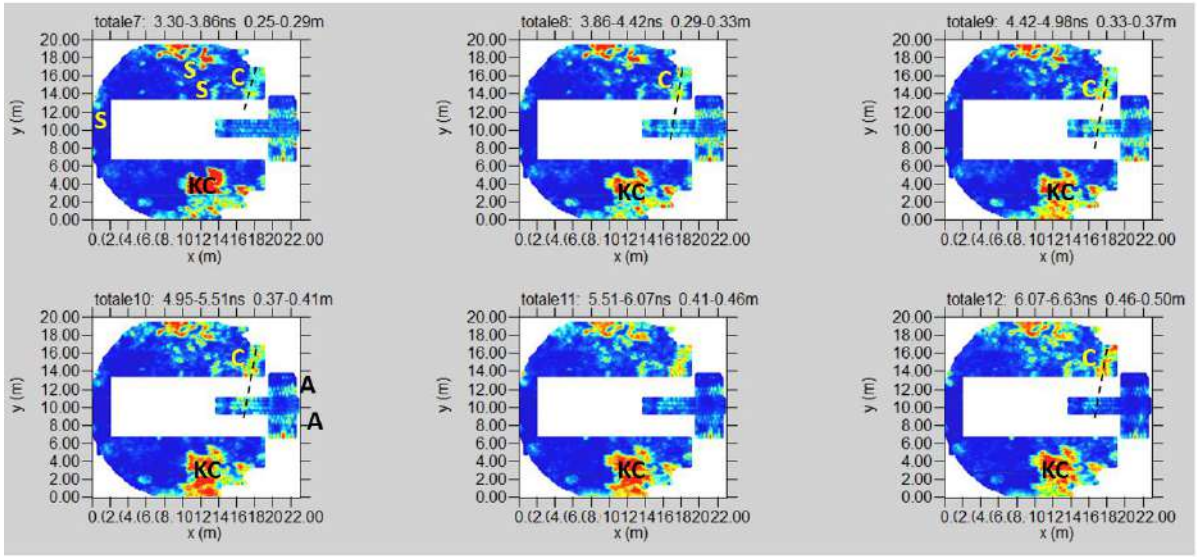

Fig. 140: the whole Area: Depth slices 0.25-0.5m (KC: Know cavity; A: archaeological structures; C: channel; S: underground services –pipes-)

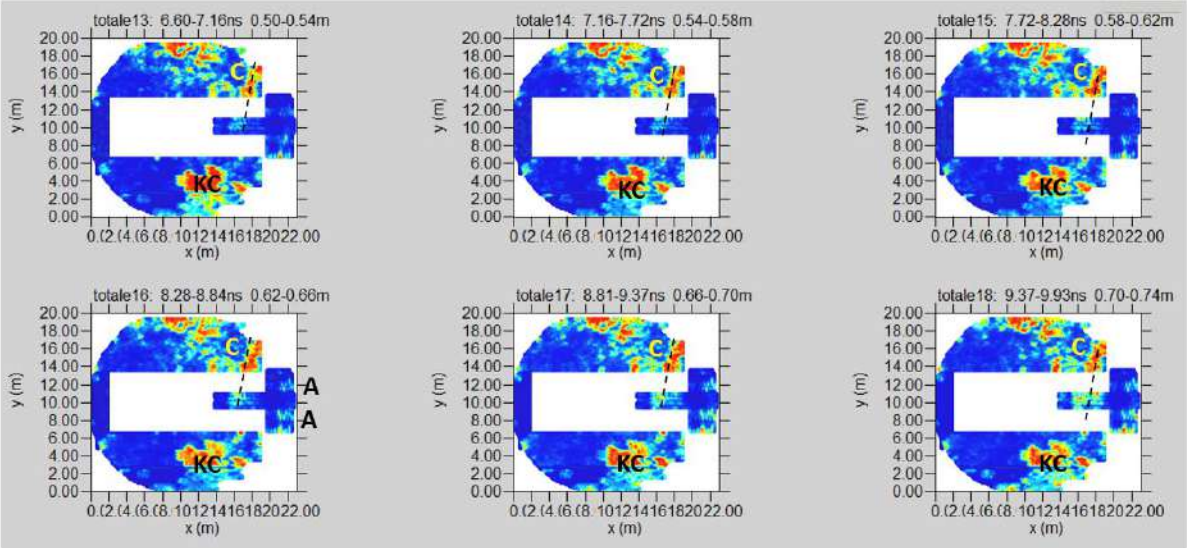

Fig. 141: the whole Area: Depth slices 0.5-0.74m (KC: Know cavity; A: archaeological structures; C: channel)

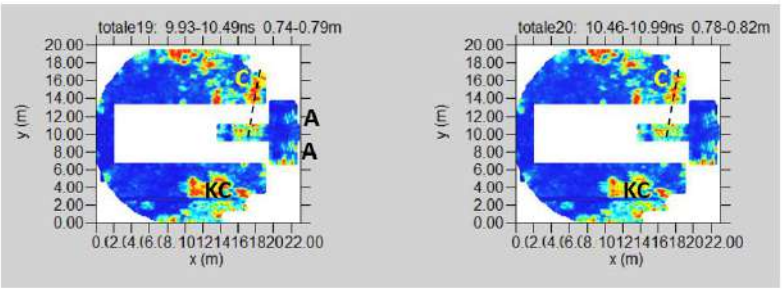

Fig. 142: the whole Area: Depth slices 0.74-0.82m (KC: Know cavity; A: archaeological structures; C: channel)

In the slices, relatively high-amplitude alignments (labelled S) are visible. These could be related to underground services (pipes). At depth, between 0.2m and 0.82m, the anomaly C represents a probable channel that develops at 0.6-0.8m in depth. The anomaly A at a depth of about 0.37m could be related to an old structure (archaeological interest- may be a wall). It is also possible to see the shallow subsurface known cavity (KC).

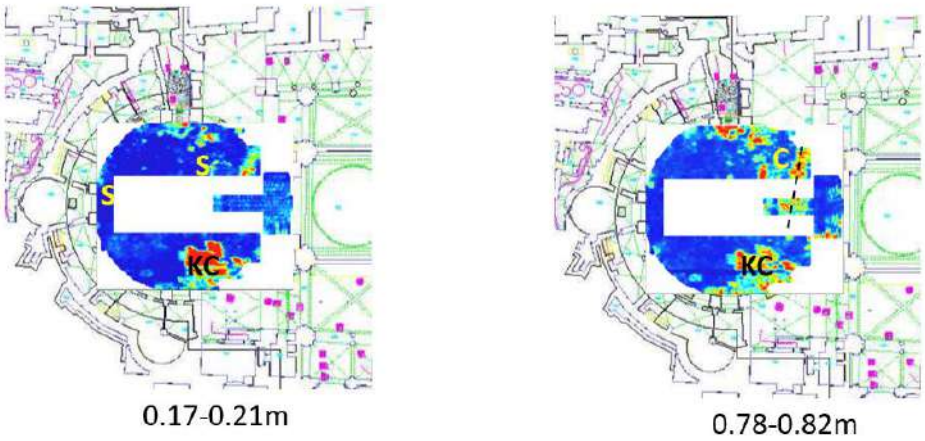

Fig. 143: the whole Area: depth slices overlapped to the planimetry

Fig 143 shows the more significant depth slices overlapped to the planimetry of the church. It is possible to see the position of the high amplitude anomalies A, the channel C, the know cavity KC and the probable pipes S.

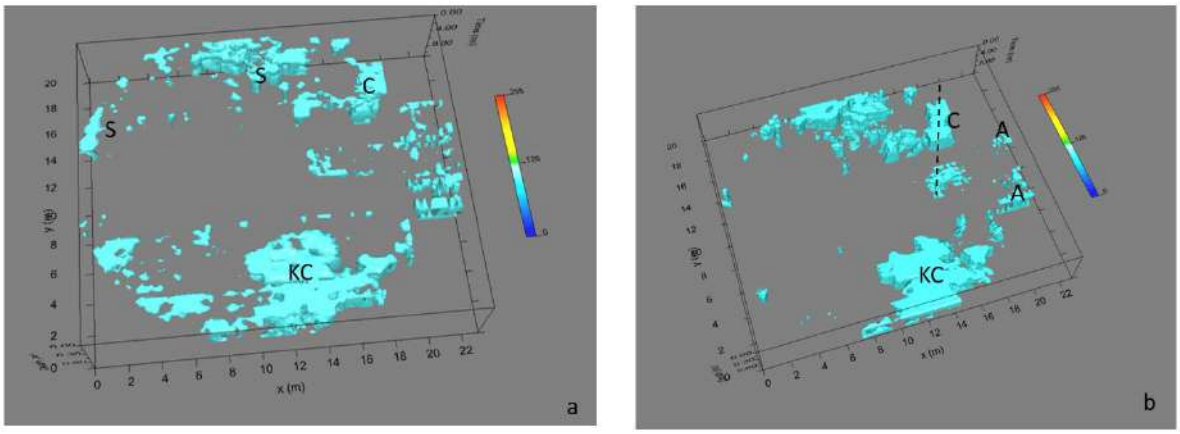

Fig. 144: the whole Area: electromagnetic amplitude isosurfaces: a) 0.0-0.17m depth threshold 40%; b) 0.37-0.79m depth threshold 38%

Fig. 144 show the iso-surface visualization. Here is possible to see the spatial position of the anomalies C, A, KC, and S. Fig. 145 show a virtual excavation. In this case, it is possible to see the position of the anomalous zones well.

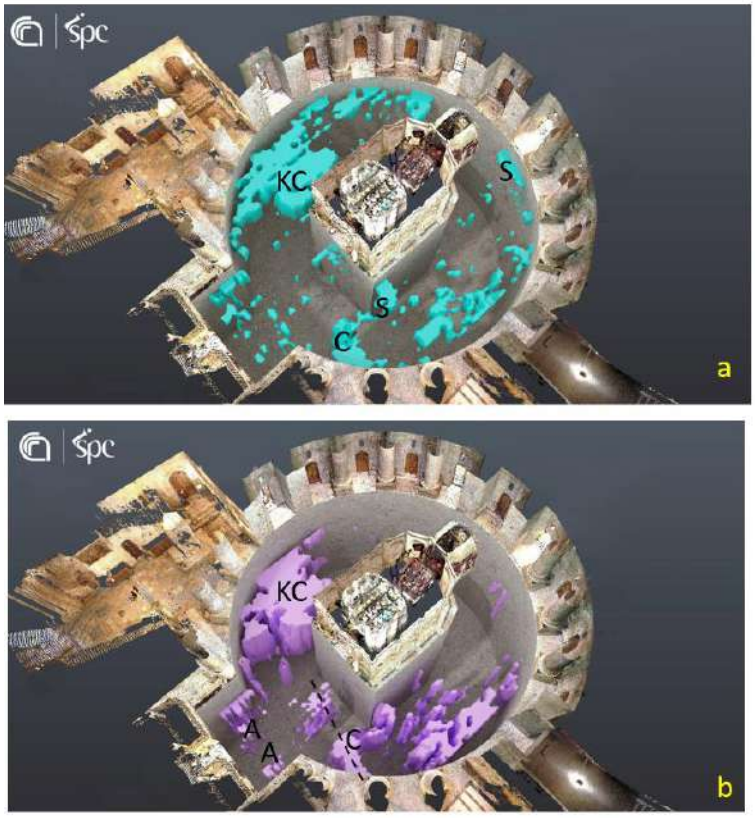

Fig. 145: the whole Area: virtual excavation: a) 0.0-0.17m depth threshold 40%; b) 0.37-0.79m depth threshold 38%

Area B+C+D+E: EM-WAVE VELOCITY ANALYSIS AND MOISTURE MAP

The EM-wave velocity plays an essential role in defining shallow subsurface water content. Numerous studies have used GPR techniques to determine subsurface moisture (Annan et al. 1990; Du and Rummel 1994; Mellet 1995; Grandjean et al. 2000; Leucci, 2019).

However, since each technique is generally considered individually and is efficient only in a specific context, it isn't easy to compare the results because of different field conditions. For the GPR frequency band, the velocity of EM-waves propagating in the ground depends on the relative dielectric permittivity (i.e. the real part of the dielectric constant K) of the material; it is given by the simplified equation (Davis and Annan 1989),

$v=c/K^{1/2}$ (1)

where c is the EM-wave velocity in a vacuum (0.30 m/ns).

Hence, K can be determined directly from the EM-wave velocity. For pure water, K is about 80, while for most dry geological material, it varies between 4 and 10. If only a tiny amount of

water is contained in the material, the value of K will increase considerably and, conversely, the EM-wave velocity will decrease significantly. Thus K is a good measure of the water content in the ground.

Several formulae have been developed, both theoretically and empirically, to give the dielectric response of heterogeneous mixtures such as water-saturated soils. One such formula is the complex refractive index method (CRIM) equation, often used to interpret EM logging data (Greaves et al. 1996). The major problem with the CRIM formula is that it does not consider the geometrical information about the internal structure of rocks and the microscopic fluid distribution. This has a significant effect on the dielectric properties of partially saturated rocks (Endrea and Knight 1992). The above restriction may be overcome by using the Hanai–Bruggeman formula (Endrea and Knight 1992).

The main problem with the two previous approaches is that it is impossible to derive both the porosity and water content from the dielectric constant. Therefore, it is impossible to obtain information about the water content without strong a priori assumptions. For this reason, it is preferable to use the well-known empirical equation derived by Topp et al. (1980), relating the dielectric response K of various soil samples (with different degrees of saturation) to their net water content w.
This formula is given by

$$w = -5.3\times10^{-2} + 2.92\times10^{-2}(K) - 5.5\times10^{-4}(K)^2 + 4.3\times10^{-6}(K)^3 \quad (2)$$

This equation was nearly independent of soil texture, soil bulk density, temperature and soil salinity (Du and Rummel, 1994). Here, the volumetric water content was determined from the dielectric properties of subsurface material, using the above empirical relationship (2).
The EM-wave velocity can be estimated from GPR data in several ways (Conyers and Goodman 1997; Huisman et al. 2003); the conventional methods involve common depth-point (CDP) and wide-angle reflection and refraction (WARR) data sets. Both ways require two antennae in separate units and relatively long acquisition times. In the first case, both antennae are simultaneously moved apart on either side of the midpoint of the profile. In the second case, the position of one antenna is fixed while the other is moved along the profile direction. The EM-wave velocity can be more quickly and easily determined from the reflection profiles acquired in continuous mode, using the characteristic hyperbolic shape of reflection from a point source (Fruhwirth et al., 1996). This is a widespread velocity estimation method, and it is based on the phenomenon that a small object reflects EM waves in almost every direction. In the data set, several hyperbolic reflections caused by objects of small dimensions are present, enabling EM wave velocity analysis to be performed. This software used for data processing (GPR-slice) allows the interactive velocity adaptation of a diffraction or reflection hyperbola by calculating a hyperbola of defined velocity and width. The velocities are combined into a 2D model using a particular interpolation method. The interpolation is performed as follows: all actual velocities are summed for every point in the x–t range, proportional to the square of their distance from the (x, t) point. This method provides only the average EM-wave velocity to the depth of the source-point reflector. The EM-wave velocity was determined from the point-source reflections. This method gives RMS EM-wave velocities to the depth of the point-source reflector. Since in all radar sections acquired in the crypt, any interfaces with changes in EM-wave velocities between the surface and the target depth level are recorded, and the errors involved, compared to those obtained using interval velocities, are about 0.35%, this early application, which uses a point-source reflection from a buried object to determine the average velocity, gives an accurate (qualitative) estimate of the subsoil volumetric water-content in the crypt. Application of this method provides both vertical (in time, hence in depth) and lateral velocity variations from 0.07 m/ns to 0.15 m/ns. By applying the empirical Topp formula (equation (2)), we then estimate the average volumetric water content of the soil down to the depth of the point-source reflector.
Figs. 146,…, 148 shows the depth slices with volumetric water content in depth between 0.1m and 0,67m. The slices show a volumetric water content that varies from 7% to 38%. The volumetric water content plan distribution shows high volumetric water content at a depth between 0.11m to 0.14m (Fig. 146). The volumetric water content seems to decrease in depth. In the deeper slices (Fig. 148), there are some zones (H) in which the volumetric water content is high (38%). There appears to be a significant rise in humidity from these zones.

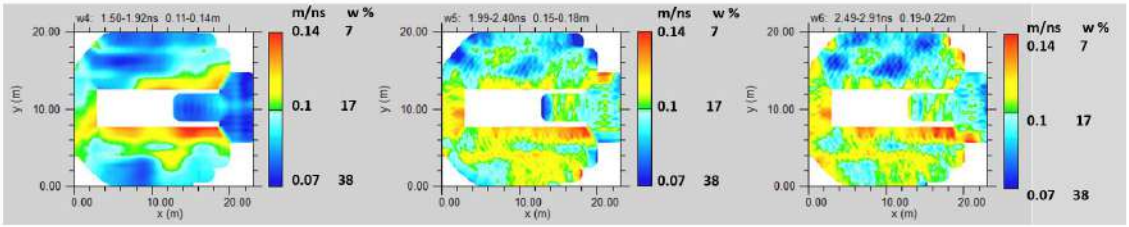

Fig. 146: the whole Area: Volumetric water content (w) and electromagnetic wave velocity (m/ns) at depth from 0.11 to 0.22m

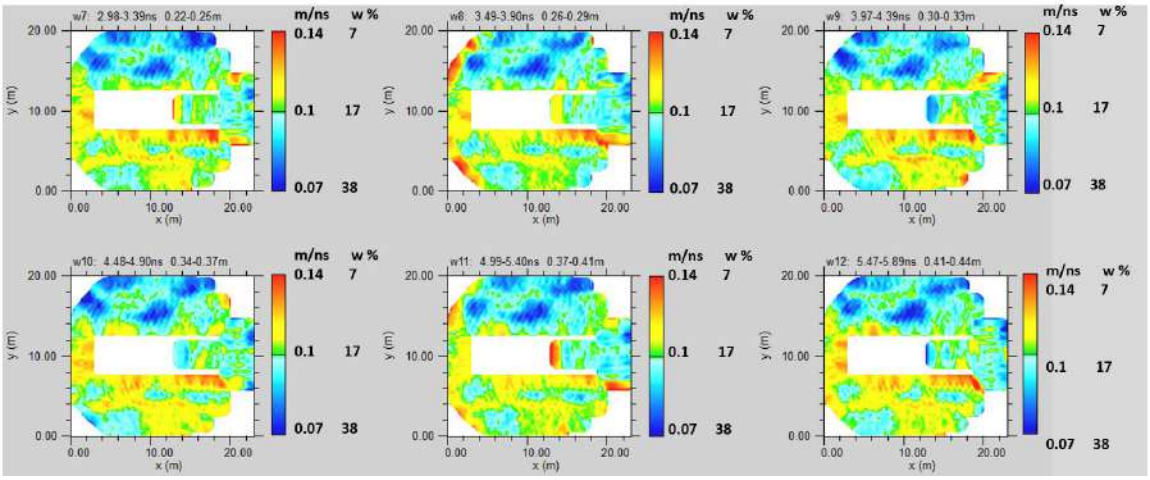

Fig. 147: the whole Area: Volumetric water content (w) and electromagnetic wave velocity (m/ns) at depth from 0.22 to 0.44m

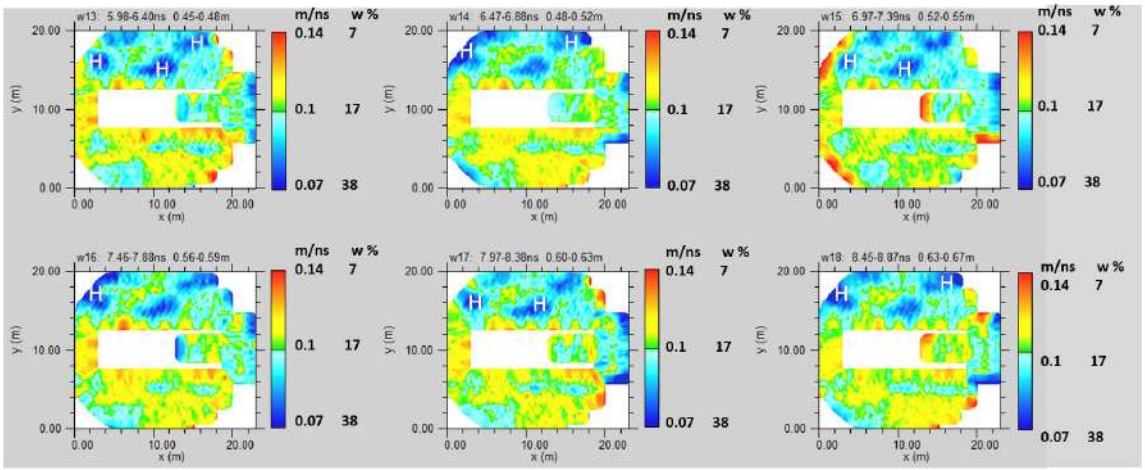

Fig. 148: the whole Area: Volumetric water content (w) and electromagnetic wave velocity (m/ns) at depth from 0.45 to 0.67m

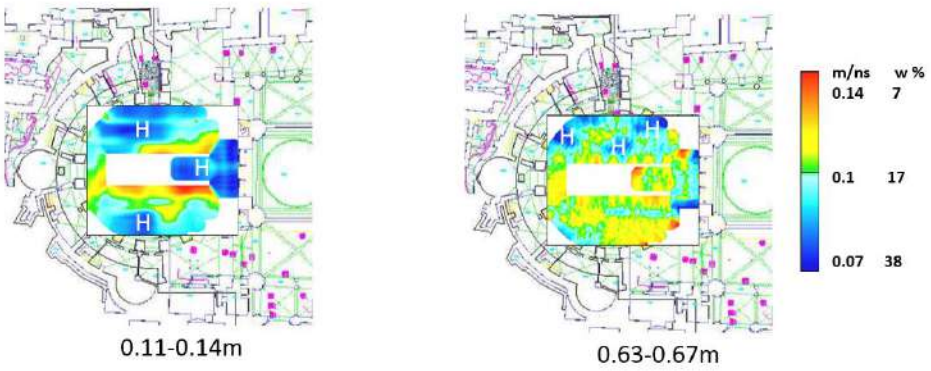

Fig. 149: the whole Area: volumetric water content depth slices overlapped to the planimetry

Fig. 149 shows the volumetric water content depth slice overlapped to the planimetry.

Area F+G+R

In the area, F+G+R have acquired 82 GPR profiles for an extension of 995.0 meters (Fig. 150).

The GPR data profiles were processed in 2D using GPR-slice software (GPR-SLICE Software (gpr-survey.com)). To eliminate a small noise component and make it easy to interpret GPR data, the following processing sequence was applied:

1) Zero-time adjust (static shift), to associate zero-time with zero-depth;
2) Background removal;
3) Frequency filtering, to remove high-frequency noise;
4) Migration, to correct the shape and dimension of reflection events related to the structure present in the subsoil.

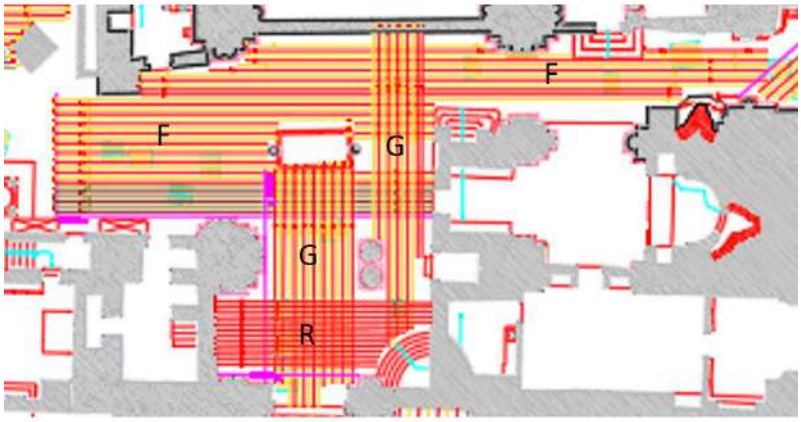

Fig. 150: Area F, G and R: location of GPR profiles

AREA F: The processed GPR profiles acquired in area F are shown in Figs. 151,…, 160.

The reflection event evidenced by a dashed yellow line (labelled P) is probably related to the paving. Here the thickness of the paving seems to vary between 0.1m and 0.3m.

The T's reflection events are related to the manholes visible on the surface.

The reflection events labelled D at a depth of about 0.7m are related to a probable old structure.

Some reflection events labelled S at a depth of about 0.3 m are probably related to underground services (pipes).

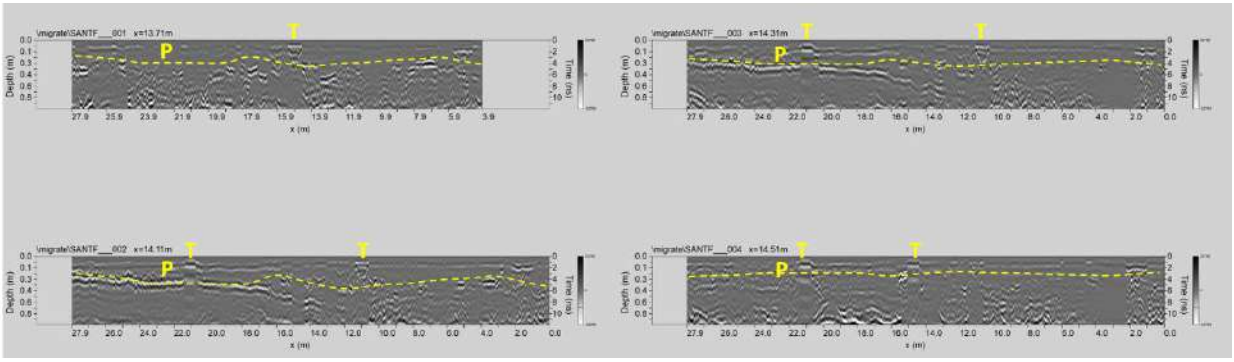

Fig. 151: Area F: processed GPR profiles 1, …, 4 (T: manhole; P: paving thickness)

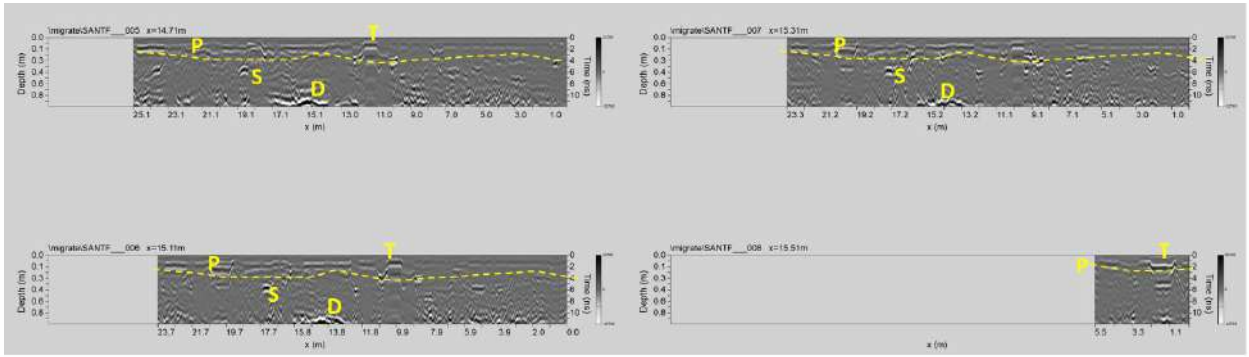

Fig. 152: Area F: processed GPR profiles 5, …, 8 (T: manhole; P: paving thickness; D: structure; S: underground services)

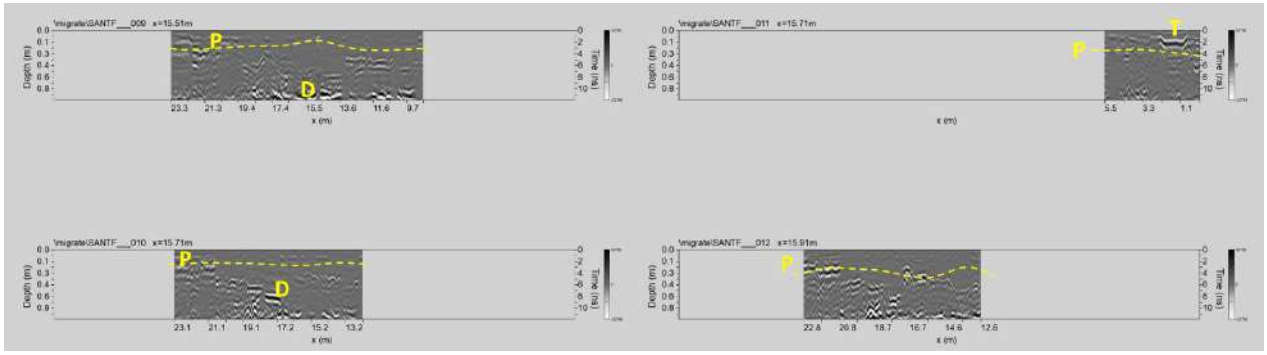

Fig. 153: Area F: processed GPR profiles 9, …, 12 (T: manhole; P: paving thickness; D: structure)

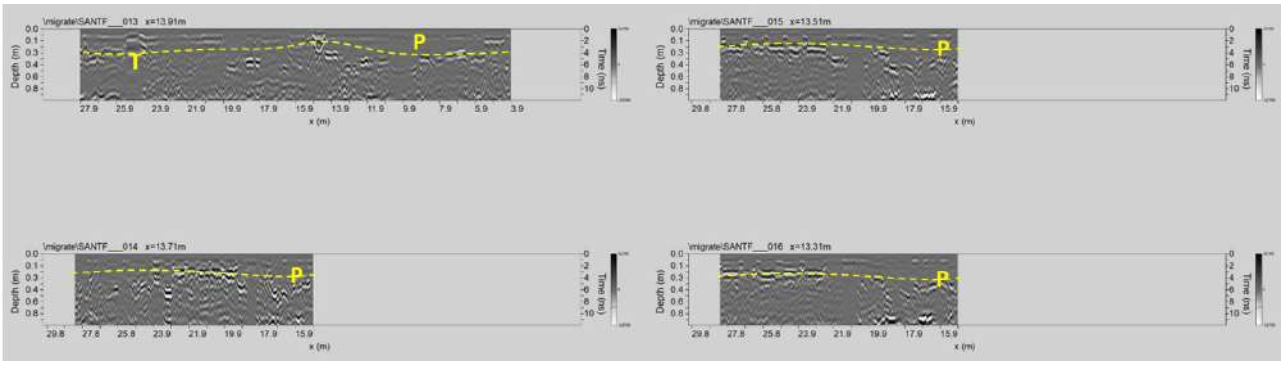

Fig. 154: Area F: processed GPR profiles 13, …, 17 (T: manhole; P: paving thickness)

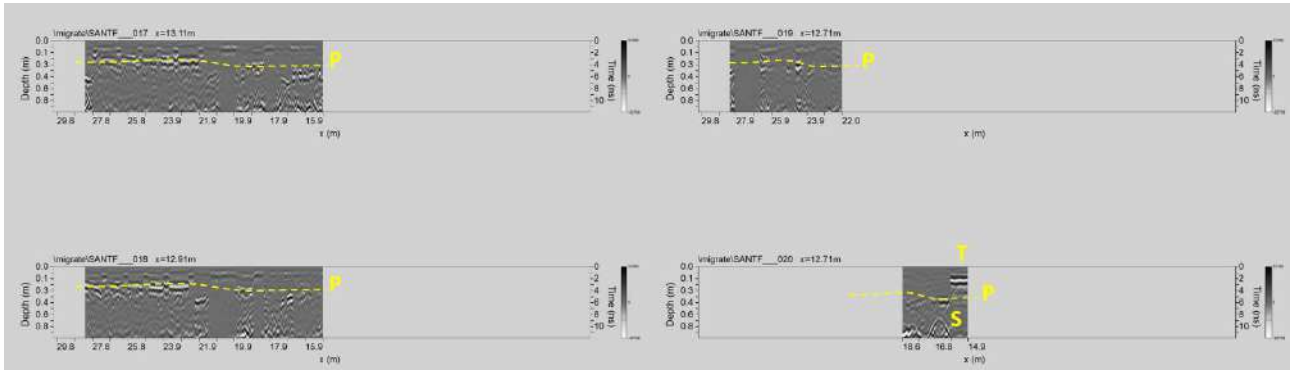

Fig. 155: Area F: processed GPR profiles 17, …, 20 (T: manhole; P: paving thickness; S: underground services)

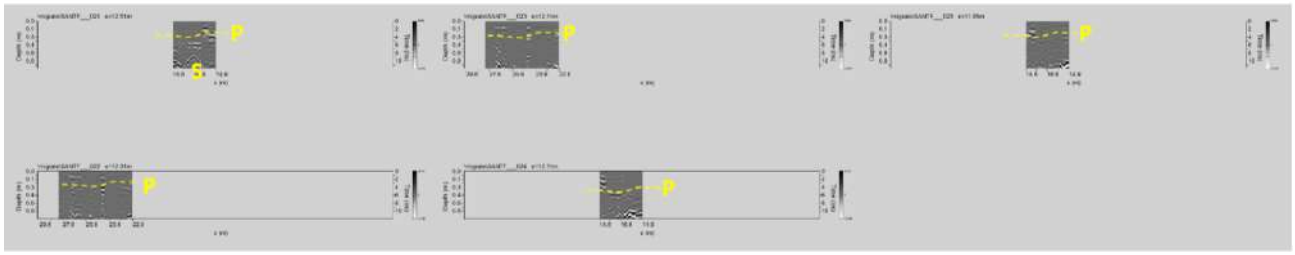

Fig. 156: Area F: processed GPR profiles 21, …, 25 (P: paving thickness; S: underground services)

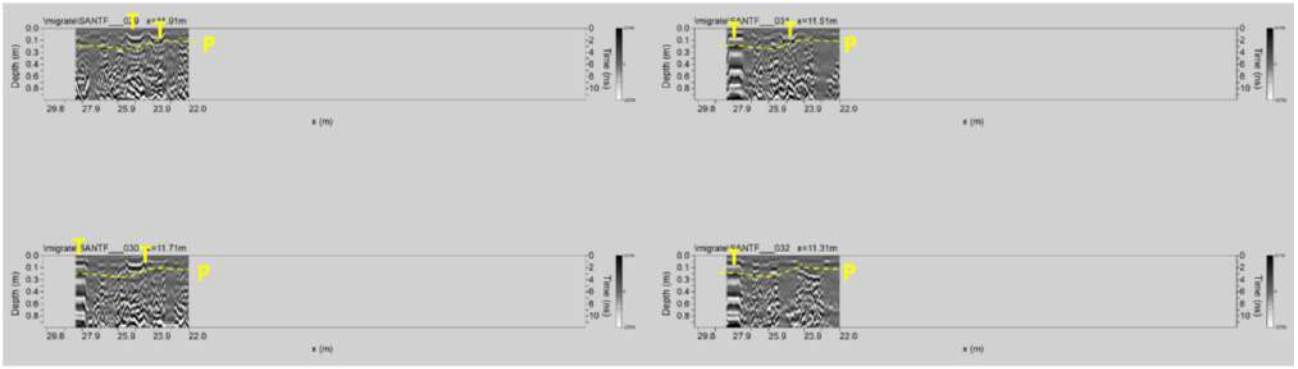

Fig. 157: Area F: processed GPR profiles 29, …, 32 (T: manhole; P: paving thickness)

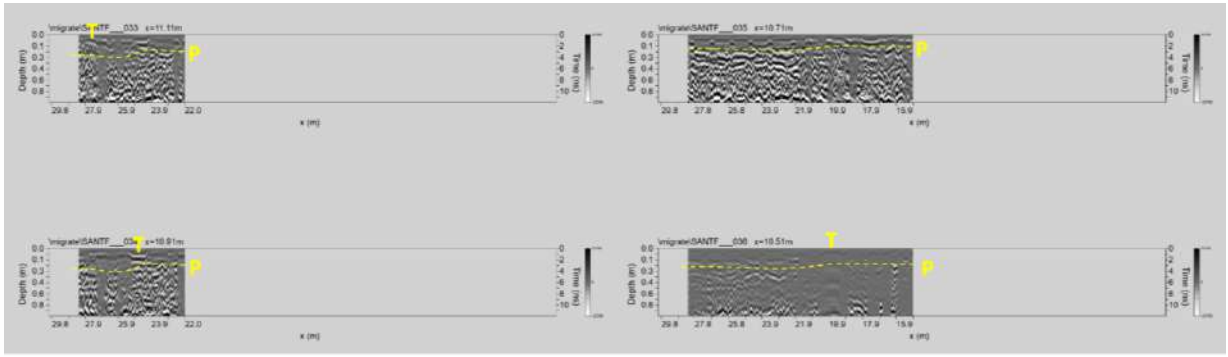

Fig. 158: Area F: processed GPR profiles 33, …, 36 (T: manhole; P: paving thickness)

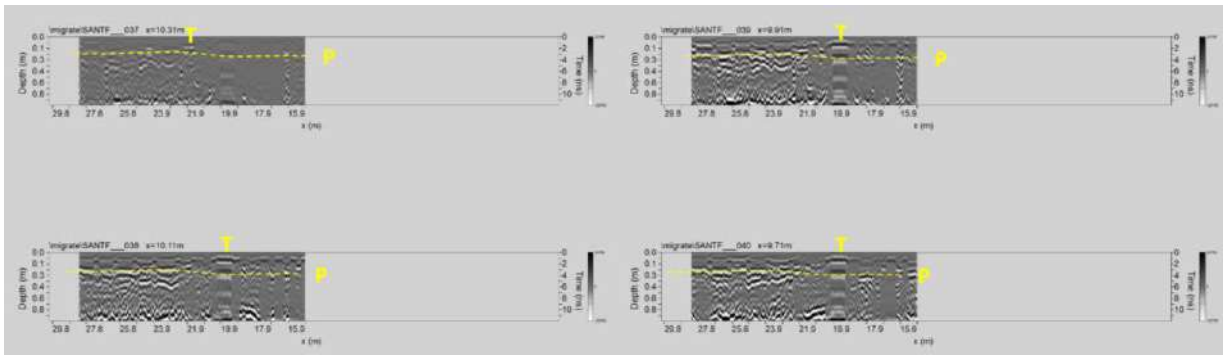

Fig. 159: Area F: processed GPR profiles 37, …, 40 (T: manhole; P: paving thickness)

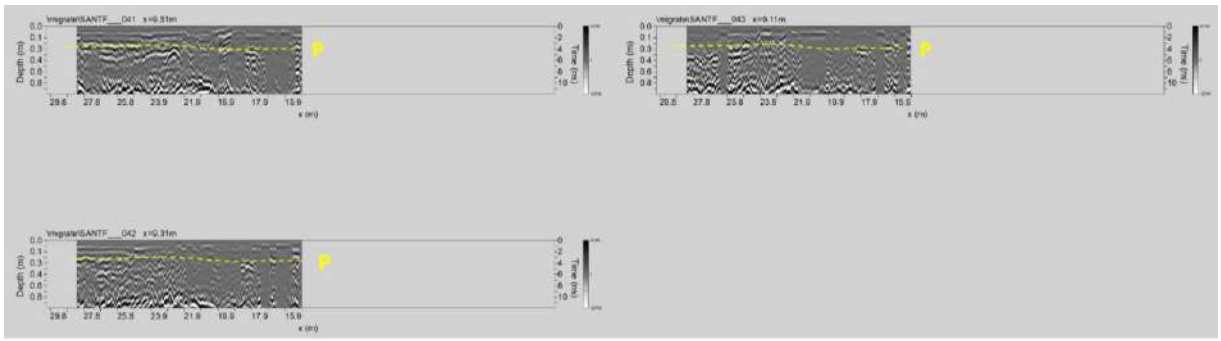

Fig. 160: Area F: processed GPR profiles 41, …, 43 (T: manhole; P: paving thickness)

AREA G: The processed GPR profiles acquired in area G are shown in Figs. 161,…, 167.
The reflection event evidenced by a dashed yellow line (labelled P) is probably related to the paving. Here the thickness of the paving seems to vary between 0.1m and 0.35m.
The T's reflection events are related to the manholes visible on the surface.
Some reflection events labelled S at a depth of about 0.3 m are probably related to underground services (pipes).

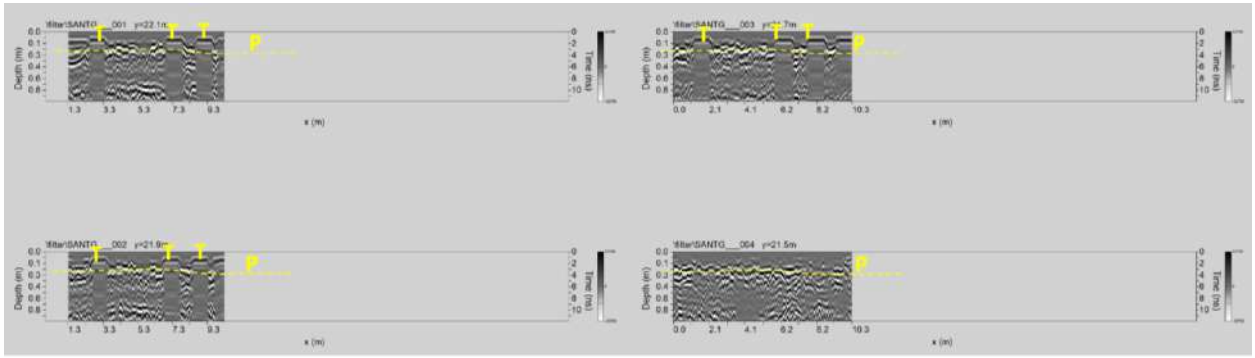

Fig. 161: Area G: processed GPR profiles 1, …, 4 (T: manhole; P: paving thickness)

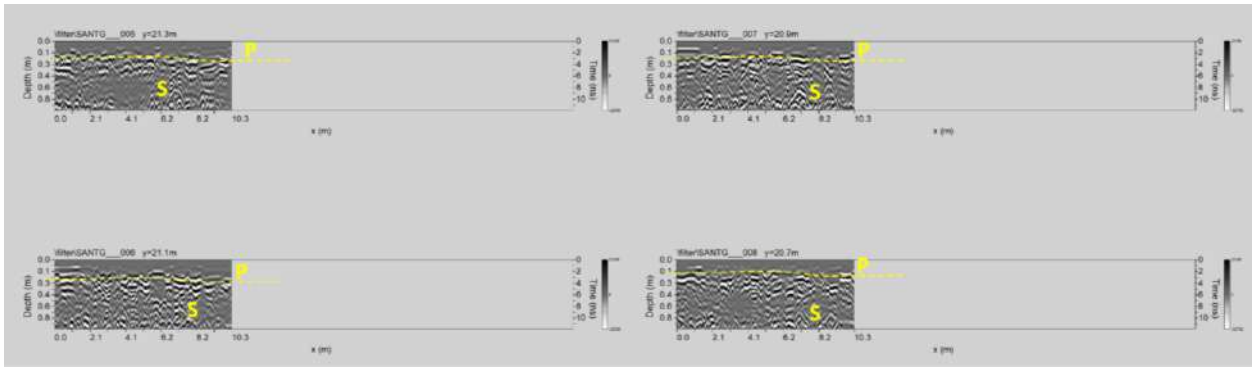

Fig. 162: Area G: processed GPR profiles 5, …, 8 (P: paving thickness; S: underground services)

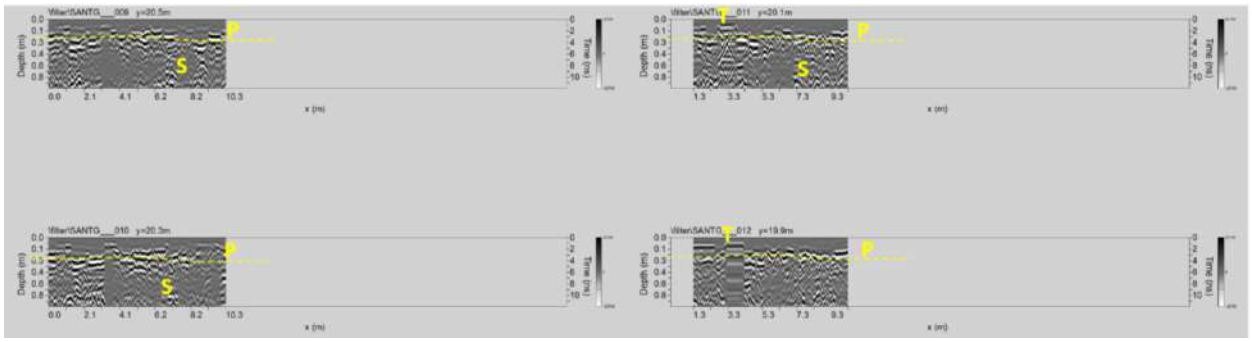

Fig. 163: Area G: processed GPR profiles 9, …, 12 (T: manhole; P: paving thickness; S: underground services)

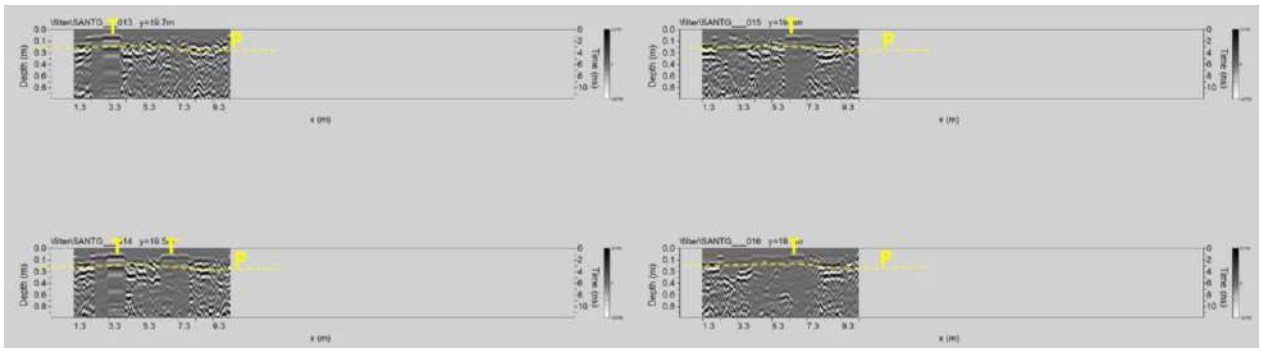

Fig. 164: Area G: processed GPR profiles 13, …, 16 (T: manhole; P: paving thickness)

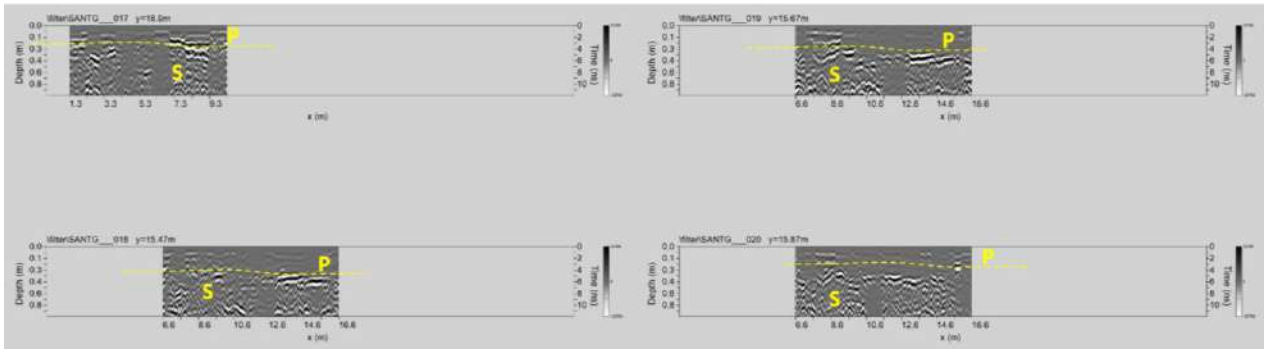

Fig. 165: Area G: processed GPR profiles 17, …, 20 (P: paving thickness; S: underground services)

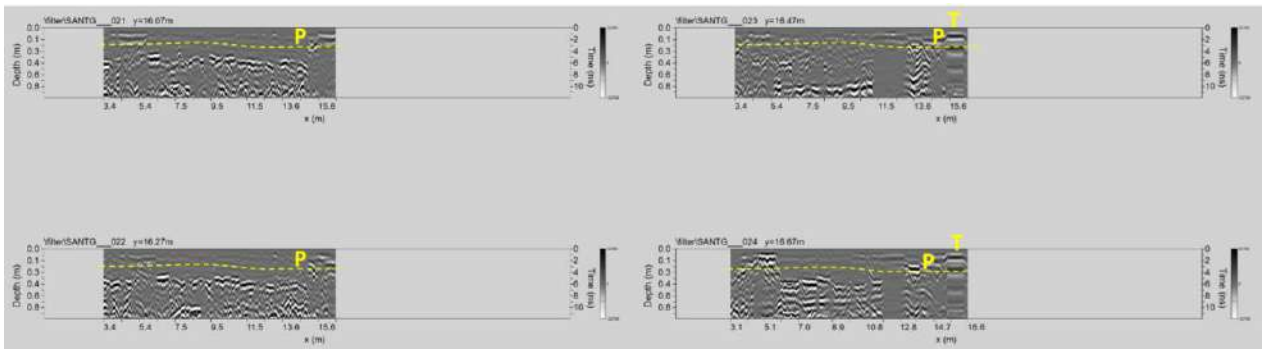

Fig. 166: Area G: processed GPR profiles 21, …, 24 (T: manhole; P: paving thickness)

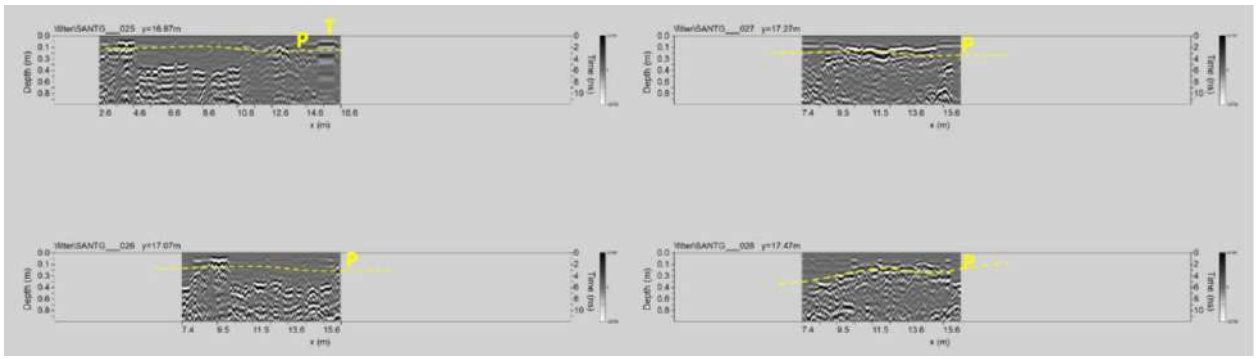

Fig. 167: Area G: processed GPR profiles 25, …, 28 (P: paving thickness; T: manhole)

AREA R: The processed GPR profiles acquired in area R are shown in Figs. 168,…, 171.
The reflection event evidenced by a dashed yellow line (labelled P) is probably related to the paving. Here the thickness of the paving seems to vary between 0.1m and 0.4m.
The reflection events labelled D visible at about 0.4m-0.5m depth could be related to an old structure.
The T's reflection events are related to the manholes visible on the surface.

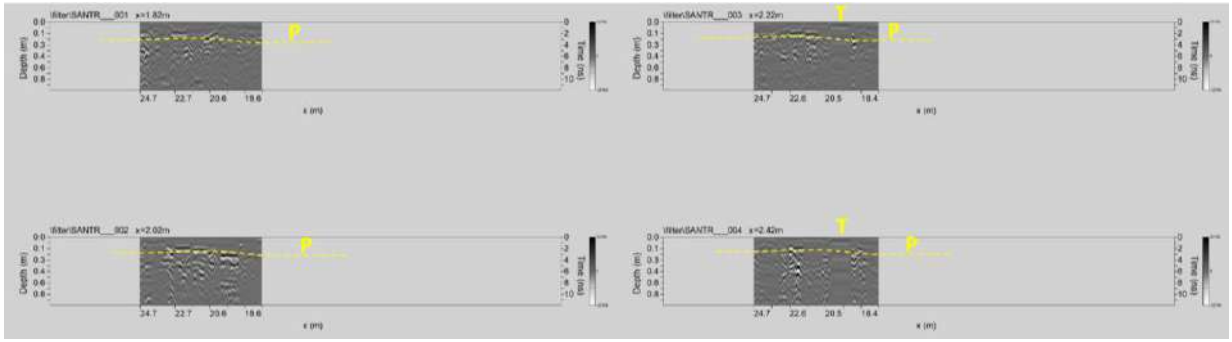

Fig. 168: Area R: processed GPR profiles 1,…, 4 (P: paving thickness; T: manhole)

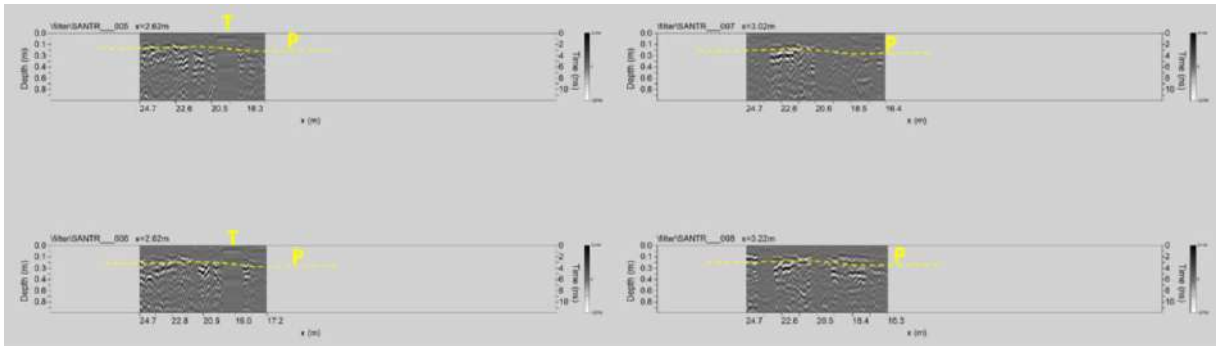

Fig. 169: Area R: processed GPR profiles 5, …, 8 (P: paving thickness; T: manhole)

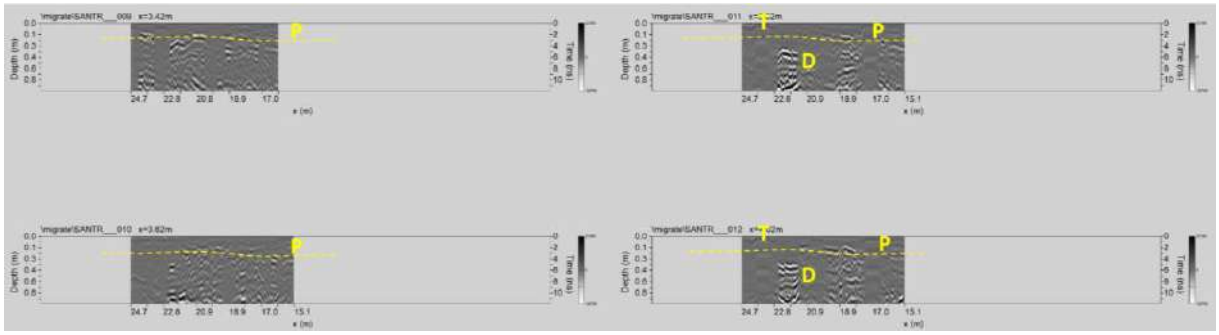

Fig. 170: Area R: processed GPR profiles 9, …12 (P: paving thickness; T: manhole; D: structure)

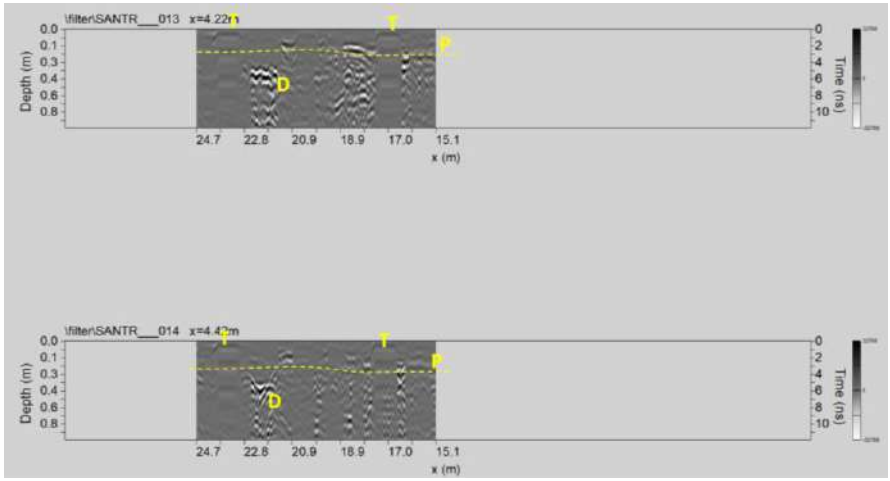

Fig. 171: Area R: processed GPR profiles 13 and 14 (P: paving thickness; D: structures; T: manhole)

Area F+G+R: 3D visualization: The time-slice technique has been used to display the amplitude variations within consecutive time windows of width Δt=1 ns.
Figs. 172,…, 175 shows the depth slices from 0.0 m to 0.74 m in depth.

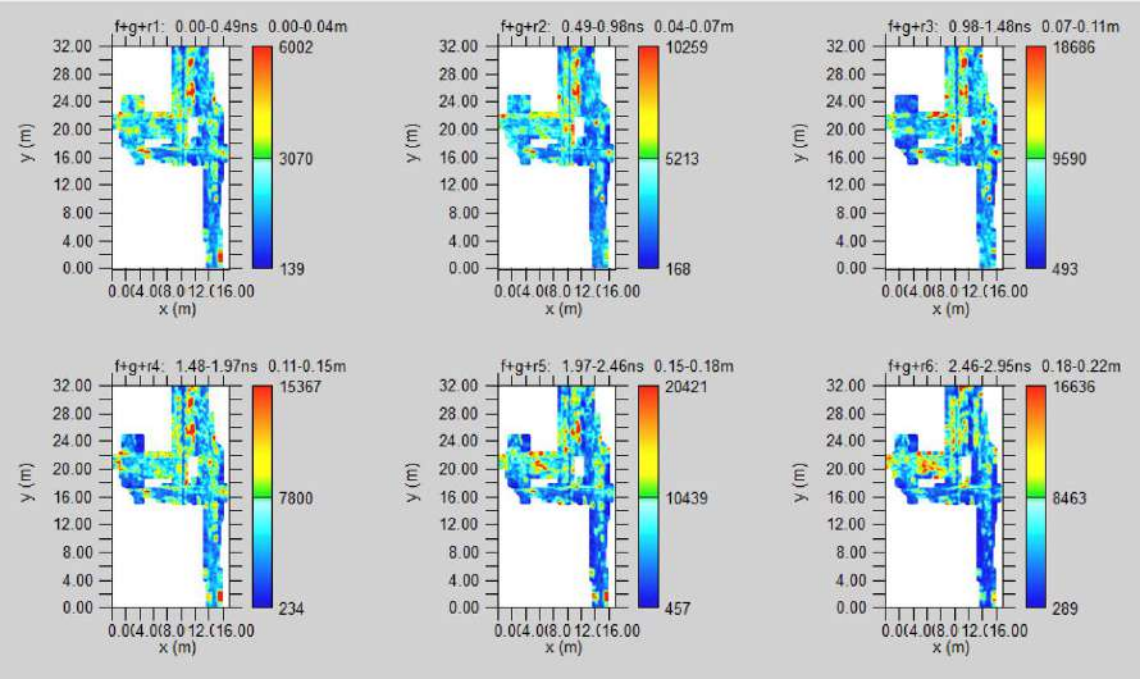

Fig. 172: the whole Area: Depth slices 0.0-0.22m

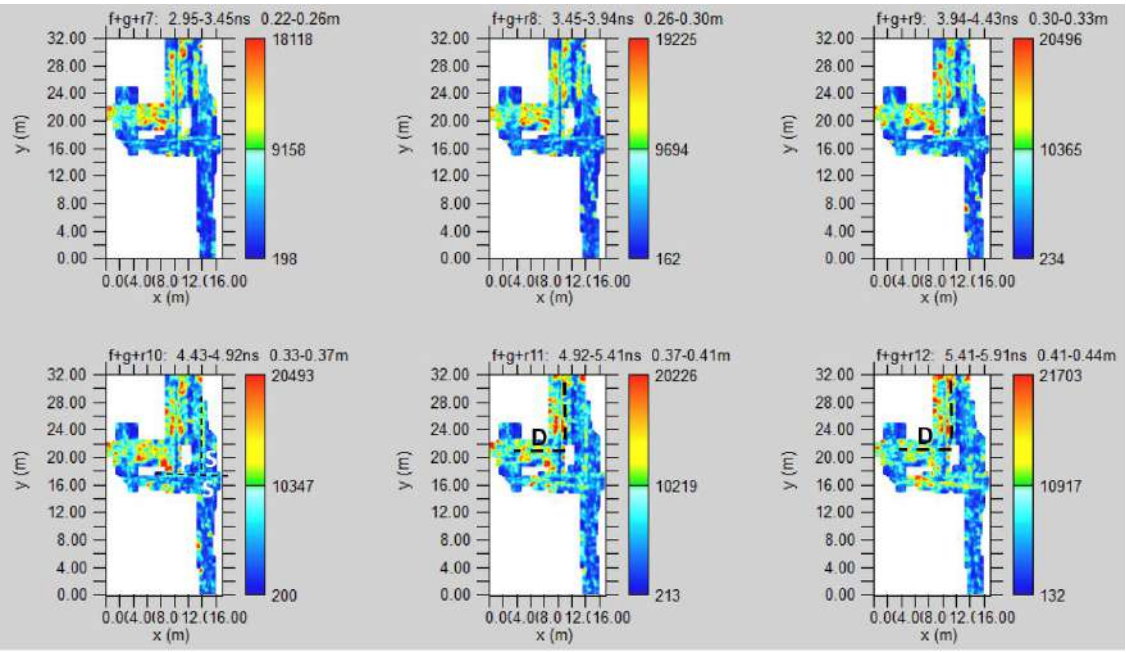

Fig. 173: the whole Area: Depth slices 0.22-0.44m (D: old structure-channel-; S: underground services –pipes-)

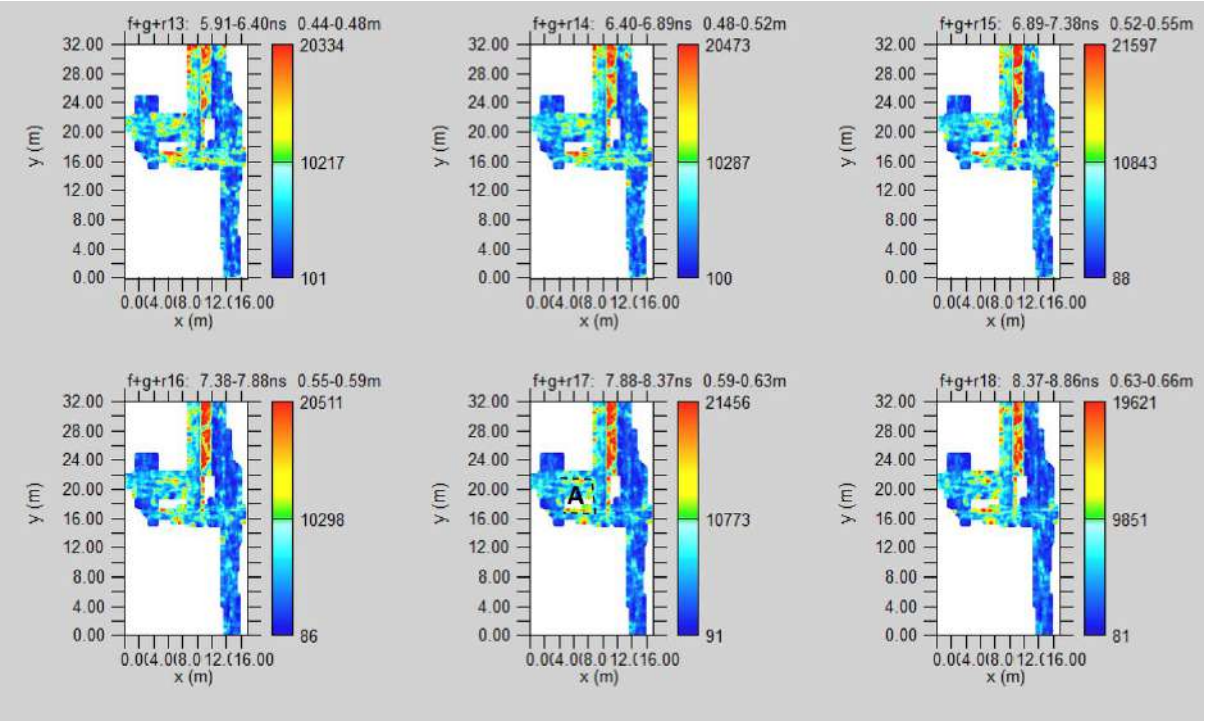

Fig. 174: the whole Area: Depth slices 0.44-0.66m (A: archaeological structures)

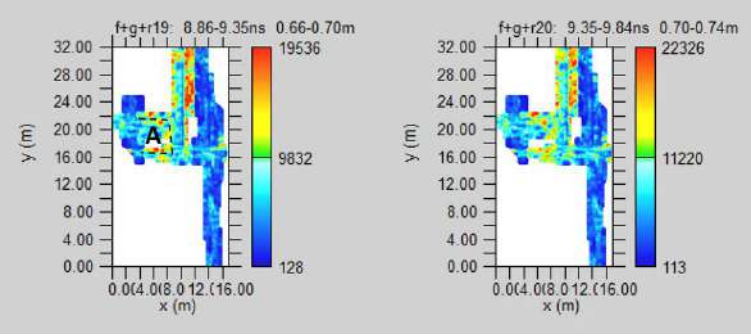

Fig. 175: the whole Area: Depth slices 0.66-0.74m (A: archaeological structures)

In the slices, relatively high-amplitude alignments (labelled S) are visible. These could be related to underground services (pipes). At depths between 0.37m and 0.44m (Fig. 173), the anomaly D represents a probable channel. The anomaly A at a depth of about 0.6m could be related to an old structure (archaeological interest- may be a wall).

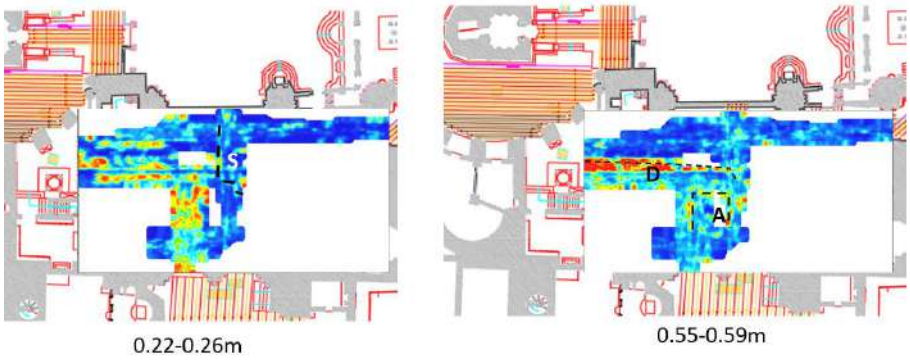

Fig. 176: the whole Area: depth slices overlapped to the planimetry (D: structure-channel-; A: archaeological structures; S: underground services)

Fig 176 shows the more significant depth slices overlapped to the planimetry of the church. It is possible to see the position of the high amplitude anomalies A, channel D, and the probable pipes S.

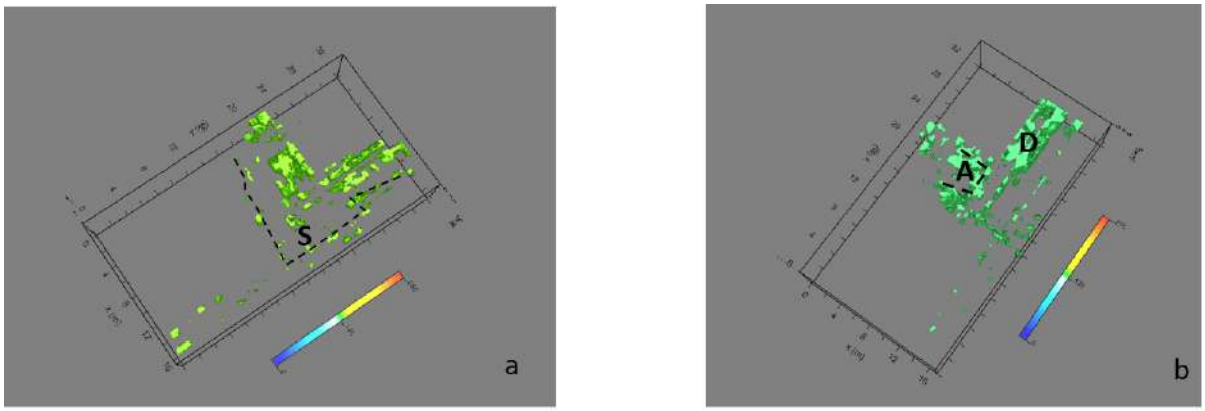

Fig. 177: the whole Area: electromagnetic amplitude isosurfaces: a) 0.15-0.33m depth threshold 55%; b) 0.33-0.59m depth threshold 50%

Fig. 177 show the iso-surface visualization. Here is possible to see the spatial position of the anomalies D, A, and S.
Fig. 178 show a virtual excavation. In this case, it is possible to see the position of the anomalous zones well.

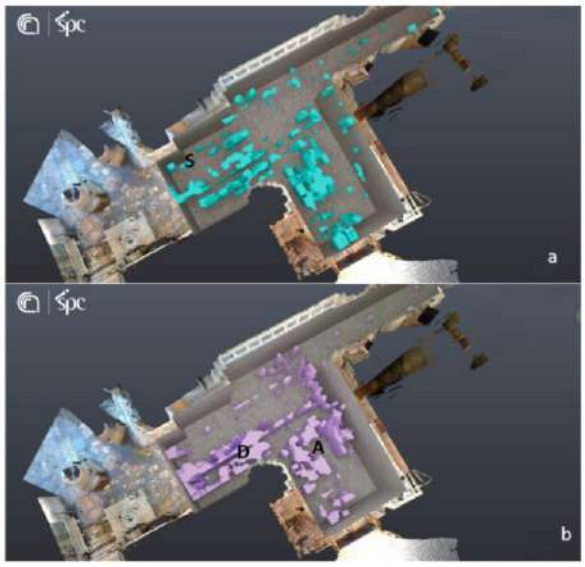

Fig. 178: the whole Area: virtual excavation: a) 0.15-0.33m depth threshold 55%; b) 0.33-0.59m depth threshold 50%

Area F+G+R: MOISTURE MAP

Figs. 179,…, 182 shows the depth slices with volumetric water content in depth between 0.11m and 0,74m. The slices show a volumetric water content that varies from 7% to 38%. The volumetric water

content plan distribution shows high volumetric water content at a depth between 0.11m to 0.63m. The volumetric water content seems to decrease in deeper slices.

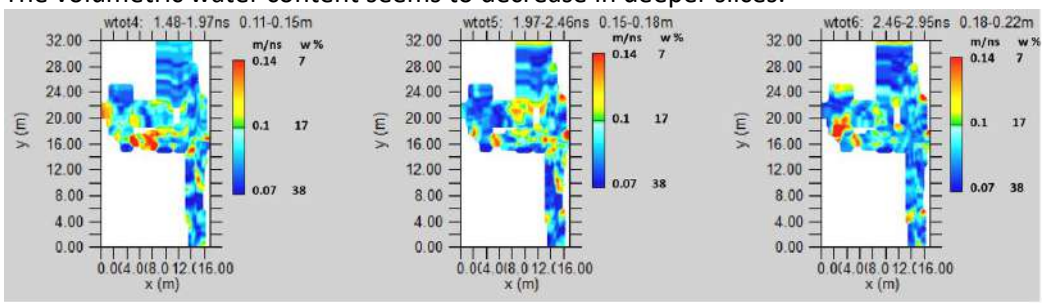

Fig. 179: the whole Area: Volumetric water content (w) and electromagnetic wave velocity (m/ns) at depth from 0.11 to 0.22m

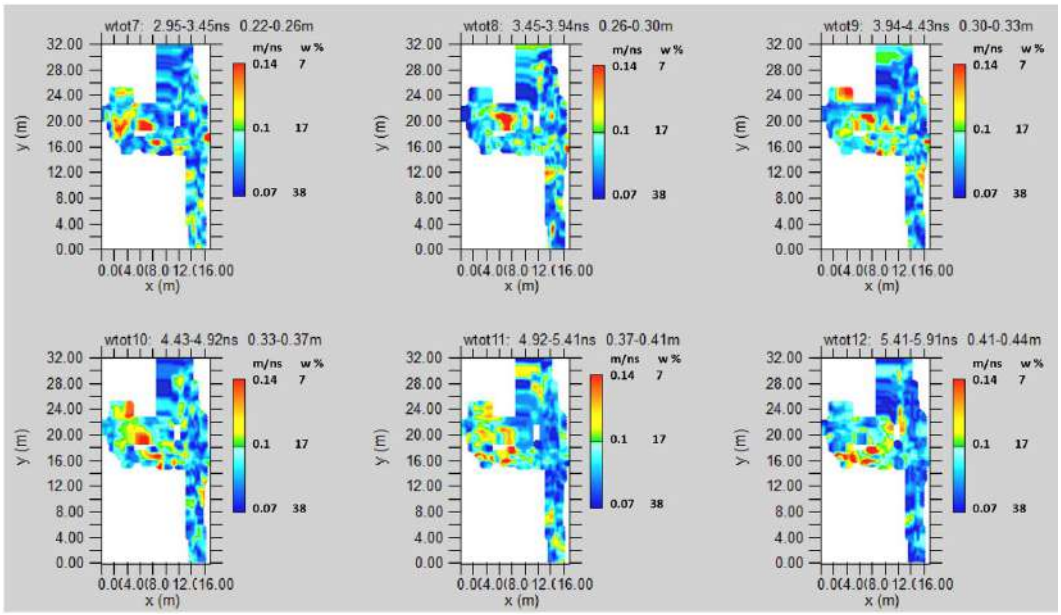

Fig. 180: the whole Area: Volumetric water content (w) and electromagnetic wave velocity (m/ns) at depth from 0.22 to 0.44m

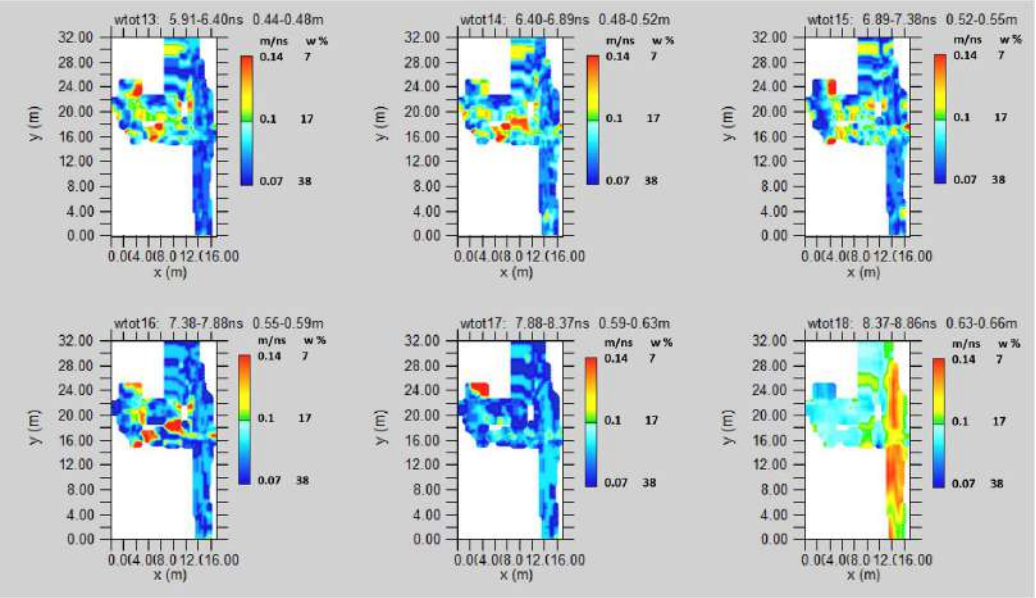

Fig. 181: the whole Area: Volumetric water content (w) and electromagnetic wave velocity (m/ns) at depth from 0.44 to 0.66m

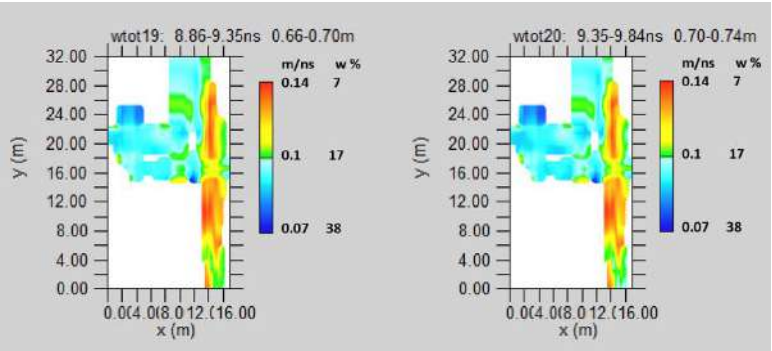

Fig. 182: the whole Area: Volumetric water content (w) and electromagnetic wave velocity (m/ns) at depth from 0.66 to 0.74m

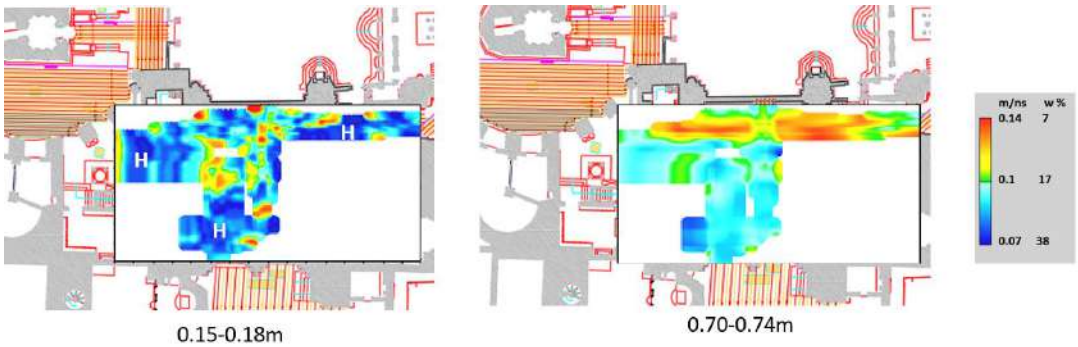

Fig. 183: the whole Area: volumetric water content depth slices overlapped to the planimetry

Fig. 183 shows the volumetric water content depth slice overlapped to the planimetry.

Area A+ H+ I+ L+ N+ M

In the area, A+H+I+L+N+M have acquired 124 GPR profiles for an extension of 980.0 meters (Fig. 184). The GPR data profiles were processed in 2D using GPR-slice software (GPR-SLICE Software (gpr-survey.com)). To eliminate a small noise component and make it easy to interpret GPR data, the following processing sequence was applied:

1) Zero-time adjust (static shift), to associate zero-time with zero-depth;
2) Background removal;
3) Frequency filtering, to remove high-frequency noise;
4) Migration, to correct the shape and dimension of reflection events related to the structure present in the subsoil.

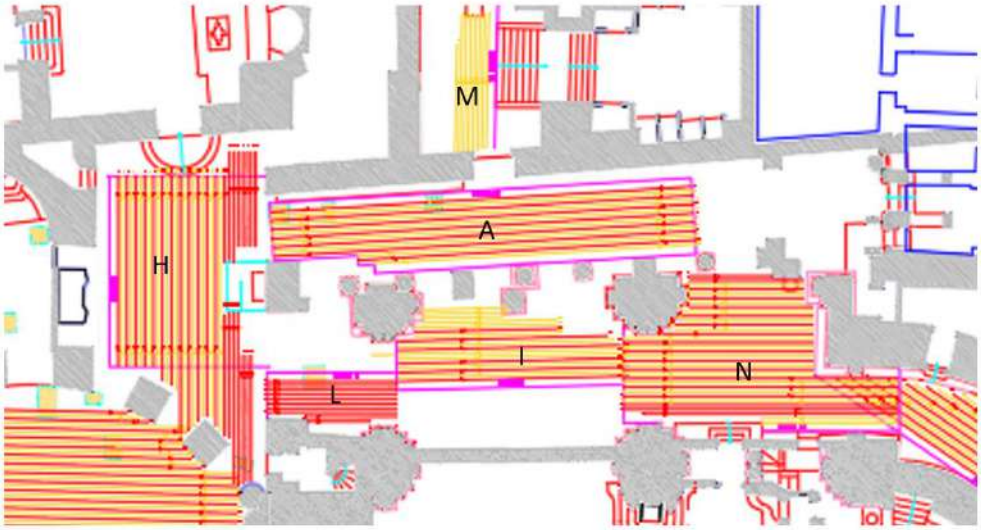

Fig. 150: Area A+H+I+L+M+N: location of GPR profiles

AREA A: The processed GPR profiles acquired in area A are shown in Figs. 185,…, 188.
The reflection event evidenced by a dashed yellow line (labelled P) is probably related to the paving. Here the thickness of the paving seems to vary between 0.1m and 0.3m.
The reflection events labelled T is related to the manholes visible on the surface.
The reflection events labelled D at a depth of about 0.6m are related to a probable old structure.
The reflection events labelled R at a depth of about 0.3-0.6m are probably related to a filling with waste material.

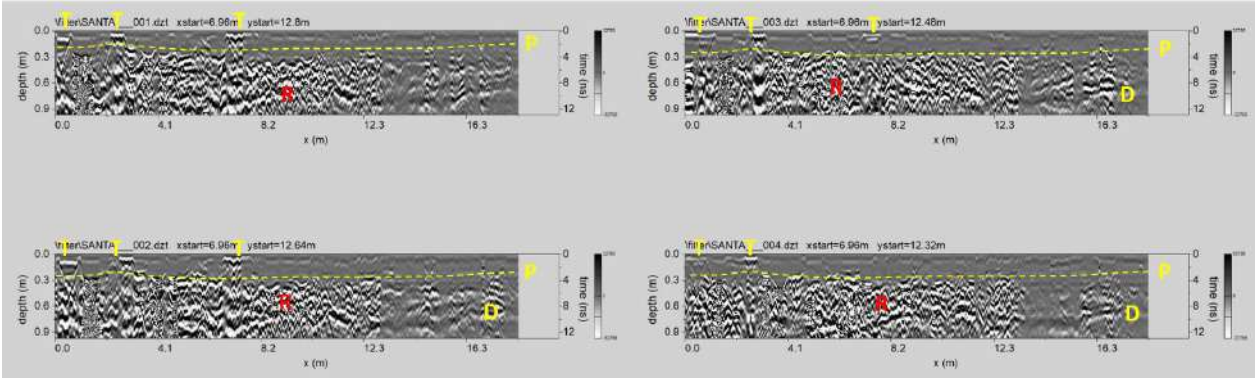

Fig. 185: Area A: processed GPR profiles 1, …, 4 (T: manhole; P: paving thickness; R: filling; D: structure)

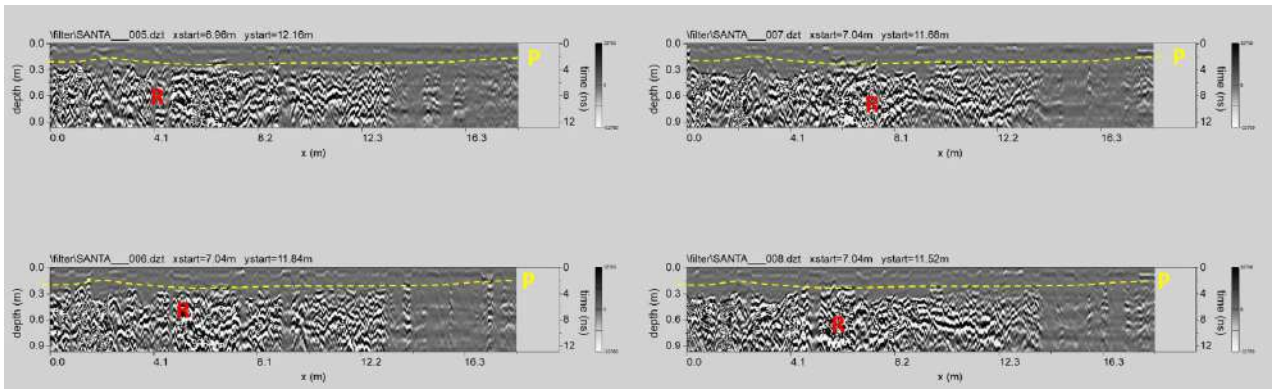

Fig. 186: Area A: processed GPR profiles 5, …, 8 (P: paving thickness; R: filling)

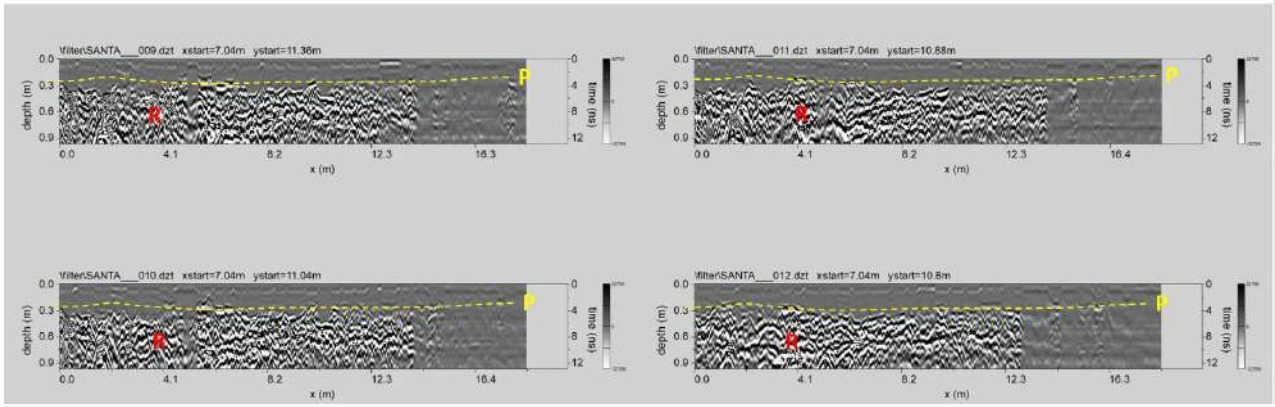

Fig. 187: Area A: processed GPR profiles 9, …, 12 (P: paving thickness; R: filling)

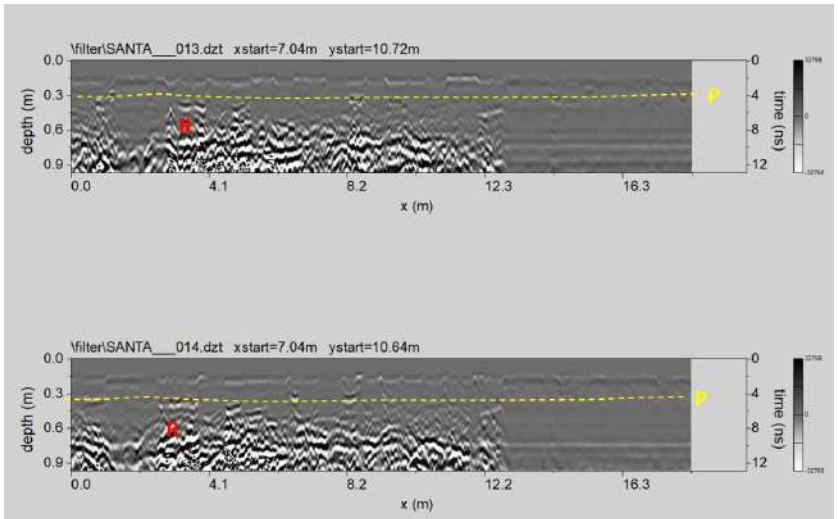

Fig. 188: Area A: processed GPR profiles 13 and 14 (R: filling; P: paving thickness)

AREA H: The processed GPR profiles acquired in area H are shown in Figs. 189,…, 198.
The reflection event evidenced by a dashed yellow line (labelled P) is probably related to the paving. Here the thickness of the paving seems to vary between 0.1m and 0.35m.

Some reflection events at a depth of about 0.7 m are probably related to archaeological structures. The reflection events labelled D at a depth of about 0.6m-0.7m are probably related to the old structure (cavity).

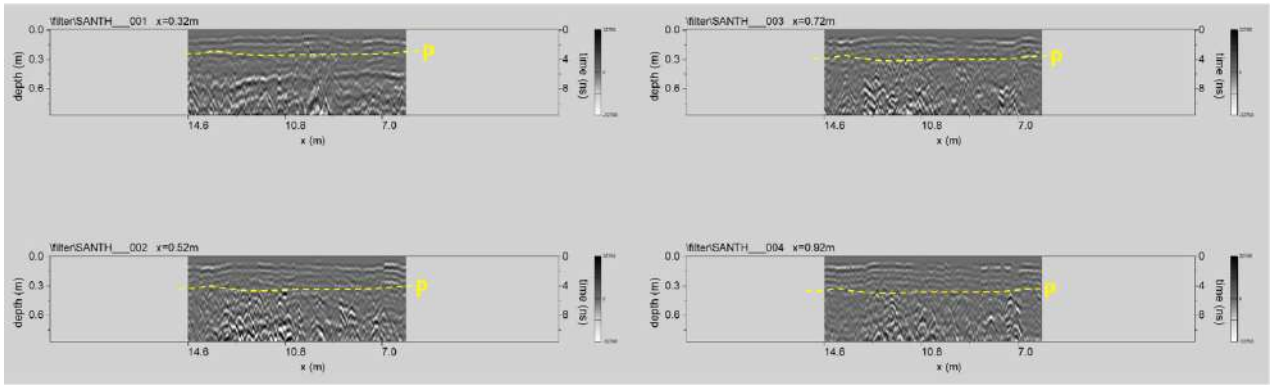

Fig. 189: Area H: processed GPR profiles 1, …, 4 (P: paving thickness)

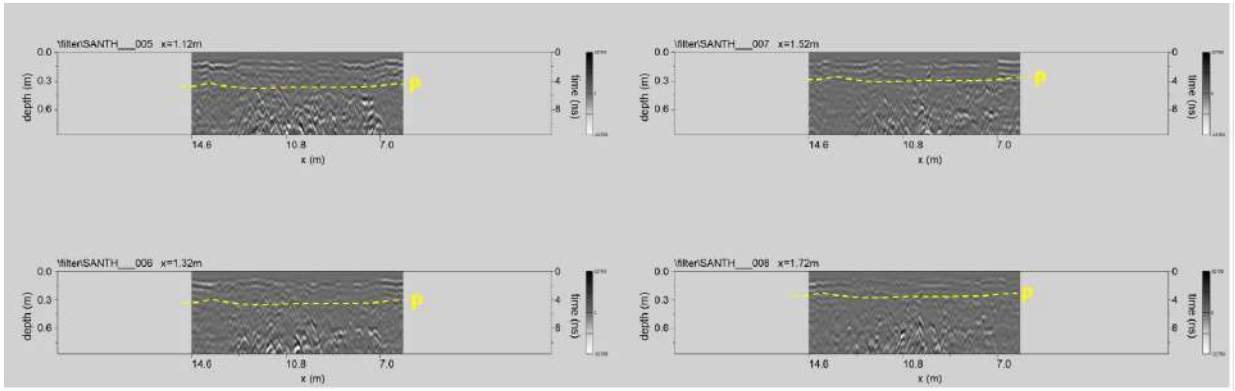

Fig. 190: Area H: processed GPR profiles 5, …, 8 (P: paving thickness)

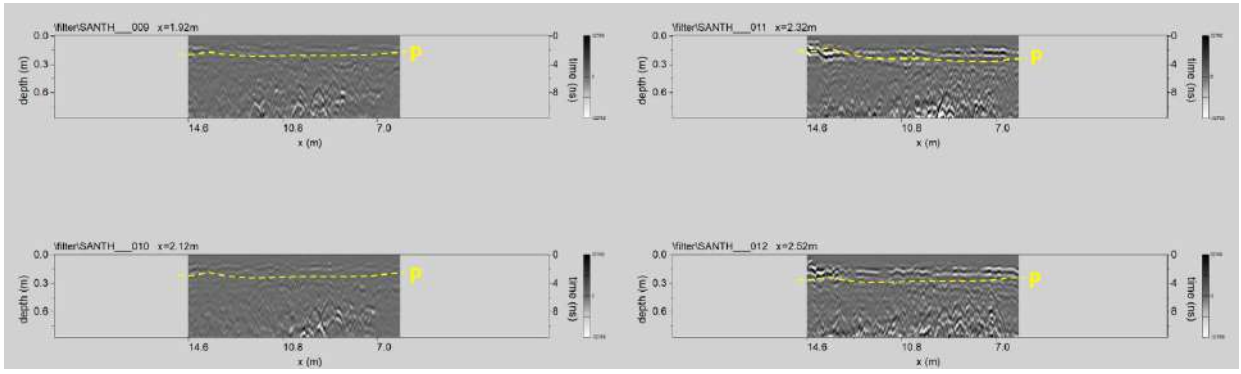

Fig. 191: Area H: processed GPR profiles 9, …, 12 (P: paving thickness)

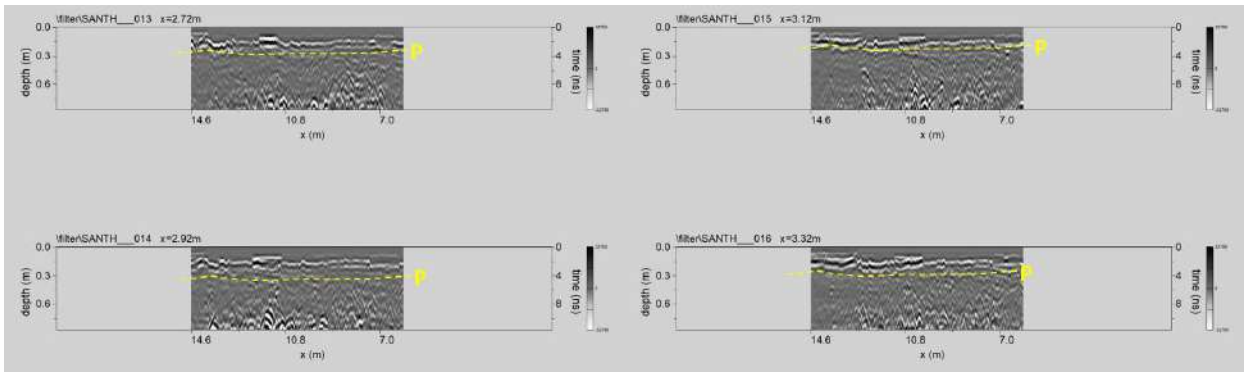

Fig. 192: Area H: processed GPR profiles 13, …, 16 (P: paving thickness)

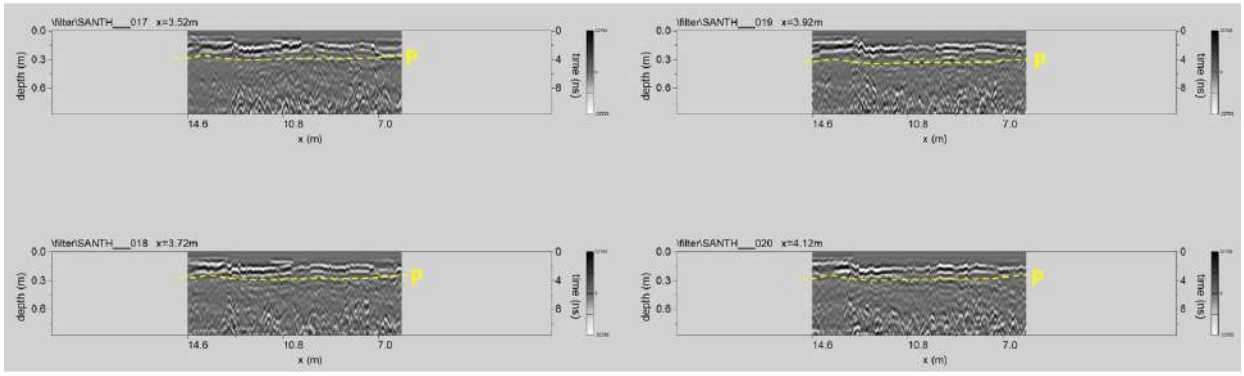

Fig. 193: Area H: processed GPR profiles 17, …, 20 (P: paving thickness)

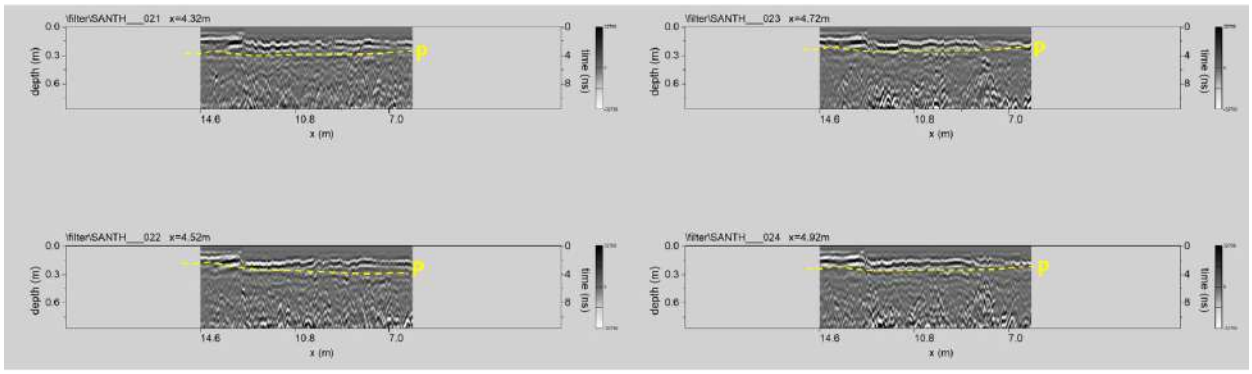

Fig. 194: Area H: processed GPR profiles 21, …, 24 (P: paving thickness)

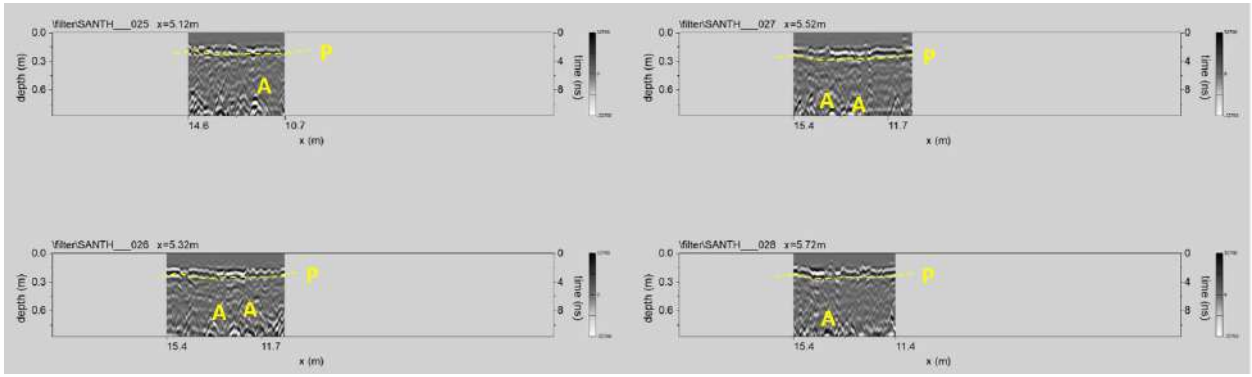

Fig. 195: Area H: processed GPR profiles 25, …, 28 (A: archaeological structure; P: paving thickness)

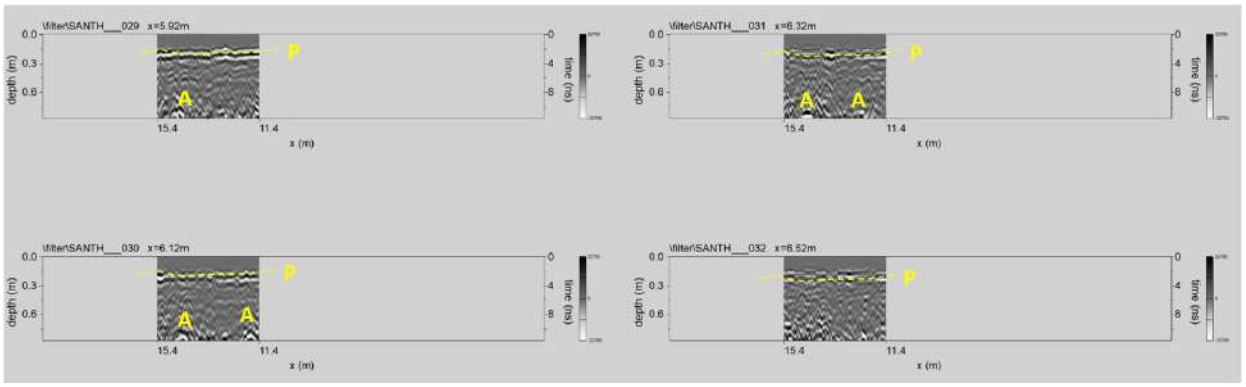

Fig. 196: Area H: processed GPR profiles 29, …, 32 (A: archaeological structure; P: paving thickness)

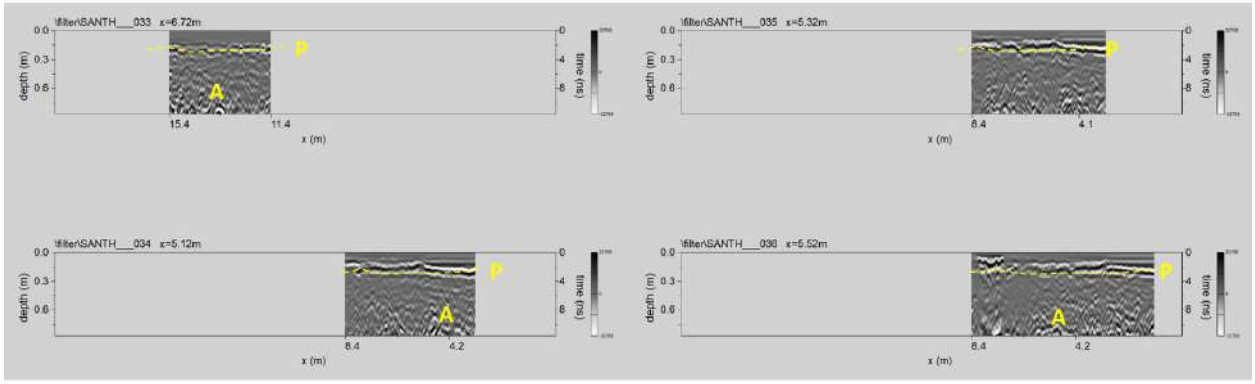

Fig. 197: Area H: processed GPR profiles 33, …, 36 (A: archaeological structure; P: paving thickness)

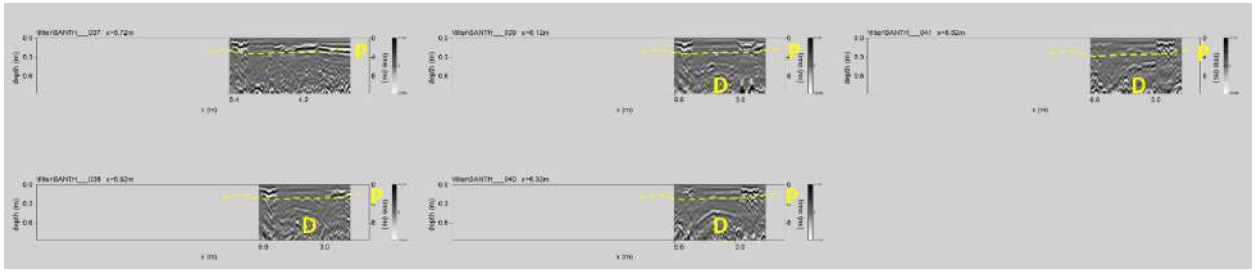

Fig. 198: Area H: processed GPR profiles 37, …, 41 (A: archaeological structure; D: structure; P: paving thickness)

AREA I: The processed GPR profiles acquired in the area I are shown in Figs. 199,…, 202.
The reflection event evidenced by a dashed yellow line (labelled P) is probably related to the paving. Here the thickness of the paving seems to vary between 0.1m and 0.3m.
The reflection events labelled D visible at about 0.4m-0.5m depth could be related to an old structure.
The reflection events labelled V at a depth between 0.35m and 0.5m are related to probable void spaces.

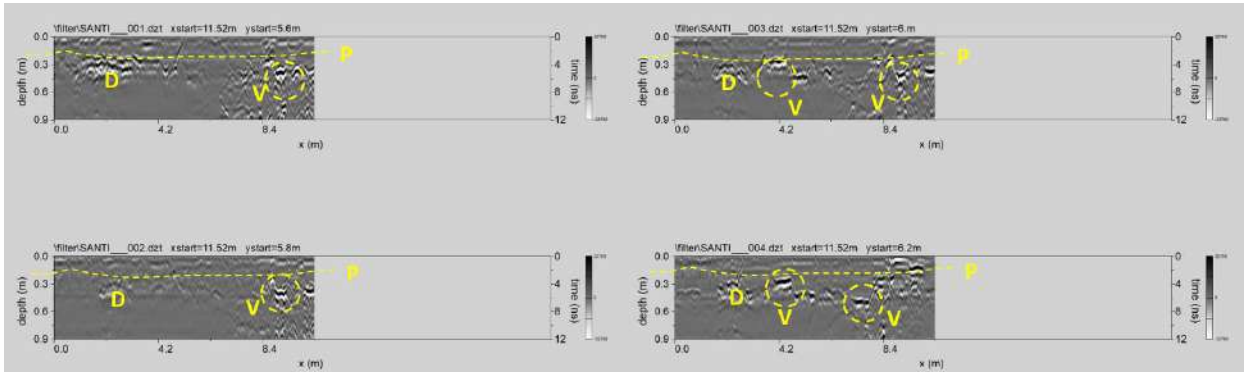

Fig. 199: Area I: processed GPR profiles 1,…, 4 (D: structure; P: paving thickness; V: void spaces)

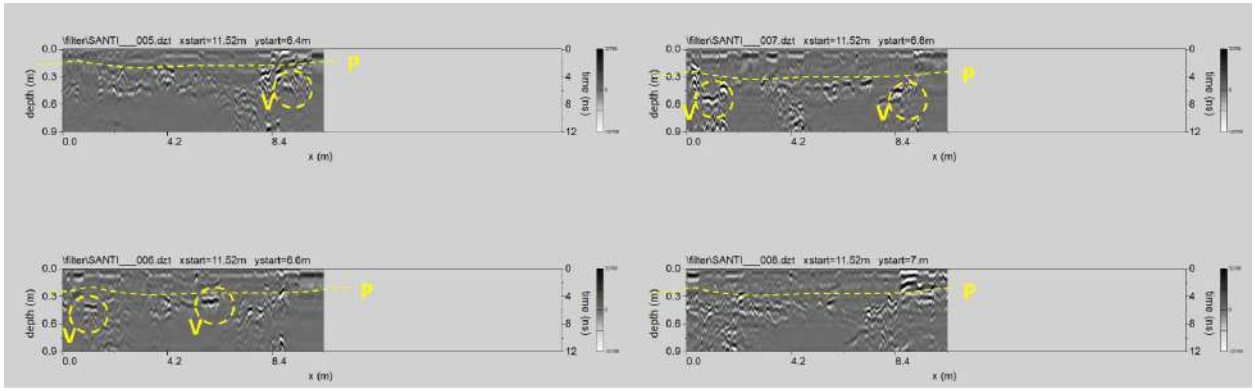

Fig. 200: Area I: processed GPR profiles 5, …, 8 (P: paving thickness; V: void spaces)

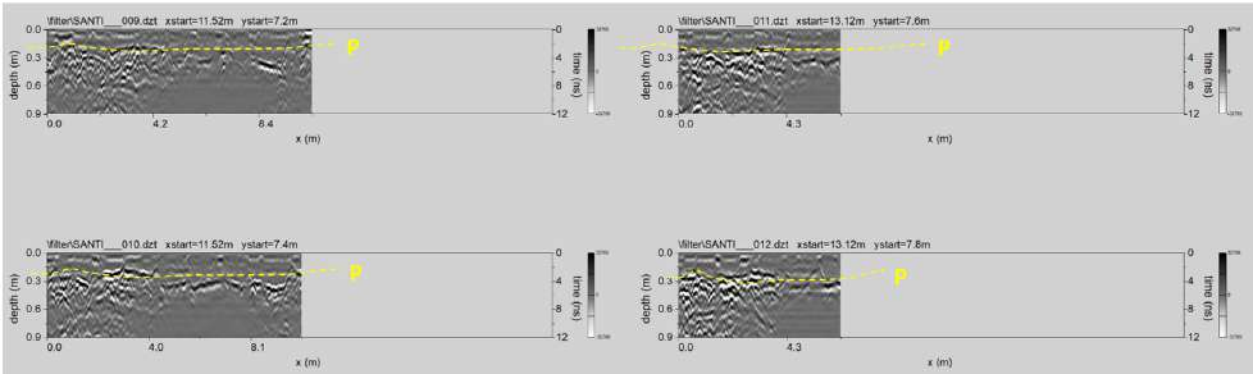

Fig. 201: Area I: processed GPR profiles 9, …12 (P: paving thickness)

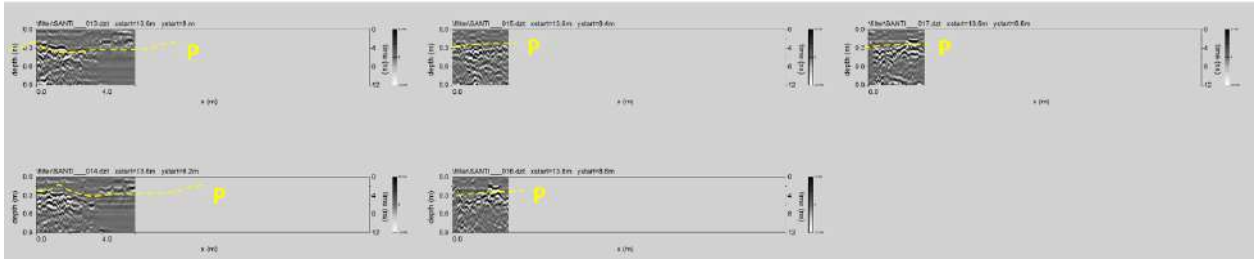

Fig. 202: Area I: processed GPR profiles 13,…, 17 (P: paving thickness)

AREA L: The processed GPR profiles acquired in area L are shown in Figs. 203,…, 205.
The reflection event evidenced by a dashed yellow line (labelled P) is probably related to the paving. Here the thickness of the paving seems to vary between 0.1m and 0.35m.
The reflection events labelled R visible at about 0.35m depth could be related to filling with waste materials.
The reflection events labelled T is related to the surface manhole.

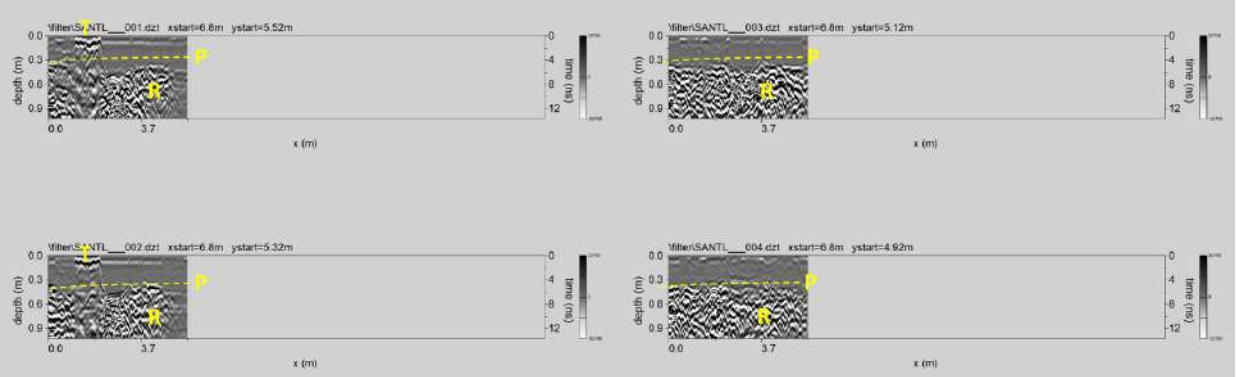

Fig. 203: Area L: processed GPR profiles 1,…, 4 (P: paving thickness; R: filling; T: manhole)

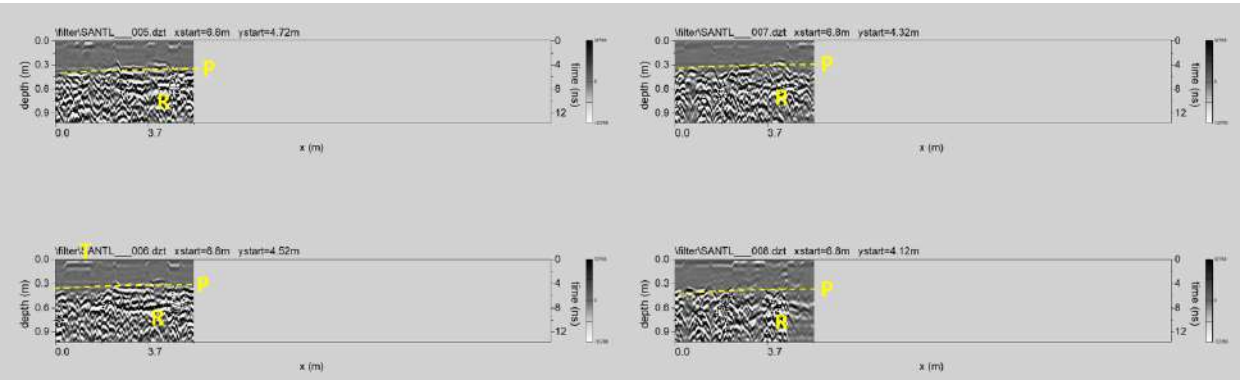

Fig. 204: Area L: processed GPR profiles 5, …, 8 (P: paving thickness; R: filling; T: manhole)

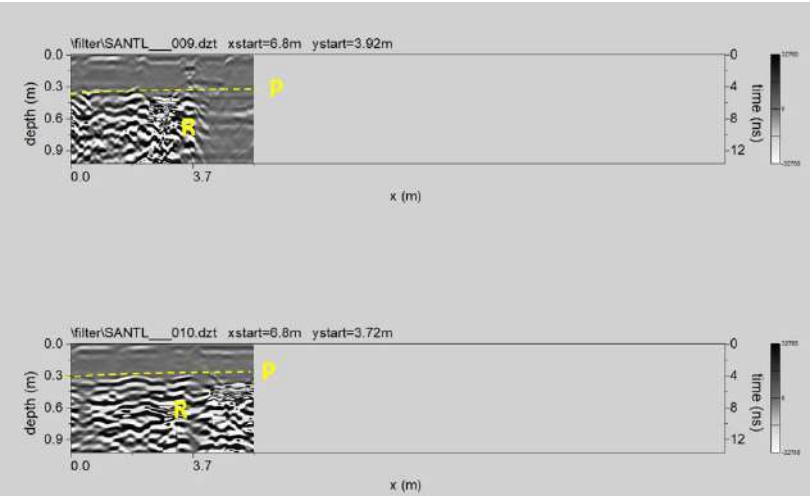

Fig. 205: Area L: processed GPR profiles 9 and 10 (P: paving thickness; R: filling)

AREA M: The processed GPR profiles acquired in area M are shown in Figs. 206 and 207.

The reflection event evidenced by a dashed yellow line (labelled P) is probably related to the paving. Here the thickness of the paving seems to vary between 0.1m and 0.35m.
The reflection events labelled E visible at about two levels, 0.35m and 0.7m depth, could be related to the presence of a metal grid.

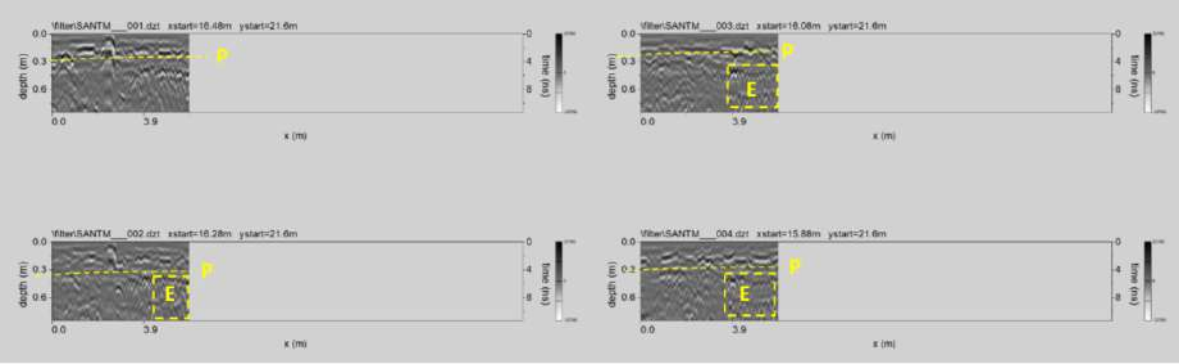

Fig. 206: Area M: processed GPR profiles 1,…, 4 (E: metal grid; P: paving thickness)

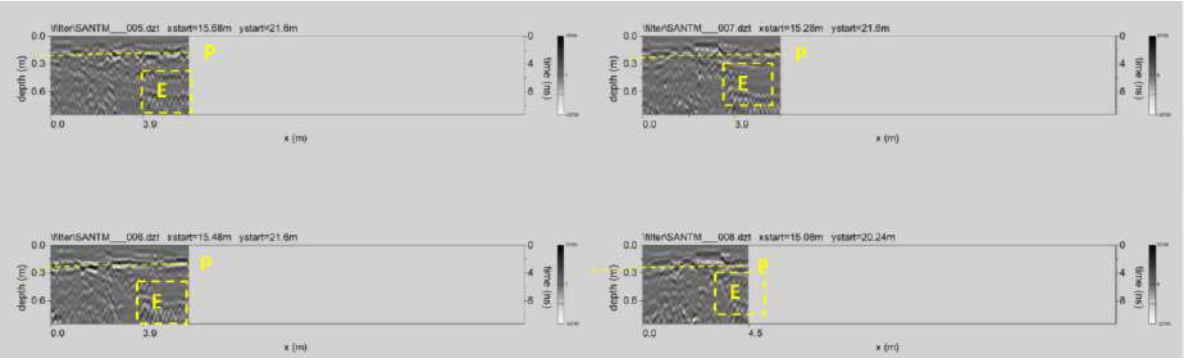

Fig. 207: Area M: processed GPR profiles 5, …, 8 (P: paving thickness; E: metal grid;)

AREA N: The processed GPR profiles acquired in area N are shown in Figs. 208 and 216.
The reflection event evidenced by a dashed yellow line (labelled P) is probably related to the paving. Here the thickness of the paving seems to vary between 0.1m and 0.3m.
The reflection events labelled A visible at about two levels 0.3m depth could be related to archaeological structures.
The reflection events D at a depth ranging from 0.45m to 0.7 m could be related to probable structures (cavities). The reflection event R indicates a probable filling with waste materials.

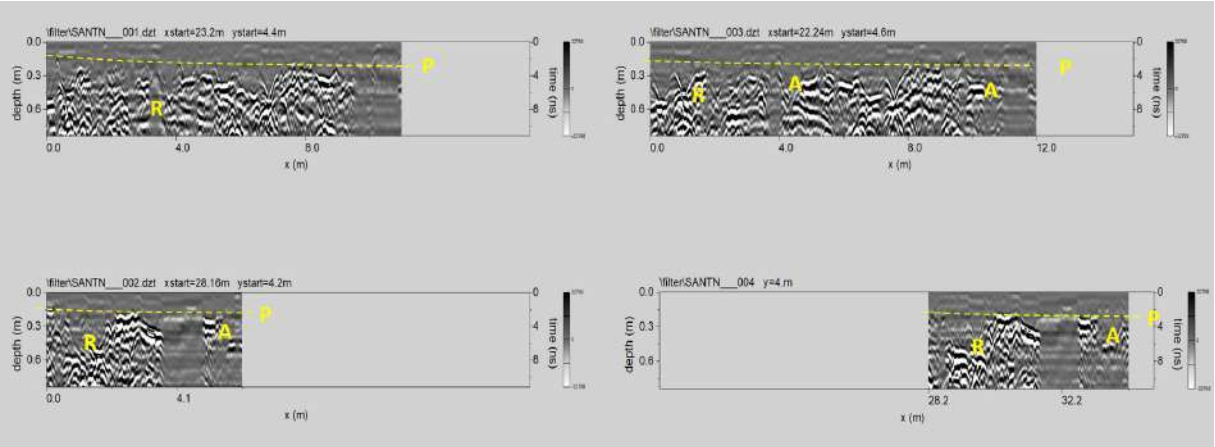

Fig. 208: Area N: processed GPR profiles 1,…, 4 (A: archaeological structure; P: paving thickness; R: filling;)

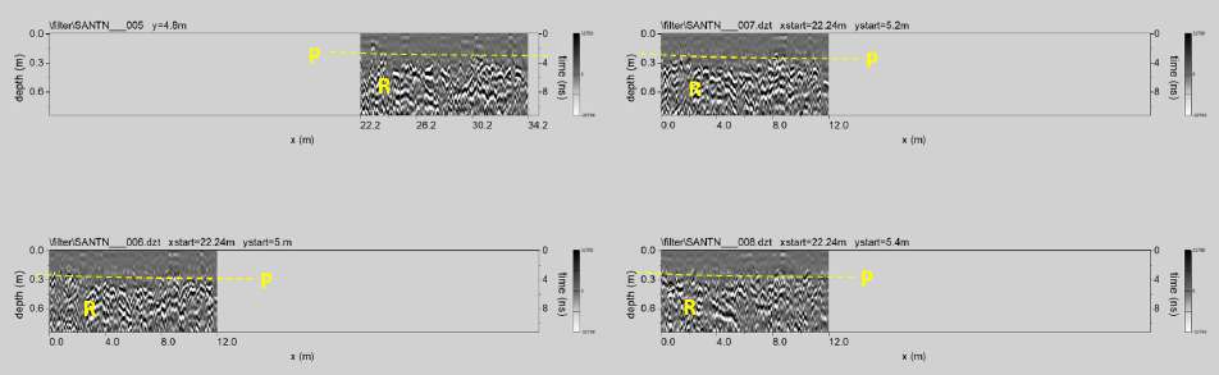

Fig. 209: Area N: processed GPR profiles 5, …, 8 (P: paving thickness; R: filling;)

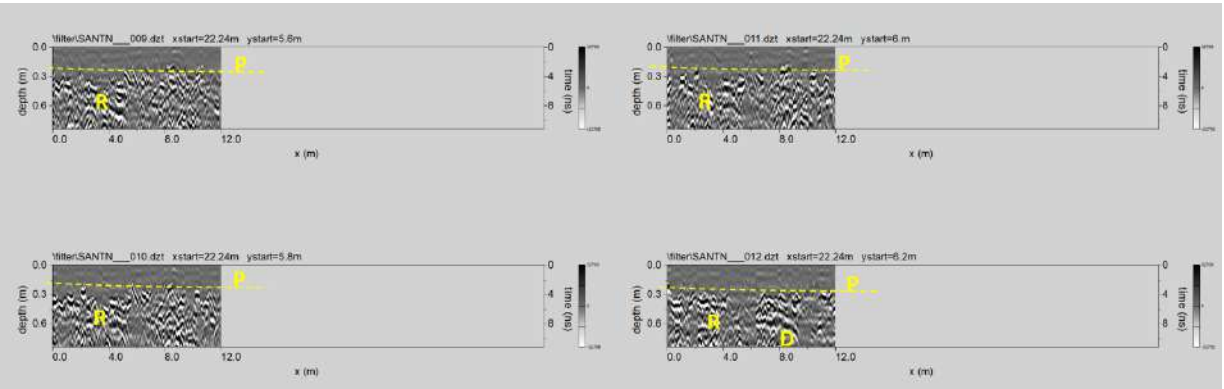

Fig. 210: Area N: processed GPR profiles 9, …, 12 (D: structure; P: paving thickness; R: filling;)

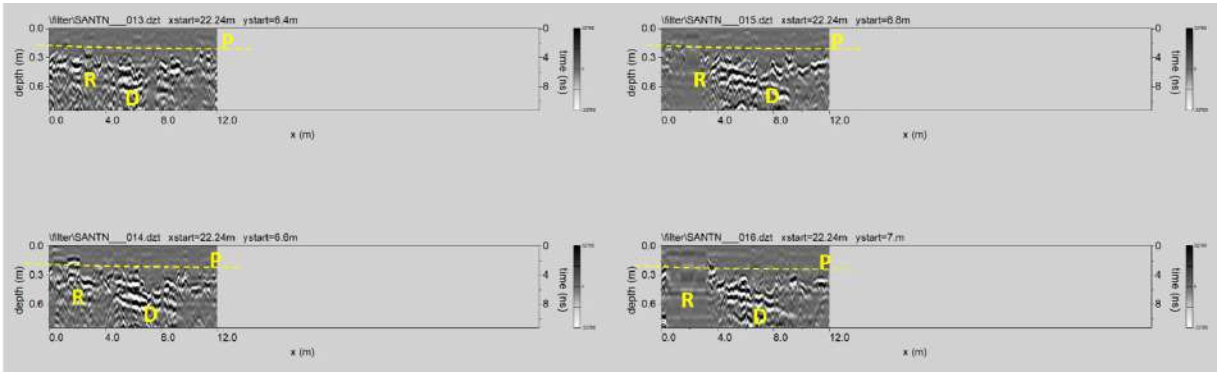

Fig. 211: Area N: processed GPR profiles 13, …, 16 (D: structure; P: paving thickness; R: filling;)

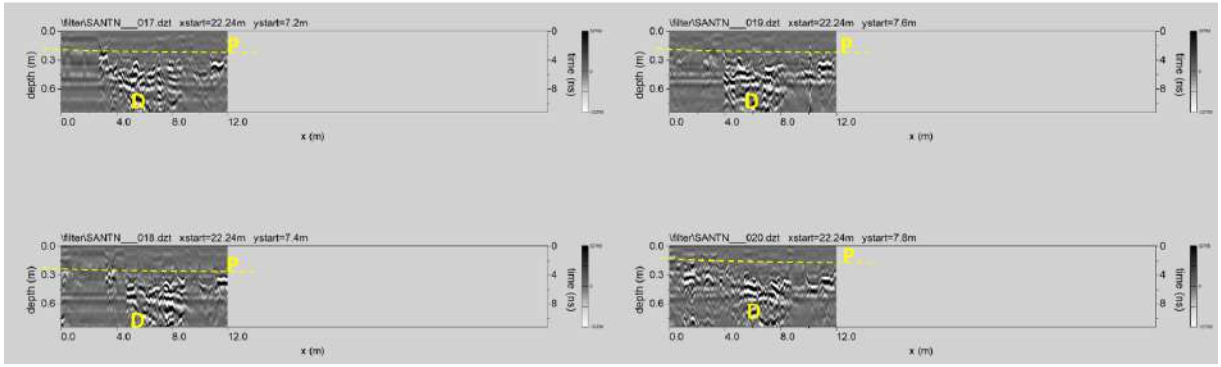

Fig. 212: Area N: processed GPR profiles 17, …, 20 (D: structure; P: paving thickness)

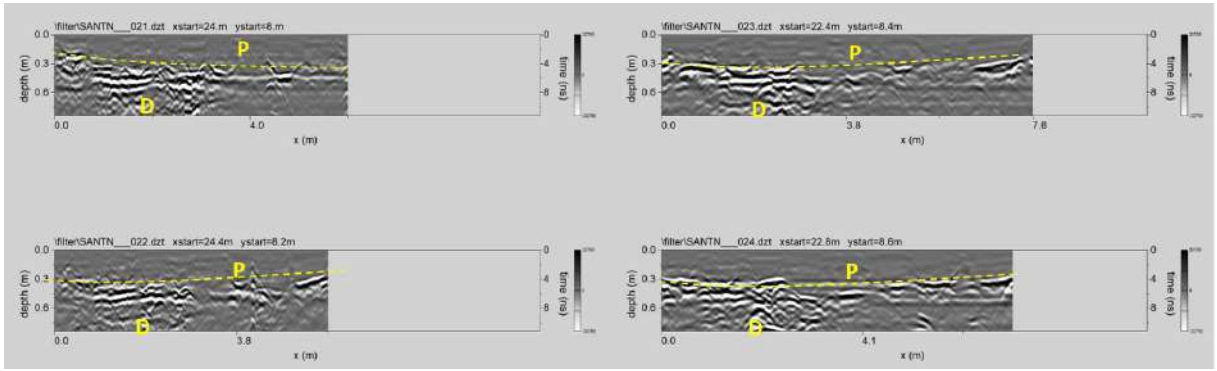

Fig. 213: Area N: processed GPR profiles 21, …, 24 (D: structure; P: paving thickness)

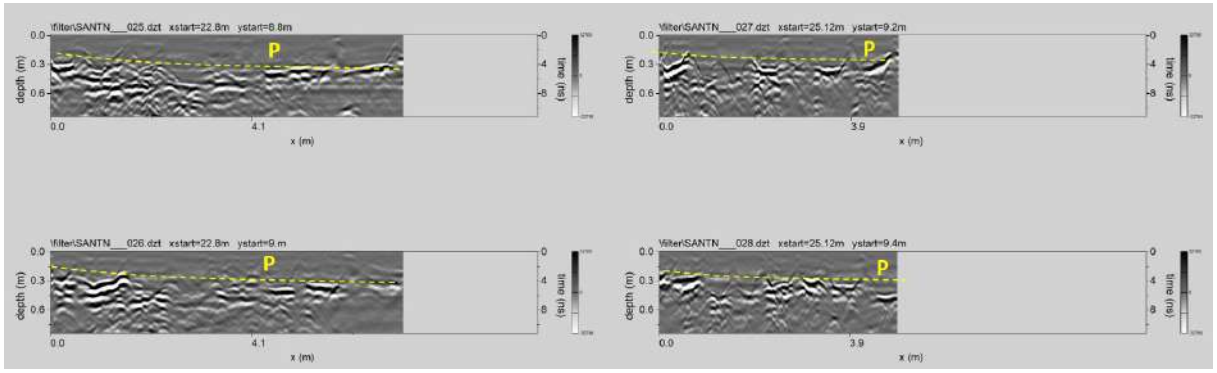

Fig. 214: Area N: processed GPR profiles 25, …, 28 (P: paving thickness)

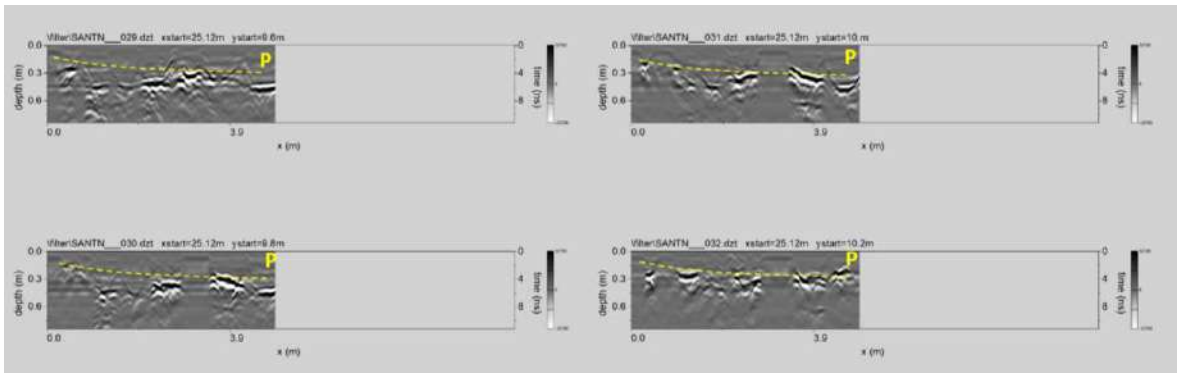

Fig. 215: Area N: processed GPR profiles 29, …, 32 (P: paving thickness)

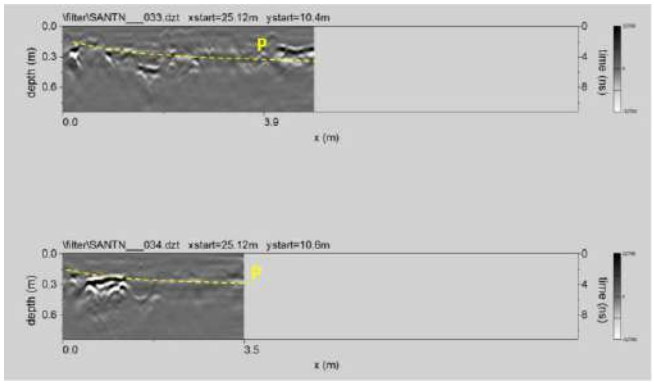

Fig. 216: Area N: processed GPR profiles 33 and 34 (P: paving thickness)

Area A+H+I+L+M+N: 3D visualization: The time-slice technique has been used to display the amplitude variations within consecutive time windows of width Δt=1 ns.
Figs. 217,…, 219 shows the depth slices from 0.0 m to 0.97 m in depth.

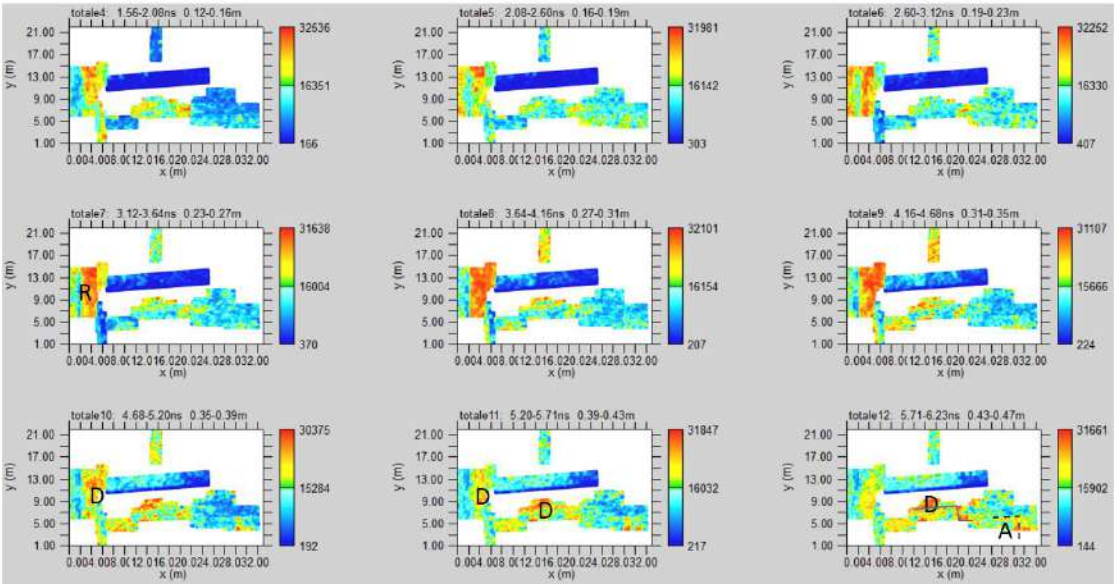

Fig. 217: the whole: Depth slices 0.0-0.47m (A: archaeological structures; R: filling; D: structures –cavities)

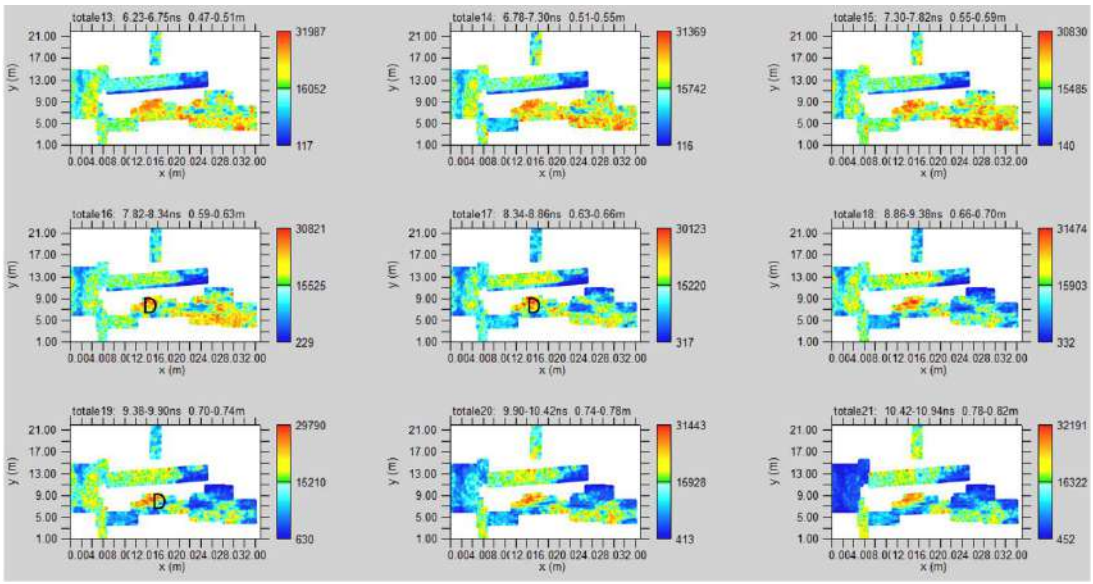

Fig. 218: the whole: Depth slices 0.47-0.82m (D: structures- cavities)

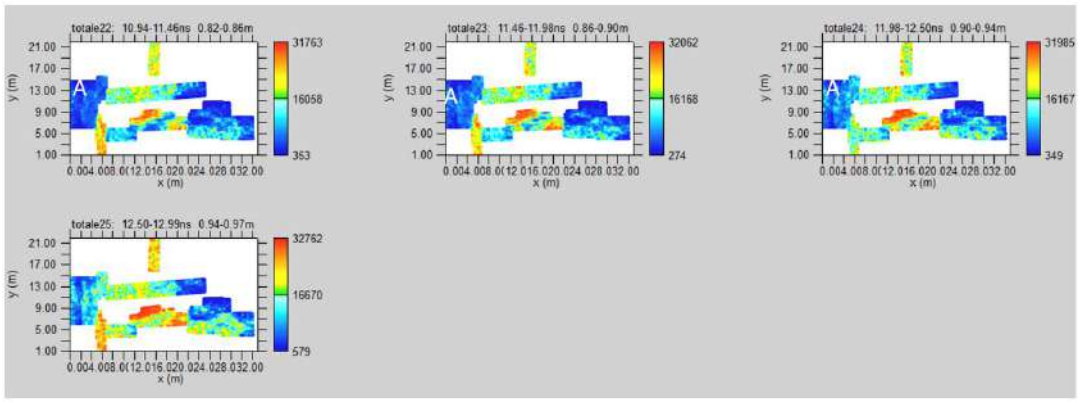

Fig. 219: the whole: Depth slices 0.82-0.97m (A: archaeological structures)

In the slices, relatively high-amplitude alignments (labelled D) are visible. These could be related to probable underground structures (cavities?). They are at a depth between 0.4m and 0.7m. At depths between 0.8m and 0.9m (Fig. 219), anomaly A represents a probable archaeological structure (walls).

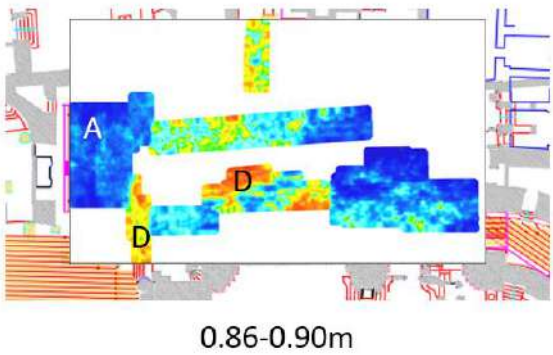

Fig. 220: the whole Area: depth slices overlapped to the planimetry (D: structure-channel-; A: archaeological structures)

Fig 220 shows the more significant depth slices overlapped to the planimetry of the church. It is possible to see the position of the high amplitude anomalies A and the probable channel D.

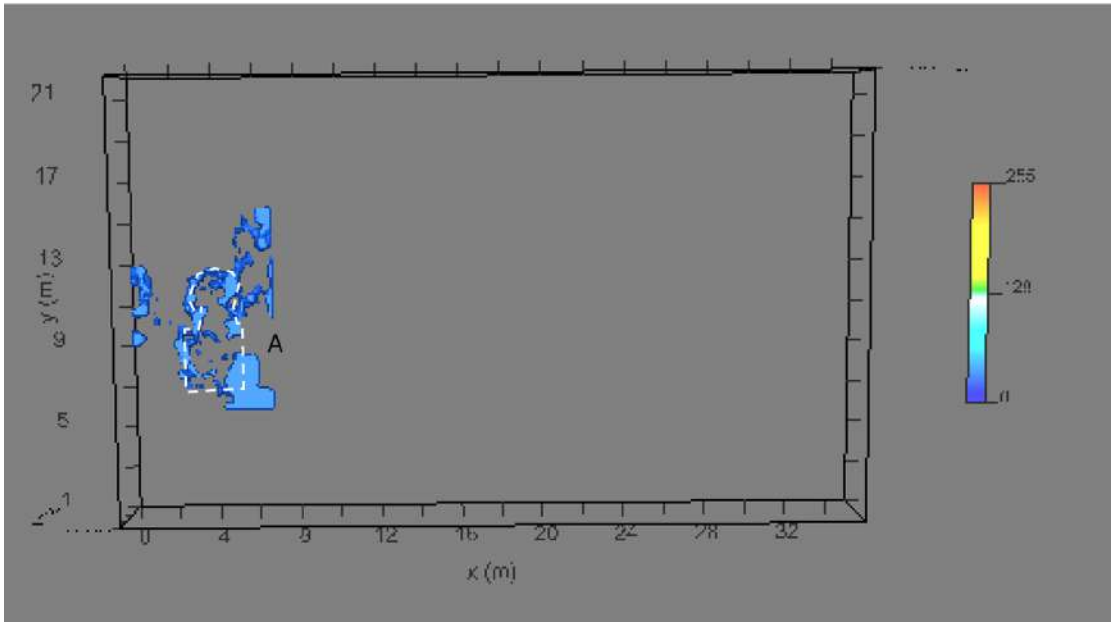

Fig. 221: the whole Area: electromagnetic amplitude isosurfaces 0.82-0.94m depth threshold 15%

Fig. 221 show the iso-surface visualization. Here is possible to see the spatial position of anomaly A.
Fig. 222 show a virtual excavation. In this case, it is possible to see the position of the anomalous zones well.

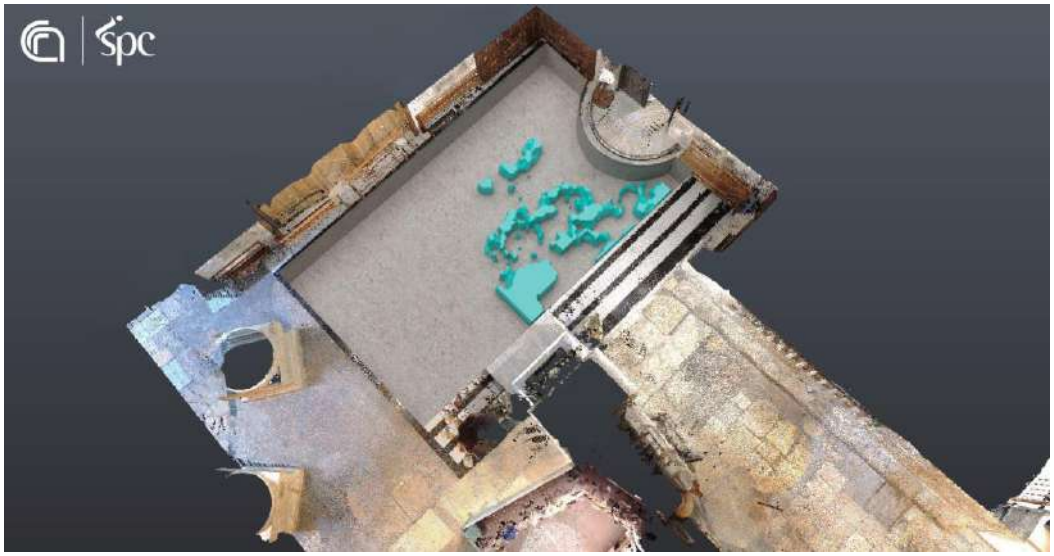

Fig. 222: the whole Area: virtual excavation 0.82-0.94m depth threshold 15%

Area A+H+I+L+M+N: **MOISTURE MAP**

Figs. 223,…, 225 shows the depth slices with volumetric water content in depth between 0.09m and 0,81m. The slices show a volumetric water content that varies from 7% to 38%. The volumetric water content plan distribution shows relatively high volumetric water content (16%) distributed in a homogeneous mode.

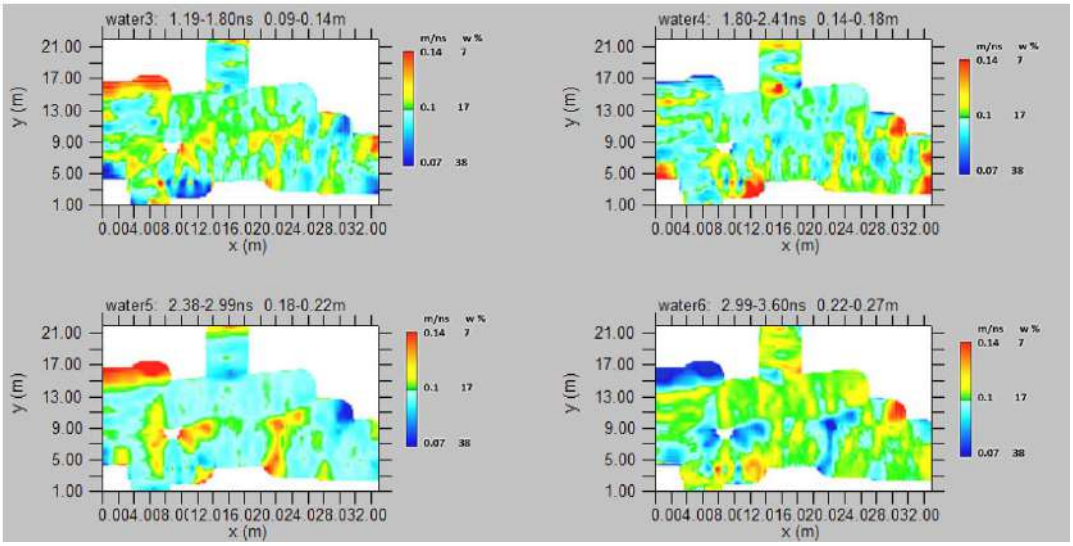

Fig. 223: the whole Area: Volumetric water content (w) and electromagnetic wave velocity (m/ns) at depth from 0.09 to 0.27m

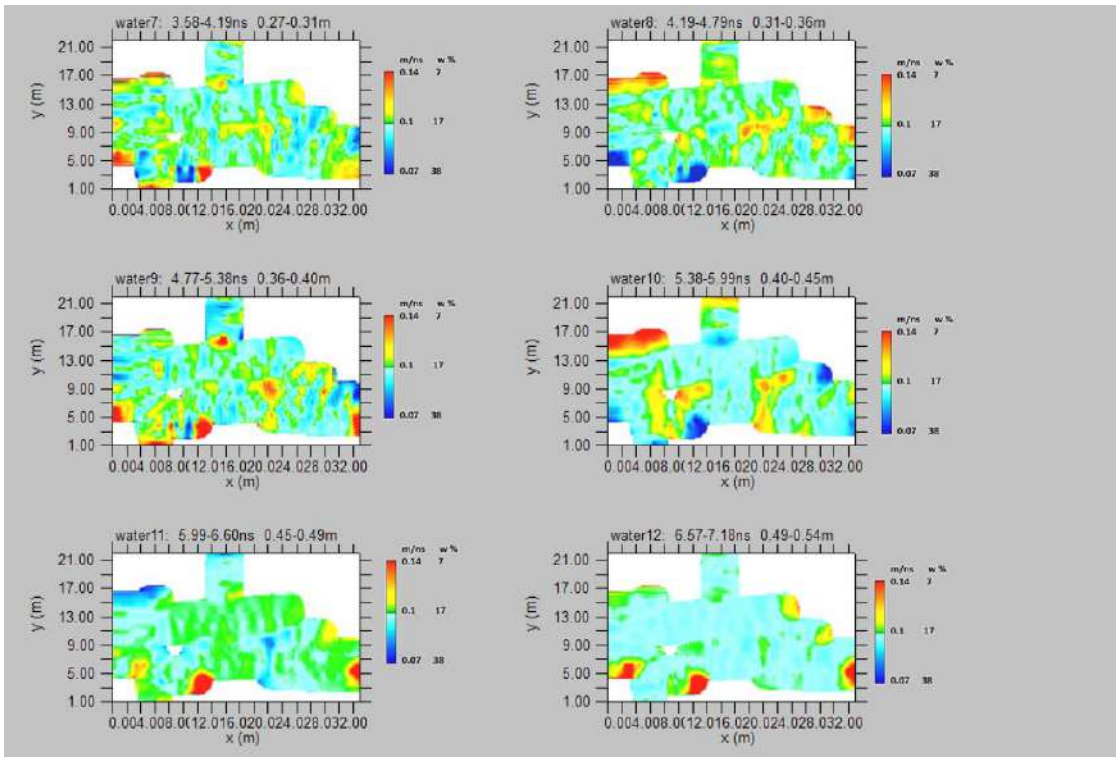

Fig. 224: the whole Area: Volumetric water content (w) and electromagnetic wave velocity (m/ns) at depth from 0.27 to 0.54m

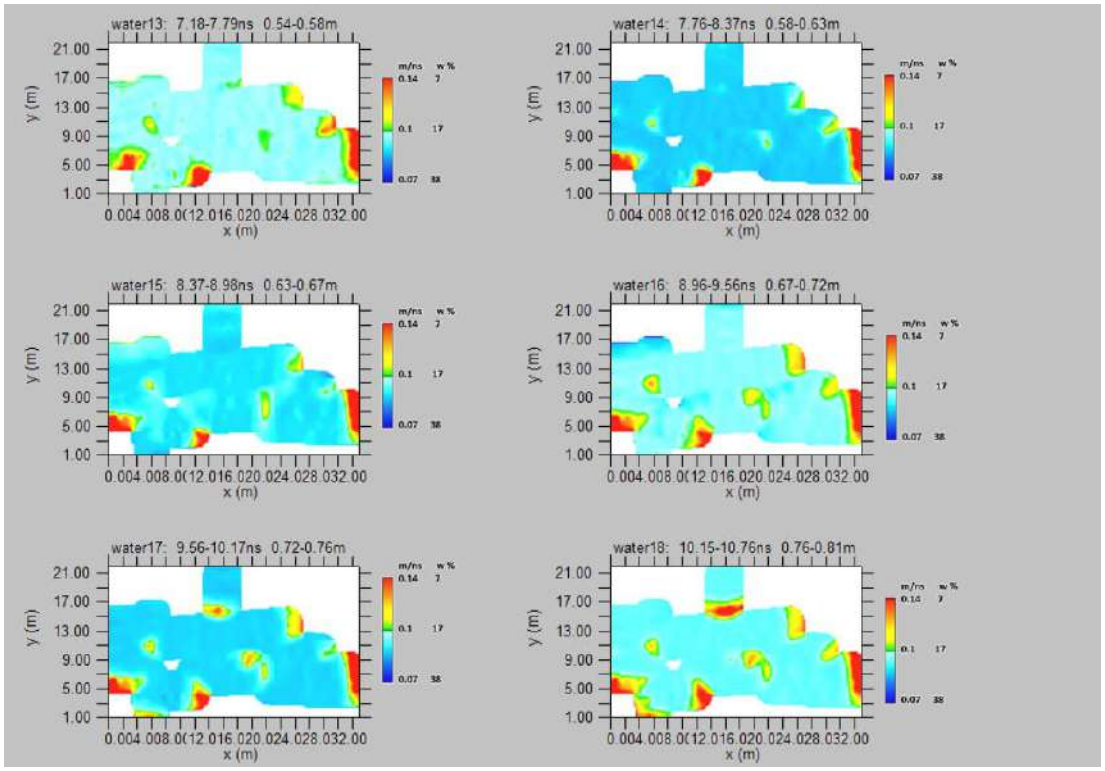

Fig. 225: the whole Area: Volumetric water content (w) and electromagnetic wave velocity (m/ns) at depth from 0.54 to 0.81m

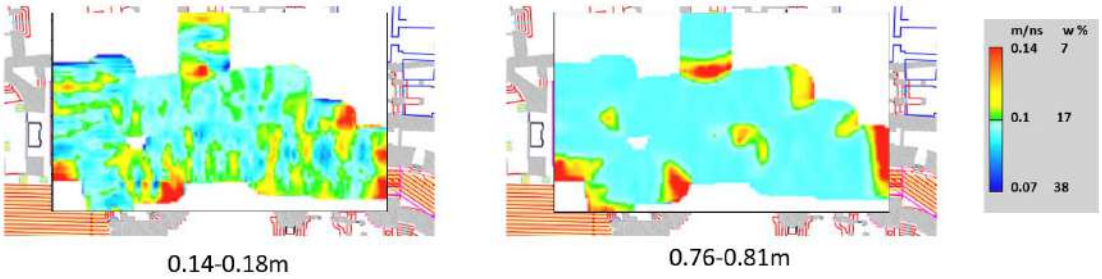

Fig. 226: the whole Area: volumetric water content depth slices overlapped to the planimetry

Fig. 226 shows the volumetric water content depth slice overlapped to the planimetry.

Area O+P+Q

In the area, O+P+Q have acquired 44 GPR profiles for an extension of 490.0 meters (Fig. 227).

The GPR data profiles were processed in 2D using GPR-slice software (GPR-SLICE Software (gpr-survey.com)). To eliminate a small noise component and make it easy to interpret GPR data, the following processing sequence was applied:

1) Zero-time adjust (static shift), to associate zero-time with zero-depth;
2) Background removal;
3) Frequency filtering, to remove high-frequency noise;
4) Migration, to correct the shape and dimension of reflection events related to the structure present in the subsoil.

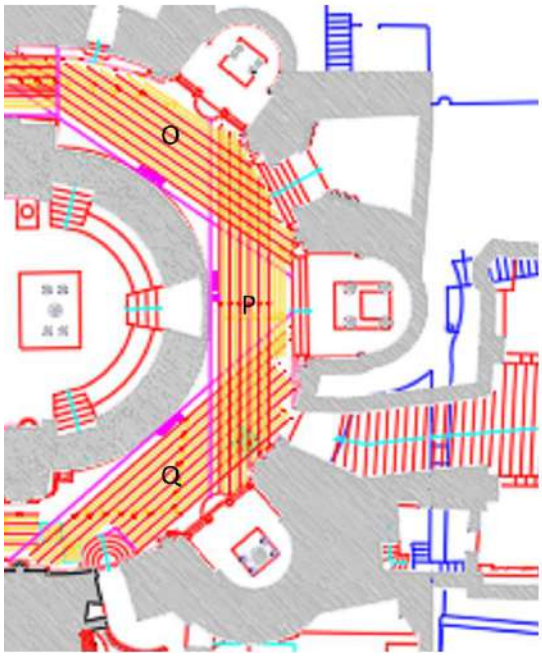

Fig. 227: Area O, P and Q: location of GPR profiles

AREA O: The processed GPR profiles acquired in area O are shown in Figs. 228,…, 231.

The reflection event evidenced by a dashed yellow line (labelled P) is probably related to the paving. Here the thickness of the paving seems to vary between 0.15m and 0.3m.

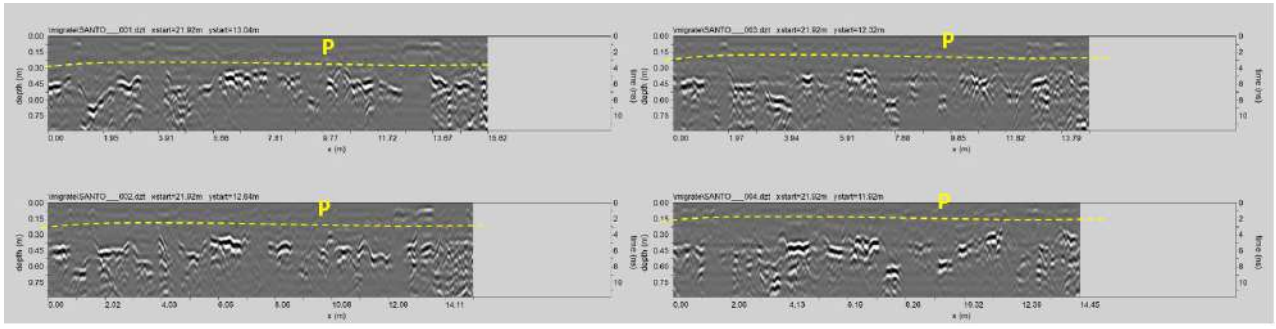

Fig. 228: Area O: processed GPR profiles 1, …, 4 (P: paving thickness)

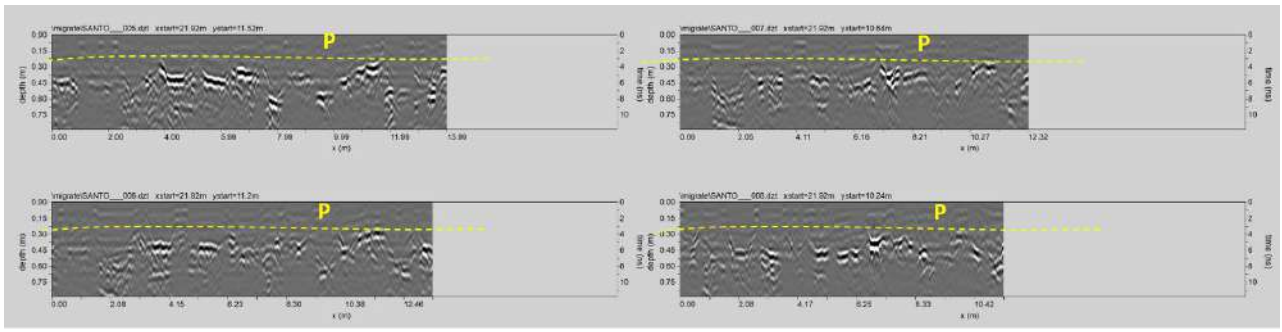

Fig. 229: Area O: processed GPR profiles 5, …, 8 (P: paving thickness)

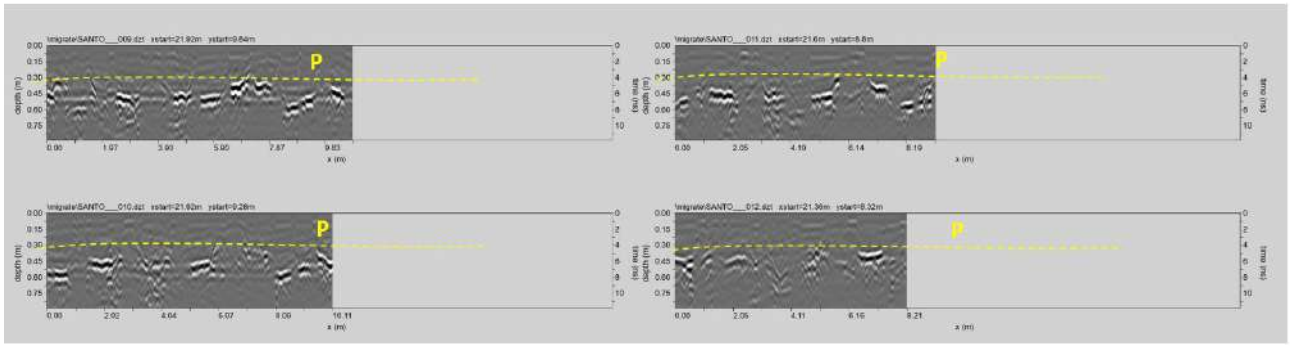

Fig. 230: Area O: processed GPR profiles 9, …, 12 (P: paving thickness)

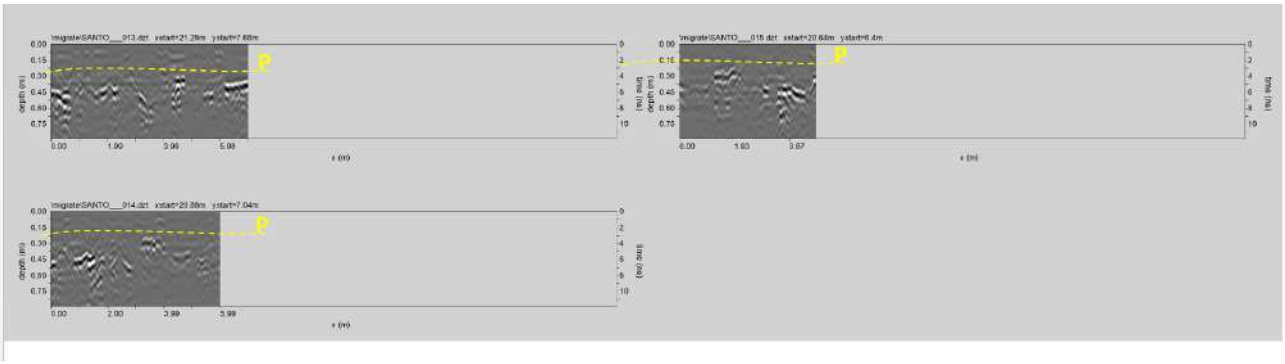

Fig. 231: Area O: processed GPR profiles 13, …, 15 (P: paving thickness)

AREA P: The processed GPR profiles acquired in area P are shown in Figs. 232,…, 235.
The reflection event evidenced by a dashed yellow line (labelled P) is probably related to the paving. Here the thickness of the paving seems to vary between 0.1m and 0.45m.
The reflection events labelled T is related to the manholes visible on the surface.

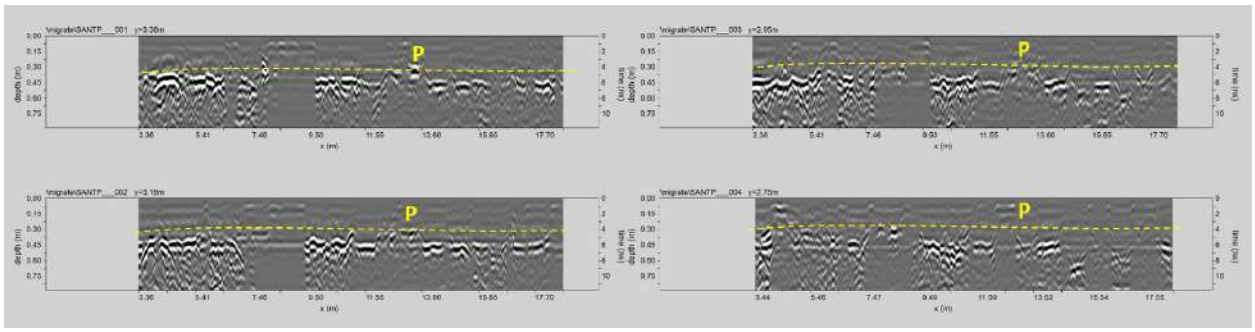

Fig. 232: Area P: processed GPR profiles 1, …, 4 (P: paving thickness)

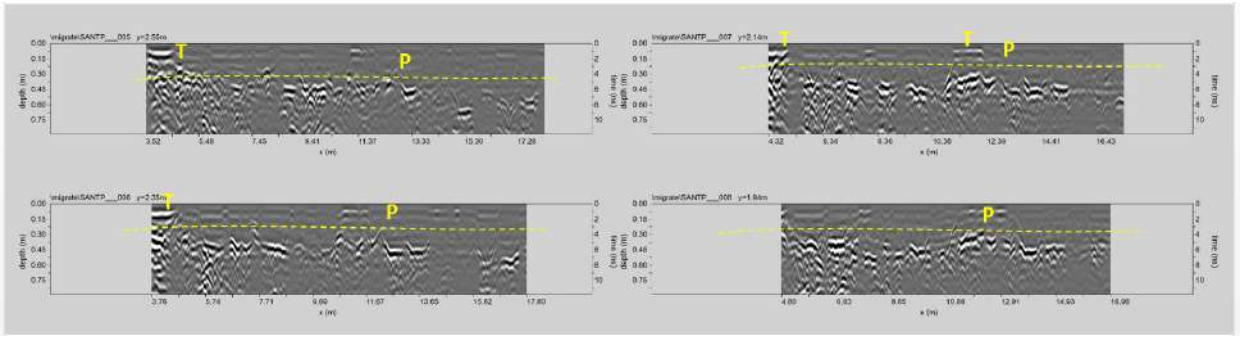

Fig. 233: Area P: processed GPR profiles 5, …, 8 (P: paving thickness; T: manhole)

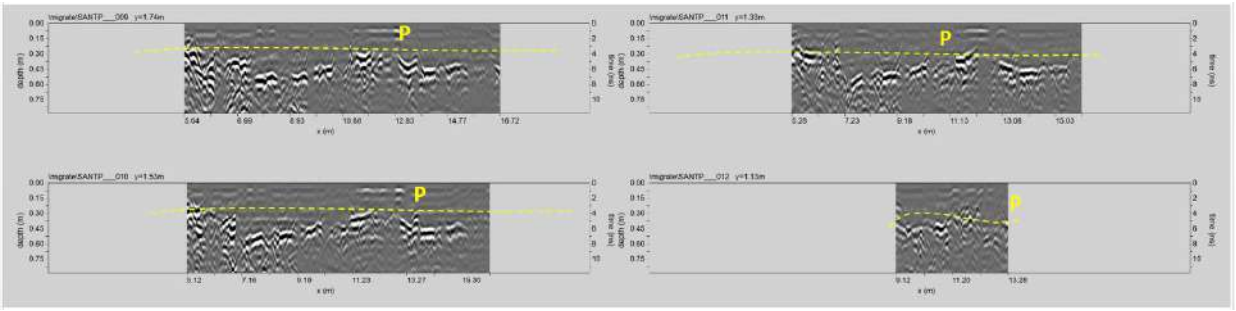

Fig. 234: Area P: processed GPR profiles 9, …, 12 (P: paving thickness)

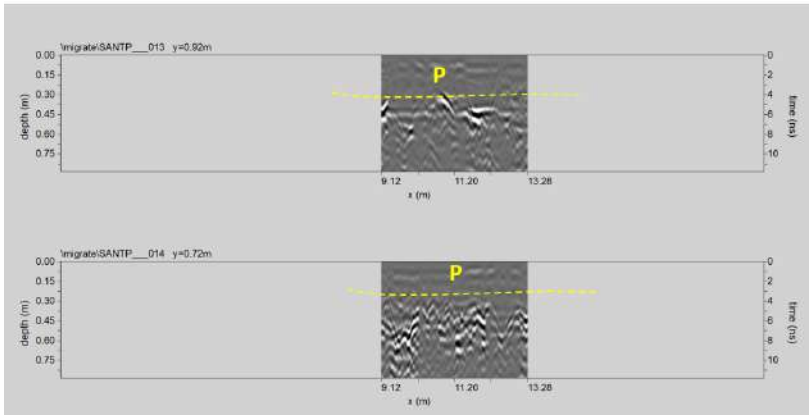

Fig. 235: Area P: processed GPR profiles 13 and 14 (P: paving thickness)

AREA Q: The processed GPR profiles acquired in area Q are shown in Figs. 236,…, 239.
The reflection event evidenced by a dashed yellow line (labelled P) is probably related to the paving. Here the thickness of the paving seems to vary between 0.1m and 0.3m.
The reflection events labelled D visible at about 0.4m-0.5m depth could be related to an old structure.
The reflection events labelled T is related to the manholes visible on the surface.

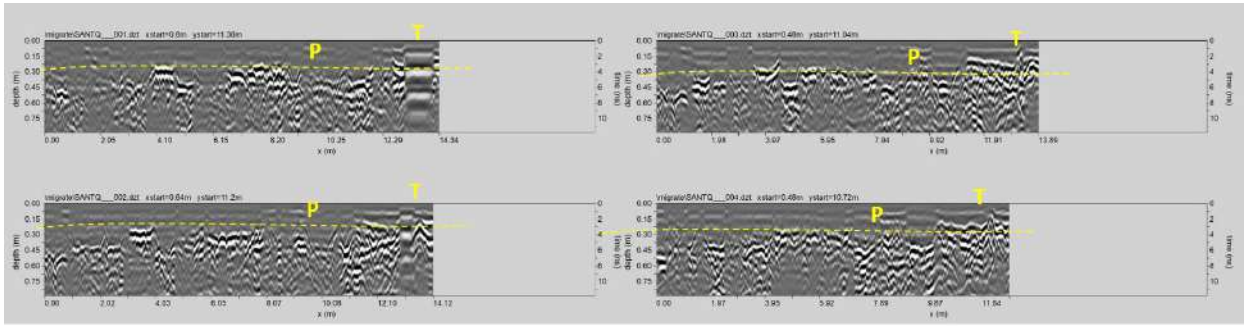

Fig. 236: Area Q: processed GPR profiles 1,…, 4 (P: paving thickness; T: manhole)

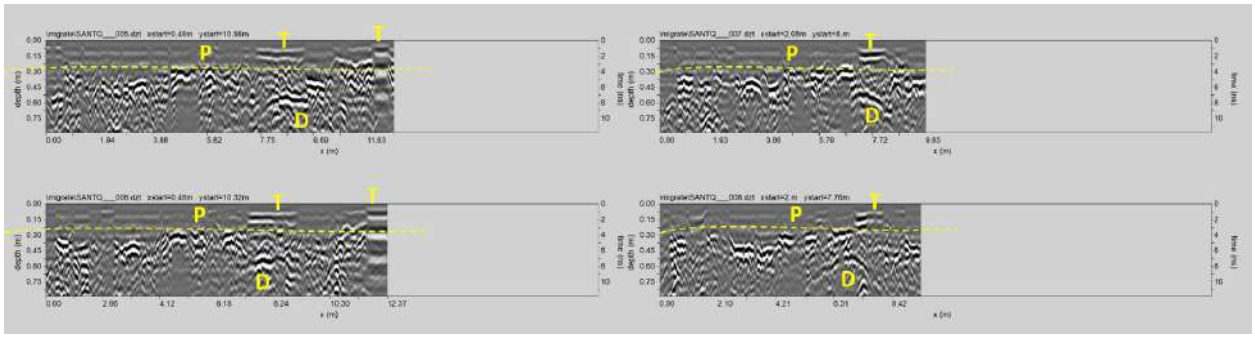

Fig. 237: Area Q: processed GPR profiles 5, …, 8 (D: structure; P: paving thickness; T: manhole)

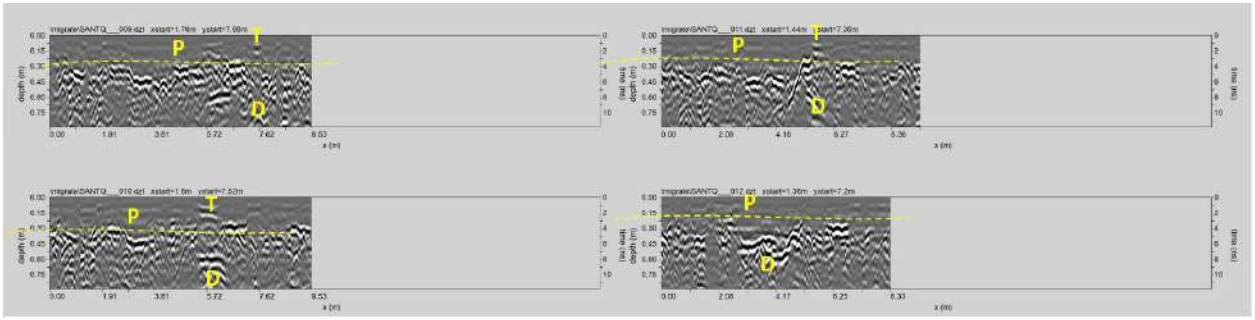

Fig. 238: Area Q: processed GPR profiles 9, …12 (P: paving thickness; T: manhole; D: structure)

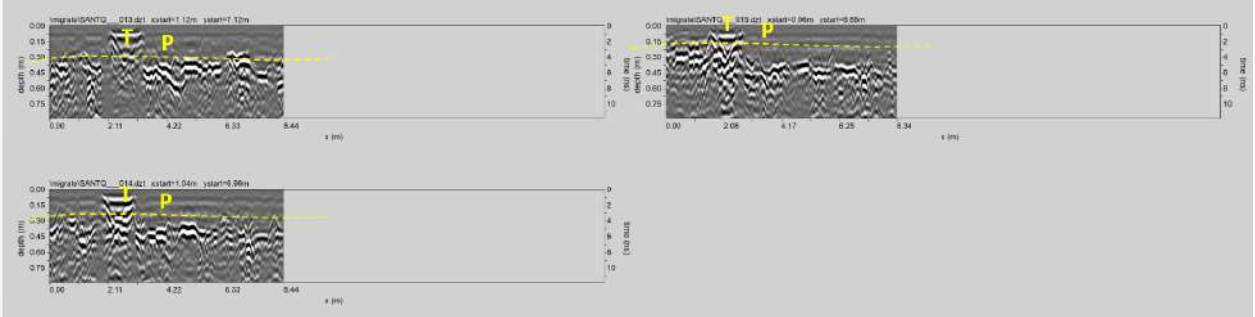

Fig. 239: Area Q: processed GPR profiles 13, …, 15 (P: paving thickness; T: manhole)

Area O+P+Q: 3D visualization: The time-slice technique has been used to display the amplitude variations within consecutive time windows of width Δt=1 ns.
Figs. 240,…, 242 shows the depth slices from 0.0 m to 0.89 m in depth.

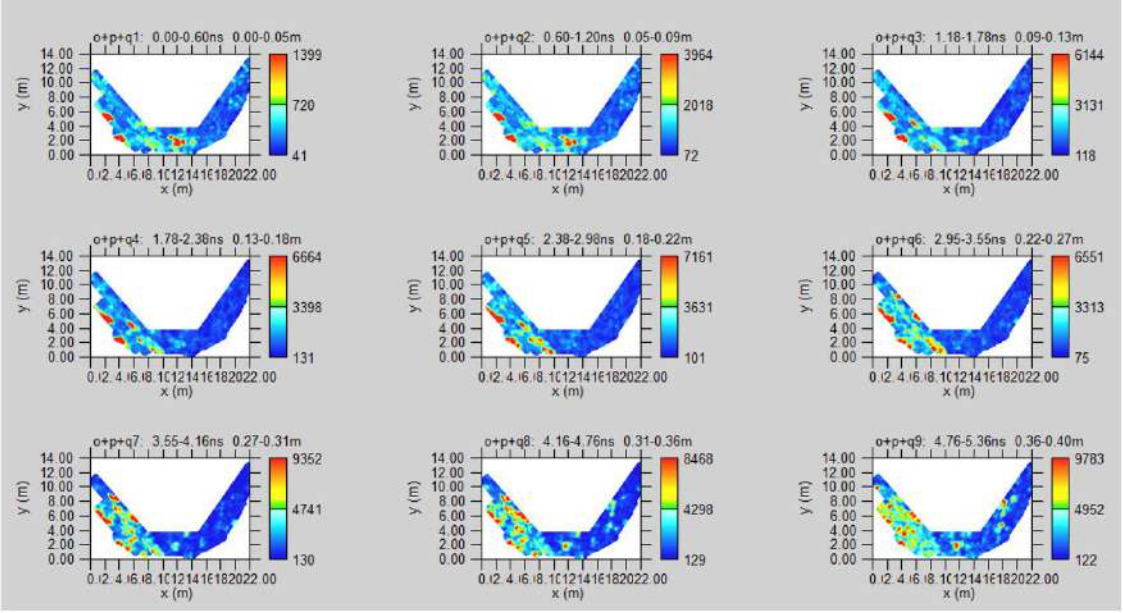

Fig. 240: the whole Area: Depth slices 0.0-0.4m

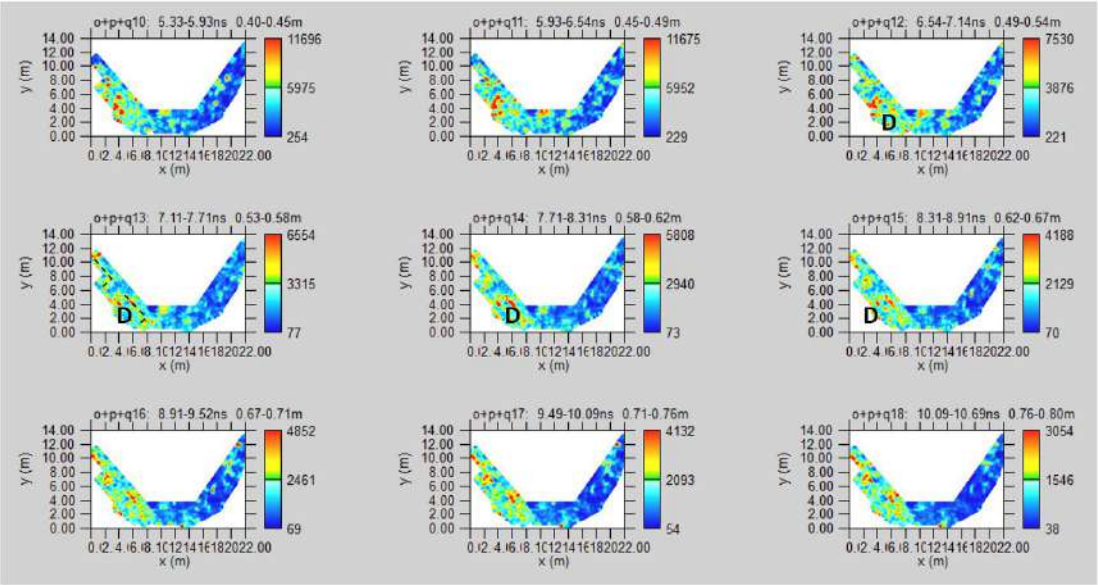

Fig. 241: the whole Area: Depth slices 0.4-0.8m (D: old structure-channel)

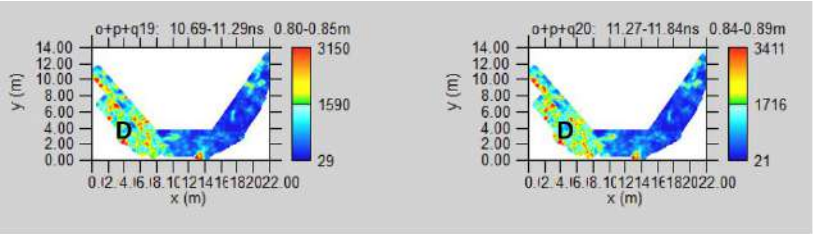

Fig. 242: the whole Area: Depth slices 0.8-0.89m (D: old structure-channel)

At depth between 0.53m and 0.89m, the anomaly D represents a probable channel.

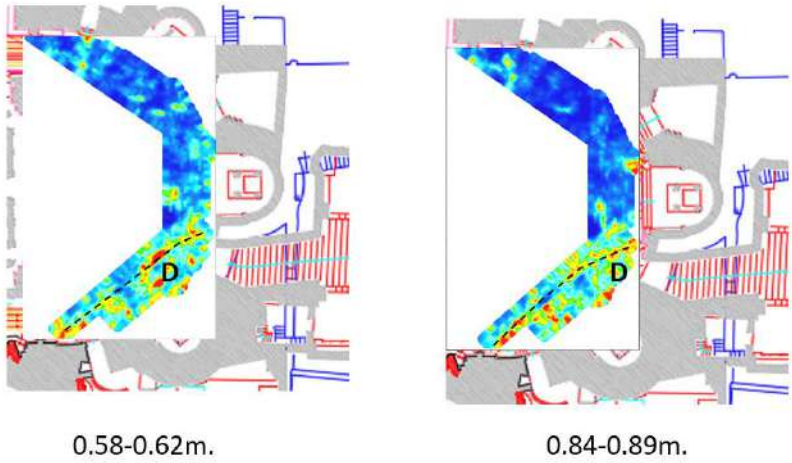

Fig. 243: the whole Area: depth slices overlapped to the planimetry (D: structure-channel-)

Fig 243 shows the more significant depth slices overlapped to the planimetry of the church. It is possible to see the position of the high amplitude anomaly D.

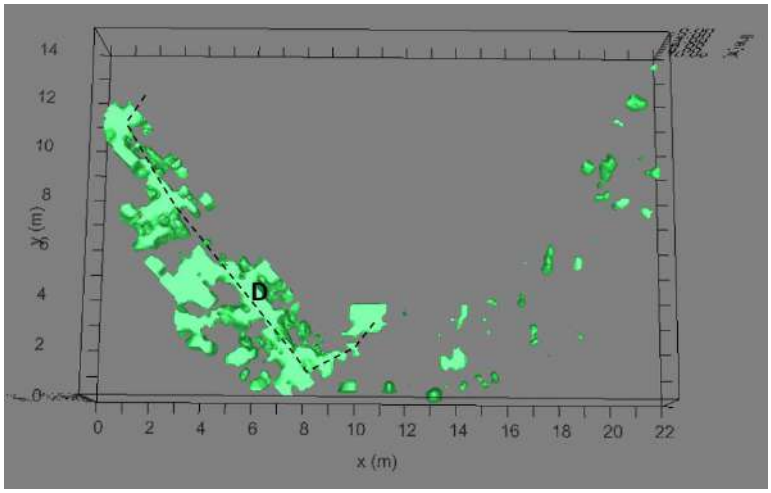

Fig. 244: the whole Area: electromagnetic amplitude isosurfaces 0.49-0.76m depth threshold 50%

Fig. 244 show the iso-surface visualization. Here is possible to see the spatial position of the anomaly D.
Fig. 245 show a virtual excavation. In this case, it is possible to see the position of the anomalous zones well.

Fig. 245: the whole Area: virtual excavation 0.49-0.76m depth threshold 50%

Area O+P+Q: MOISTURE MAP

Figs. 246,…, 248 shows the depth slices with volumetric water content in depth between 0.13m and 0,88m. The slices show a volumetric water content that varies from 7% to 15%. The volumetric water content plan distribution shows relatively high volumetric water content (15%) distributed in a homogeneous mode.

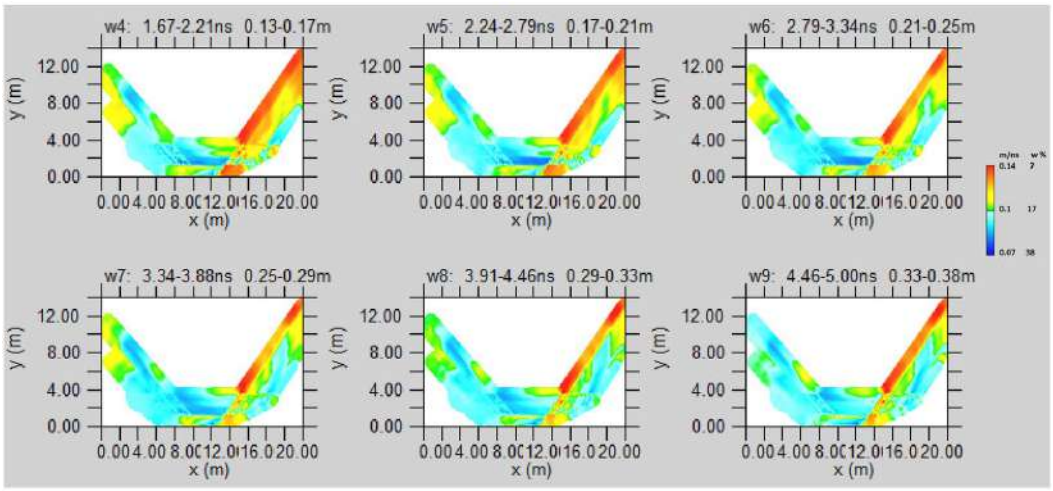

Fig. 246: the whole Area: Volumetric water content (w) and electromagnetic wave velocity (m/ns) at depth from 0.13 to 0.38m

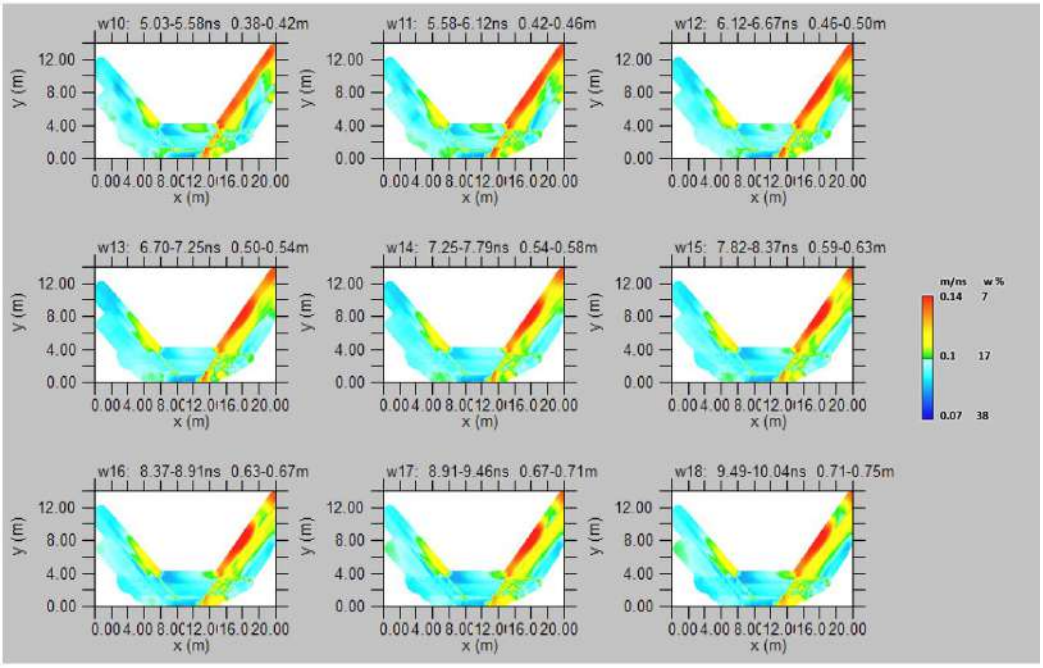

Fig. 247: the whole Area: Volumetric water content (w) and electromagnetic wave velocity (m/ns) at depth from 0.38 to 0.75m

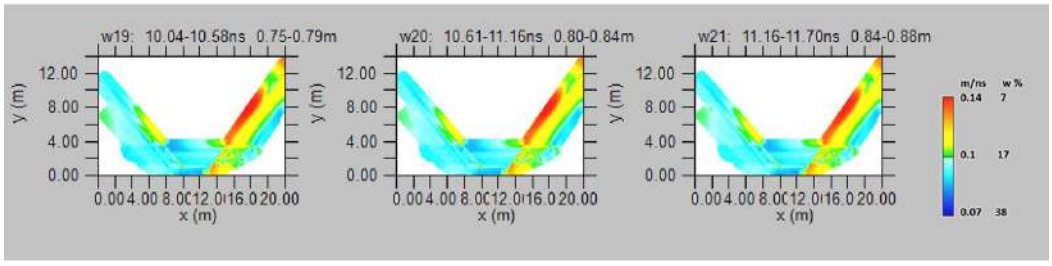

Fig. 248: the whole Area: Volumetric water content (w) and electromagnetic wave velocity (m/ns) at depth from 0.75 to 0.88m

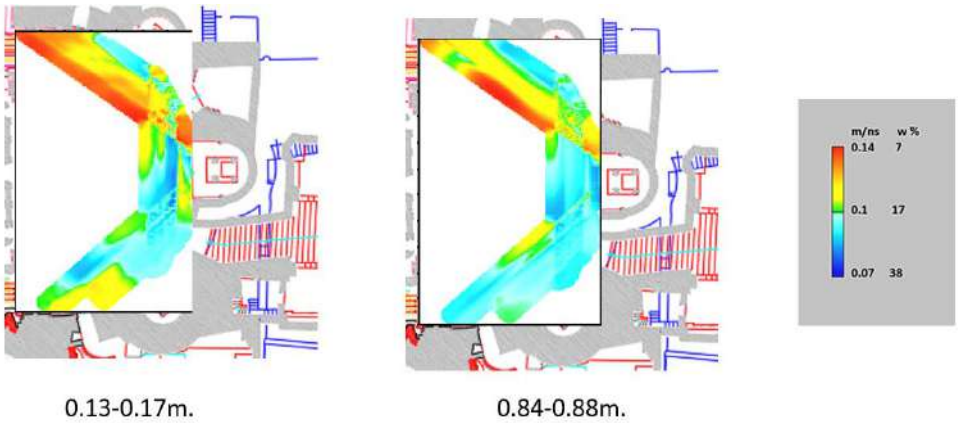

Fig. 249: the whole Area: volumetric water content depth slices overlapped to the planimetry

Fig. 249 shows the volumetric water content depth slice overlapped to the planimetry.

Area Y

In the area, Y has acquired 39 GPR profiles for an extension of 751.0 meters (Fig. 250).

The GPR data profiles were processed in 2D using GPR-slice software (GPR-SLICE Software (gpr-survey.com)). To eliminate a small noise component and make it easy to interpret GPR data, the following processing sequence was applied:

1) Zero-time adjust (static shift), to associate zero-time with zero-depth;
2) Background removal;
3) Frequency filtering, to remove high-frequency noise;
4) Migration, to correct the shape and dimension of reflection events related to the structure present in the subsoil.

Fig. 250: Area Y: location of GPR profiles

The processed GPR profiles acquired in area Y are shown in Figs. 251,…, 260.

The reflection event evidenced by a dashed yellow line (labelled P) is probably related to the paving. Here the thickness of the paving seems to vary between 0.1m and 0.2m.

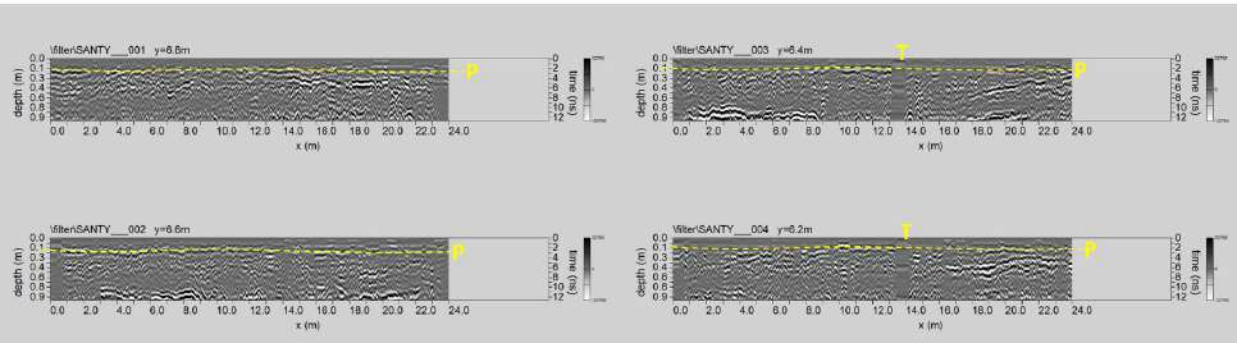

Fig. 251: Area Y: processed GPR profiles 1, …, 4 (P: paving thickness; T: manhole)

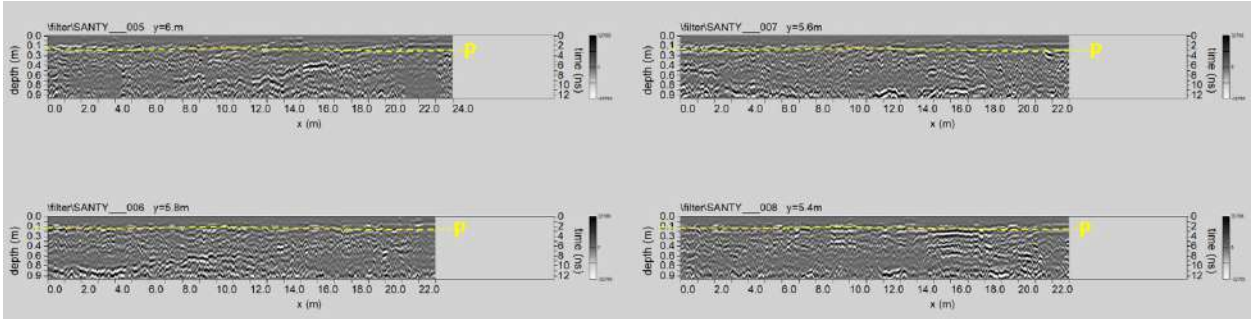

Fig. 252: Area Y: processed GPR profiles 5, …, 8 (P: paving thickness)

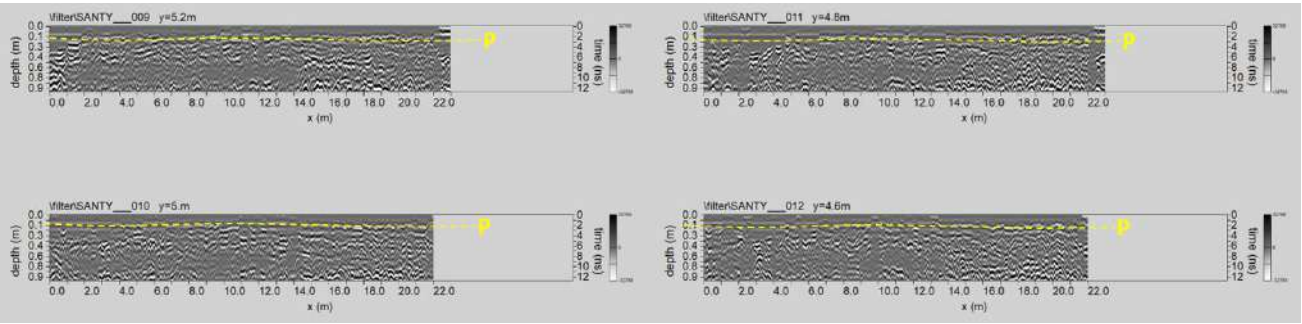

Fig. 253: Area Y: processed GPR profiles 9, …, 12 (P: paving thickness)

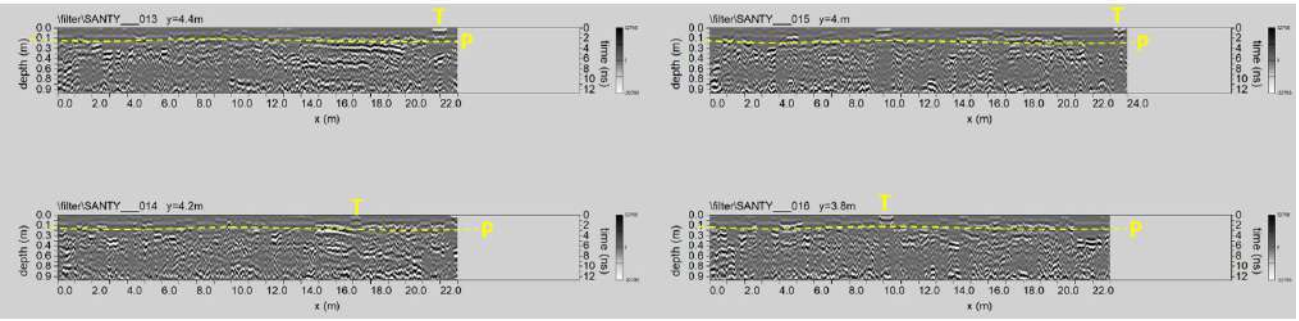

Fig. 254: Area Y: processed GPR profiles 13, …, 16 (P: paving thickness; T: manhole)

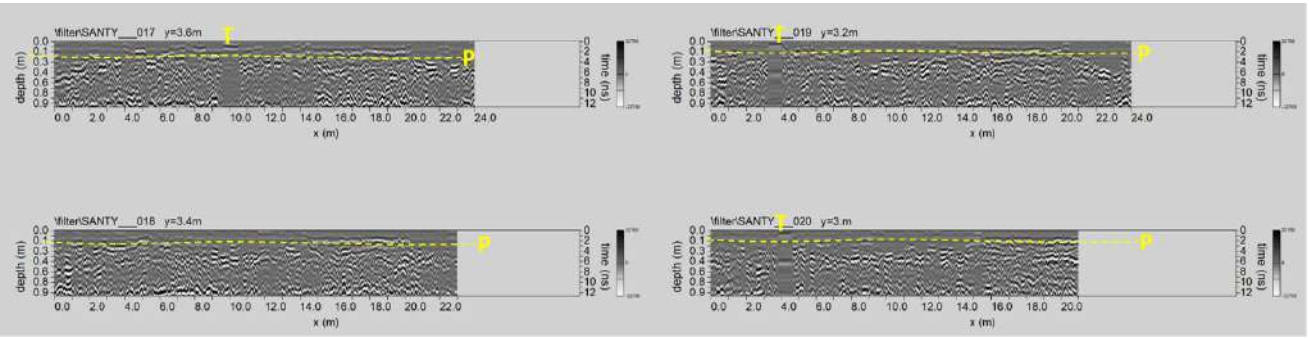

Fig. 255: Area Y: processed GPR profiles 17, …, 20 (P: paving thickness; T: manhole)

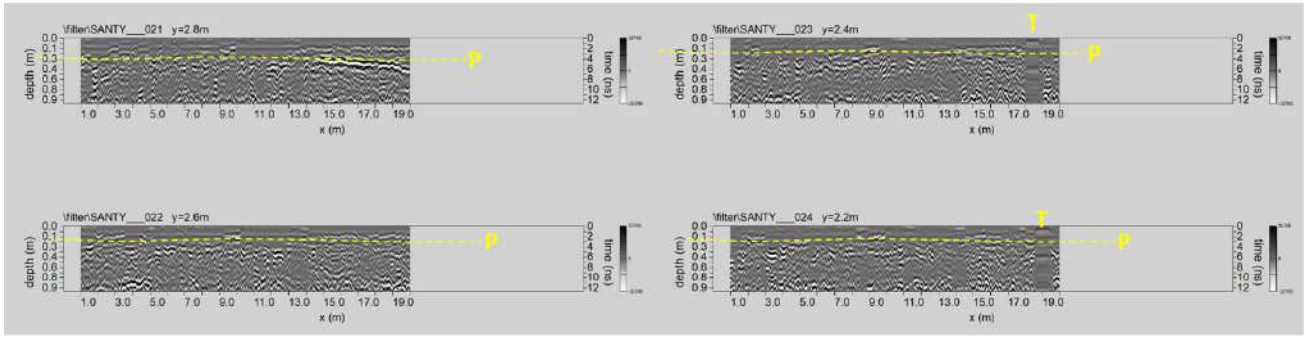

Fig. 256: Area Y: processed GPR profiles 21, …, 24 (P: paving thickness; T: manhole)

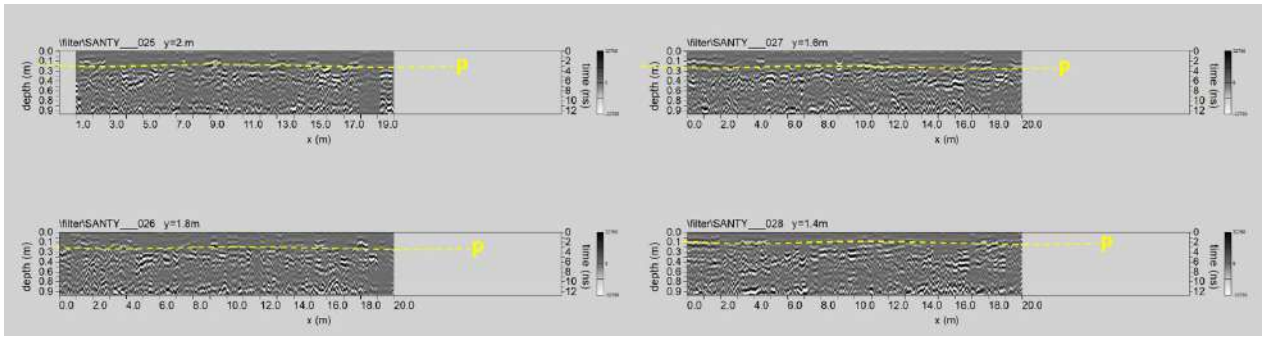

Fig. 257: Area Y: processed GPR profiles 25, …, 28 (P: paving thickness)

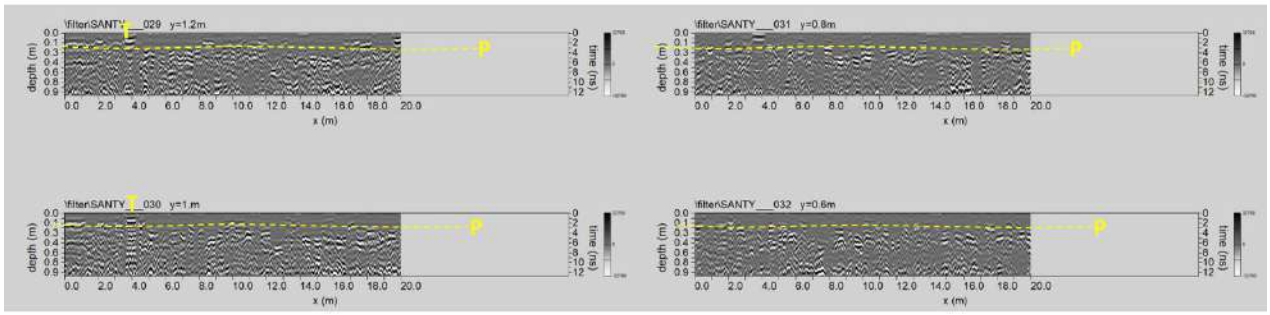

Fig. 258: Area Y: processed GPR profiles 29,.., 32 (P: paving thickness; T: manhole)

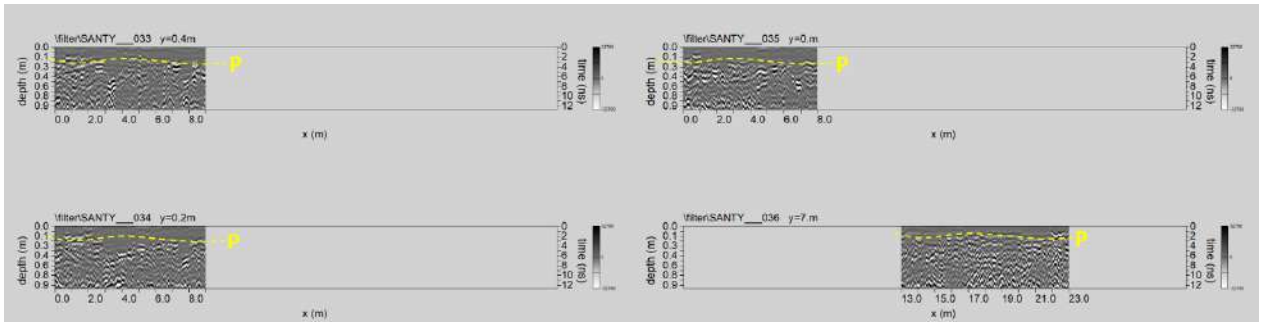

Fig. 259: Area Y: processed GPR profiles 33,…, 36 (P: paving thickness)

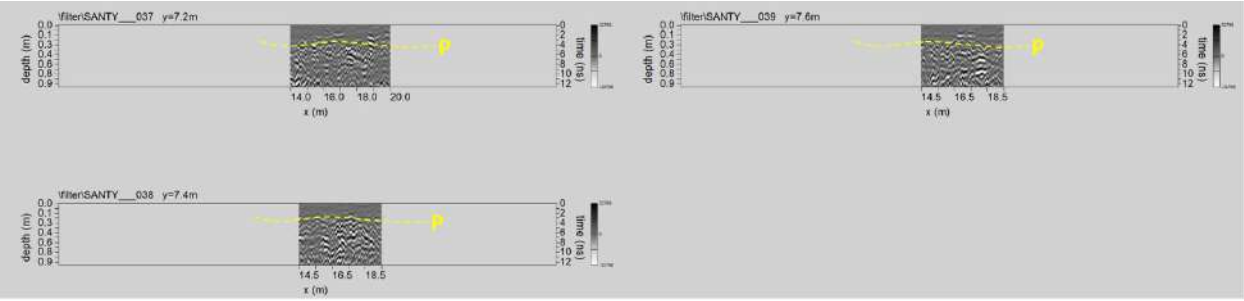

Fig. 260: Area Y: processed GPR profiles 37, …, 39 (P: paving thickness)

Area Y: 3D visualization: The time-slice technique has been used to display the amplitude variations within consecutive time windows of width Δt=1 ns.
Figs. 261,…, 264 shows the depth slices from 0.0 m to 0.96 m in depth.

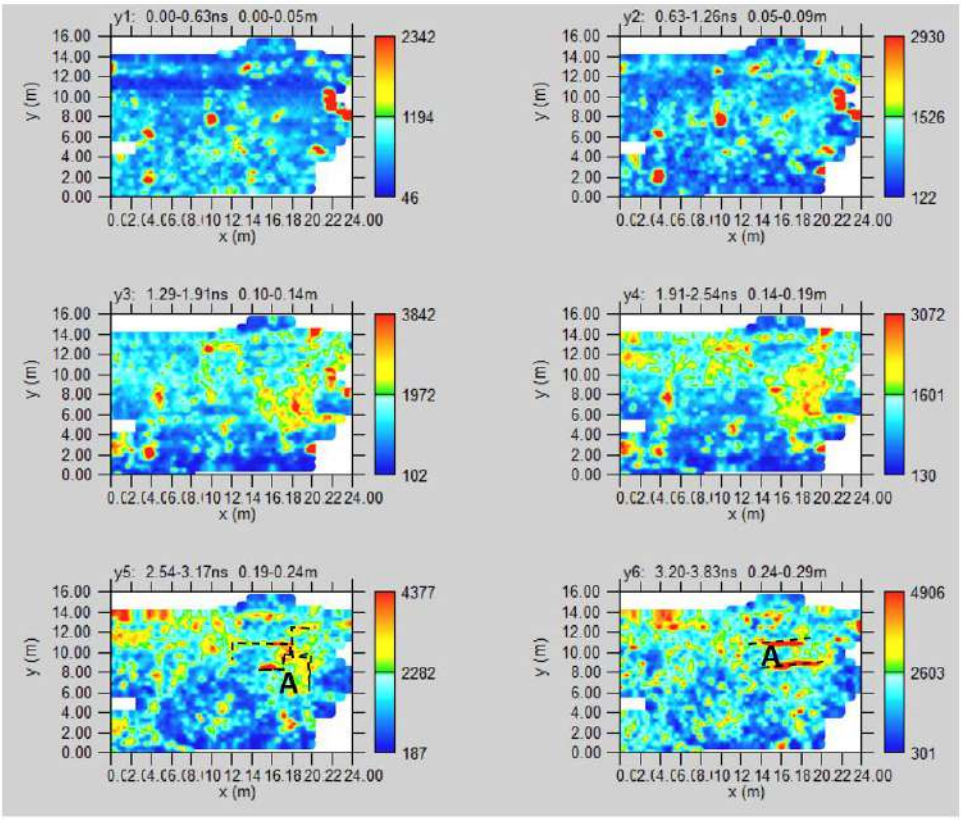

Fig. 261: the whole: Depth slices 0.0-0.29m (A: archaeological structures)

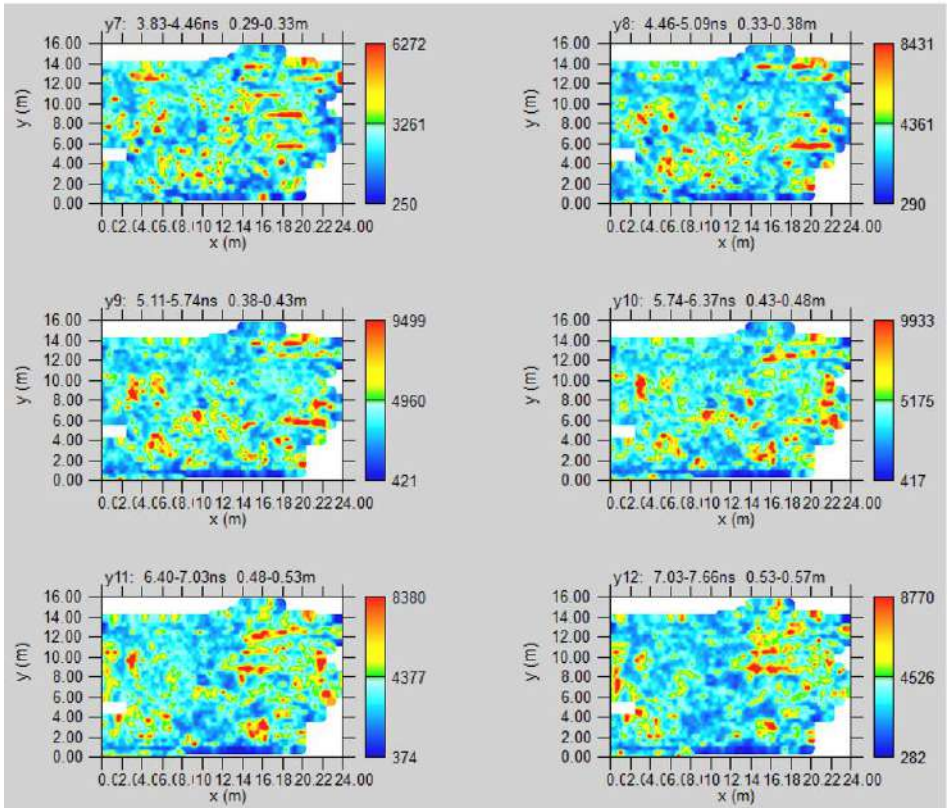

Fig. 262: the whole: Depth slices 0.29-0.57m

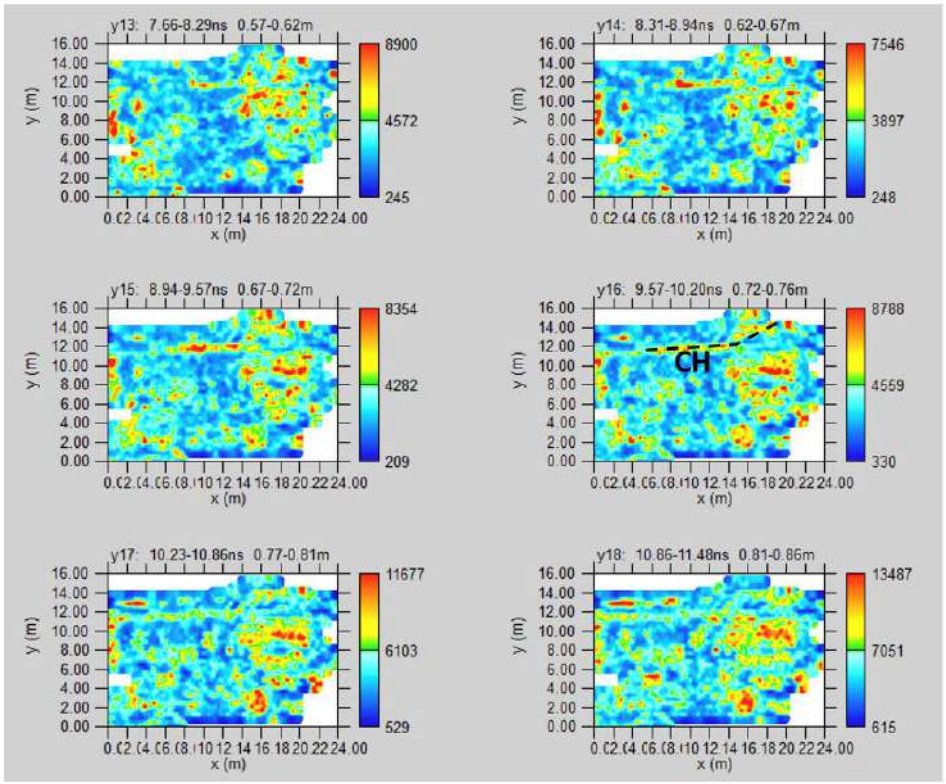

Fig. 263: the whole: Depth slices 0.57-0.86m (A: archaeological structures; CH: channel)

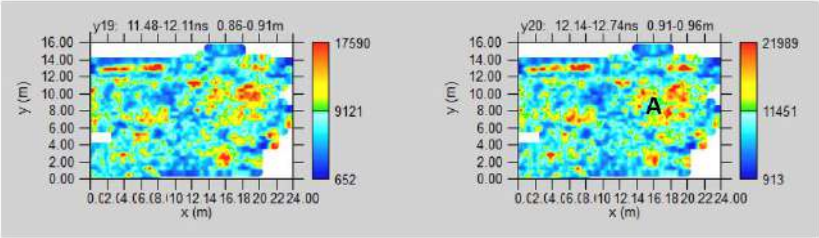

Fig. 264: the whole: Depth slices 0.86-0.96m (A: archaeological structures)

The slices reveal anomalies zone A at depth between 0.24m and 0.96m, representing probable archaeological structures (walls). A confirmation of the channel CH is visible on the slices 0.72-0.76m depth

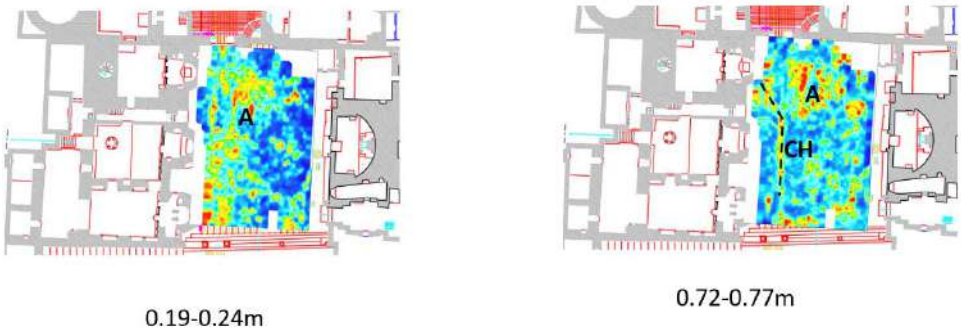

Fig. 265: the whole Area: depth slices overlapped to the planimetry (A: archaeological structures; CH: channel)

Fig 265 shows the more significant depth slices overlapped to the planimetry of the church. It is possible to see the position of the high amplitude anomalies A and CH.

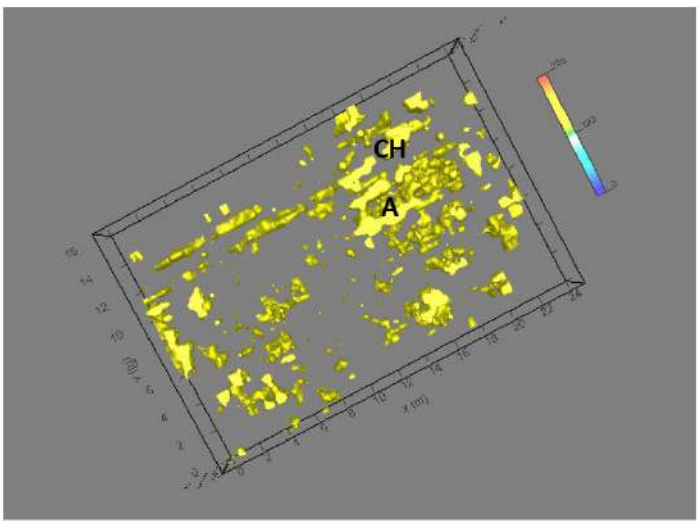

Fig. 266: the whole Area: electromagnetic amplitude isosurfaces 0.53-0.86m depth threshold 65%

Fig. 266 show the iso-surface visualization. Here is possible to see the spatial position of the anomalies A and CH.
Fig. 267 show a virtual excavation. In this case, it is possible to see the anomalous zones' position.

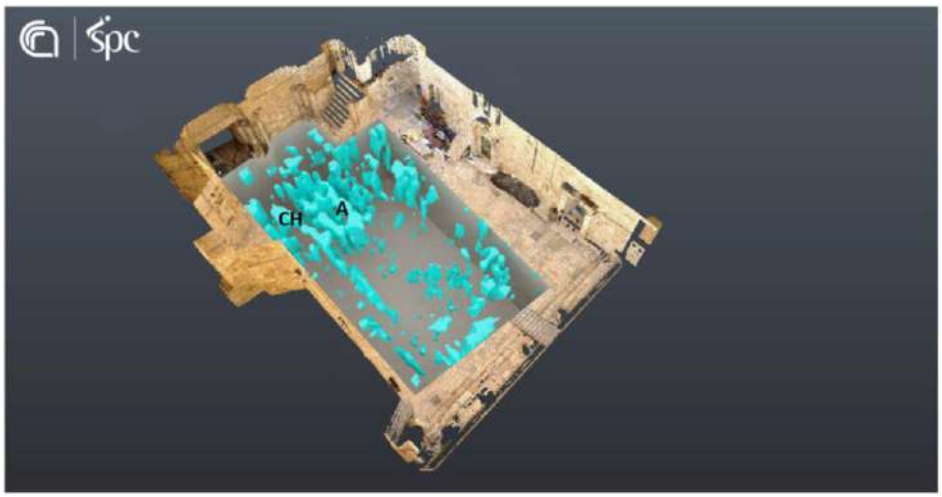

Fig. 267: the whole Area: virtual excavation 0.53-0.86m depth threshold 65%

Area Y: MOISTURE MAP

Figs. 268,…, 270 shows the depth slices with volumetric water content in depth between 0.09m and 1.04m. The slices show a volumetric water content that varies from 7% to 35%. The volumetric water content plan distribution shows high volumetric water content (35%) distributed in deeper slices.

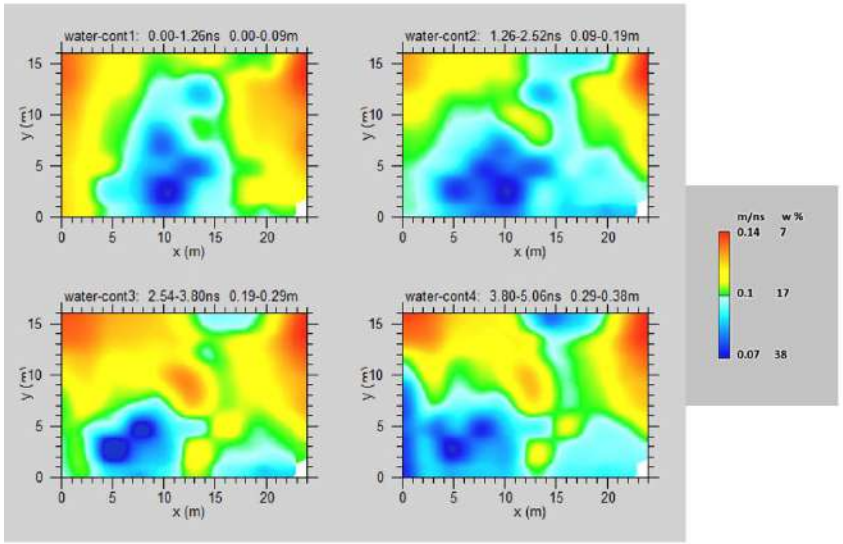

Fig. 268: the whole Area: Volumetric water content (w) and electromagnetic wave velocity (m/ns) at depth from 0.0 to 0.38m

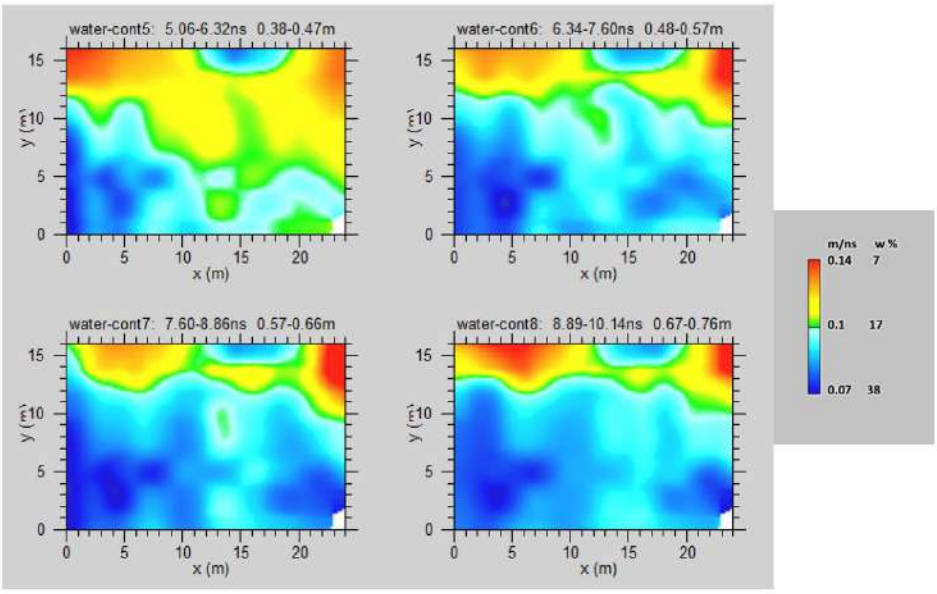

Fig. 269: the whole Area: Volumetric water content (w) and electromagnetic wave velocity (m/ns) at depth from 0.38 to 0.76m

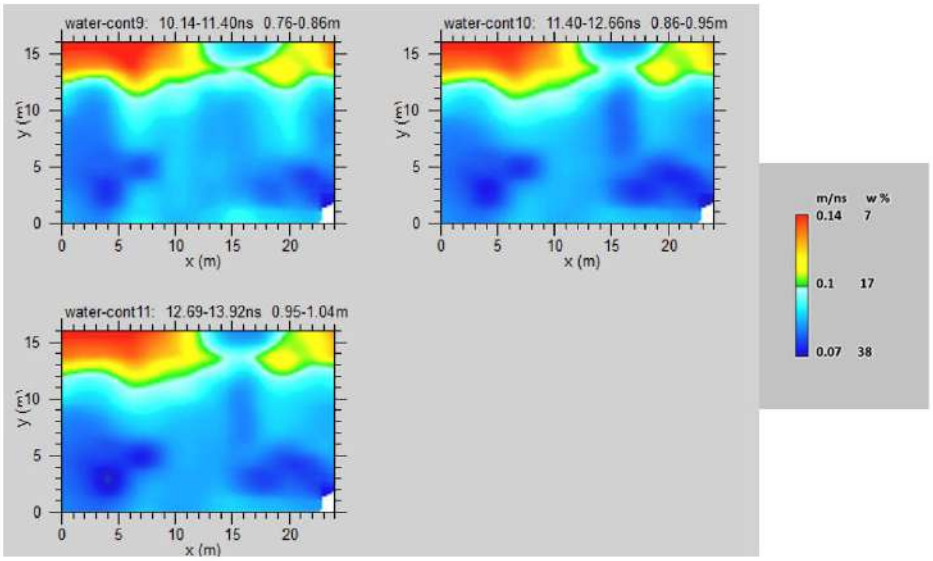

Fig. 270: the whole Area: Volumetric water content (w) and electromagnetic wave velocity (m/ns) at depth from 0.76 to 0.95m

Fig. 271: the whole Area: volumetric water content depth slices overlapped to the planimetry

Fig. 271 shows the volumetric water content depth slice overlapped to the planimetry. It seems that there may be a probable rise in humidity from the subsoil

CONCLUSIONS

GPR results are encouraging. They evidenced the potentiality of the GPR method in the context of the Basilica of the holy sepulchre. The data had allowed evidence of the bedrock's depth (sacred rock). It ranges from 0.3m to 2.5m (Fig. 272).

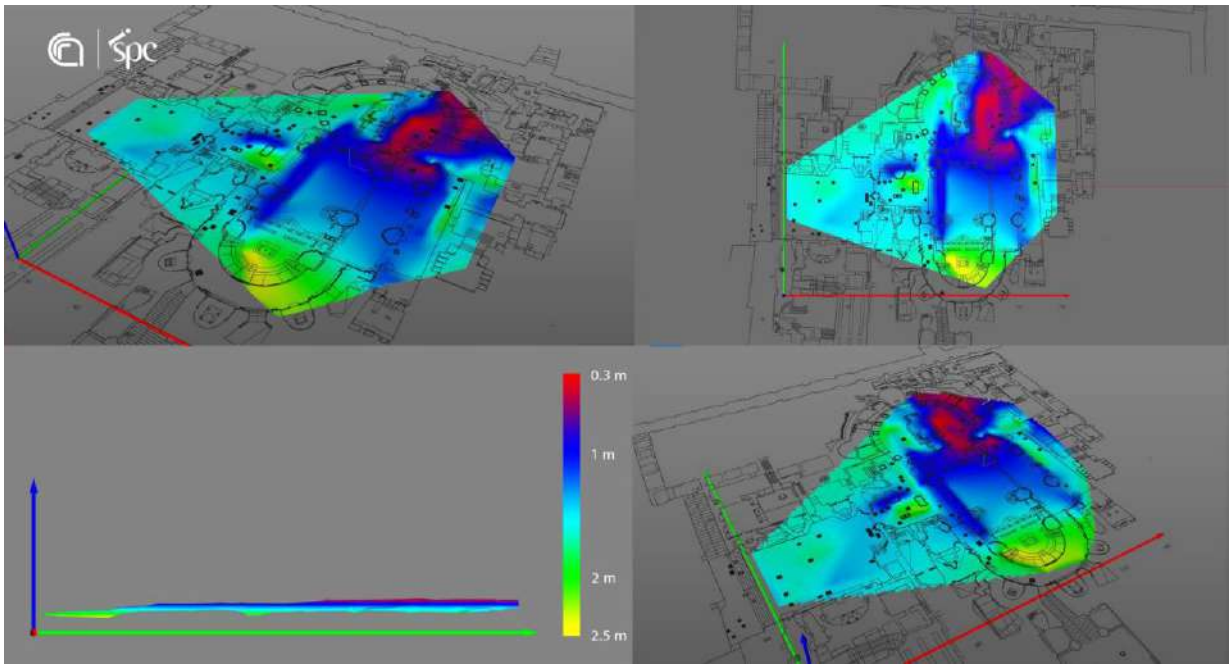

Fig. 272: the pseud 3D visualization of the isosurfaces representing the depth of the bedrock

The paving thickness varies from 0.15m to 0.45m.
The GPR survey highlighted various structures of probable archaeological interest.
GPR survey highlighted probable carriage tracks called A in Fig. 273 in the roundabout area.

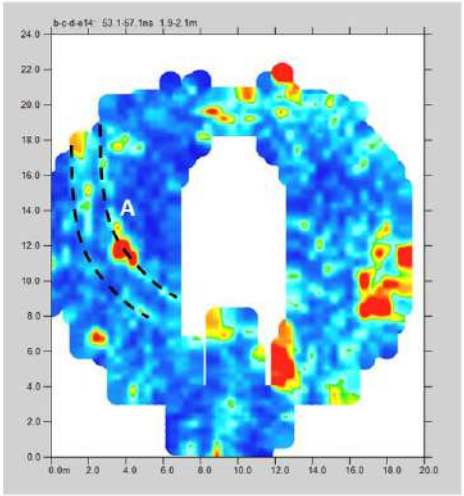

Fig. 273: the probable carriage tracks A

GPR data highlighted an interesting structure called A in Fig. 274.

Fig. 274: the whole Area: virtual excavation 0.82-0.94m depth threshold 15%

Furthermore, the known cavities (Fig. 275) and several channels (Fig. 276).

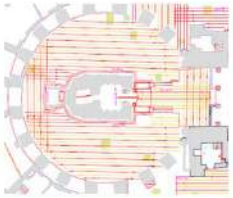

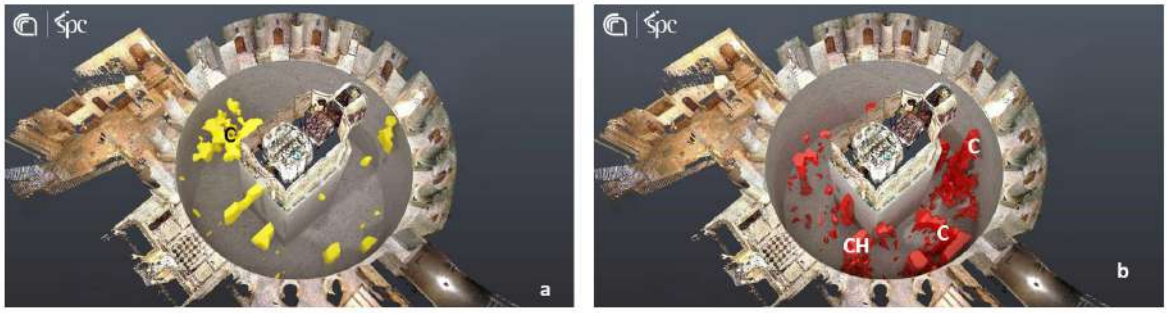

Fig. 275: virtual-excavation: a) 0.6m depth; b) 0.7 m depth. (C: known cavities; CH: channel)

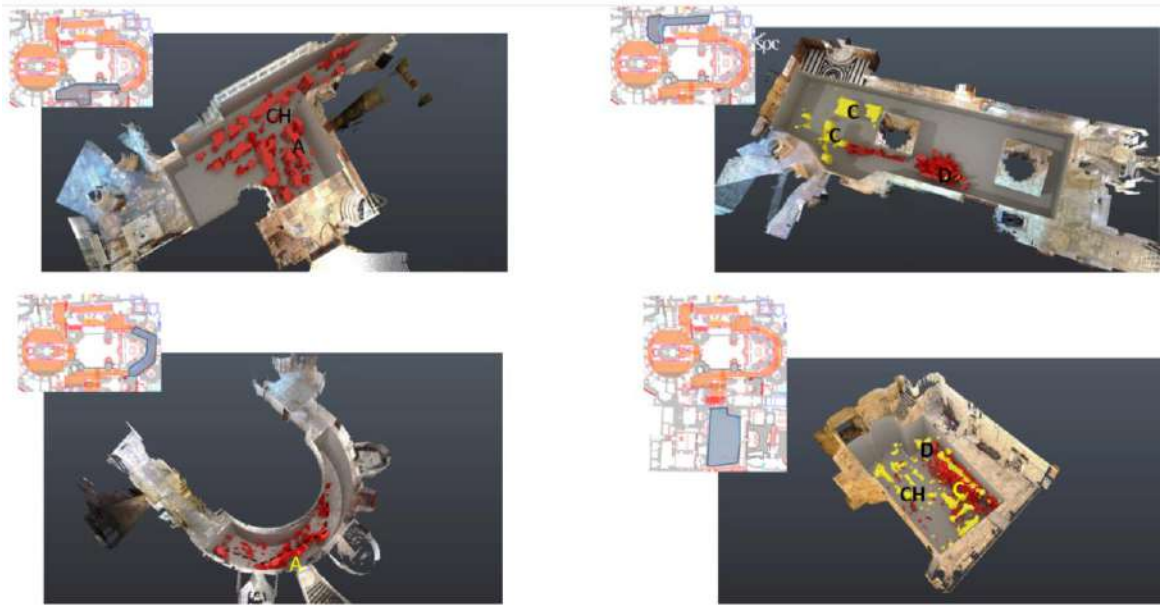

Fig. 276: results of GPR survey: C: cavities; CH: channel; A: archaeological structures; D: old structures)

The volumetric water content seems to rise from the bottom upwards (Fig. 277).

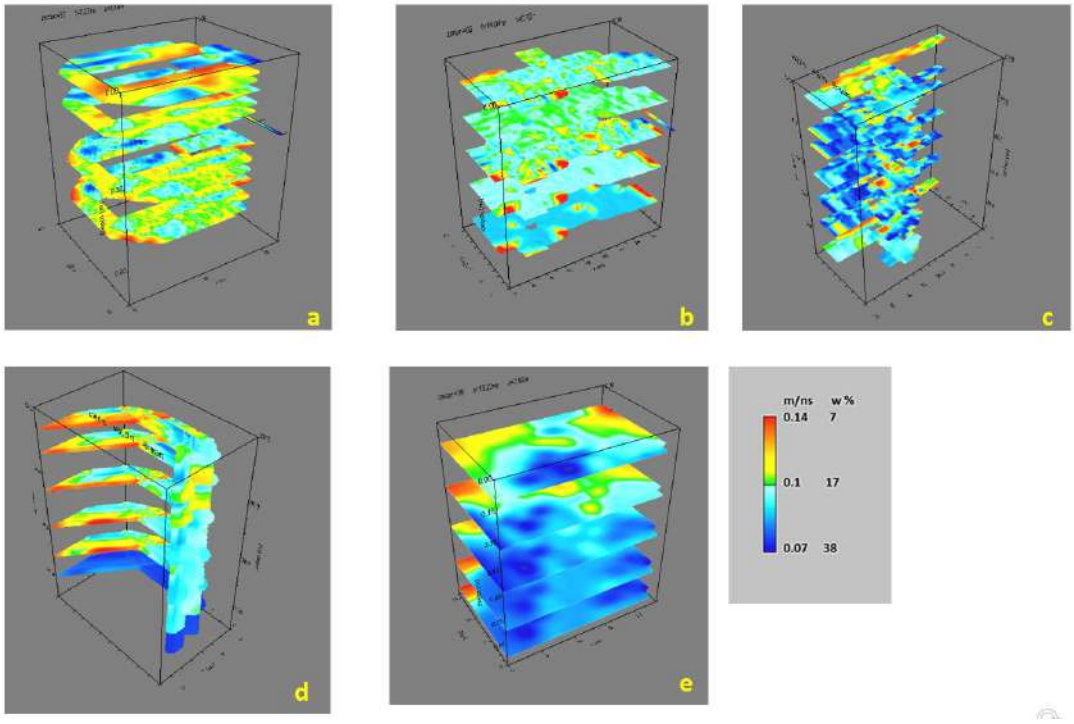

Fig. 277: water content; a) area B+C+D+E; b) A+H+I+L+M+N; c) area F+G+R; d) area O+P+Q; d) area Y

REFERENCES

Annan, A.P. and Davis, J.L., 1978, Methodology for Radar Transillumination Experiments: Report of Activities, Geological Survey of Canada, Paper, 78-1B, p. 107-110.

Annan A.P., Scaife J.E. and Giamou P. 1990. Mapping buried barrels with magnetics and ground penetrating radar. 60th SEG Meeting, San Francisco, USA, Expanded Abstracts, 422–423

Conyers, Lawrence B., 2004, Moisture and soil differences as related to the spatial accuracy of amplitude maps at two archaeological test sites. Proceedings of the Tenth International Conference on Ground Penetrating Radar, Delft, The Netherlands, June 21–24, 2004.

Conyers, Lawrence B. and Dean Goodman, 1997, Ground-penetrating Radar: An Introduction for Archaeologists. AltaMira Press, Walnut Creek, California.

Conyers LB. 2006. Innovative ground-penetrating radar methods for archaeological mapping. Archaeological Prospection 13(2): 139–141.

Conyers LB (2012) Interpreting ground-penetrating radar for archaeology. Left Coast Press, Walnut Creek

Davis J.L. and Annan A.P. 1989. GPR for high resolution mapping of soil and rock stratigraphy. Geophysical Prospecting 37, 531–551.

Du S. and Rummel P. 1994. Reconnaissance studies of moisture in the subsurface with GPR. Proceedings of the 5th International Conference on Ground Penetrating Radar, pp. 1224–1248.

Endrea A.L. and Knight R. 1992. A theoretical treatment of the effect of microscopic fluid distribution on the dielectric properties of partially saturated rocks. Geophysical Prospecting 40, 307–324.

Fruhwirth R.K., Schmoller R. and Oberaigner E.R. 1996. Some aspects of the estimation of electromagnetic wave velocities. Proceedings of the 6th International Conference on Ground Penetrating Radar, Tohoku University, Sendai, Japan, pp. 135–138.

Gaffney, Chris and John Gater, 2003, Revealing the Buried Past: Geophysics for Archaeologists. Tempus, Stroud, Gloucestershire.

Giannino F. and Leucci G., 2021. Electromagnetic Methods in Geophysics: Applications in GeoRadar, FDEM, TDEM, and AEM. Wiley, pp 352, ISBN: 978-1-119-77098-5

Goodman, Dean and Piro, Salvatore, Nishimura, Yasushi, Patterson, Helen and Vince Gaffney, 2004, Discovery of a 1st century AD Roman amphitheatre and other structures at the Forum Novum by GPR. Journal of Environmental and Engineering Geophysics 9: 35–42.

Goodman D. 2013. GPR Slice Version 7.0 Manual. http://www.gpr-survey.com (accessed June 2013).

Goodman D, Piro S. 2013. GPR Remote Sensing in Archaeology. Geotechnologies and the Environment Series, Vol. 9, Springer-Verlag: Berlin; 233 pp.

Goodman D, Steinberg J, Damiata B, Nishimure Y, Schneider K, Hiromichi H, Hisashi N. 2006. GPR overlay analysis for archaeological prospection. Proceedings of the 11th International Conference on Ground Penetrating Radar, Columbus, Ohio; CD-rom.

Grandjean G., Gourry J.C. and Bitri A. 2000. Evaluation of GPR techniques for civil-engineering applications: study on a test site. Journal of Applied Geophysics 45, 141–156.

Grasmueck M. 1996. 3-D ground-penetrating radar applied to fracture imaging in gneiss. Geophysics 61, 1050–1064. Greaves R.J., Lesmes D.P., Lee J.M. and Toksöz N. 1996. Velocity variations and water content estimated from multi-offset, ground-penetrating radar. Geophysics 61, 683–695.

Huisman J.A., Hubbard S.S., Redman J.D. and Annan A.P. 2003. Measuring soil water content with ground penetrating radar: A review. Vadose Zone Journal 2, 476–491.

Leckebusch, J., 2003, Ground-penetrating radar: A modern three-dimensional prospection method. Archaeological Prospection 10: 213–240.

Leucci G., 2008. ground penetrating radar:the electromagnetic signal attenuation and maximum penetration depth, Scholarly Research Exchange: Volume 2008 • Article ID 926091 • doi:10.3814/2008/926091;

Leucci G., 2015, Geofisica Applicata all'Archeologia e ai Beni Monumentali. Dario Flaccovio Editore, Palermo, pp. 368. ISBN: 9788857905068

Leucci G., 2019, Nondestructive Testing for Archaeology and Cultural Heritage: A practical guide and new perspective. Springer editore pp 217, ISBN 978-3-030-01898-6

Leucci G., 2020, Advances in Geophysical Methods Applied to Forensic Investigations: New Developments in Acquisition and Data Analysis Methodologies. Springer editore, pp 200, ISBN 978-3-030-46241-3

Mellet J.S. 1995. Ground penetrating radar applications in engineering, environmental management, and geology. Journal of Applied Geophysics 33, 157–166.

Miller, M.L., Freeland, R.S., and Koppenjan, S.K., 2002. Searching for Concealed Human Remains using GPR Imaging of Decomposition, Ninth International Conference on Ground Penetrating Radar, Santa Barbara, California, USA, April 30-May 2, pp. 539- 544.

Topp G.C., Davis J.L. and Annan A.P. 1980. Electromagnetic determination of soil water content: measurements in coaxial transmission lines. Water Resources Research 16(3), 574–582.

Ylmaz O., Seismic Data Processing, in: E.B. Neitzel (Ed.), Seismic Data Processing, Society of Exploration Geophysicists, Tulsa USA, 1987.

.